Structural and chemical relationships in metal phosphine complexes relevant to homogeneous catalysis

A thesis submitted to meet the requirements for the degree

PHILOSOPHIAE DOCTOR

In the

DEPARTMENT OF CHEMISTRY

At the

UNIVERSITY OF THE FREE STATE

By

BUNGU PETER NDULA

Promoter

PROF. STEFANUS OTTO

Co-promoter

PROF. ANDREAS ROODT

March 2010

Preface

I will first of all wish to thank the almighty God for his infinite wisdom and for giving me peace, strength and good health during the course of this work.

I remain indebted to the following people:

- My beloved wife, Kuvin Florence Ntuchu and children Ikeh Tracey and Fanwi Jesse for their love, encouragement and understanding during my time of study.
- Prof. Stefanus Otto and Prof. Andreas Roodt for their guidance, patience and enthusiasm during the course of the work.
- Dr. Fanie Muller and Leo Kirsten for X-ray crystallographic data collection and Prof. Stefanus Otto for refining and solving the crystal structures.
- My colleagues both in Sasol and UFS for their kind support.

Finally, I wish to thank Sasol Technology R & D for providing me with a job and giving me the opportunity to pursue this study.

Dedication

This thesis is dedicated to my late parents Pa Ndula David Nkeusse Kumsike and Mama Nchewe Ikeh Agnes Ndula and my late uncle Pa Lambi Umaru Kumsike Ndanyi.

Publications and presentation

- P. N. Bungu and S. Otto *J. Organomet Chem*; 2007,**692**, 3370. "*Steric and electronic properties in bicyclic phosphines; Crystal and molecular structures of Se-Phoban-Q (Q = C_2, C_3Ph, Cy and Ph)*".
- P. N. Bungu and S. Otto, *Dalton Trans.*, 2007, 2876. "*Bicyclic phosphines as ligands for cobalt catalyzed Hydroformylation. Crystal structures of [Co(Phoban[3.3.1]-Q)$(CO)_3]_2$ (Q= C_2H_5, C_5H_{11}, $C_3H_6NMe_2$, C_6H_{11})*".
- P. N. Bungu and Stefanus Otto (Unpublished). "*Evaluation of ligand effects in the modified cobalt hydroformylation of 1-octene. Crystal structure of [Co(L)(CO)3]2 (L = PA-C_5, PCy_3 and PCp_3)*".
- P. N. Bungu and S. Otto, *Acta Cryst.*, 2009, **E65,** o560. "2-Isobutyl-2-phosphabicyclo[3.3.1]nonane 2-selenide".
- P. N. Bungu and S. Otto, *Acta Cryst.*, 2009, **C65**, m152. *"Cis* - dichloridobis{dimethyl[3-(9-phosphabicyclo[3.3.1]non-9-yl)propyl]amine-kP}platinium(II)".
- P. N. Bungu and P. C. Pistorius, *Canadian Metallurgical Quarterly*, 2009, **48(1)**, 45. "Mineralogy and initial chlorination of water granulated high titania slag".
- An oral lecture on the work was presented at an international conference, The South African Chemical Institute (SACI) in Bloemfontein on the 13th Sept. 2009. Title: "*Structure and activity relationships in MeI oxidative addition and migratory insertion reactions in Rh-phosphine complexes".*
- A poster was presented at the national conference, Catalysis South Africa (CATSA) in Richards Bay in 2007. Title: "*Crystallographic and NMR investigation on steric and electronic properties of bicyclic phosphines".*

Table of contents

Abbreviations and symbols

*A*0	Initial absorbance
*A*1	Final absorbance
acac	Acetyl acetonato
A_{obs}	Observed absorbance
Bislim	1, 2-bis-(8-bicyclo-2,6-dimethyl-8-phospha(3.3.1)nonyl)ethane
$CDCl_3$	Deuterated chloroform
Cy	Cyclohexyl
DCM	Dichloromethane
DME	Dimethyl ether
Ea	Activation energy
Et	Ethyl
h	Plank's constant
I	Iodide
IMes	1,3-bis(2,4,6-trimethylphenyl)imidazol-2-ylidene
IR	Infrared.
IUPAC	International Union of Pure and Applied Chemistry
K	Equilibrium constant
k_1	Oxidative addition rate constant
k_{-1}	Reductive elimination rate constant
k_B	Boltzmann's constant
k_{obs}	Pseudo first order rate constant
Lim-C_5	Mixture of (4R, 8S) and (4S, 8S) 4,8-dimethyl-2-pentyl-2-phosphabicyclo [3.3.1]nonane
Lim-Cp	Mixture of (4R, 8S) and (4S, 8S) 4,8-dimethyl-2-cyclopentyl-2-phosphabicyclo[3.3.1]nonane
Lim-Ph	Mixture of (4R,8S) and (4S,8S)-4,8-dimethyl-2-phenyl-2-phosphabicyclo[3.3.1]nonane
LPG	Liquified petroleum gas

VAZO	1,1'-Azobis(cyclohexane-carbonitrile)
VCH-C_5	2-pentyl-2-phosphabicyclo[3.3.1]nonane
VCH-^{i}Bu	Mixture of 2-isobutyl-2-phosphabicyclo[3.3.1 and 3.2.2]nonane
VCH-Ph	Mixture of 2-phenyl-2-phosphabicyclo[3.3.1 and 3.2.2]nonane
$\Delta H^{\neq}$	Activation enthalpy change
ΔG^{o}	Standard Gibbs free energy change
$\Delta G^{\neq}$	Gibbs free energy change
$\Delta S^{\neq}$	Activation entropy change
ν	Stretching frequency on IR
θ	Tolman cone angle

1 Introduction and aim

1.1. General concept of catalysis

The phenomenon of catalysis was recognized over 150 years ago by Berzelius who referred to it as the "catalytic power of substances" that were able to "awake affinities that are asleep at a given temperature by their mere presence and not by their own affinity". Once the principle of thermodynamics was developed and the concept of equilibrium established by the turn of the twentieth century, scientists realized that catalysts are defined as substances that increase the rate at which a chemical reaction approaches equilibrium without being consumed in the process.[1] Consider the following reaction for the formation of water:

$$H_2\,(g) + \frac{1}{2}O_2 \overset{K_p}{\rightleftharpoons} H_2O\,(g) \qquad 1$$

$\Delta G°$ = -228.6 kJ mol^{-1} and K_p = 1.19 x 10^{40} atm^{-1} at 298 K, indicating that at equilibrium this system lies completely to the right.[2] However, if hydrogen and oxygen are carefully mixed in a pure state nothing happens. Nevertheless, by adding some finely divided platinum to the mixture, the reaction takes place very rapidly. Thermodynamics tell us a lot about the equilibrium state of the system, but it tell us nothing about the speed at which the state could be achieved. A catalyst cannot make a reaction happen that is not thermodynamically allowed. Before embarking on any catalyst design, it is imperative to check the thermodynamic feasibility of the desired reaction. It

1 W. Keim, *Homogeneous Catalysis for Industries*, Institut für Technische chemie und Makromoleculare Chemie der Rheinisch-Westfälischen, Technischen Hochschule Aachen, Worringerweg 1, D-52074, Aachen.

2 C. Masters, *Homogeneous Transition-metal Catalysis*, 1980 and references there in.

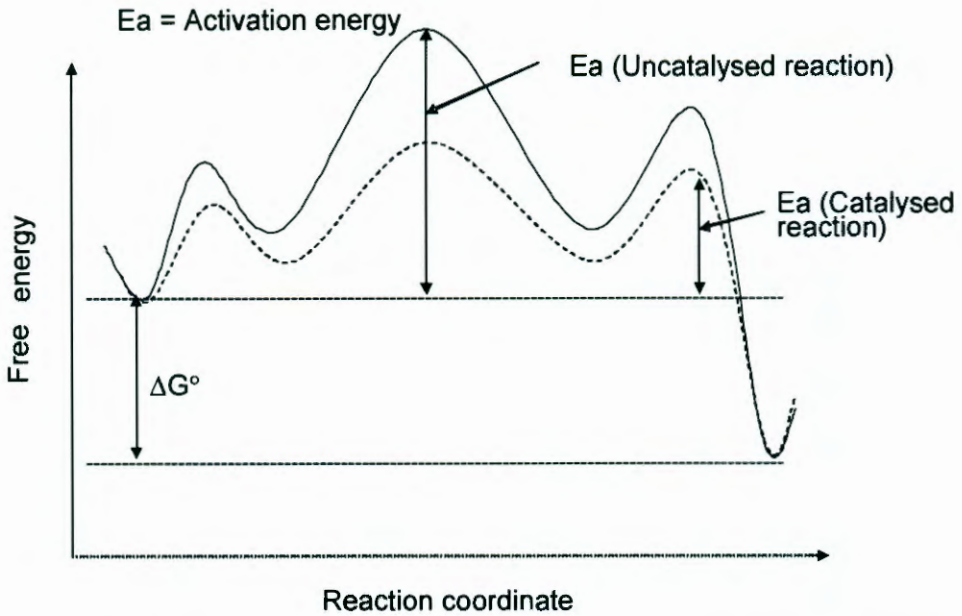

Figure 1.1: Free energy plot for hypothetical uncatalysed and catalysed reactions.

A catalyst provides a new reaction pathway with a low barrier of activation and may involve many intermediate steps. The sequence of steps is called the mechanism, which also refers to the more detailed description of a reaction at the molecular bonding level. In this sense, the catalyst itself remains chemically unchanged during the catalytic conversion.

Typically, catalysts are intimately involved with reactants (often called substrates) in a cyclic series of bond making, and bond breaking steps. During each cycle, the catalyst is regenerated so that it may go through another cycle. Each cycle, producing a molecule of product, is called a turnover and an effective catalyst may undergo hundreds, even thousands of turnovers before deactivating. In a stoichiometric reaction, the "catalyst" (actually reagent) undergoes only one turnover per molecule of product produced.[3] During the catalytic cycle, the catalyst may be present in several intermediate forms when one looks more closely at the molecular level. When

3 R. H. Crabtree, *The Organometallic Chemistry of the Transition metals*, Yale University, 1988, 185.

1.2. Importance of catalysts

Catalysts are widely used in nature, in industry, in the laboratory and it is estimated that they contribute up to one-sixth of the value of all manufactured goods in industrialised countries.[7] Catalysis plays a vital role in the production of fuels, chemicals as well as providing the means for strengthening environmental safeguards all over the world. The products produced by the chemical industry can be differentiated into commodity chemicals (large volume ethylene, vinyl chloride, etc.), specialized chemicals (oil field chemicals, lubricants, etc.) and fine chemicals (pharmaceuticals). For example, a key step in the production of sulphuric acid is the catalytic oxidation of sulphur dioxide to sulphur trioxide using vanadium pentoxide (V_2O_5) as catalyst.[8] Ammonia, another chemical essential for industry and agriculture, is produced by the catalytic reduction of nitrogen with hydrogen[4] using porous iron as catalyst.[9] Inorganic catalysts are also important in energy sources, cracking of higher hydrocarbons, reforming and hydrotreating.[1, 7] In addition, the conversion of synthesis gas to paraffins and olefins via Fischer Tropsch technology[1], conversion of the olefins to high valued oxygenates[10], conversion of ethylene to 1-hexene and 1-octene[11] as done by Sasol cannot be achieved without the use of catalysts.

---

7 D. F. Shriver, P. W. Atkins and C. H. Langford, *Inorg. Chem.*, 2nd ed., Oxford University Press: Oxford, Chapter 7, 1994, 709.

8 http://www.chemguide.co.uk/physical/equilibria/contact.html, accessed on the 24/12/2009.

9 http://www.ausetute.com.au/haberpro.html, accessed on the 24/12/2009.

10 P. J. Steynberg, H. van Rensburg, C. J. J. Grove, S. Otto and C. Crause, *WO. Patent*, 2003, 068719A2.

11 M. J. Overett, K. Blann, A. Bollmann, J. T. Dixon, F. Hess, E. Killian, H. Maumela, D. H. Morgan, A. Neveling and S. Otto, *Chem. Commun.*, 2005, 622.

use of enzymes and microorganisms in chemical reactions taking place in living cells/organisms.[12]

Organometallic catalysts consist of a central metal surrounded by organic and inorganic molecules, called ligands, with at least one metal-carbon bond. Both the metal and the large variety of ligands determine the properties of the catalyst. The success of organometallic catalysts lies in the relative ease of catalyst modification by changing the ligand environment. The catalyst is usually deployed in solution and most commonly exists in a molecularly dispersed form. All sites are potentially active for catalysis and in many cases catalysis is observed under much milder reaction conditions than found with heterogeneous catalysis using metals and metal oxides catalysts.[13]

Homogeneous catalysis presents a great opportunity in that, unlike heterogeneous catalysis, there is a far better understanding of the reaction mechanism (catalytic cycle) with the possibility of being able to influence the steric and electronic properties of these molecularly defined catalysts.[12] It is thus possible to optimize the homogeneous catalyst, tailoring it to the specific system, by adapting the chemical and structural nature of the catalyst.

Crucial properties to be influenced are the rate of the reaction (relates to the amount of reactants the catalyst can convert per unit time), stability (relates to how long the catalyst remains functional before deactivating) and the selectivity (relates to the amount of desired product as opposed to undesirable products that the catalysed reaction forms) of certain products.[4]

---

12 B. Cornils and W. A. Herrmann, "*Applied Homogeneous Catalysis with Organometallic. Compounds*", VHC Publishers, Weinheim, 1998.

13 S. P. Parker and McGraw-Hill, *Encyclopedia of Chemistry*, 1983.

polymerisation of olefins or deposition of heavy fractions such as waxes during petrochemical processes.[16] Inefficient catalyst recovery in homogeneous catalysis will influence productivity due to the high cost of the precious metal and the ligands.[17] A summary of some of the differences of homogenous and heterogeneous catalysis is given in Table 1.4.

Table 1.4: Homogeneous versus heterogeneous catalysis

	Homogeneous	**Heterogeneous**
Catalytic forms	soluble metal complexes, usually mononuclear	solid, often metal or metal oxide usually supported.
Mode of use	dissolved in reaction medium	fixed or slurry bed
Diffusion	facile	can be very important
Selectivity	high	low
Activity	moderate	high
Solvent	required, can be product or by-product	usually not required
Stability	often decomposed at high temperature	stable at high temperature
Temperature	low (<250° C)	high (250 - 500° C)
Heat transfer	facile	can be problematic
Product separation	problematic	facile
Catalyst recycle	difficult and expensive	simple
Reaction mechanisms	reasonable well understood	poorly understood
Fouling	problematic	Does not cause problem

1.5. Ligands in catalytic reactions

A ligand is defined as any element or combination of elements that form a chemical bond with a transition metal. Ligands can be ionic such as Cl^-, H^-, OH^-, CN^-, alkyl, aryl, etc. or neutral such as CO, alkene, 3°, 2°, 1° phosphines, arsines, phosphites, H_2O or amines.[2]

In catalytic reactions ligands that take actively part in a catalytic cycle and end up in the product(s) of the cycle are called participating ligands. Examples are alkenes, alkyl, carbonyl and hydride. Equally important are non-

16 http://en.wikipedia.org/wiki/Fouling, accessed on the 22/12/2009.

17 A. Cybulski, J. A. Moulijn, M. M. Sharma and R. A. Sheldon, *Fine Chemicals Manufacture: technology and engineering*, 2001, 112.

In an attempt to improved our fundamental understanding of the role different phosphine ligands play in modified cobalt-catalyzed hydroformylation the following study was undertaken:

The electronic and steric properties of Phoban derived ligands, Phoban-Q (Q = CH_2CH_3 (C_2), $(CH_2)_4CH_3$ (C_5), $(CH_2)_9CH_3$ (C_{10}), $(CH_2)_{19}CH_3$ (C_{20}), $(CH_2)_3N(CH_3)_2$ (C_3NMe_2), C_6H_{11} (Cy) and C_6H_5 (Ph), were systematically manipulated by altering the side chain on the phosphorus atom. The effects of the electronic and steric properties of the Phoban derived ligands were determined in cobalt-catalyzed hydroformylation of linear internal decene.

A list of other bicyclic ligands: a mixture of 4S, 8S- and 4R, 8S isomers of Lim-C_5 and Lim-Cp, [3.3.1] and [3.2.2] isomers of VCH-^{i}Bu and VCH-C_5, PA-C_5 and Phoban-C_5, added for comparison, were selected based on differences in their electronic and steric properties. The bicyclic ligands were compared in terms of their electronic, steric properties to conventional ligands such as P^nBu_3, P^tBu_3, P^iBu_3, PCy_3, PCp_3, $P(p\text{-}C_6H_4OCH_3)_3$, PPh_3 and $P(2\text{-furyl})_3$. Their effects on the rates and product distributions in cobalt-catalyzed hydroformylation of 1-octene were also evaluated.

To gain further information on some of the ligands used in the hydroformylation studies, their effect on the MeI oxidative addition reaction was investigated in a model [Rh(acac)(CO)(L) (L = Phoban[3.3.1]-Ph, Phoban[4.2.1]-Ph, a mixture of 4R, 8S- and 4S, 8S-Lim-Ph, a mixture of VCH[3.3.1]-Ph and VCH[3.2.2]-Ph and PA-Ph) system. This system involves the formation of metal alkyl and acyl complexes, present in the hydroformylation catalytic cycle, which can be studied at ambient temperature and pressure.

Solid-state properties as well as solution behaviours were investigated and proper characterisation of all ligands, complexes and products were done.

2 Homogeneous carbonylation chemistry

2.1. Introduction

The oil crisis of 1973 emphasized the vulnerability of chemical industries based on a single raw material such as crude petroleum. Since then there has been a scramble for alternative sources of energy and raw materials some of which include coal, oil shale, tar sands, biomass and natural gas. In this context synthesis gas (syngas), which is a mixture of carbon monoxide and hydrogen has assumed great importance specifically because it can be produced from any carbon source, from methane to manure and from fossil fuels to farm wastes.[1]

Chemicals derived from synthesis gas (syngas) or syngas based feedstocks are of considerable interest to the chemical industry.[2] Today, syngas is commonly produced directly from the methane component in natural gas rather than from coal. Methane reacts with steam on a nickel catalyst to produce syngas at temperatures of about 850 °C and moderate pressure of about 10 to 20 bar. The reaction is endothermic and is commonly known as steam-methane reforming (SMR). Methane can also exothermically undergo partial oxidation with molecular oxygen to produce syngas. The heat given off during this process can be used in situ to drive the steam-methane reforming reaction. When the two processes are combined, it is known as autothermal reforming. Chemicals such as dimethyl ether (DME) can be derived from synthesis gas either *via* direct or indirect routes. In the direct route, DME can be produce in one-step directly from syngas and the process is at the

1 P. D. Sunavala and B. Raghunath, *J. Sci. and Ind. Res.*, 1986, **45**, 327.

2 H. Bahrmann and B Cornils, in J. Falbe (Ed) *New Synthesis with Carbon monoxide*, Springer Verlag, New York, 1980, 226.

- The well-known Fischer-Tropsch reaction that involves the hydrogenation of CO to paraffins, alkenes and heteroatoms such as oxygen and nitrogen containing products such as methanol.[2]

Selected indirect routes involve the use of the following intermediates: olefins, methanol, methyl formate formaldehyde. These intermediates undergo consecutive reactions and can yield a variety of desired products. For instance, acetic acid can be synthesized directly from syngas but due to selectivity problems, the carbonylation of methanol is by far the better process.[7] Although oxidation and biologically (i.e. wood distillation and fermentation) based routes still contribute significantly to the quantities of acetic acid produced worldwide, the carbonylation of methanol has become generally accepted as the method of choice for large scale production.[8]

The first major commercial process for the production of synthetic acetic acid was based on the oxidation of acetaldehyde. Significant cost advantages resulted from the use of carbon monoxide (derived from natural gas) and of low cost methanol (derived from syngas) as feedstocks.[9]

Other indirect routes through which chemicals can be derived from these intermediates include:

- Methanol can be used in the manufacturing of formaldehyde industrially by catalytic oxidation using silver metal or a mixture of iron molybdenum or vanadium oxides. In this process, commonly known as the FORMOX process, methanol and oxygen react at about 250 – 400

---

7 W. Keim, *J. Organomet. Chem.*, 1989, **372**, 15.

8 J. R. Zoeller, *Eastman Chemical Company*, Kingsport, Tennessee, 1993, **49**, 35.

9 C. M. Thomas and S. Fink, *Coord. Chem. Rev.*, 2003, **243**, 125 and references there in.

- Hydroformylation is a hydrocarbonylation process that involves the addition of both carbon monoxide and hydrogen to unsaturated organic compounds such as alkenes. The reaction requires metal catalysts mostly cobalt[12, 13] or rhodium[14] that binds the CO, H_2, alkene allowing these substrates to combine within its coordination sphere. The reaction with the cobalt metal resulted in alcohols directly while the reaction with rhodium resulted in aldehydes which could latter be converted to the corresponding alcohol by hydrogenation.

- Another potential indirect route is the hydrocarbonylation of methanol with hydrogen and carbon monoxide to ethanol in the presence of a water soluble cobalt catalyst at high temperatures and pressures.[15]

- A new process for acetic acid directly from the oxidation of ethylene has been established and commercialized. The catalyst system consist of Pd and heteropoly acid and exhibit excellent activity and selectivity. Adding Se and Te to the catalyst system helps to suppress the formation of carbon dioxide hence the process is environmentally friendly.[16]

2.2. Carbonylation reactions and applications

Carbonylation reaction in general is a broad and valuable field of homogeneous catalysed reactions, which utilises carbon monoxide as a reactant. It refers to reactions that introduce carbon monoxide alone or

---

12 O. Roelen, *Angew. Chem.*, 1948, **60**, 62.

13 C. Crause, L. Bennie, L. Damoense, C. L. Dwyer, C. Grove, N. Grimmer, W. Janse van Rensburg, M. M. Kirk, K. M. Mokheseng, S. Otto and P. J. Steynberg, *Dalton Trans.*, 2003, 2036.

14 P. W. N. M. van Leeuwen, *Homogeneous catalysis, Understanding the art*, 2004, and references there in.

15 B. G. Gane and D. G. Stewart, *US. Patent*, 1982, 4319056.

16 K. Sano, H. Uchida and S. Wakabayashi, *Catalysis surveys from Japan*, 1999, **3**, 55.

$$RCH_2OH + CO + H_2O \rightarrow RCH_2COOH \qquad 2.4$$

If alcohol replaces water, the process is called hydroesterification. The Reppe reactions thus represent routes for the manufacturing of unsaturated and saturated acids, anhydrides, amides etc. from a wide variety of feedstocks. Acrylic acid in Eqn. 2.2 is an important feedstock for various types of polymer materials that have excellent weather and UV resistant abilities, hence are used in making water resistant and heat resistant materials. It is also used in coating, adhesive, chemical fibres, paper, printing and dyeing.[20, 21] The world production of crude acrylic acid is given in Table 2.1.

Table 2.1: Capacity of world production of crude acrylic acid in tons per year.[23]

Producer	**Capacity, tons per year**
BASF, Freeport, Tex.	242500
American Acryl, Pasadena, Tex	132500
Celanese, Clear Lake, Tex	320000
Dow Chemicals, Taft, La	120000
Rohm and Hans/StoHaas, Deer Park, Tex	632500

The attractive feature of using carbon monoxide as a raw material for the manufacture of chemicals is the fact that it can be made readily from any available carbon source.[1, 8] The carbonylation of methanol is currently the preferred route for the industrial manufacture of acetic acid and account for about 60% of the world acetic acid production.[38] Important industrial applications of this type of chemistry are the BASF, Monsanto and Cativa processes which uses cobalt, rhodium and iridium metals respectively to convert methanol to acetic acid.

---

23 http://www.the-innovation-group.com/ChemProfiles/Acrylic%20Acid.htm, accessed on 12/12/2009.

BASF described the first carbonylation of methanol using cobalt catalyst at high temperature and pressure in 1913. Due to the extreme conditions as well as corrosion problems, commercialization was not successful.[29, 30]

Reppe extensively studied carbonylation with homogeneous nickel catalysts in the thirties and forties and the results of the findings were not published until 1953. Based on the outcome, an acetic acid manufacturing process was commercialized in 1955.[31]

In 1941, Reppe demonstrated the potential of many metal carbonyls in several reactions, including hydroformylation. This work resulted in the hydroformylation process that was commercialized in 1960 by BASF.[7] It uses a CoI_2 catalyst and required very high pressure (600 bar) as well as high temperatures (230 °C) and the selectivity for acetic acid was ~90%. Corrosion problems were overcome by applying Hastelloy C in constructing the reactor vessel.[30] The selectivity and stability of the catalyst system can be enhanced by addition of suitable ligands such as phosphines.

2.2.1.1. Reaction mechanism of cobalt-catalysed carbonylation

The active species in the cobalt-catalysed carbonylation of methanol to acetic acid are generally considered as either the tetracarbonylcobalt anion or the hydride. In the BASF process, the tetracarbonyl cobalt anion, $[Co(CO)_4]^-$, is produced from cobalt iodide according to Eqns. 2.6 and 2.7[32]:

$$2CoI_2 + 2H_2O + 10CO \rightleftharpoons [Co_2(CO)_8] + 4HI + 2CO_2 \qquad 2.6$$

29 E. E. Donath, *History of Catalysis in Coal Liquefaction*, in J. R. Anderson and M. Boudart (Editors), *Catalysis, Science and Technology*, Springer Verlag, Berlin, 1982, **3**, 1.

30 A. J. B. Robertson, *The Early History of Catalysis*, *Platinum Metals Rev.*, 1975, **19(2)**, 64.

31 R. A. Santen, P. W. N. M. van Leeuwen, J. A. Moulijn and B. A. Averill, *Catalysis: An Integrated Approach*, 1999, 15.

32 N. von Kutepow, W. Himmele and H. Hohenshutz, *Chem. Ing. Techn.*, 1965, **37**, 297.

In the promoted system as shown in Figure 2.1, iodide compounds (organic and inorganic) were added to the methanol carbonylation process and have been found to increase the reaction rate.

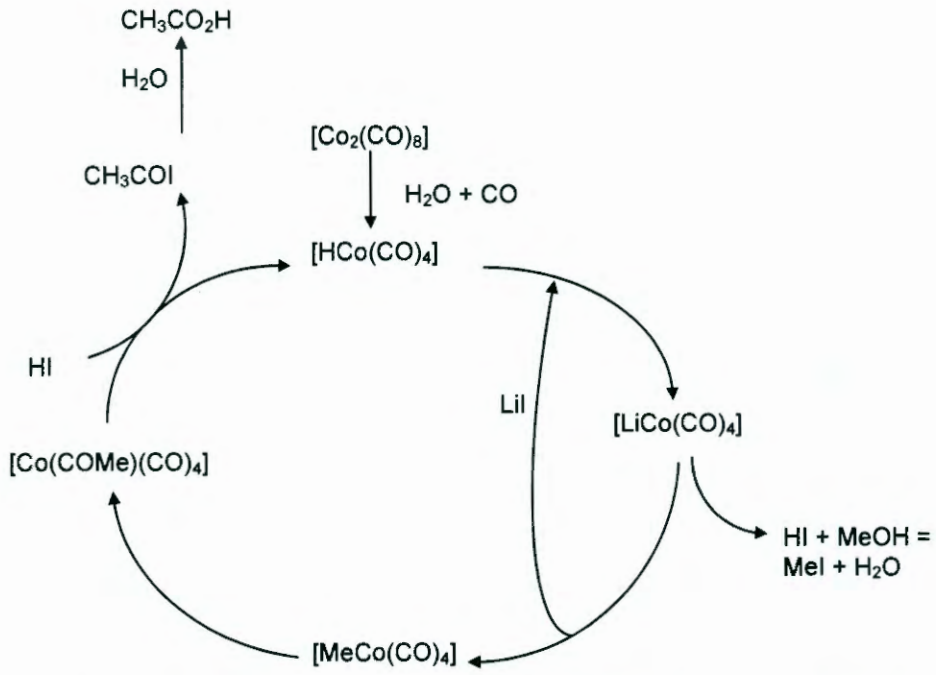

Figure 2.1: Catalytic cycle of the cobalt-catalysed methanol carbonylation process as used by BASF for the production of acetic acid in the presence of an iodide promoter.

The nature of the iodide promoter was also studied and it was found that the covalent iodide, CH_3I, was more active than ionic iodides such as LiI, KI, and $MePBu_3I$. However, a surprising synergistic effect was found when using a mixture of both covalent and ionic iodides.[35] Originally, it was proposed that the function of the ionic iodide was to produce methyl iodide which then reacts with the nucleophilic anion $[Co(CO)_4]^-$ followed by the elimination of the iodide anion to give the alkyl-cobalt species.[24, 36] In the presence of iodide promoters, methyl iodide is the likely intermediate since it reacts much faster than methanol in carbonylation/hydrocarbonylation reactions. The probable

35 J. Gauthier-Lafaye, R. Perro and Y. Colleuille, *J. Mol. Catal.*, 1982, **17**, 339.

36 Y. Sugi, K. Takeuchi, H. Arakawa, T. Matsuzaki and K. Bando, *C1 Mol. Chem.*, 1986, **1**, 423.

conditions the catalytic species, *cis*-$[Rh(CO)_2I_2]^-$, was generated and identified with high-pressure IR spectroscopy.[42]

Protic solvents such as methanol accelerated the oxidation addition step as compared to aprotic solvents. The addition of iodide salts such as LiI or Bu_4NI lead to an enhanced reaction rate and was attributed to the formation of a highly nucleophilic dianionic species, $[Rh(CO)_2I_3]^{2-}$.[43]

2.2.2.1. Reaction mechanism of the Monsanto process

The catalytic cycle for the Monsanto MeOH carbonylation process for the production of acetic acid is given in Figure 2.2.

High-pressure IR spectroscopy showed (**i**) to be the most prevalent complex in solution. One of the key elements of the catalytic cycle was the ability of a Rh(I) complex to undergo facile oxidative addition with a methyl halide (especially iodide).[34] During a typical oxidative addition reaction, a molecule X-Y adds to a transition metal in such a way that the metal becomes bonded to both X and Y. This is accompanied by an increase in the formal oxidation state of the metal by 2.[44] In some other cases, the addition of X-Y to the metal centre may be accompanied by elimination of a ligand, such as a molecule of carbon monoxide for instance.[45]

---

42 A. Hayes, J. Mcnish and J. M. Pearson, *J. Organomet. Chem.*, 1998, **551**, 339.

43 A. Fulford, C. E. Hickey and P. M Maitlis, *J. Organomet. Chem.*, 1990, **398**, 311.

44 A. J. Hart-Davis and W. A. G. Graham, *Inorg. Chem.*, 1970, **9(12)**, 2658.

45 (a) R. B. King, *Inorg. Chem.*, 1966, **5**, 82; (b) R. Kummer and W. A. G. Graham, *Inorg. Chem.*, 1968, **7**, 1208.

with CO to regenerate the 18 electron species $[Rh(CH_3CO)(CO)_2I_3]^-$ (**iv**), see Figure 2.2. The 18-electron species subsequently undergoes reductive elimination to give acetyl iodide and regenerates the rhodium(I) anion again. The final reaction of acetyl iodide with compounds containing hydroxyl groups such as water, methanol or acetic acid leads to the formation of hydrogen iodide and the corresponding acetyl derivatives.

The overall rate of the carbonylation reaction showed a first-order dependence on the concentrations of both rhodium and MeI. Hence, the oxidative addition step was proposed to be the rate-determining step of the overall catalytic reaction. The oxidative addition reaction was believe to occur via S_N2 nucleophilic attack of the rhodium(I) complex on the carbon of MeI followed by iodide coordination to Rh(III) to give the *trans*-Rh(I) alkyl species complex.[47] This implies that by changing the electronic property of the metal centre one could influence the nature and rate of the oxidative addition reaction.[48] Consequently, more nucleophilic ligands attached to the Rh should speed up the rate of the reaction.

2.2.2.2. Water gas shift in the Monsanto process

Although rhodium-catalysed carbonylation of methanol is highly selective and efficient, it suffers from some disadvantageous side reaction such as the water gas shift reaction. The water gas shift reaction catalysed by rhodium occurs via the competing oxidative addition of HI on $[Rh(CO)_2I_2]^-$ according to Figure 2.3.

---

47 D. Forster, *J. Am. Chem. Soc.*, 1976, **98**, 846.

48 J. G. Leipoldt, E. C. Steynberg and R. Van Eldik, *Inorg. Chem.*, 1987, **26**, 3068.

complex occurs and is also a precursor for the formation of insoluble RhI_3. This would eventually precipitate out of the reaction mixture resulting in a major catalyst loss. One of the key features of the original Monsanto process is that the conditions in the reactor must be maintained within certain limits to prevent catalyst precipitation. The reactor composition is maintained within limits on water, methyl acetate, methyl iodide and rhodium concentrations.[38] This problem could be dealt with by adding ionic iodides especially lithium iodide along with methyl iodide to stabilized the rhodium catalyst, prevent the water gas shift reaction and the formation of $[RhI_4CO]^-$. This reduces catalyst precipitation of the reaction mixture resulting in enhanced reaction rates.[51] Catalyst precipitation can also be prevented by maintaining a minimum CO partial pressure and high water concentration. This condition decrease productivity and increase operating costs since the distillation section of the plant has to remove a considerable amount of water from the acetic acid product.[38] Propionic acid is also a major by-product generated from the carbonylation of ethanol derived from the reduced acetaldehyde present in the methanol feed as high boiling impurities.[52]

2.2.3. Iridium-based carbonylation process

Due to the limitations of the rhodium catalysed process and the very high price difference between rhodium ($167 per gram) and iridium ($10 per gram) which existed in 1990, research into the use of iridium (the Cativa process) as a catalyst for methanol carbonylation was pursued.[52] Two such plants have been constructed; the sterling plant in Texas City, USA and the Samsung plant in the Republic of Korea in 1996 and 1997 respectively.[38] In Kertih, Malaysia, another iridium base plant, BP Petronas, started operations in 2000 with an output of 500000 tonnes per annum.[53, 52]

---

51 B. L. Smith, P. G. Torrence, A. Aguilo´and J. S. Aider, *US. Patent*, 1991, 5001259.

52 J. H. Jones, *Platinum Metals Rev.*, 2000, **44**, 94.

53 http://www.catalysis-ed.org.uk/ethacid/ethacid10.htm, accessed on 12/12/2009.

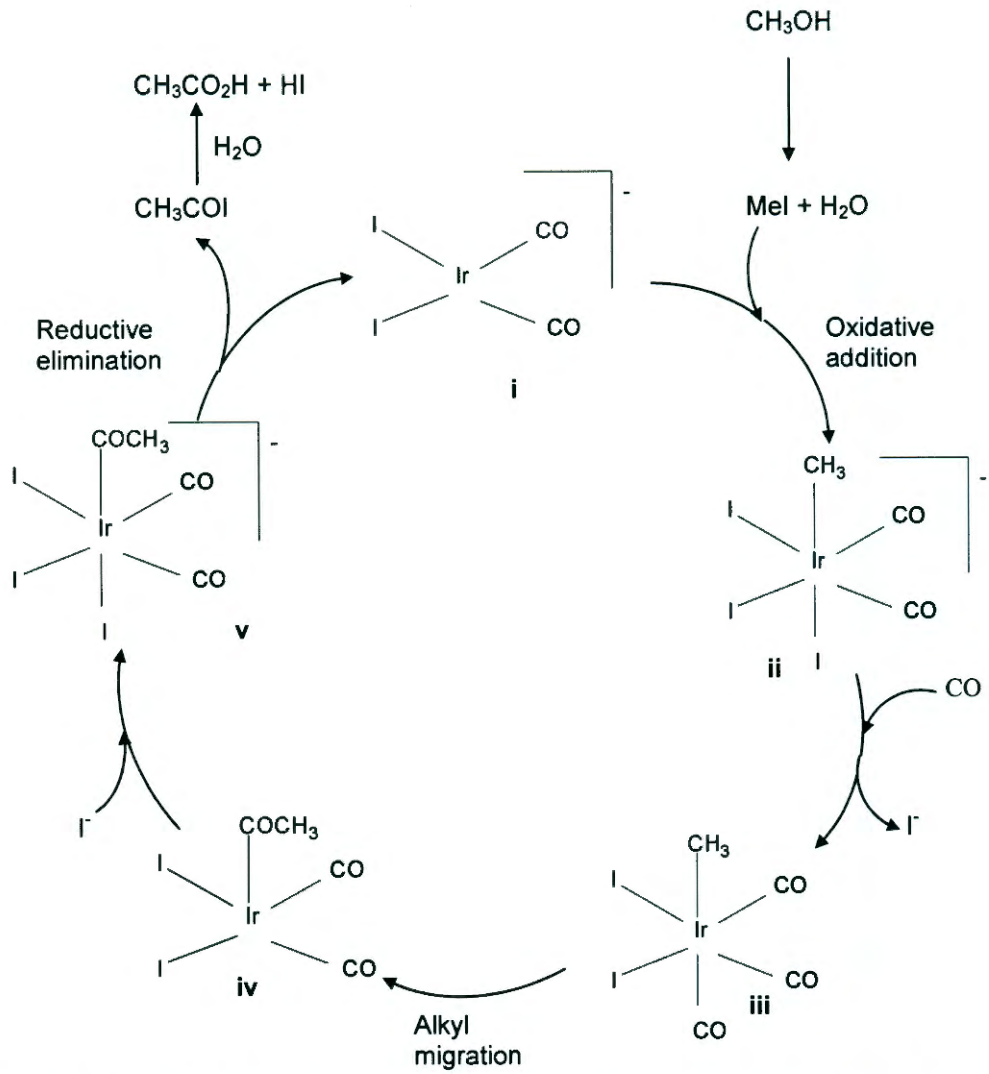

Figure 2.4: Catalytic cycle of the iridium-catalysed methanol carbonylation (Cativa) process for the production of acetic acid.[52]

The catalytically active species is the anion, *cis*-$[Ir(CO)_2I_2]^-$ (**i**) which undergoes oxidative addition with MeI to form the hexacoordinated anion (**ii**). Model studies have shown that the oxidative addition of methyl iodide to the metal centre was about 150 times faster than the equivalent reaction with rhodium.[55] The anion (**ii**) rapidly undergoes elimination of iodide anion and coordination of CO ligand to give a neutral species (**iii**). The rate law given in Eqn. 2.11.[54]

---

55 P. M. Maitlis, A. Haynes, G. J. Sunley and M. J. Howard, *J. Chem. Soc., Dalton Trans.*, 1996, 2187.

neutral species, the migration was about 800 times faster accounting for the relatively high reactivity observed.[56]

2.2.4. Evaluation of the three carbonylation processes

Regardless of the current low price of cobalt metal ($0.04 per gram) the low product selectivity as well as the high pressure and temperature required for the methanol carbonylation process would result in higher capital cost involve in constructing such a plant and eventual low profitability. Consequently, rhodium and iridium based processes, due to their milder reaction conditions and high product selectivity of about 99%, are considered the method of choice for making acetic acid from methanol.

The Cativa and Monsanto processes are sufficiently similar that they can used the same chemical plant. The initial studies have shown iridium to be less active than rhodium for the carbonylation of methanol. Subsequent research showed that the iridium catalyst could be promoted by ruthenium and this combination leads to a catalyst that is superior to the rhodium-based process.

Unlike the large price differences, $167 and $10 per gram, between the rhodium and iridium metals respectively in 1990 that favoured the iridium process, the current prices of these precious metals given as rhodium ($58 per gram) and iridium ($15 per gram)[37] as well as the 3 equivalents of ruthenium ($3 per gram) required in the Cativa process favours the rhodium process.[38]

High water concentrations in excess of 10% is required in the Monsanto process to prevent catalyst precipitation but result in low productivity, increase high boiling by-products and increase operating costs since the distillation section of the plant has to remove a considerable amount of water from the acetic acid product.[38] Since 1980, Celanese has achieved great

---

56 A. P. Wright, *Abstacts of Paper, 222nd ACS National Meeting*, Chicago, IL, U.S., 2001, 26.

into the origin of oxygenated products occurring in cobalt catalysed Fischer-Tropsch (FT) reactions.[59] In his investigation, he passed a mixture of ethylene and synthesis gas over a fixed-bed cobalt containing catalyst at 150 °C and 100 bar. The first hydroformylation catalyst was a solid mixture containing (66% silica, 30% cobalt, 2% thorium oxide and 2% magnesium oxide). Only later was the conclusion reached that the actual catalytic species was homogeneous.[60] This reaction was termed oxo synthesis and Adkins introduced the named hydroformylation in 1948.[61] A transition metal catalyst usually based on cobalt[12, 13] or rhodium[14], homogeneously catalyses this reaction and all atoms of the starting materials are incorporated into the products.[62] Many other carbonyl-forming metals have been claimed to be active in the oxo reaction and include Mn, Re, Cr, Cu, Mo, Pt, Ir, and Ni.[63, 64, 65] Cobalt or rhodium among the transition metals were the most active metals.[66] Rhodium based catalysts are about 10^4 times more active than cobalt. The reaction is exothermic[67] with a heat of reaction for propylene of 125 kJ mol^{-1} and 115 – 145 kJ mol^{-1} for other olefins depending on the olefin structure and molecular weight. During the hydroformylation process, isomeric mixtures of straight and branched-chain aldehydes, depending on the extent of anti-Markovnikov vs Markovnikov additions, are produced. The ratio of linear (n) to branched (iso) aldehydes, which is commonly referred to as the n/iso ratio, is one of the most important features of the process. Generally, the maximum selectivities to straight-chain products are preferred due to the high economic value associated with it. Undesirable competing

---

59 O. Roelen, *Ger. Patent*, 1938, 949548.

60 I. Wender, M. Orchin and H. Storch, *J. Am., Chem. Soc.*, 1950, **72**, 4842.

61 H. Adkins and G. Krsek, *J. Am. Chem. Soc.*, 1948, **70**, 383.

62 B. Breit and W. Seiche; Recent advances on Chemo, Regio and stereoselective hydroformylation, *Rev. Synth.*, 2001, **1**, 36.

63 E. V. Gusevskaya, E. N. dos Santos, R. Augusti, A. de O. Dias and C. M. Foca, *J. Mol. Catal. A: Chem.*, 2000, **152**, 15.

64 T. A. Ayers and T. V. Rajanbabu, *US. Patent*, 1995, 5475146.

65 C. Tang, Y. Zeng, P. Cao, X. Yang and G. Wang, *Catal. Lett.*, 2009, **129(1)**, 189.

66 J. Falbe, *New synthesis with carbon monoxide*, 1980, 38.

67 R. Whyman, *Appl. Organomet. Chem. and Catal.*, ed, 2001.

rhodium catalyst which can be applied as $[Rh_6(CO)_{16}]$ or made in situ from a variety of starting materials have been reported. It was found to be more active than $[Co_2(CO)_8]$ by several orders of magnitude under comparable reaction conditions.[70] Some of these rhodium catalysts are uniquely thermally stable hence favours catalyst recycling.[71, 72] Despite the advantages of rhodium over cobalt in the hydroformylation process, rhodium metal ($58 per gram) is currently significantly more expensive than cobalt ($0.70 per gram). In addition, the rhodium catalyst will easily be poisoned by feed impurities while the cobalt catalyst system is more robust.[73] The first commercial plant of the low-pressure oxo process was lunched by Hoecst Celanese Corporation in 1974 followed by Union Carbide Corporation (UCC) in 1976.[74] Other commercial rhodium based hydroformylation processes include the BASF and Mitsubishi technologies, which are parallel to the UCC process.[75] Sasol announced the commercialisation of a rhodium catalysed low-pressure hydroformylation process licensed from Kvaerner (previously Davy McKee) for the conversion of it's Fischer Tropsch C_{11}/C_{12} olefin fraction of the Synthol product stream to detergent range alcohols on a 120 kt per year scale in 2001.[75, 76, 77] The Ruhrchemie/Rhone-Poulenc process uses a two-phase system in the hydroformylation of propene on a commercial scale in the presence of TPPTS as a ligand in a stirred tank reactor. In this system, the catalyst and products are in two different immiscible phases. The main advantage of this system is that the product and the catalyst can be separated

---

70 B. Heil and L. Marko, *Chem. Ber.*, 1969, **102**, 2238.

71 J. H. Craddock, A. Hershman, F. E. Paulik and J. F. Roth, *Ind. Eng. Chem. Prod. Res. Dev.*, 1969, **8**, 291.

72 A. Hershman, K. K. Robinson, J. H. Craddock and J. F. Roth, *Ind. Eng. Chem. Prod. Res. Dev.*, 1969, **8**, 372.

73 C. Dwyer, H. Assumption, J. Coetzee, C. Crause, L. Damoense and M. Kirk, *Coord. Chem. Rev.*, 2004, **248**, 653.

74 Anon, *Celanese Corp.* Annual Report; 1974, 9.

75 a) http://edu.chem.tue.nl/6KM00/New%20Hydroformylation%20Techniques.pdf, accessed on the 11/12/2009; b) *Chem. Eng. News*, 1999, 20; c) http://www.sasoltechdata.com/tds/SAFOL23.pdf accessed on the 12/12/2009.

76 I. P. Greager and J. C. Crause, *US Patent*, 2009, 0203804.

77 B. M. Justin, D. M. Eberhard, G. Arie and R. G. J. Hendricus, *US Patent*, 2004, 67566411.

of the double bond.[82, 83] The reactivities of the olefins decrease in the series 1-alkenes > substituted 1-alkenes >> internal alkenes.

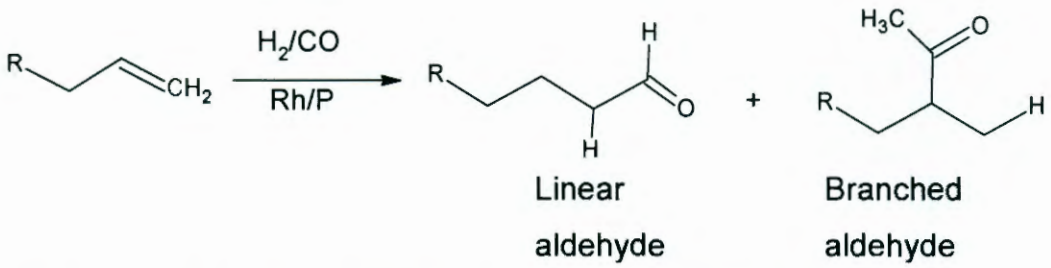

Figure 2.5: Modified hydroformylation catalysed by rhodium.

The key to the successful progress of homogeneous hydroformylation has been the exploitation of the effect that the electronic and steric properties of the ligand exert on the metal centre in the complex. By tuning the electronic and steric properties of a catalytically active metal site, one can alter selectivities and rates significantly.[14, 84] A comparative study of 1-dodecene with rhodium using triphenyl phosphine, triphenylarsine, triphenylantimony and triphenylbismuth as ligands proved the superiority of triphenylphosphine over the other group V ligands.[85] This work was later confirmed using three different metals, rhodium, cobalt and ruthenium.[86]

Steric effects are very important in the phosphine- and phosphite-modified rhodium hydroformylation of olefins. The reaction rate decreases with an increase in steric bulk of the ligand and the substrate with a corresponding

---

82 J. H. Craddock, A. Hershman, F. E. Paulik and J. F. Roth, *Ind. Eng. Chem. Prod. Res. Dev.*, 1969, **8**, 291.

83 A. Hershman, K. K. Robinson, J. H. Craddock and J. F. Roth, *Ind. Eng. Chem. Prod. Res. Dev.*, 1969, **8**, 372.

84 C. D. Frohning and C. W. Kohlpainter, in B. Cornils, W. A. Hermann (Eds), *Applied Homogeneous Catalysis with Organometallic Compounds*, Wiley-VCH, Weinheim, 2000, **1**, 29.

85 J. T. Carlock, *Tetrahedron*, 1984, **40**, 185.

86 V. K. Srivastava, R. S. Shukla, H. C. Baksh and R. V. Jasra, *Appl. Catal. A: Gen.*, 2005, **282**, 31.

observed.[92] Previous studies with this catalyst system mainly reported the initial rate data at ambient conditions. It was also reported that the rate of the reaction was first-order with respect to H_2, olefin, catalyst and negative order with respect to CO.[90, 91, 93] The rate expression for the hydroformylation of propene at typical reaction conditions was reported as in Eqn. 2.12 but with a zero order with respect to hydrogen.[94]

$$\text{Rate} = k[C_3H_6]^{0.6}[PPh_3]^{-0.7}[CO]^{-0.1}[Rh]^{1}[H_2]^{0} \qquad 2.12$$

Bulky substituted triphenylphosphites have been shown to be better ligands compared to PPh_3 in the hydroformylation of 1-octene in terms of activity and product selectivity.[95] Unfortunately, they could easily hydrolyze and would react with the aldehydes produced during the hydroformylation process.[96] Adamantane cage (PA-Ph) bulky ligands have also been shown to be good ligands for rhodium-catalysed hydroformylation of linear terminal and branch olefins. They are inert to decomposition and stereoelectronically similar to bulky phosphonites.[97] Phosphonites have been reported to result in highly active rhodium-catalysed hydroformylation.[97]

Diphosphines are a class of chelating ligands that contain two phosphine groups connected to each other by a bridge, referred to as the backbone. The backbone may consist of one or more methylene groups or multiple aromatic rings with heteroatoms attached. The structure of the backbone and

---

93 J. Hjortkjaer, *J. Mol. Catal.*, 1979, **5**, 377.

94 (a) P. Cavalieri, L. Raimondo, G. Pagani, G. Montrasi, G. Gregorio and A. Andreetta, *Chim. Ind. (Milan)*, 1980, **62**, 572; (b) G. Gregorio, G. Montrasi, M. Tampieri, P. Cavalieri, G. Pagani and A. Andreetta, *Chim. Ind. (Milan)*, 1980, **62**, 389.

95 A. van Rooy, E. N. Orij, P. C. J. Kamer and P. W. N. M. van Leeuwen, *Organometallics*, 1995, **14**, 34.

96 P. W. N. M. van Leeuwen and C. Claver, *Rhodium Catalysed Hydroformylation*, Ed. Kluwer Academic Publishers, Dordrecht, 2000.

97 R. A. Baber, M. L. Clarke, K. M. Heslop, A. C. Marr, A. G. Orpen, P. G. Pringle, A. Ward and D. E. Zambrano-Williams, *Dalton Trans.*, 2005, 1079 and references there in.

Examination of the molecular model indicates that the bite angles of BISBI and the derivatives of Xantphos were much greater than 90°, the most common bite angles for bidentate ligands such as DPPE and DPPP. The bite angle is a geometric parameter used to classify chelating ligands in inorganic and organometallic chemistry. The relationship between selectivity and bite angle for different diphosphines ligands were studied and a good correlation between the bite angle of the diphosphines and the regioselectivity were obtained.[99] Together with the Tolman cone angle, this parameter is relevant to diphosphine ligands which are used in industrial processes such as hydroformylation, hydrocyanation and hydrogenation.[100] Hydroformylation of linear olefins have shown that ligands with wider bite angles have a significant effect on the l:b ratio of the products. While, DPPE and DPPP gave l:b ratio ranges from 1 to 5 during the hydroformylation of linear olefins under standard condition, bidentate ligands BISBI, Xantphos, Thixantphos, Nixantphos and Benzylnixantphos gave l:b ratios of 25, 52.2, 50, 50.6 and 69.4 respectively.[14]

Some bidentate ligands such as 2, 5-dppm-nor as shown in Figure 2.7, with a natural bite angle of 126°, gave an unexpectedly low l:b ratio of 2.6.

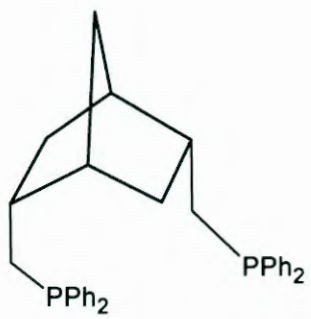

2, 5-dppm-nor (126°)

Figure 2.7: Bidentate ligand with wide natural bite angle.

---

99 C. P. Casey, G. T. Whiteker, M. G. Melville, L. M. Petrovich, J. A. Jr. Gavney and D. R. Powell, *J. Am. Chem. Soc.*, 1992, **114**, 5535.

100 http://en.wikipedia.org/wiki/Bite_angle, accessed on the 12/12/2009.

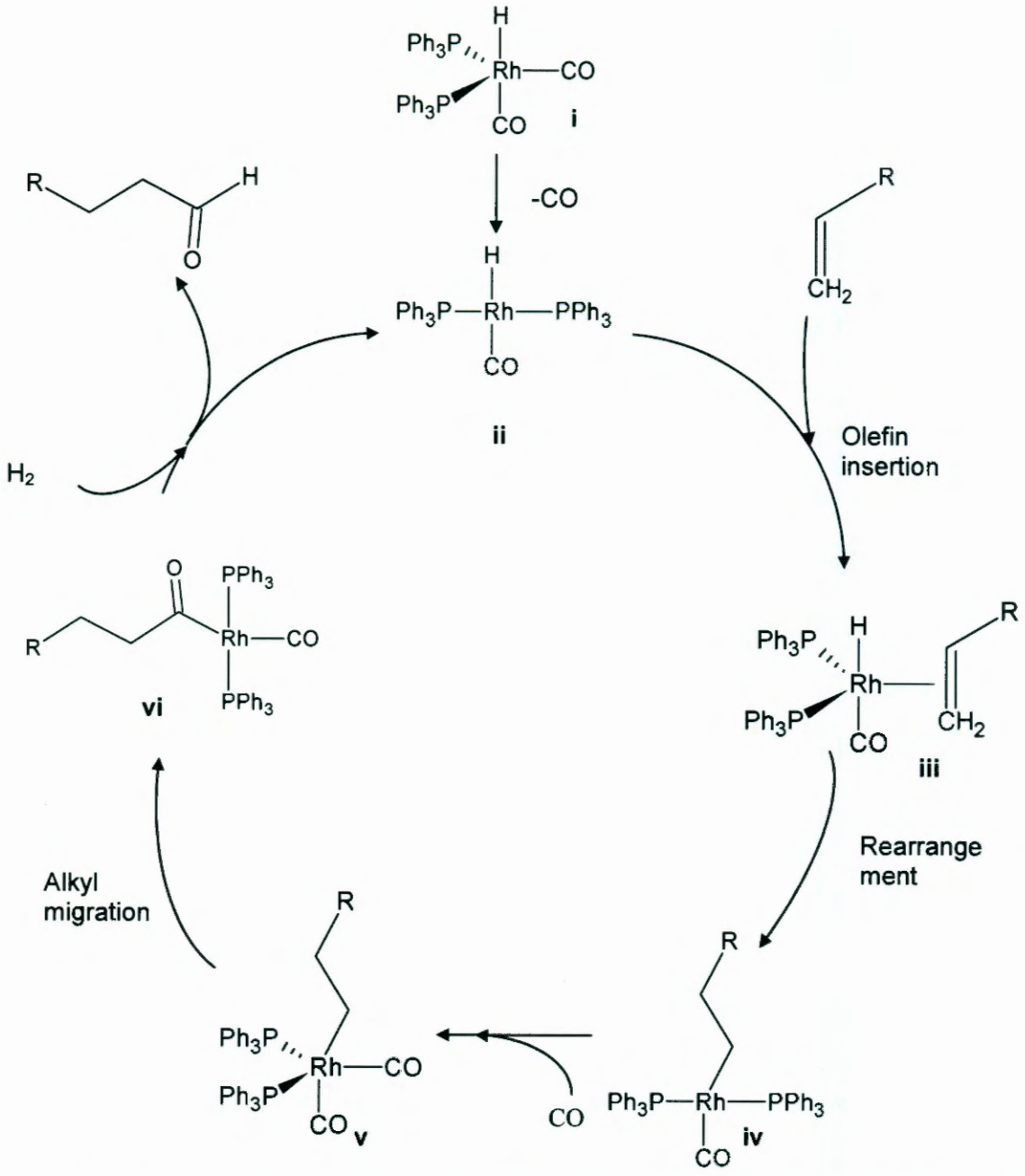

Figure 2.8: Proposed catalytic cycle for modified rhodium catalysed hydroformylation.

Complex (**v**) undergo migratory CO-insertion to form the acyl complex (**vi**) which can either react with CO to give the saturated trigonal bipyramidal acyl intermediate which have been observed spectroscopically or with H_2 via oxidative addition followed by reductive elimination to give aldehyde products and the unsaturated square planar complex (**ii**).[15]

Dicobalt octacarbonyl, $[Co_2(CO)_8]$, is an orange, pyrophoric, microcrystalline solid which sublimes readily (Mp = 51 °C). It is soluble in organic solvents, thermally unstable and slowly loses CO at room temperature to give $[Co_4(CO)_{12}]$ and eventually cobalt metal.

The crystal structure of $[Co_2(CO)_8]$ in Figure 2.9 shows that, in the solid state, the molecule has two bridging carbonyl groups as in structure (i). In the liquid and gaseous states, the carbonyl-bridged structures coexist in equilibrium with the isomeric non-bridging forms, structures (ii) and (iii).[108]

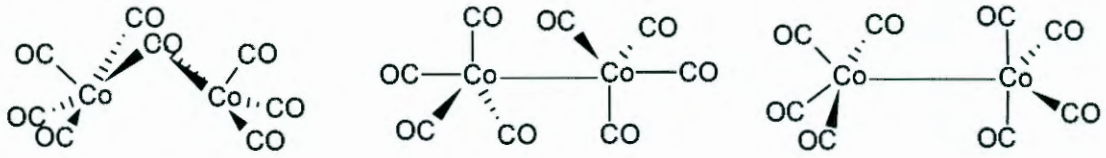

Figure 2.9: Isomeric structures of $[Co_2(CO)_8]$.

A mixture of butene and butane has been hydroformylated with the use of cobalt of fatty acid such as $Co(COOR)_2$ (where R = derivative of naphthalene or 2-ethylhexanoic acid) as a catalytic precursor forming pentaldehyde and pentanol.[109] In the presence of molecular hydrogen at high temperatures and pressures, the dicobalt octacarbonyl is converted to the true catalyst, $[HCo(CO)_4]$ as shown in Eqn. 2.13.[105]

$$[Co_2(CO)_8] + H_2 \rightarrow 2[HCo(CO)_4] \qquad 2.13$$

$[HCo(CO)_4]$ is a gas at ambient conditions with an estimated boiling point considerably below room temperature. It is very toxic, has an unpleasant odour and great caution must be exercised while working with it. In the gas phase it is quite stable, especially in the presence of CO, however on slow cooling the hydride condenses to a whitish-yellow solid. On melting the liquid

---

108 G. G. Sumner, H. P. Klug and L. E. Alexander, *Acta Crystallogr.*, 1964, **17**, 732.

109 Y. T. Vigranenko, V. M. Gavrilova, G. N. Gvozdovskii, V. A. Rybakov, G. V. Kuz'mina, V. A. Pavlova and L. A. Bogdanova, Russ. *J. Org. Chem.*, 1996, **32(12)**, 1774.

2.3.2.1. Effect of reaction parameters and reaction mechanism

Natta and co-workers made some important discoveries concerning the kinetics of the hydroformylation reaction.[112, 113] In their initial work, they showed that the rate was proportional to the concentration of the olefin and $[Co_2(CO)_8]$ but independent of the pressure of syngas (H_2:CO, 1:2) in the range of 120 to 380 bars.[114] It was later shown that during the reaction at constant CO partial pressures the rate was directly proportional to the hydrogen pressure. At constant hydrogen partial pressures the rate increases with CO partial pressures up to about 10 bars, but thereafter decreases with higher CO partial pressure. The reaction rate can therefore be expressed as in Eqn. 2.16.

$$\text{Rate} = k[\text{olefin}][\text{Co}][H_2][\text{CO}]^{-1} \qquad 2.16$$

The inverse dependence on CO partial pressure is consistent with the mechanistic requirement for CO dissociation from the initial 18-electron species to open up a coordination site for olefin or H_2 binding. When using a 1:1 ratio of H_2/CO, the reaction rate was essentially independent of pressure due to the opposing orders of H_2 and CO. Increasing the H_2/CO ratio is of limited use for increasing the overall reaction rate because $[HCo(CO)_4]$ is only stable under certain minimum CO partial pressures at a given reaction temperature. The reaction conditions for cobalt catalysed hydroformylation were largely governed by the thermal instability of $[HCo(CO)_4]$ which produces metallic cobalt if the CO partial pressure is not kept high enough. As the reaction temperature is increased, the CO partial pressure required to maintain stability of the catalytic species increases.[115, 116]

---

112 G. Natta, R. Ercoli, S. Castellano and F. H. Barbieri, *J. Am. Chem. Soc.*, 1954, **76**, 4049.

113 G. Natta, R. Ercoli and S. Castellano, *Chim. Ind. (Milan)*, 1955, **37**, 6.

114 G. Natta and R. Ercoli, *Chim. Ind.*, 1952, **34**, 503.

115 M. F. Mirbach. *J. Organomet. Chem.*, 1984, **265**, 205.

116 W. R. Moser and D. W. Slocum, *ACS*, Washington D.C., 1992, **230**, 14.

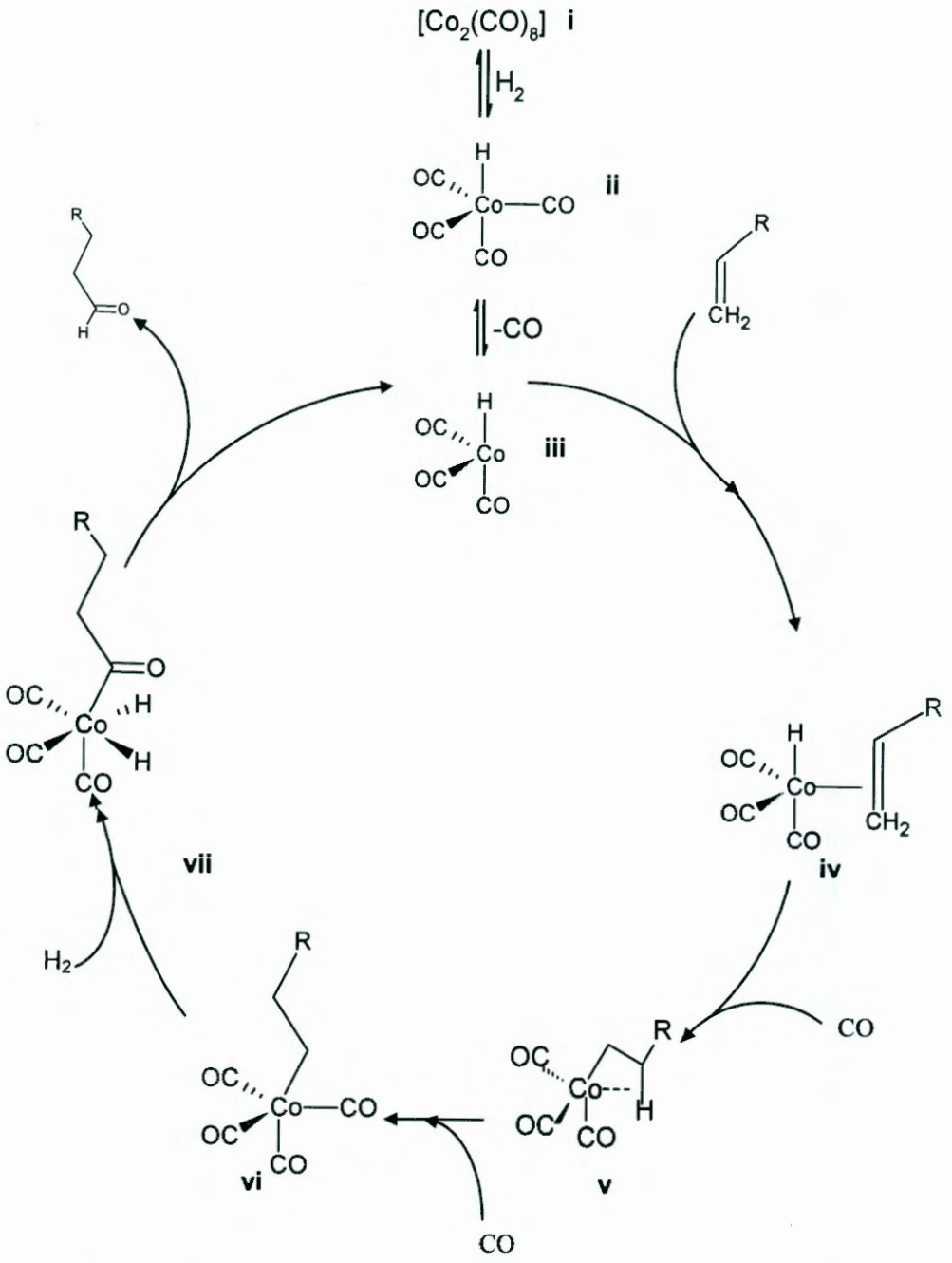

Figure 2.10: Accepted mechanism for unmodified cobalt catalysed hydroformylation of olefins.[102, 110]

Accordingly, an increase in the CO partial pressure will decrease the hydroformylation reaction rate and olefin isomerisation side reaction leading to an increase in the linear to branched product ratio. The reduced probability of direct olefin coordination with the saturated $[HCo(CO)_4]$ complex is consistent with the reduced activity at higher CO partial pressures.[115, 116]

1.2:1 was obtained. The product distribution in Figure 2.11 indicates that alkene isomerisation resulting in branched product was slow for internal olefins and fast for α-olefins.[120]

According to Keulemans et. al., the distribution of alcohols derived from 1- and 2-pentene was about the same, i.e. 1-hexanol (50 - 55%), 2-methyl-1-pentanol and 2-ethyl-1-butanol (35 - 40%).[121] It has also been reported that 1-hexanol (80%) and (70%), and 2-methyl-1-pentanol (14 -18%) and (26 - 30%) were obtain from 1-pentene and 2-pentene respectively with both olefins yielded 2-ethyl-1-butanol (2 - 4%).[122] This implies that one can start with a considerably less expensive mixture of terminal and internal alkenes and get a product distribution favouring the linear aldehyde. Labelling studies have shown that alkene isomerisation generally occurs without dissociation of the alkene from the cobalt catalyst.[123]

In the case of branched alkene starting materials, it was shown that very little hydroformylation occurs at the carbon centre containing the branch, even if it was part of the double bond.[124] Again, the terminal aldehydes were favoured as shown in Figure 2.12.

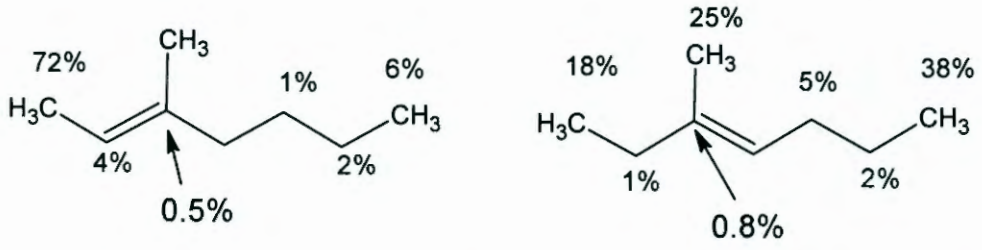

Figure 2.12: Product distribution for the hydroformylation of 3-methyl-2-heptene and 3-methyl 3-heptene respectively.

---

121 A. I. M. Keulemans, A. Kwantes and T. Van Bavel, *Rec. Irav. Chem.*, 1948, **67**, 298.

122 I.J. Goldfarb and M. Orchin, "*Advances in Catalysis*", Academic Press, Inc., New York, 1957, **9**, 609.

123 M.Bianchi, F.Parcenti, P .Freudiani and U. Matteili, *J. Organomet. Chem.*, 1977, **137**, 361.

124 B. L. Haymore, A. van Asselt and G. R. Beck, *Ann. New York Acad. Sci.*, 1984, **415**, 159.

2.3.3. Modified cobalt catalysed hydroformylation

In a patent, reported in 1966, Shell claimed that phosphines (or arsines) could replace CO as electron donating ligands on the cobalt carbonyl complex. The modified cobalt complex obtained had a significant effect on the product composition during cobalt-catalysed hydroformylation of olefins. In general, the trialkylarsine/carbonyl cobalt catalysts were somewhat less stable than the corresponding tertiary phosphine-containing complexes.[127] The replacement of a CO by a phosphine, originally P^nBu_3, the electron back-donation from cobalt to the carbonyl ligand is enhanced and strengthen the M-CO bond stabilising the catalyst at significantly lower CO partial pressures with commercial operations using < 100 bar at temperatures ranging from 160 to 220 °C.[127] Such a reaction is classified as modified cobalt hydroformylation. The modified hydroformylation catalysts were generally formed in situ by treating $[Co_2(CO)_8]$ with the phosphine ligand (ligand to cobalt mole ratio = 1:1 or 2:1), carbon monoxide and hydrogen (H_2:CO mole ratio =~2:1) at elevated temperatures and pressures. The olefin substrate was added either with the catalyst precursors or after preforming the catalyst. Cobalt salts e.g. cobalt acetate and cobalt octanoate could be used instead of $[Co_2(CO)_8]$.[66] In these cases, the cobalt salt is rapidly reduced to give the cobalt complex dimer $[Co_2(CO)_6(PR_3)_2]$ and hydride $[HCo(CO)_3PR_3]$ under syngas pressure.[73, 128] The reduction reaction is highly dependent on mass transfer and temperature effects and does not occur at temperature ≤ 150 °C as shown in HP-NMR studies.[73] However, pre-forming from $[Co_2(CO)_8]$ gave cobalt hydride complex at temperature as low as 90 °C and the catalyst solutions had a characteristic deep red colour due to the presence of the modified dimer. The reaction proceeds through a dicarbonyl bis(phosphine) salt $[Co(CO)_3P_2]^+[Co(CO)_4]^-$. These cobalt complexes are highly unstable and could decompose to metallic cobalt in the absence of CO pressure.

---

127 L. H. Slaugh and R. D. Mullineaux, *US. Patent*, 1966, 3239569.

128 L. H. Slaugh and R. D. Mullineaux; *J. Organomet.Chem.*, 1968, **13**, 469.

- The modified carbonyl hydride complex is much more stable[128, 132] and robust toward feed impurities.[73]

It has been claimed that the high selectivity of the modified catalyst towards linear products could be attributed to the larger steric demand of a tertiary phosphine as compared to CO as it would influence the orientation of the olefin during insertion into the Co-H bond.[133, 134]

Although hydroformylation is the oldest homogeneous process in use today, research groups worldwide are still actively pursuing improvements to obtain a highly selective catalyst system with low percentage hydrogenation and reasonable reaction rates. In 1969, Shell patented a new class of phosphine ligands for modified cobalt hydroformylation.[135] The ligands were described as hetero-bicyclic tertiary phosphines where the phosphorous atom is a member of a bridge linkage, but not a bridgehead atom. The smallest phosphorous containing ring should contain at least five atoms, see Figure 2.15.

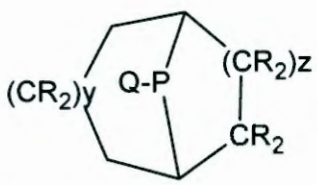

Figure 2.15: The generic phosphine structure as patented by Shell.

The integers y and z represents numbers, which sums from 2 to 3 and has a minimum value of 1 and R represents hydrogen or lower alkyl group containing 1 to 4 carbons. The third substituent, Q, may consist of only carbon and hydrogen, or contain functional groups such as carbonyl,

---

132 O. Roelen, *Angew. Chem.*, 1948, **60**, 62.

133 J. P. Collman, L. S. Hegedus, J. R. Norton and R. G. Finke, *Principles and Applications of Organometallic Metal Chemistry*, University Science Books, Mill Valley, California, 1987.

134 M. Beller, B. Cornils, C. D. Frahning and C. W. Kohlpainer, *J. Mol. Catal. A: Chem.*, 1995, **104**, 17.

135 J. L. van Winkle, S. Lorenzo, R. C. Morris and R. F. Mason, *US. Patent*, 1969, 3420898.

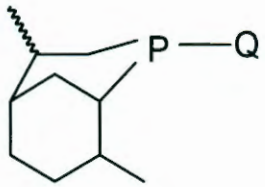

Figure 2.17: The generic Lim-Q structure as patented by Sasol.

The secondary phosphine (Lim-H) used as the precursor for making this tertiary phosphine ligands was synthesized from the addition of (R)-(+)-limonene to PH_3 in the presence of AIBN as the free radical initiator resulting in a mixture of the (4R, 8S) and (4S, 8S) isomers.[136] It was reported that hydroformylation of 1-dodecene in C9-C11 paraffin as solvent at typical reaction conditions gave product linearities ranging from 54 to 71 % with Lim-$(CH_2)_3CN$ yielding the most branched product and Lim-$(CH_2)_4CH_3$ the most linear product. Hydrogenation of the olefin was very low ranging from 5 to 6%.[13]

Sasol also reported another bicyclic phosphine ligand (VCH-R) with the P-atom forming part of the largest ring structure of the molecule and the side chain R could be alkyl, branched alkyl, cycloalkyl or aryl groups. This family of ligands was derived from vinylcyclohexene and consists of two isomers the 3.3.1 and 3.2.2 as shown in Figure 2.18.[137]

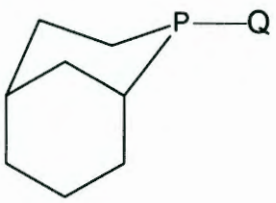

VCH[3.3.1]-R

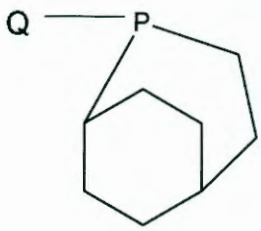

VCH[3.2.2]-R

Q = alkyl, branched alkyl, cycloalkyl or aryl groups

Figure 2.18: Two isomers of VCH-Q ligands.

---

136 A. Robertson, C. Bradarie, C. S. Frampton, J. McNulty and A. Capretta, *Tetrahedron Lett.*, 2001, **42**, 2609.

137 P. J. Steynberg, H. Van Rensburg, J. J. C. Grove, S. Otto and C. Crause, *WO Patent*, 2003, 03068719A2.

equilibria have been detected at low cobalt concentration and it was suggested that $[Co_2(CO)_7PR_3]$ might be an important intermediate which then reacts with hydrogen to yield $[HCo(CO)_4]$ and $[HCo(CO)_3PR_3]$.[140] In the absence of syngas, the phosphine ligands react with $[Co_2(CO)_8]$ by displacement of CO to form the complex salt which converts directly to the corresponding dimer at high temperature.[73]

2.3.3.1. Reaction mechanism of modified cobalt hydroformylation

In 1960 Heck and Breslow presented their currently accepted mechanism for the unmodified cobalt system based on the postulated formation of $[HCo(CO)_4]$, from $[Co_2(CO)_8]$ and hydrogen and its subsequent dissociation into $[HCo(CO)_3]$ and CO as shown in Figure 2.10.[102] This unmodified catalytic cycle can be generalised and extrapolated to the modified systems in which the pre-catalytic species is the mono-phosphine hydride $[HCo(CO)_3P]$ as shown in Figure 2.20.

The catalytic cycle is made up of six steps starting from the disubstituted phosphine dimer. The first step (**a**) involves the activation of molecular hydrogen to give the tricarbonyl phosphine hydride $[HCo(P)(CO)_3]$. This 18 electron complex then loses CO to form an unsaturated cobalt dicarbonyl phosphine hydride, $[HCo(P)(CO)_2]$, step (**b**). The reaction of the modified hydrido-cobalt dicarbonyl, $[HCo(P)(CO)_2]$, and an olefin give a π-complex step (**c**).

---

140 M. van Boven, N. H. Alemdaroglu and J. M. L. Penninger, *J. Organomet. Chem.*, 1975, **14**, 259.

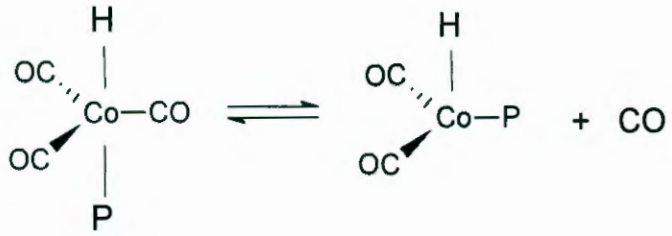

Figure 2.21: CO dissociation from the modified cobalt hydride.

The steric size of the ligands can also affect reaction rates. The size of the ligands could influence the equilibrium dissociation reactions, the tendency of metal complexes to undergo oxidative addition reactions as well as reactions with olefins to form π-complexes.[142] Increasing the steric demand of the ligands tends to favour the followings:

- Lower coordination number of the complexes.
- The formation of less sterically crowded systems.
- Increased rate and equilibria in dissociative reactions.[143, 144]

Hydride migration to the coordinated olefin step (**d**) occurs through two routes, either anti-Markovnikov migration to give the linear alkyl species or Markovnikov migration to give the branched alkyl species. The further reaction of these alkyl groups determines the nature of the products obtained.[145] The resultant alkyl complexes would either react with hydrogen to form alkanes or undergo alkyl migration to a coordinated CO group to form the corresponding acyl complexes.

The migration of the alkyl group to a coordinated *cis*-carbonyl to give an acyl complex is step (**e**) of the catalytic cycle. This is an intramolecular nucleophilic attack of the coordinated alkyl group on to the carbon atom of the carbonyl to form the metal acyl species. Several factors are known to govern

---

142 C. A. Tolman, *Organometallics*, 1983, **2**, 1391.

143 C. A. Tolman, *Chem. Rev.*, 1977, **77**, 313.

144 M. M. Rahman, H. Ye. Liu, A. Prock and W. P. Giering, *Organometallics*, 1987, **6**, 650.

145 E. J. Cammell and J. M. Andersen, *J. Organomet. Chem.*, 2000, **604**, 7.

adjacent carbonyl ligand more slowly than the smaller linear group.[145, 150, 151] In a phosphine induce migratory CO-insertion reaction, the migration of a bulkier branched alkyl group adjacent to the incoming nucleophile such as PPh_3 will experience some resistance.

In a conventional intramolecular rearrangement, bulkier (branched) alkyl group should react faster since the steric strain is being alleviated on going from the more hindered alkyl to an open acyl complex. These different views concerning the steric effects on the rate of alkyl migration were studied further and the concept of a steric window was introduced within which reactivity is enhanced.[151] A number of other articles also claimed that bulkier alkyl groups undergo migratory insertion slower than smaller groups.[149, 150] It has been shown that the alkyl migration reactions of $[Mn(R)(CO)_5(PPh_3)]$ initially increases as the alkyl chain length $CH_3(CH_2)_n$- increases from n = 0 to n = 2, then decrease rapidly until n = 6. Beyond this point, the alkyl chain lengths no longer influence the rate of alkyl migration.[149]

The effect of the entering ligand is closely related to the solvent. It has been found that electron donating solvents increases the rate of alkyl migration in substituted benzyl manganese penta-carbonyl compounds, $[Mn(CH_2C_6H_{5-n}X_n)(CO)_5]$.[152] The donor solvent attack the metal centre during alkyl migration and this reaction is influenced by the steric size of the solvent molecule.[153] Alkyl migration in $[Mn(R)(CO)_3]$ is assumed to follow a concerted reaction pathway, namely, concomitant bond breaking and bond formation forming a three-centred transition state. The activation energy of 61.9 kJ/mol for the alkyl migration process was found to be lower than the bond dissociation energy of 184 kJ/mol for the manganese-methyl carbon bond in $[Mn(CH_3)(CO)_5]$, supporting the concerted mechanism.[154]

---

151 J. D. Cotton and R. D. Markwell, *J. Organomet. Chem.*, 1990, **388**, 388.

152 T. L. Bent and J. D. Cotton, *Organometallics*, 1991, **10**, 3156.

153 M. J. Wax and R. G. Bergman, *J. Am. Chem. Soc.*, 1981, **103**, 7928.

154 F. Calderazzo and F. A. Cotton, *Inorg. Chem.*, 1962, **1**, 30.

It was recently shown that aldehydes could be formed from the stoichiometric reaction between manganese hydride and acyl rhodium or acyl cobalt species and in both cases these reactions were the rate determining steps.[158] The reactions with molecular hydrogen took place as well but at a slower rate than with manganese hydride. The reactions with dihydrogen involve oxidative addition rapidly followed by reductive elimination as shown in Eqn. 2.9.

$$[RC(O)Co(CO)_4] + H_2 \rightarrow RCHO + [HCo(CO)_4] \qquad 2.19$$

Evidence of the reaction shown in Eqn. 20 in the presence of bulkier olefins such as 3,3-dimethylbutene and cyclohexene at room temperature was reported.[159] Isotopic exchange studies have confirmed that the hydrogenolysis occurred by molecular hydrogen and not by $[HCo(CO)_4]$. The ratio of the final products RCHO and RCDO, corresponded to the ratio of H_2 and D_2 in the gas phase and not to the ratio of $[HCo(CO)_4]$ and $[DCo(CO)_4]$ in solution.[160] More over, in many experiments where the formation of acyl metal species were detected, these species survived longer in the reaction mixtures than the hydrides while the formation of aldehydes continued to take place.[160] This agrees with the fact that the hydrogenolysis of the acyl complexes to the corresponding aldehydes occurs with molecular hydrogen.

2.3.3.2. Formation of multi-substituted phosphine cobalt carbonyl hydrides

Pregaglia and co-worker combined HP-IR and HP-NMR to demonstrate that, in the presence of CO, a series of reversible reactions took place at room temperature between the mono-, di-, and tri-substituted cobalt hydrides, Eqn. 2.20.

---

158 T. Onoda, *Chem. Tech.*, 1993, 34.

159 R. Tannenbaum and G. Bor, *J. Mol. Catal. A: Chem.*, 2004, **215**, 33.

160 P. Pino, A. Major, F. Spindler, R. Tannenbaum, G. Bor and I. T. Horvath, *J. Organomet. Chem.*, 1991, **417**, 65.

2.3.3.3. The use of phosphites as ligands

It has been shown that phosphite ligands in the presence of cobalt metal can successfully be used to catalyse the hydroformylation of 1-pentene to the corresponding aldehydes. During this process, some of the 1-pentene was converted to internal olefins due to isomerisation. From HP-IR studies the isomerised products with large cone angles were obtained only with $P(OPh)_3$ (128°) and not with bulkier ligands such as $P(O\text{-}2,4\text{-}^tBu_2C_6H_3)_3$ (175°). It was suggested that the isomerisation was catalysed by the formation of the bis(phosphito)cobalt hydride species.[162] As earlier claimed, the large amount of bis(phosphito)cobalt hydride formed from the less bulky ligand at high ligand to metal ratios was inactive towards hydroformylation but enhances the isomerisation of the α-olefins to less-reactive internal alkenes.[163] Generally, since phosphites should decrease the electron density on the metal centre relative to phosphines, they are expected to yield fewer hydrogenation products.

2.3.3.4. The use of carbenes (alkylidene) as ligands

Carbenes are complexes containing M-C double bonds with the structure given in Figure 2.22.[119]

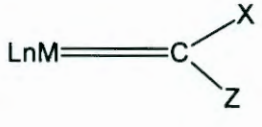

Figure 2.22: The structure of a carbene complex, where both X and Z are electronegative atoms such as N, S, O or the halogens, the compound is called Fischer carbenes and when X and Z = hydrogen atoms the compound is called Schrock carbenes.

---

162 R. Meijboom, M. Haumann, A. Roodt and L. Damoense, *Helvetica Chim. Acta*, 2005, **88**, 676.

163 M. Haumann, R. Meijboom, J. R. Moss and A. Roodt, *Dalton Trans.*, 2004, 1679.

pallanium-catalysed C-C coupling between aryl halide or vinyl halide and activated alkene in the presence of a base.[119]

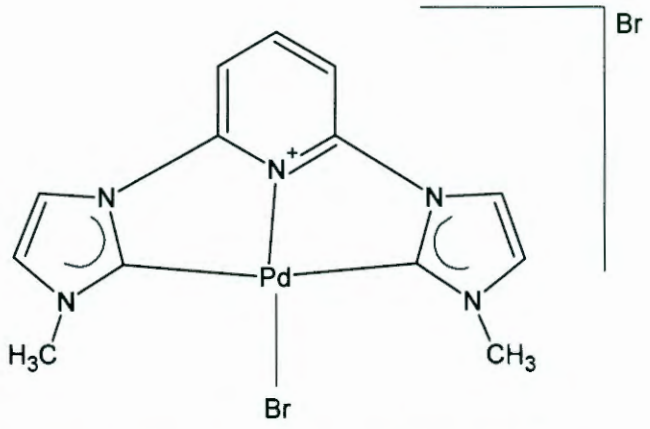

Figure 2.23: Palladium pincer-type carbene complex.[167]

Recently, metal complexes containing the N-heterocyclic carbenes (NHCs) have provided air and moisture-stable catalysts for a variety of reactions.[169] The steric bulk of 1,3-diarylimidazol-2-ylidene type ligands IMes and IPr account for the stability of these complexes. Rhodium carboxylato complexes bearing these ligands have been shown to be active for the regioselective hydroformylation of both aryl and aliphatic alkenes with regioselectivity of about 40:1 favouring the branch product without isomerisation or hydrogenation of the feed.[169] Others use these carbene ligands as modifiers in rhodium hydroformylation of vinylarenes with selectivity up to 97% of the branch product.[166, 170] The branched products from vinylarenes are more desirable, since oxidation generates the corresponding 2-arylpropionoic acids that are important class of analgesic drugs, including ibuprofen and naproxen.[169]

---

169 J. M. Praetorius, M. W. Kotyk, J. D. Webb, R. Wang and C. M. Crudden, *Organometallics*, 2007, **26**, 1057.

170 A. C. Chen, D. P. Allen, C. M. Crudden and A. Decken, *Can. J. Chem.*, 2005, **83**, 943.

The next Chapter will deal with the synthesis and characterisation of bicyclic tertiary phosphine ligands for evaluation in cobalt-catalysed hydroformylation.

3 Synthesis and characterisation of phosphine ligands and Se-P complexes

3.1. Introduction

Prior to Tolman's studies in 1970 the effect of phosphorus ligands on reactions and on the properties of metal complexes were rationalized mainly in terms of electronic effects, although there were some scattered references on steric effects.[1] However, systematic studies had shown that steric effects are as important as electronic effects and in terms of stability of complexes, they could even be dominant.[2]

The metal-phosphorus (M-P) bond is formed by a combination of sigma and pi contributions. The σ-bond is formed by donation of lone pair of electrons from the P atom to the M atom while the π-bond is formed by accepting electron density from the metal by back-donation into the empty 3d-orbitals and π*-orbital of the P atom.[2]

Tolman claimed that by replacing one or more CO ligands of transition metal carbonyl complexes by phosphine ligands causes the CO stretching frequencies of the remaining carbonyl to decrease by an amount depending on the number and nature of the phosphine ligands.[1, 3] Strohmeier and Horrocks[4] had also shown that phosphine ligands can be ranked in a "π-

1 C. A. Tolman, *J. Am. Chem. Soc.*, 1970, **92**, 2953.

2 G. O. Spessard and G. L. Miessler, *Organometallic Chemistry*, Prentice-Hall, Englewood Cliffs, NJ, 1997.

3 C. A. Tolman, *Chem. Rev.*, 1977, **77**, 313 and references there in.

4 (a) W. Strohmeier and F. J. Müller, *Chem. Ber.*, 1967 **100**, 2812. (b) W. D. Horrocks Jr. and R. C. Taylor, *Inorg. Chem.*, 1963, **2**, 723.

basicity. The *s* character is the percentage of s orbital of the total number of orbitals used in a hybridized bond.[12]

A second factor influencing the coordination of phosphine ligands is the spatial demand, or steric size associated with the specific ligand.[9] Consequently, the steric attributes of the phosphine ligands are easily controlled during ligand synthesis. The ability to control the bulk of the ligand permits one to tune the reactivity of the transition metal complexes. For example, if the dissociation of a phosphine ligand is the first step in a reaction, the reaction can be accelerated by utilizing a larger phosphine ligand.[13]

Ligand exchange on Ni(0) complexes was carried out using a range of phosphorus ligands L' and [NiL_4] complexes. From the product distributions after solutions of [NiL_4] and L' in toluene were equilibrated, the ligands could be ranked in a series according to the stability of the complexes.[1] The order of ligands in the series did not correlate with the electronic properties of the phosphorus ligands. Cone angle measurements from atomic models were therefore used to define a quantitative steric effect, which correlated well with the stability data. Displacement of CO from [$Ni(CO)_4$] by various phosphorus ligands confirmed the expectation that the degree of replacement would decrease as the size of the ligand increased. A crude but effective measure of the steric demand of a symmetrical ligand is the Tolman cone angle θ given in Eqn. 3.1 and θ/2 is the half angle.[3]

$$\theta = 2/3(\Sigma\, \theta/2) \qquad 3.1$$

The steric parameter θ for the phosphine ligands is the apex angle of a cylindrical cone, 2.28 Å from the centre of the P atom. The cylindrical cone must be large enough to enclose the Van der Waals radii of the outermost atoms of the phosphine ligand,[13] see Figure 3.1.

---

12 a) H. A. Bent, *Chem. Rev.*, 1961, **61**, 275; b) www.britannica.com/eb/topic-514672/s-character, accessed on the 12/12/2009.

13 http://www.liv.ac.uk/Chemistry/Links/links.html, accessed on the 12/12/2009.

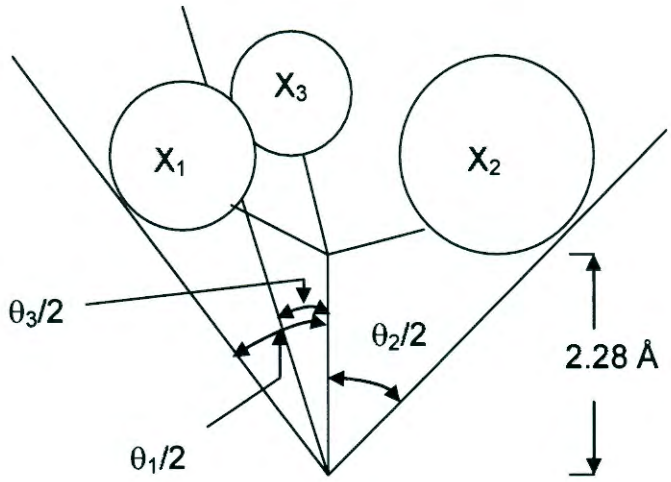

Figure 3.2: Measurement of cone angle for unsymmetrical phosphine ligands.

Clearly, the steric and electronic properties of tertiary phosphines can significantly influence the reactivities of metal centres and lead to marked changes in chemical reactions. The steric bulk and electron donor-acceptor abilities of phosphine ligands are difficult properties to quantify, and indeed, the two properties are closely related. For example, as the steric bulk of the R groups in a tertiary phosphine of the type PR_3 are increased, it is expected that the interorbital angles about the phosphorus atom will increase.[12]

In this chapter, the synthesis of some of the phosphine ligands as well as the phosphorus selenide compounds of all the ligands included in the study will be discussed. The electronic properties of the ligands are determined from the first-order selenium-phosphorus ($^1J_{Se\text{-}P}$) coupling constants.[11] The steric sizes of the ligands are determined from the cone angles of their solid state crystal structures of phosphorus selenides, cobalt dimers (discussed in Chapter 4) and Rh(I) complexes (discussed in Chapter 5). In all these structures the cone angles are calculated based on Tolman's model using a Van der Waals H-atom radius of 1.2 Å.[1] The actual M-P bond distances are used in the calculation to give what is referred to as the effective cone angles.[14, 15]

---

14 S. Otto, *Acta Cryst.*, 2001, **C57**, 793.

15 S. Otto, A. Roodt and J. Smith, *Inorg. Chim. Acta*, 2000, **303**, 295.

The synthesis of tertiary bicyclic phosphine ligands are classified into three main groups depending on the third substituent on the ligand backbone. In the first and second groups the third substituent on the bicyclic backbone were the aliphatic and alicyclic side chains respectively while in the third group the substituent was the phenyl group. Several distinct methodologies were used for the synthesis of these three groups of compounds as described in sections 3.2.2 and 3.2.3. The different secondary phosphines used in the synthesis of these ligands are given in Figure 3.3.

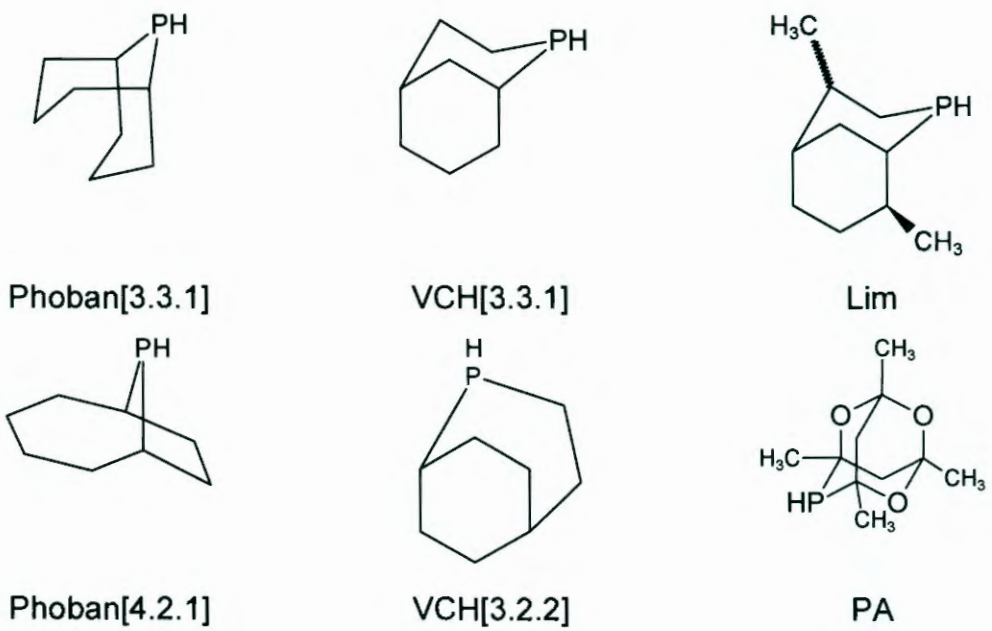

Figure 3.3: Bicyclic secondary phosphines used as precursors for making tertiary phosphine ligands.

3.2.2. Radical addition of an olefin to Phoban-H

Two different methods for the synthesis of bicyclic ligands containing the aliphatic or alicyclic side chains were evaluated.[17, 18] The first method

17 A. Robertson, C. Bradarie, C. S. Frampton, J. McNulty and A. Capretta, *Tetrahedron Lett.*, 2001, **42**, 2609.

18 C. Crause, L. Bennie, L. Damoense, C. L. Dwyer, C. Grove, N. Grimmer, W. Janse van Rensburg, M. M. Kirk, K. M. Mokheseng, S. Otto and P. J. Steynberg, *Dalton Trans.*, 2003, 2036.

was subsequently heated overnight at 100 °C as described above, bp = 240 °C.

A toluene solution containing a mixture of the Phoban[3.3.1 & 4.2.1]-C_2 isomers were prepared under argon and the concentration of the isomers were determined as [3.3.1] = 1.626 mol dm^{-3} and [4.2.1] = 1.429 mol dm^{-3} by integration of the ^{31}P NMR peak areas against an internal standard (PPh_3). An aqueous solution of HCl (48 mL, 1.0 mol dm^{-3}, 48 mmol) was added to the ligand solution (30 mL) containing Phoban[3.3.1] (49 mmol) and Phoban[4.2.1] (43 mmol). The mixture was stirred for 3 minutes and the phases were allowed to separate. The aqueous phase containing the [3.3.1] isomer was transferred into a Schlenk tube and Na_2CO_3 (5.312 g, 50.11 mmol) was added to neutralize the acid. The ligand was then extracted with toluene (20 x 3 mL), filtered through silica and ^{31}P NMR indicated that pure [3.3.1] isomer was isolated. To the remainder of the ligand mixture aqueous HCl (4 mL, 1.0 mol dm^{-3}, 4 mmol) was added and the reaction mixture was stirred for 3 minutes. After phase separation, the organic phase containing the Phoban[4.2.1] isomer was transferred into a Schenk tube and neutralized with an excess degassed concentrated aqueous Na_2CO_3 solution. The organic solution containing the Phoban[4.2.1] isomer was washed three times with degassed distilled water (20 x 3 mL), dried with anhydrous $MgSO_4$ and filtered through silica to remove any possible phosphine oxide. ^{31}P NMR analysis of the resultant solution indicated isolation of the pure Phoban[4.2.1] isomer, yield = 30.20 g, 81%.

Phoban[3.3.1]-C_2 isomer:

^1H NMR ($CDCl_3$): δ_H 1.63 (dt, 3H, CH_3 on C_2 chain), 1.57 (m, 2H, CH_2CH_3), 1.64 - 1.80 (m, 6H), 1.92 - 2.14 (m, 8H).

^{31}P NMR ($CDCl_3$): δ_P = -31.5.

Phoban[4.2.1]-C_2 isomer:

^{1}H NMR ($CDCl_3$): δ_H 0.83 (t, 3H, CH_3 on C_5 chain), 1.22 - 1.26 (2 x s, 6H, 2 x CH_3 closer to P), 1.28 and 1.29 (s, 3H, CH_3 away from P), 1.30 - 1.60 (m, 8H, CH_2 on the C_5 side chain), 1.59 - 1.92 (m, 4H, CH_2 on the PA backbone).
^{31}P NMR ($CDCl_3$): δ_P = -28.5.

3.2.2.6. Synthesis of VCH-C_5

A toluene solution of VCH-H was reacted with 1-pentene according to the procedure described in section 3.2.2.1. Since the VCH-H starting material contained a primary phosphine contaminant, full details of the synthesis and purification is given below.

A mixture containing both primary and secondary VCH phosphines was standardised with ^{31}P NMR using an internal standard (PPh_3) and found to contain 5.16 mol dm^{-3} of VCH-H. The starting reaction mixture (6.80 mL, 35 mmol) was added to 3 molar equivalent of 1-pentene (11.50 mL, 7.40 g, 106 mmol) and VAZO (1.64 g) in a pipe reactor under argon. The reaction was left overnight at 100 °C and ^{31}P NMR analysis the next morning showed the reaction to be complete. The solvent was removed under vacuum resulting in a yellow oily liquid. Purification by Kugelrohr distillation resulted in the final product, bp = 293 – 313 °C, yield = 4.21 g, 56.5%.

^{1}H NMR ($CDCl_3$): δ_H 0.78 - 0.84 (t, 3H, CH_3 on C_5 chain), 1.20 - 2.02 (m, 20H, CH_2 and CH on C_5 chain and VCH backbone).
^{31}P NMR ($CDCl_3$): δ_P = -31.9 (VCH-C_5).

3.2.3. Radical addition of *cis,cis*-1,5-cyclooctadiene to H_2PCy

The second method involved radical addition of *cis,cis*-1,5-cyclooctadiene to H_2PCy and was used to make Phoban-Cy.

3.2.4.1a. Action of phenyl lithium on Phoban-Cl

This was a two step approach which involved the synthesis of Phoban-Cl and coupling with phenyl lithium to give the final product as shown in Figure 3.6. The Phoban-Cl was synthesised according to a modification of the procedure described by Weferling.[19]

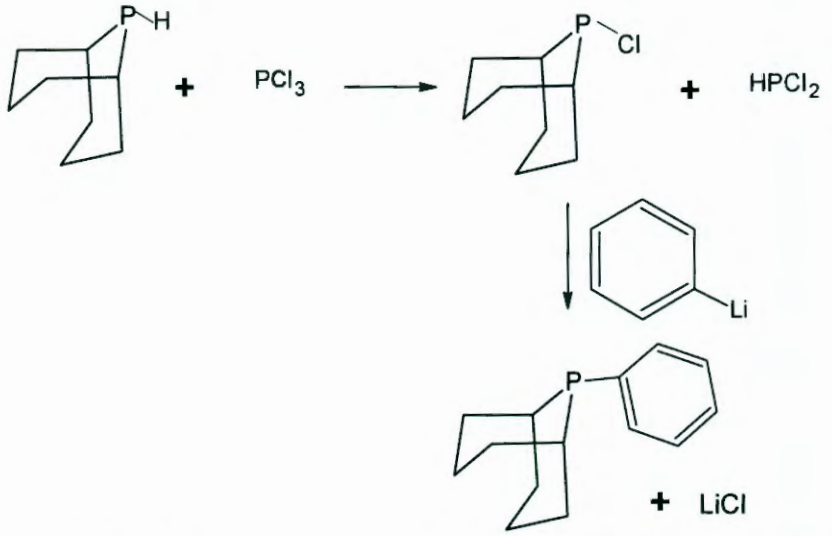

Figure 3.6: Synthesis of Phoban-Ph via Phoban-Cl; Phoban-Cl was synthesized from PCl_3 and Phoban-H in toluene at room temperature and couple with PhI in ether at -78 °C.

Phoban-Cl: PCl_3 (13 mL, 20.46 g, 149 mmol) was added drop-wise to a toluene solution of Phoban-H (50 mL, 43.50 g 60% solution, 26.10 g Phoban-H; 184 mmol) at room temperature. After the addition was complete, the reaction mixture was stirred for 1 h. All volatile components were removed under vacuum and the remaining orange solids were repeatedly extracted with diethyl ether (3 x 30 mL). The solvent fractions were combined and filtered through a celite plug. The material obtained in this way was normally of sufficient purity for further use, yield = 19.91 g, 61% as determined by ^{31}P NMR.

---

19 N. Weferling, *Z. Anorg. Allg. Chem.*, 1987, **548**, 55.

allowed to heat up to about -30 °C followed by the addition of fluorobenzene (0.7 mL, 7.44 mmol). The reaction mixture was allowed to warm up to 5 °C during which time the initial light yellow solution changed to a deep red. After stirring for another 1 h degassed aqueous NH_4Cl was added and the two phases were separated. The organic phase was dried with anhydrous sodium sulphate and filtered through a short silica plug to remove some phosphine oxides that was formed during the reaction. The resultant mixture was shown to contain (0.77 g, 63%) of the desired ligand and 31% of Phoban-H.

3.2.4.1c. Palladium catalysed P-C coupling

The palladium catalysed P-C coupling reaction was performed according to a modification of the procedure reported by Stelzer and co-workers as shown in Figure 3.8.[21]

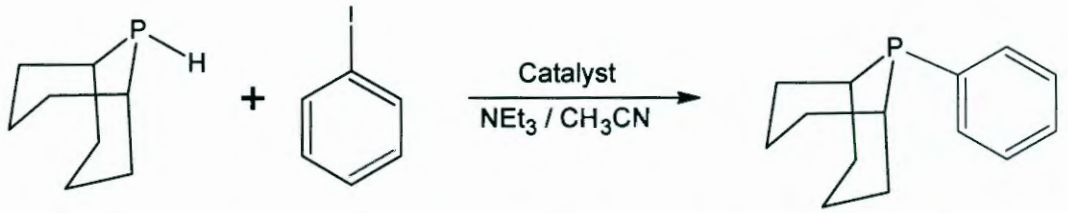

Figure 3.8: Synthesis of Phoban-Ph from Phoban-H and PhI via P-C coupling reaction with palladium catalyst in acetonitrile at 120 °C.

A reaction mixture containing Phoban-H (24 mL, 20.59 g 60% solution in toluene, 12.35 g Phoban-H, 86.9 mmol), iodobenzene (10 mL, 18.23 g, 89.3 mmol), NEt_3 (12 mL, 8.71 g, 86.1 mmol), $[Pd(PPh_3)_4]$ (250 mg, 0.022 mmol) and acetonitrile (15 mL) was prepared in an autoclave under an argon atmosphere and heated to 120 °C for 96 h. ^{31}P NMR analysis of the reaction mixture indicated 83% of all the phosphorus-containing components corresponded to the desired product. The reaction mixture was allowed to cool to room temperature and degassed toluene (30 mL) was added to

---

21 A. Heßler, K. W. Kottsieper, S. Schenk, M. Tepper and O. Stelzer, *Z. Naturforsch.*, 2001, **56b**, 347.

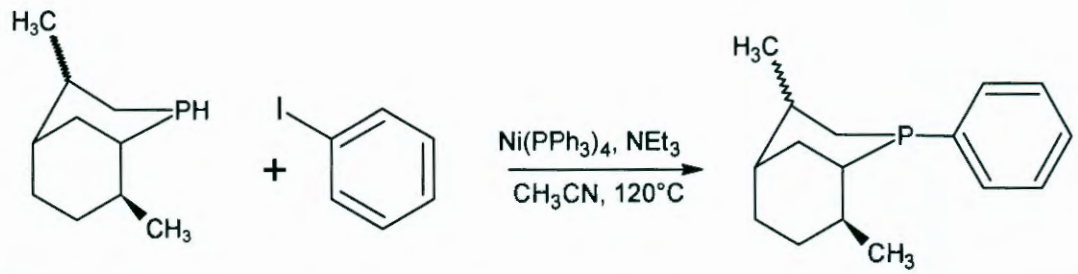

Figure 3.9: Synthesis of Lim-Ph from Lim-H and PhI via P-C coupling reaction with nickel catalyst in acetonitrile.

A reaction mixture containing Lim-H (15.75 mL, 13.62 g 50% solution in toluene, 6.81 g Lim-H, 40 mmol), iodobenzene (10.7 mL, 8.78 g, 42 mmol), NEt_3 (5 mL, 3.63 g, 39 mmol), $[Ni(PPh_3)_4]$ (11 mg, 0.01 mmol) and acetonitrile (10 mL) was prepared in an autoclave under an argon atmosphere and heated to 120 °C for 87 h. After this time ^{31}P NMR analysis of the reaction mixture indicated 80% of all the phosphorous containing components corresponded to the desired product. The reaction mixture was allowed to cool to room temperature and degassed toluene (20 mL) was added, the mixture was shaken and filtered through silica to removed the bulk of the $[Et_3NH]I$. All volatiles were removed from the golden yellow solution under vacuum and the final purification was done by Kugelrohr distillation to give a whitish compound, yield = 14.59 g, 74%, bp = 343 °C.

^1H NMR ($CDCl_3$): δ_H 1.20 (d, 3H, CH_3 (4R, 8S-Lim)-closer to P); 1.06 (d, 3H, CH_3 (4R,8S-Lim)-away from P); 1.32 (d, 3H, CH_3 (4S, 8S-Lim)-closer to P); 1.13 (d, 3H, CH_3 (4S, 8S-Lim)-away from P); 1.35 – 2.21 2 x (m, 12H, 4CH, $4CH_2$) for both isomers, 7.43 – 7.52 (m, 4H, *m*-ArH); 7.33 – 7.40 (m, 6H, *p/o*-ArH).

^{31}P NMR ($CDCl_3$): δ_P -32.7 (4R, 8S-Lim), -43.9 (4S, 8S-Lim).

3.2.4.3. Synthesis of PA-Ph

The same procedure was used as described in section 3.2.4.1c as shown in Figure 3.10, bp = 315 °C.

analysis of the reaction mixture indicated 80% conversion of all the phosphorous starting materials. The reaction mixture was allowed to cool to room temperature, degassed toluene (3 x 20 mL) was added and the resulting mixture was filtered through silica to remove the ammonium salts yielding a yellow solution. ^{31}P NMR ($CDCl_3$) analysis of the resultant solution indicated four major peaks at -3.34, -15.91, -20.61 and -23.94 ppm. The last two peaks were assigned to the two isomers of the VCH[3.3.1]-Ph (80%) and VCH[3.2.2]-Ph (20%) ligands respectively while the first two peaks were assigned to the tertiary ligands formed from the primary phosphine impurities. All volatiles were removed under vacuum and the final purifications were done at 2 mbar and 150 – 160 °C by Kugelrohr distillation, yield = 6.19 g, 55%, bp = 330 °C.

^{1}H NMR ($CDCl_3$): δ_H 1.2 - 2.6.(m, 28H, 4CH, 12CH_2). Mixtures of protons for the VCH[3.3.1] and VCH[3.2.2] isomers; 7.40 - 7.45 (m, 4H, *m*-ArH); 7.29 - 7.35 (m, 6H, *p/o*-ArH).
^{31}P NMR ($CDCl_3$): δ_P VCH[3.3.1] = -20.5, VCH[3.2.2] = -23.8.

A summary of the ^{31}P NMR data, boiling points and cone angles of selected bicyclic phosphine derivatives are given in Table 3.1.

3.2.4.5 Preparation of phosphine selenides

The phosphorus selenide complexes were synthesized and first-order Se-P coupling constants were determined according to procedure reported previously.[22]

Figure 3.12 illustrate a typical ^{31}P NMR spectrum of the selenium-phosphorus complex of Lim-Ph exhibiting coupling associated with the Se-P interaction (^{77}Se 7.58% spin 1/2).

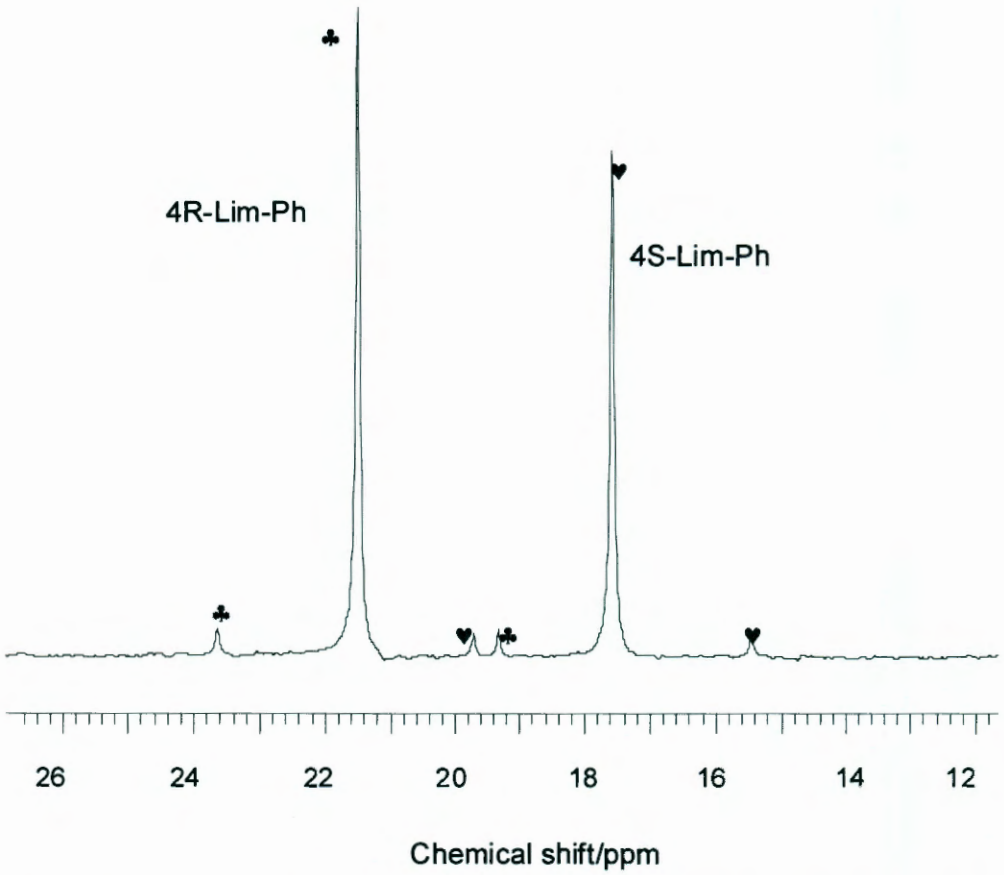

Figure 3.12: ^{31}P NMR spectrum of the phosphorus selenium complex of Lim-Ph showing the satellites of the two isomers of the ligand.

The synthesis of the selenide complex of Phoban-C_2 is described below as an example.

---

22 S. Otto, A. Ionescu and A. Roodt, *J. Organomet. Chem.*, 2005, **690**, 4337.

3.2.4.5a and will be discussed in section 3.4.2. These conventional as well as the bicyclic ligands will be evaluated in cobalt-catalysed hydroformylation of α-olefins as described in Chapter 4.

3.3. Crystallographic characterisation

Crystals suitable for X-ray diffraction were obtained from slow evaporation of the solvent from the samples in $CDCl_3$, CH_2Cl_2 or acetone. The data collection was done on either a Bruker X8 ApexII 4K Kappa CCD or a Bruker SMART 1K CCD diffractometer using ϕ-scans and Mo K_α (0.71073 Å) radiation. All reflections were merged and integrated using SAINT-Plus and XPREP[23] and were corrected for Lorentz, polarization and absorption effects using multi-scans. After completion of the data collection, the first 50 frames were repeated to check for decay of which none was observed. The structures were solved by the direct method and refined through full-matrix least squares cycles using the SHELXL97 software package with $\Sigma(|F_o|-|F_c|)^2$ being minimized.[24] All non hydrogen atoms were refined with anisotropic displacement parameters while the hydrogen atoms were constrained to parent sites using a riding model. The co-crystallization of both the [3.3.1] and [4.2.1] isomers in Se-Phoban-Ph and Se-Phoban-Cy were refined with the occupancy of the cyclooctyl component as a free variable. Bonds and anisotropic restrains were used to keep the refinements of the disorders stable. The graphics were done with DIAMOND.[25] Cone angle calculations were done according to the Tolman model as described before but by using the actual P-Se bond distances.[15, 15] A summary of the general crystal data and refinement parameters is given in Table 3.3.

---

23 Bruker, SAINT-Plus. *Version 7.12 (including XPREP). Bruker AXS Inc.*, Madison, Wisconsin, USA, 2004.

24 G. M. Sheldrick, *SHELXL97, Program for refinement of crystal structures*, University of Göttingen, Germany, 1997.

25 K. Brandenburg and M. Berndt, *DIAMOND, Version 2.1e, 2001*, Crystal Impact GbR, Bonn, Germany, 1999.

3.4.1. Synthesis of phosphine ligands

Different synthetic routes A to F for the synthesis of Phoban-Ph ligand were evaluated as illustrated in Figure 3.13. Some of these routes involving the radical addition of 1° or 2° phosphine to an appropriate diene or alkene have been well established.[26] This method was used to prepare phosphine ligands with aliphatic and acyclic side chains. The reaction of cyclohexene with Phoban-H was very slow (method A) and resulted in significant formation of undesired side products such as P-P dimers. Radical addition of *cis*,*cis*-1,5-cyclooctadiene to H_2PCy, (method B) however proceeded smoothly and produced Phoban-Cy in acceptable yields.[27]

Other bicyclic ligands with aliphatic side chains were synthesized according to method A. The one step reaction went smoothly with yields in excess of 70% for the Phoban, Lim and PA ligands while that for VCH was about 50-60%. The starting reagent for the synthesis of the VCH derivatives consisted of a mixture of primary and secondary phosphines as well as other unknown impurities. These phosphines reacted to give a mixture of tertiary bicyclic and acyclic phosphines with different boiling points. Some of the final product was lost during purification accounting for the lower yields.

---

26 F. Krech, B. Krauss and C. Mugge, *Z. Anorg. Allg. Chem.*, 2003, **629**, 1475.

27 P. N. Bungu and S. Otto, *J. Organomet. Chem.*, 2007, **692**, 3370.

Both methods were moderately effective, but method C especially yielded some P-P dimeric species because of lithium/halogen scrambling. Additional unidentified side products were also observed and may be linked to deprotonation on one or both of the two 2 °C atoms of the cyclooctyl group attached directly to P. Even though nucleophilic aromatic substitution is normally an unfavourable process the use of fluorobenzene as electrophile in the preparation of aryl phosphines has been demonstrated.[20, 28] Method D is superior to Method C since the additional preparation of Phoban-Cl can be circumvented.

The palladium catalysed P-C coupling reaction (Method E) was performed according to a modification of the procedure reported by Stelzer[21] and co-workers see Figure 3.13. This methodology is usually employed when functional groups incompatible with Grignard or organolithium reagents are present in some of the reactants. This protocol has the added advantage that it is not particularly sensitive towards moisture and only inert conditions needed to be maintained to avoid oxidation of the phosphine. The iodobenzene, NEt_3 and acetonitrile were thus used straight from the bottle without any further purification or drying steps performed on it. Even though this procedure took significantly more time than methods C and D it was not labour intensive and is superior in terms of product yield while no detectable side products were observed. Different palladium sources such as $[Pd(PPh_3)_4]$ and $[Pd(OAc)_2]$ were evaluated and gave comparable results.

Two different nickel sources $[Ni(PPh_3)_4]$ and [Ni(2-ethylhexanoate)$_2$] were evaluated in place of palladium in the P-C coupling reactions. [Ni(2-ethylhexanoate)$_2$] gave lower conversions due to the formation of 37% of an unknown compound at ^{31}P NMR ($CDCl_3$) δ = 16.95 ppm. By replacing the Ni source with $[Ni(PPh_3)_4]$, higher conversions were obtained as could be seen in the synthesis of Lim-Ph and PA-Ph described in sections 3.2.4.2 and 3.2.4.3 respectively.

---

28 O. Herd, A. Heßler, K. P. Langhans, O. Stelzer, W. S. Sheldrick and N. Weferling, *J. Organomet. Chem.*, 1994, **475**, 99.

nucleus. The difference in chemical shifts of the isomers is in the range of 35 ppm for Phoban-Q and ~ 25 ppm for the Se-Phoban-Q derivatives respectively, see Table 3.1.

The effect of the Q-substituent of the Phoban derivatives seems to be moderate as only minor differences could be induced by all groups evaluated. In this regard a maximum $^{1}J_{Se-P}$ of 14 Hz could be induced between the [4.2.1] isomers for Q = Cy and Q = Ph; the most electron donating and electron withdrawing substituents respectively. The effect of the substituent seems to be slightly amplified as a difference of only 7 Hz was observed between the [4.2.1] and the corresponding [3.3.1] Phoban isomers. In this regard, the Q-substituent is available for manipulation of the physical properties (melting point, boiling point, solubility) of the Phoban ligands without affecting the chemical properties of the ligands drastically.

The difference in chemical properties of the Phoban[3.3.1] and Phoban[4.2.1] isomers, as noted before was exploited to separate a mixture of 9-H-9-phosphabicyclo[3.3.1]nonane and 9-H-9-phosphabicyclo[4.2.1]nonane by a sequence of hydrophosphination/ dehydrophosphination reactions.[31] Furthermore the difference in coordinating ability has been used to separate the isomers by selectively coordinating the [3.3.1] isomer by the addition of a metal to a solution containing both isomers.[32, 33] This difference could also account for the increased reactivity in all cases where an increase in electron density has a beneficial effect. This is manifested in the preferred oxidation of the [3.3.1] isomer as well as the reaction with $SeCN^-$ where a two-electron oxidation is required. During our investigation it was also qualitatively observed that the [3.3.1] isomer reacts preferentially with the $SeCN^-$ when <1 molar equivalent was added. Most notably the superior coordinating ability of the [3.3.1] isomer during cobalt hydroformylation was illustrated by high-

31 J. H. Downing, V. Gee and P. G. Pringle, *Chem. Commun.*, 1997, 1527.

32 H. C. L. Abbenhuis, U. Burckhardt, V. Gramlich, C. Köllner, P. S. Pregosin, R. Salzmann and A. Togni, *Organometallics*, 1995, **14**, 759.

33 J. Fawcett, P. A. T. Hoye, R. D. W. Kemmitt, D. J. Law and D. R. Russell, *J. Chem. Soc., Dalton Trans.*, 1993, 2563.

The $^1J_{Se-P}$ coupling constant of VCH-^{i}Bu, VCH-C_5 and VCH-Ph, determined as 673, 678 and 696 Hz respectively indicated that the first two ligands were the most electron donating bicyclic ligands included in the study. VCH-Ph was synthesized as an 80:20 mixture of the [3.3.1] and [3.2.2] isomers, VCH-^{i}Bu was obtained from Cytec as a 48:52 mixture respectively while in the synthesis of the VCH-C_5 only the [3.3.1] isomer was obtained. The [3.3.1] isomers of these ligands resonate upfield from the [3.2.2] due to shielding effects.

The two isomers of VCH-Ph differ by 1 Hz while that of VCH-^{i}Bu differ by 15 Hz indicating that the isomers of the ligand with the phenyl side chain were similar in electronic properties while those with the iso-butyl side chain were different. This illustrates how different the side chains on the VCH affect the electronic property of the ligand. The two isomers of VCH-Ph exhibits the largest $^1J_{Se-P}$ coupling constant indicating that it is the most electron withdrawing among the VCH ligands.

Generally, the ligands can be classified according to the following groups based on their $^1J_{Se-P}$ coupling constants: (VCH[3.3.1]-^{i}Bu, VCH[3.3.1]-C_5) = 673 – 678 Hz < (Phoban[3.3.1]-Cy, 4R- Lim-C_5, 4S- Lim-C_5, Phoban[3.3.1]-C_5, Phoban[3.3.1]-C_3NMe_2, Phoban[3.3.1]-C_2) = 682 – 688 Hz < (Phoban[3.3.1]-Ph, 4R-Lim-Ph, VCH[3.2.2]-Ph, VCH[3.3.1]-Ph, 4S-Lim-Ph) = 689 – 699 Hz < (Phoban[4.2.1]-Cy, Phoban[4.2.1]-C_2 ~ Phoban[4.2.1]-C_5 ~ Phoban[4.2.1]-C_3NMe_2, Phoban[4.2.1]-Ph) = 703 - 717 Hz < PA-C_5 ~ PA-Ph = 751 - 752 Hz. The trend indicates that the VCH ligands, except those with the phenyl side chain, were the most electron donating ligands in the series. The two isomers of Lim-C_5 were similar to each other and to all the derivatives of Phoban[3.3.1]. The third group in the series consist of all the Phoban[4.2.1] ligands and finally the PA ligands were the most electron withdrawing ligands evaluated in this study. The $^1J_{Se-P}$ coupling constants of the bicyclic ligands were compared to those of conventional ligands in Table 3.4.

structures determined in this study are presented in Table 3.5 while comparisons with literature analogues are given in Table 3.6.

3.4.3.1. Crystallographic analysis of Se-Phoban[3.3.1]-C_2

Se-Phoban[3.3.1]-C_2 as shown in Figure 3.14 crystallises on the general positions in the triclinic space group $P\bar{1}$. The calculation of the cone angle was based on the half angles as shown in Table 3.5 resulting in a value of 172°.

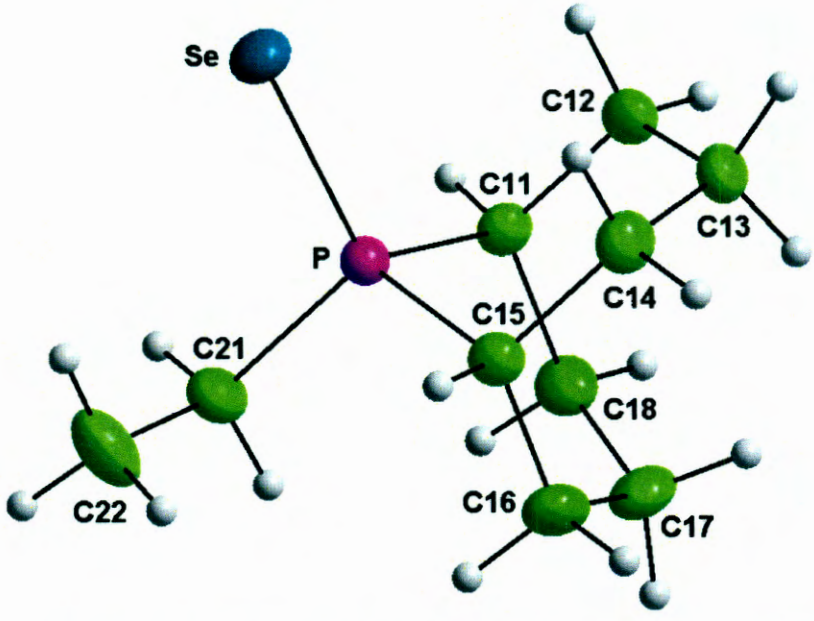

Figure 3.14: Molecular diagram showing the numbering scheme and thermal displacement ellipsoids (30% probability level) for Se-Phoban[3.3.1]-C_2, hydrogen atoms are of arbitrary size.

The bicyclic backbone, the C_2 side chain and the selenium atom coordinate to the phosphorus atom in a tetrahedral fashion. The molecules in the crystal align themselves without any interaction between them indicating that Van der Waals forces alone are responsible for the packing of the molecules in the asymmetric unit.

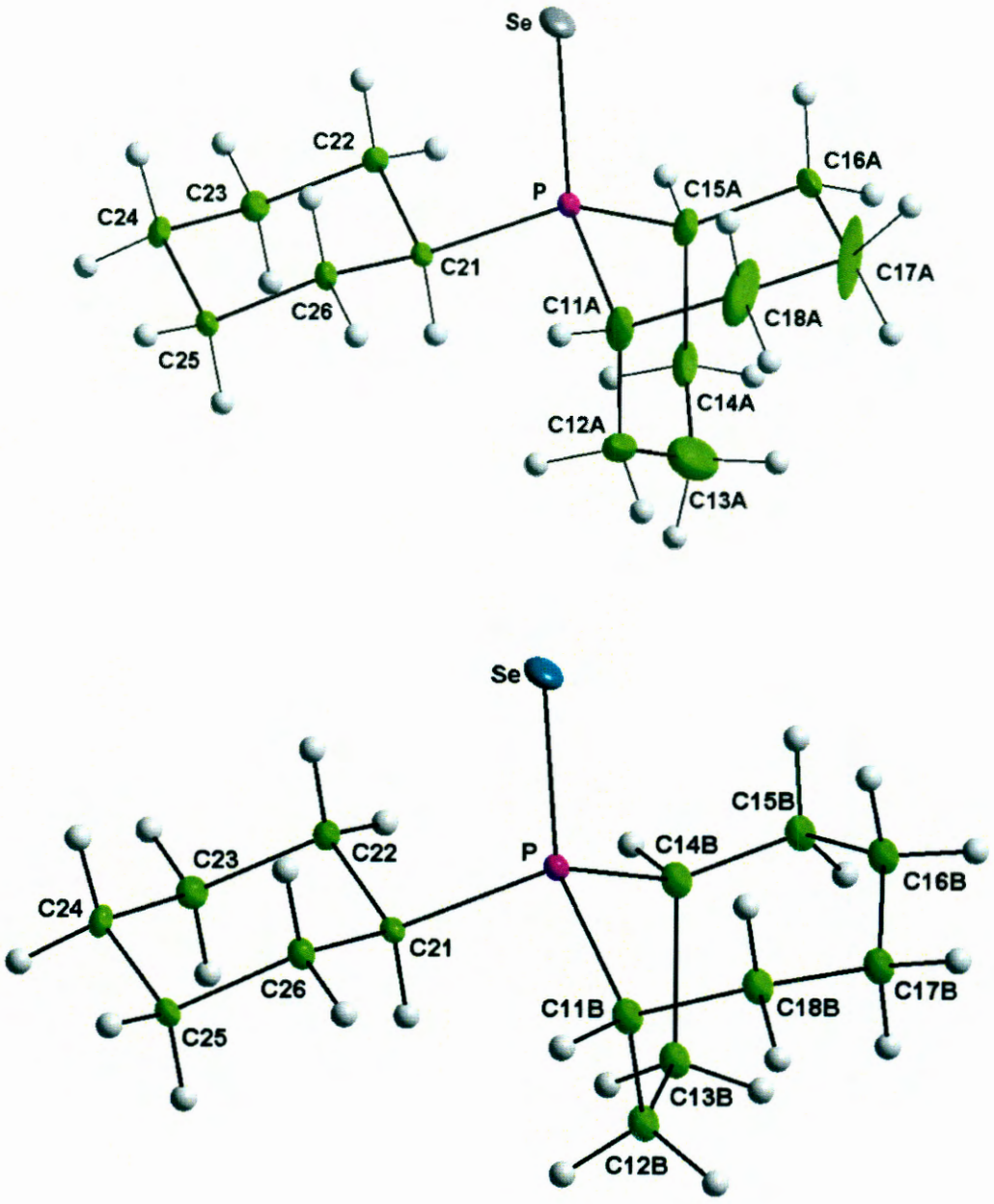

Figure 3.15: Molecular diagrams showing the numbering schemes and thermal displacement ellipsoids (30% probability level) for Se-Phoban[3.3.1]-Cy (**top**, 68%) co-crystallizing with Se-Phoban[4.2.1]-Cy (**bottom**, 32%) on the same position in the unit cell, hydrogen atoms are of arbitrary size.

On closer inspection it became apparent that it was again both the [3.3.1] and the [4.2.1] isomers co-crystallizing within the same structure also occupying the same position as encountered for the cyclohexyl derivative mentioned above, see Figure 3.17. The occupancy of the two isomers was refined to yield 60% [3.3.1] and 40% of the [4.2.1] isomers respectively. The cone angles for Se-Phoban[3.3.1]-Ph and Se-Phoban[4.2.1]-Ph were calculated as 167° and 165° respectively.

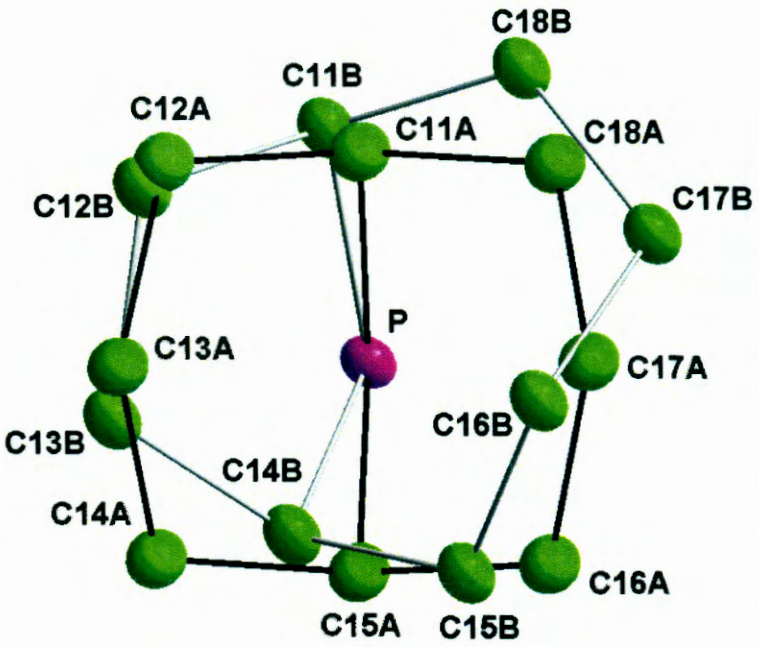

Figure 3.17: Molecular diagram illustrating the disordered packing between Se-Phoban[3.3.1]-Ph (solid bonds, 60%) and Se-Phoban[4.2.1]-Ph (open bonds, 40%) on the same position in the unit cell. The Se and H atoms as well as the Ph ring have been omitted for clarity.

3.4.3.4. Crystallographic analysis of Se-VCH-^{i}Bu

Se-VCH[3.3.1]-^{i}Bu, represents the first structure of a phosphine containing the VCH backbone. The VCH ligand consists of [3.3.1] and [3.2.2] isomers with the phosphorus selenide complex of the [3.3.1] isomer selectively crystallized resulting in the structure given in Figure 3.18. It contains two chiral centres on

bonded to the two central carbon atoms dividing the bicyclic cyclooctyl moiety into two equal halves resulting in a symmetrical molecule. The VCH[3.3.1] structure was very similar to that of the Phoban[3.3.1] except that the P-atom was bonded to two carbons on one of the six membered rings as shown in Figure 3.11. This resultant unsymmetrical molecule accounts for the two chiral centres the molecule display on the VCH backbone. The Phoban[4.2.1] isomers differ from those of Phoban[3.3.1] and VCH[3.3.1] in that the P-atom is bonded to two carbon atoms dividing the bicyclic cyclooctyl moiety into two unequal portions. The first portion is a seven membered ring while the other is a five membered ring that might result in some strain in the molecule.

All P-C bond lengths and Se-P-C and C-P-C angles for the Phoban[3.3.1] isomers and VCH[3.3.1]-^{i}Bu are very similar, see Table 3.5. The geometry of the Se-Phoban[4.2.1] isomers differ from the corresponding Se-Phoban[3.3.1] and Se-VCH[3.3.1] isomers with the most noticeable deviations in the P-C bond distances and the C-P-C angles. The strain in the five membered ring of the [4.2.1] isomers result in C-P-C angles of only 90.8(6) and 93.4(4)° respectively with corresponding large Se-P-C angles of > 120°. This deviation from an ideal tetrahedral geometry results in slightly longer than normal P-C bond distances as compared to those of the Phoban[3.3.1] and VCH[3.3.1]isomers. In addition, the deviation from the ideal geometry with resulting less effective orbital overlap and elongated P-C bonds should account for the [4.2.1] isomer being less electron rich than the Phoban[3.3.1] and VCH[3.3.1] isomers. The VCH[3.2.2] isomer consists of six and seven membered rings in the bicyclic structure resulting in strain in the molecule. No crystals of a Se-VCH[3.2.2] isomer have been obtained to date.

The two instances of the Phoban isomers co-crystallizing represent truly rare examples of random disorders and enable one to obtain crystallographic data for both isomers from the same crystal structures. This phenomenon presents strong evidence that the steric demand of the two isomers is very similar as also evident from the cone angle calculations. Because of the common geometry for the different derivatives the resulting cone angles were also very similar to that obtained from the other crystallographic studies.

Selected geometrical and electronic properties obtained during this study are compared with representative data from the literature in Table 3.6.

Table 3.6: Se-P bond distances, $^1J_{Se-P}$ coupling constants and Tolman cone angles for selected phosphines.

Phosphine	**Se-P / Å**	**$^1J_{Se-P}$ / Hz**	**Tolman / θ / °**	**Ref**
Phoban[3.3.1]-C_2	2.1171(9)	688	172	37
Phoban[3.3.1]-Cy	2.1160(9)	682	175	37
Phoban[4.2.1]-Cy	2.1160(9)	703	170	37
Phoban[3.3.1]-Ph	2.1090(9)	689	167	37
Phoban[4.2.1]-Ph	2.1090(9)	717	165	37
VCH[3.3.1]-^{i}Bu	2.1360(16)	673	168	41
PCy_3	2.108(1)	676	170	42
PMe_3	2.111(3)	684	118	43
$P(2\text{-}Me\text{-}C_6H_4)_3$	2.116(5)	708	194	44
PPh_3	2.106(1)	733	145	45
$P(NMe_2)_3$	2.120(1)	797	157	46

It is expected that a decrease in the Se-P bond distance, resulting in more effective s-orbital overlap should correspond with an increase in the first-order coupling constants. The Se-P bond distances of Se-VCH[3.3.1]-^{i}Bu given as 2.1360(16) Å was longer than those of the rest of the ligands ranging from 2.106(1) – 2.120(1) Å listed in Table 3.6. The first-order coupling constants, however, differ considerably (Δ^1J_{Se-P} = 124 Hz), but not necessarily systematically with distance.

---

41 P. N. Bungu and S. Otto, *Acta Cryst.*, 2009,**C65**, o560.

42 J. A. Davies, S. Dutremez and A. A. Pinkerton, *Inorg. Chem.*, 1991, **30**, 2380.

43 A. Cogne, A. Grand, J. Laugier, J. B. Robert and L. Wiesenfeld, *J. Am. Chem. Soc.*, 1980 **102**, 2238.

44 T. S. Cameron and E. Dahlen, *J. Chem. Soc., Perkin Trans.*, 1975, **2**, 1737.

45 P. W. Kodding and K. A. Kerr, *Acta Crystallogr.*, 1979, **B35**, 1261.

46 C. Rømming and J. Songstad, *Acta Chem. Scand.*, 1979, **A33**, 187.

constants: (VCH[3.3.1]-^{i}Bu, VCH[3.3.1]-C_5) = 673 – 678 Hz < (Phoban[3.3.1]-Cy, 4R- Lim-C_5, 4S- Lim-C_5, Phoban[3.3.1]-C_5, Phoban[3.3.1]-C_3NMe_2, Phoban[3.3.1]-C_2) = 682 – 688 Hz < (Phoban[3.3.1]-Ph, 4R, 8S-Lim-Ph, VCH[3.2.2]-Ph, VCH[3.3.1]-Ph, 4S, 8S-Lim-Ph) = 689 – 699 Hz, (Phoban[4.2.1]-Cy, Phoban[4.2.1]-C_2 ~ Phoban[4.2.1]-C_5 ~ Phoban[4.2.1]-C_3NMe_2, Phoban[4.2.1]-Ph) = 703 - 717 Hz < PA-C_5 ~ PA-Ph = 751 - 752 Hz.

- The different side chains (Q) on the Phoban derivatives did not affect their chemical properties but can be used to manipulate their physical properties such as boiling points, solubilities etc..
- In the crystal structures of the Se-P complexes the bicyclic backbones, the alkyl or aryl side chains and the selenium atoms coordinate to the phosphorus atoms in a tetrahedral fashion.
- The crystal structures of the following selenide complexes are reported: Se-Phoban[3.3.1]-C_2, Se-Phoban[3.3.1]-Cy, Se-Phoban[4.2.1]-Cy, Se-Phoban[3.3.1]-Ph, Se-Phoban[4.2.1]-Ph and Se-VCH[3.3.1]-^{i}Bu.
- The Phoban[4.2.1] isomer deviates from tetrahedral geometry resulting in slightly longer P-C bond lengths as compared to those of Phoban[3.3.1] and VCH[3.3.1]-^{i}Bu.
- The selenide complexes of the [3.3.1] and [4.2.1] isomers of Phoban-Cy and Phoban-Ph ligands co-crystallized within the same unit cell indicating that both isomers were similar in steric size.
- The average cone angles of the Phoban[3.3.1] derivatives (171°) Phoban[4.2.1] derivatives (168°) were similar to that of VCH[3.3.1]-^{i}Bu (168°).
- The slightly longer P-C bond lengths account for the Phoban[4.2.1] isomer being less electron donating than the Phoban[3.3.1] isomer.

4 Ligand evaluation in modified cobalt hydroformylation

4.1. Introduction

In this Chapter, the role which different phosphine ligands play in modified cobalt-catalysed hydroformylation is evaluated. The crystallographic characterization of cobalt dimers of selected phosphine ligands are included for additional information.

The electronic and steric properties of Phoban derived ligands, Phoban-Q (Q = CH_2CH_3 (C_2), $(CH_2)_4CH_3$ (C_5), $(CH_2)_9CH_3$ (C_{10}), $(CH_2)_{19}CH_3$ (C_{20}), $(CH_2)_3N(CH_3)_2$ (C_3NMe_2), C_6H_{11} (Cy) and C_6H_5 (Ph)) are systematically manipulated by altering the side chain on the phosphorus atoms. The effects of the electronic and steric properties of the Phoban derived ligands were determined in cobalt-catalysed hydroformylation of internal decene and are discussed in section 4.3.2.

Other bicyclic ligands including mixtures of (4S, 8S) and (4R, 8S) isomers of Lim-C_5 and Lim-Cp, [3.3.1] and [3.2.2] isomers of VCH-^{i}Bu and VCH-C_5, PA-C_5 and a mixture of [3.3.1] and [4.2.1] isomers of Phoban-C_5, added for comparison, were selected based on differences in their electronic and steric properties. The bicyclic ligands were compared to conventional ligands such as P^nBu_3, P^tBu_3, P^iBu_3, PCy_3, PCp_3, $P(p\text{-}C_6H_4OCH_3)_3$, PPh_3 and P(2-furyl)$_3$ and their effects on cobalt-catalysed hydroformylation of 1-octene were evaluated, see section 4.3.3. Bislim was included to evaluate the effect of a bisphosphine on the reaction system. Electronic properties of all the ligands were determined from their $^1J_{Se\text{-}P}$ coupling constants as discussed in Chapter 3.

temperature resulting in the formation of dark brown crystals. Crystals of the cobalt dimer of PCp_3 was obtained from the reaction mixture used for the hydroformylation of 1-octene in toluene. The solvent was removed from the reaction solution under vacuum at 40 °C and the resultant mixture containing the catalyst was placed in a fridge for several days.

The data collections were done on either a Bruker X8 ApexII 4K Kappa CCD or a Bruker SMART 1K CCD diffractometer using ϕ-scans and Mo K_α (0.71073 Å) radiation. All reflections were merged and integrated using SAINT-Plus and XPREP[2] and were corrected for Lorentz, polarization and absorption effects using multi-scans. After completion of the data collection, the first 50 frames were repeated to check for decay but none was observed. The structures were solved by the direct method and refined through full-matrix least squares cycles using the SHELXL97 software package with $\Sigma(|F_o|-|F_c|)^2$ being minimized.[3] All non-hydrogen atoms were refined with anisotropic displacement parameters while the hydrogen atoms were constrained to parent sites using a riding model. The graphics were done with DIAMOND.[4] The cone angle calculations were done based on Tolman's model using a Van der Waals H-atom radius of 1.2 Å. According to the definition, the Tolman cone angles were calculated from a fixed distance of 2.28 Å between the phosphorous atom and the metal[5] while in this study the actual P-Co bond distances were used in calculating what is referred to as the effective cone angles.[6, 7] A summary of the general crystal data and refinement parameters are given in Table 4.1 and the IUPAC names of the complexes are given in Table 4.2.

---

2 Bruker, *SAINT-Plus. Version 7.12 (including XPREP). Bruker AXS Inc.*, Madison, Wisconsin, USA, 2004.

3 G. M. Sheldrick, *SHELXL97, Program for refinement of crystal structures*, University of Göttingen, Germany, 1997.

4 K. Brandenburg and M. Berndt, *DIAMOND, Version 2.1e, 2001*, Crystal Impact GbR, Bonn, Germany, 1999.

5 C. A. Tolman, *Chem. Rev.*, 1977, **77**, 313.

6 S. Otto, *Acta. Cryst.*, 2001, **C57**, 793.

7 S. Otto, A. Roodt and J. Smith, *Inorg. Chim. Acta*, 2000, **303**, 295.

parameters

GooF	1.199	1.025	1.031	1.034	1.013	1.045	1.053
R ($I>2\sigma I$) R^a	0.0925	0.0396	0.0559	0.0253	0.0550	0.0227	0.0586
wR^b	0.2109	0.0927	0.1412	0.0626	0.1197	0.0571	0.1717
R (all data) R^a	0.1004	0.0671	0.0790	0.0310	0.0975	0.0274	0.0736
wR^b	0.2145	0.1048	0.1563	0.0655	0.1392	0.0600	0.1854
$\Delta\rho_{max}$; $\Delta\rho_{min}$/ e.Å^{-3}	0.714; -0.997	0.348; -0.280	1.068; -0.490	0.444; -0.228	1.472; -0.966	0.395; -0.235	2.366; -0.514

[a] $R = [(\Sigma\Delta F)/(\Sigma F_o)]$ [b] $wR = \Sigma[w(F_o^2 - F_c^2)^2]/\Sigma[w(F_o^2)^2]^{1/2}$

Table 4.2: IUPAC names of $[[Co_2(L)_2(CO)_6]$.

L	**IUPAC nomenclatures**
Phoban[3.3.1]-C_2	Hexacarbonylbis(9-ethyl-9-phosphabicyclo[3.3.1]nonane)dicobalt(0)
Phoban[3.3.1]-C_5	Hexacarbonylbis(9-pentyl-9-phosphabicyclo[3.3.1]nonane)dicobalt(0)
Phoban[3.3.1]-C_3NMe_2	Hexacarbonylbis(*N*,*N*-dimethyl-*N*-[3-(9-phosphabicyclo[3.3.1]non-9-yl)propyl]amine)dicobalt(0)
Phoban[3.3.1]-Cy	Hexacarbonylbis(9-cyclohexyl-9-phosphabicyclo[3.3.1]nonane)dicobalt(0)
PA-C_5	Hexacarbonylbis(1,3,5,7-tetramethyl-8-pentyl-2,4,6-trioxa-8-phosphatricyclo[3.3.1.1^{3,7}] decane)dicobalt(0)
PCy_3	Hexacarbonylbis(tricyclohexylphosphine)dicobalt(0)
PCp_3	Hexacarbonylbis(tricyclopentylphosphine)dicobalt(0)

syngas pressure. A representative reaction mixture for the Phoban-C_5 modified system at a ligand to metal ratio of 8:1 is given in Table 4.3.

Table 4.3: Reaction mixture makeup for Phoban-C_5 as ligand at a L:M ratio of 8:1.

Component	Mass / g	Vol. / mL	Comments
Feed	27.79	37.50	75% of final volume.
Cobalt required	4.05	4.68	Calculated to have 0.12g, (39.95 mM) Co in solution.
Phoban-C_5	3.61	-	L:M of 7:1 (93.90% purity)
Toluene	3.16	3.65	Adjusted to reach desired volume and mass.
Total	38.6	50	

A density of 0.772 g.cm^{-3} is used for the final reaction mixture resulting in a total mass of 38.6 g.

4.2.4. Autoclave studies of the other ligands

In this case, 1-octene (containing 1-dodecane and o-xylene as internal standards) used in the reactions was degassed with argon prior to use and cobalt (II) acetylacetonate was used as catalyst precursor. While passing argon through the autoclave, the reactor was charged with the reaction components to finally contain 60% 1-octene, [Co] = 1000 ppm (13.15 mmol dm^{-3}), the desired amount of phosphine and toluene as solvent. The reaction was carried out at 180 °C and 60 bar syngas pressure. A representative reaction mixture make-up for the Phoban-C_5 modified system at a ligand to metal ratio of 8:1 is given in Table 4.4.

Table 4.4: Reaction mixture makeup for Phoban-C_5 at L:M ratio of 8:1.

Component	Mass / g	Vol. / mL	Comments
Feed	21.45	30	60% of final volume.
Cobalt	0.1702	-	Calculated to have 13.2 mM Co in solution.
*Phoban-C_5	2.54	2.93	L:M of 8:1 (94.40% purity)
Toluene	14.59	16.86	Adjusted to reach desired volume and mass.
Total	38.75	50	

A density of 0.775 g.cm^{-3} is used for the final reaction mixture resulting in a total mass of 38.75 g. * [Phoban-C_5] = 105.2 mM in toluene, the density of toluene (0.865 g.cm^{-3}) was used to calculate the volume.

4.3. Results and discussion

4.3.1. Crystallographic studies

X-ray crystallographic studies were performed on representative cobalt dimers; see sections 4.3.1.1 – 4.3.1.7 for the molecular diagrams and numbering schemes and Tables 4.5 and 4.6 for selected geometrical parameters.

The [3.3.1] isomer of the Phoban ligands were found in most of the crystal structures as expected from its superior crystalline ability compared to the [4.2.1] isomers. Because of the symmetrical nature of the molecules, the complexes crystallises on special positions in their respective crystal systems. The cobalt centres display the expected distorted trigonal bipyramidal geometries associated with these types of molecules.

4.3.1.1. $[Co(Phoban[3.3.1]\text{-}C_2)(CO)_3]_2$

The complex in Figure 4.2 crystallises in the orthorhombic space group *Cmca* and possesses 2/m symmetry with the mirror plane running through C21, P, Co, C2, O2, C13 and C17 results in a 50% statistical disorder in C22. Atoms such as C1", C11" and C18" are generated by the mirror plane. The molecule also possesses an inversion centre in the middle of the Co-Co' bond and atoms such as C1'", O1'" and C11'" are all generated by the inversion centre.

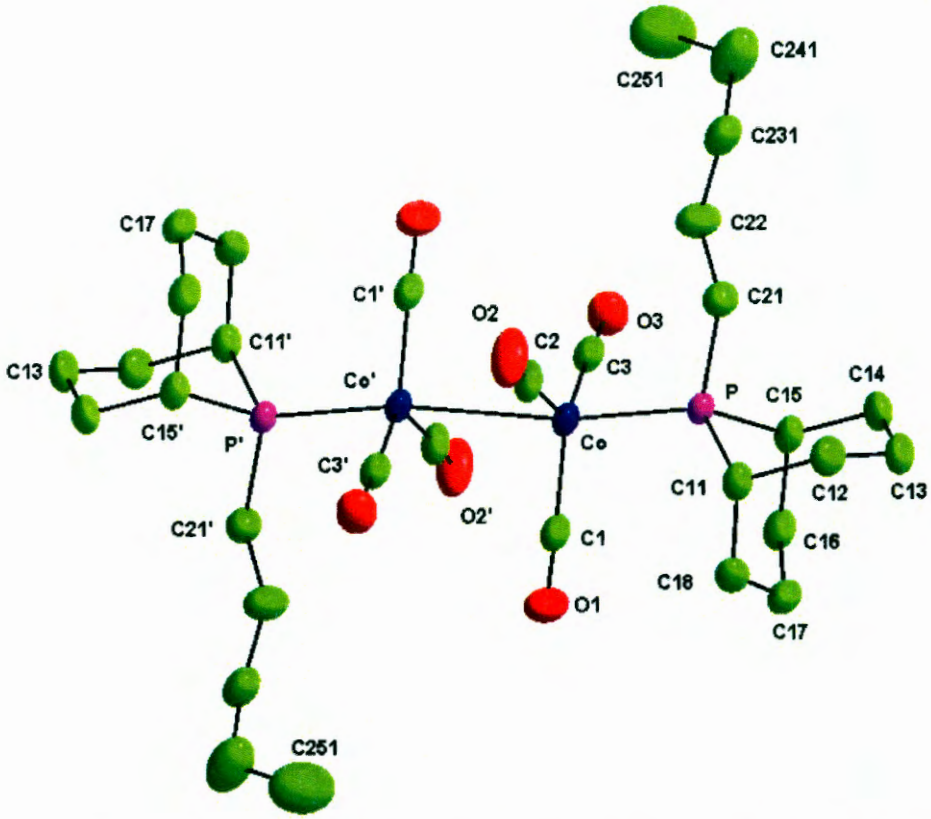

Figure 4.3: Molecular diagram showing the numbering scheme and displacement ellipsoids (30% probability) for $[Co(Phoban[3.3.1]\text{-}C_5)(CO)_3]_2$. The hydrogen atoms and the random disorder on the pentyl group were omitted for clarity. Symmetry operators: ' = 1-x, 1-y, 1-z.

4.3.1.3. $[Co(Phoban[3.3.1]\text{-}C_3NMe_2)(CO)_3]_2$

$[Co(Phoban[3.3.1]\text{-}C_3NMe_2)(CO)_3]_2$ crystallises in the monoclinic space group $P2_1/n$ and possesses an inversion centre between the two cobalt atoms. Half of the molecule, containing atoms like C11', C1', O1, C2' Co', P' etc., are generated via the inversion centre. The atomic numbering scheme and thermal displacement ellipsoids are shown in Figure 4.4. The selected geometrical parameters are given in Table 4.5 and the cone angle of the Phoban[3.3.1]-C_3NMe_2 ligand was calculated as 165°. The molecules packed in a linear fashion along the c-axis. The molecules seem to be independent and far from each other, indicating that significant forces of repulsion between them were not evident.

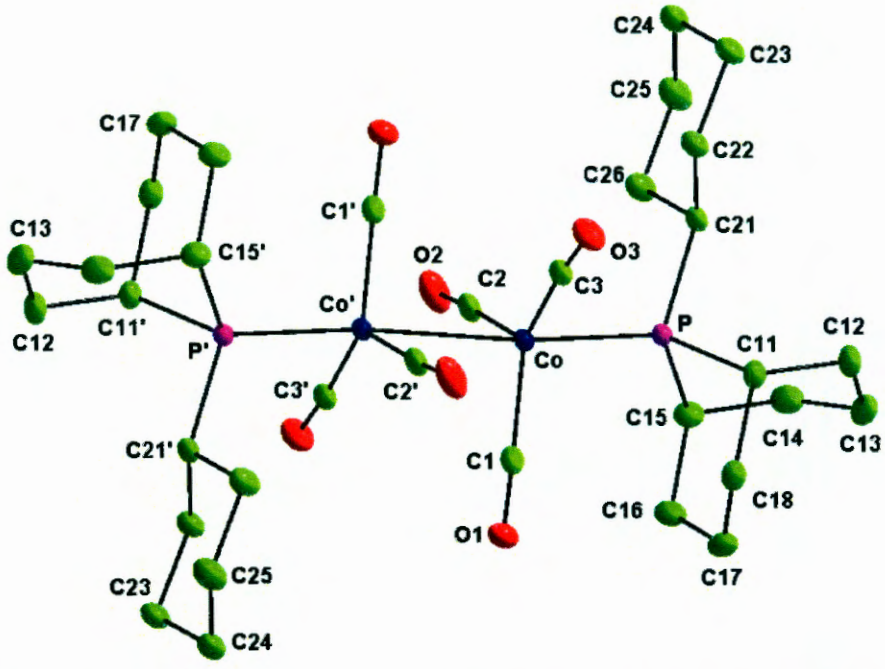

Figure 4.5: Molecular diagram showing the numbering scheme and displacement ellipsoids (50% probability) for $[Co(Phoban[3.3.1]\text{-}Cy)(CO)_3]_2$, the hydrogen atoms were omitted for clarity. Symmetry operators: ' = 1-x, -y,1-z.

4.3.1.5. $[Co(PA\text{-}C_5)(CO)_3]_2$

$\{[Co(PA\text{-}C_5)(CO)_3]_2\}_3.C_{10}H_{22}$ crystallises in the triclinic space group $P\bar{1}$ as three independent dimer molecules. Each of the molecules possesses an inversion centre and the three molecules crystallises with a single decane solvent molecule. The atomic numbering scheme and representative thermal ellipsoids are shown in Figure 4.6 for molecule 1.

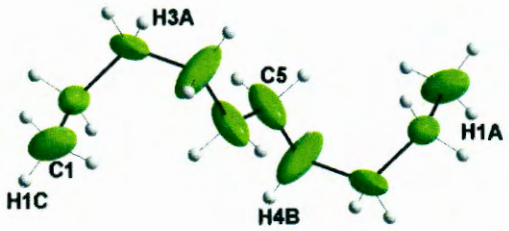

Figure 4.7: Decane molecule that crystallises with the three independent $\{[Co(PA\text{-}C_5)(CO)_3]_2\}_3$ molecules.

One of the dimer molecules has a 60/40% random disorder on the last three C atoms of the pentyl group as shown in Figure 4.8. The crystal structure of the PA-C_5 compound presented the opportunity to obtain geometrical data for three chemically equivalent molecules subjected to potentially different packing forces. The packing in the unit cell is governed by van der Waals forces alone, so no inter- or intramolecular hydrogen bonding were observed.

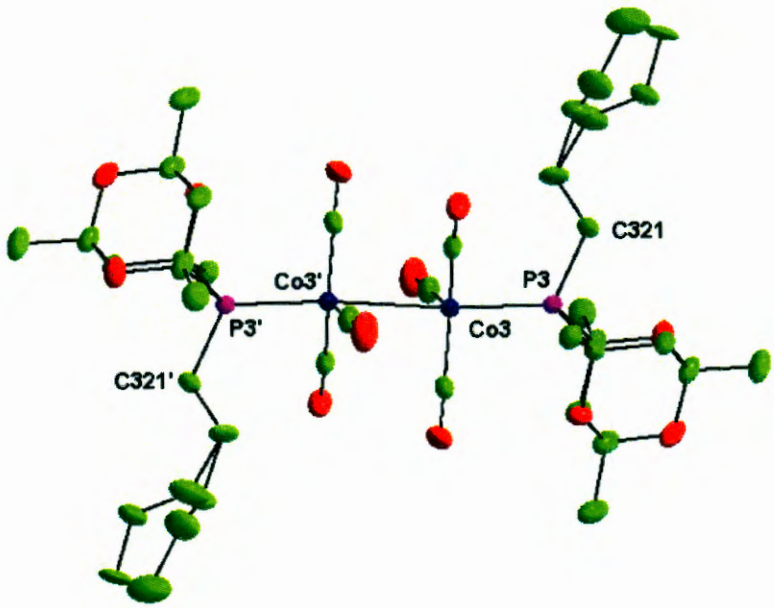

Figure 4.8: Molecular diagram showing the numbering scheme and displacement ellipsoids (30% probability) for molecule 3 of $\{[Co(PA\text{-}C_5)(CO)_3]_2\}_3.C_{10}H_{22}$, showing disorder on the pentyl side chain. Hydrogen atoms and the decane solvent molecule were omitted for clarity.

The Co-P bond distances 2.1887(13), 2.1882(11) and 2.1857(12) Å for molecules 1, 2, and 3 respectively as shown in Table 4.5 are almost identical.

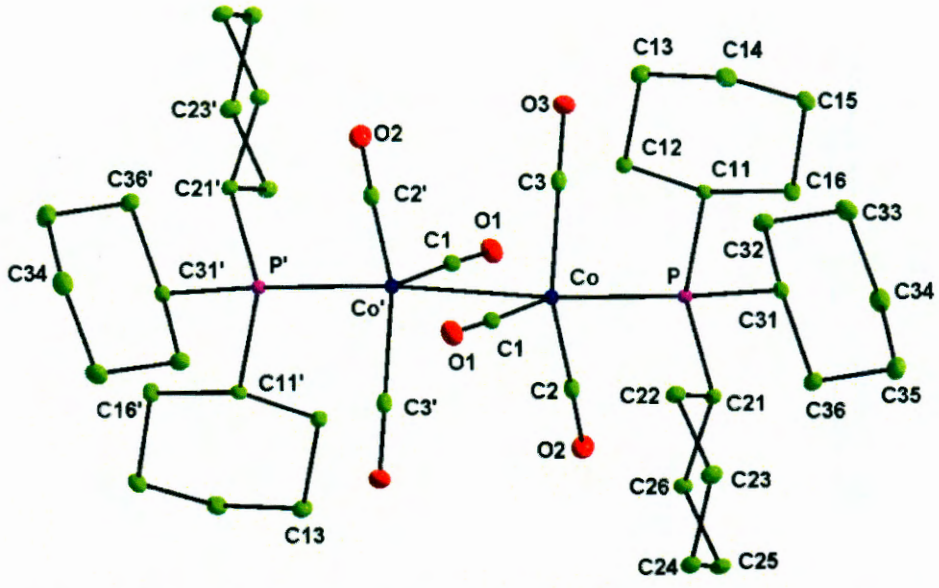

Figure 4.9: Molecular diagram showing the numbering scheme and thermal displacement ellipsoids (30% probability) for $[Co(PCy_3)(CO)_3]_2$; hydrogen atoms were omitted for clarity. Symmetry operators: ' = 1-x, 1-y, -z.

4.3.1.7. $[Co(PCp_3)(CO)_3]_2$

$\{[Co(PCp_3)(CO)_3]_2\}_2$ crystallises in the triclinic space group $P\bar{1}$ as two independent molecules each containing an inversion centre. The atomic numbering scheme and representative thermal ellipsoids for molecule 1 are shown in Figure 4.10.

withdrawing ligand in the series as reflected by the largest $^{1}J_{Se\text{-}P}$ coupling constant of 752 Hz, see Appendix A, Table A3.1.2. This accounts for the shorter average Co-P bond length of 2.1875(12) Å compared to the rest of the ligands. PCy_3 with a $^{1}J_{Se\text{-}P}$ coupling constant of 676 Hz is the most electron-donating ligand in the series. This induced higher electron density into the metal-metal bond resulting in the shortest Co-Co bond distance of 2.6478(3) Å, which represents the shortest Co-Co obtained in this study. The cone angles for all the Phoban derivatives reported are very similar ranging from 159 - 165° while the cone angles for the other ligands range from 169 - 174° for PCp_3 and PCy_3 respectively. The three carbonyls in all the dimers have staggered conformations at the Co atom relative to the Co' atom to which it is linked. Two sets of torsion angles ranging from 34.82(17) to 83.15(18) and 153.21(17) to 180.00(1) for all the seven cobalt complexes were observed as shown in Table 4.5.

In Table 4.6, the range of bond distance was established as Co-Co = 2.6478(3) - 2.707(3); Co-P = 2.1224(4) - 2.2074(9) and Co-C = 1.724(10) - 1.784(2) Å.

Both the Co-Co (0.059(3) Å) and Co-C (0.060(10) Å) bonds vary within a narrow range while the Co-P bonds (0.085(10) Å) are slightly more sensitive to the nature of the P-ligand. More specifically if the phosphite ligands are excluded from the range the Co-P (P = phosphine) range is 2.166(28) - 2.2074(9) Å, a difference of only 0.041(29) Å.

Table 4.6: Selected geometrical parameters for $[Co(L)(CO)_3]_2$ complexes.

Ligands	Co-Co / Å	Co-L_{avg} / Å	Co-C_{avg} / Å	Ref
Phoban[3.3.1]-C_2	2.707(3)	2.199(4)	1.765(13)	TW
$P(O\text{-}2,4\text{-}^tBu_2C_6H_3)_3$	2.706(5)	2.134(4)	1.776(9)	8
*IMes	2.6973(19)	1.925(10)	1.735(11)	9
Phoban[3.3.1]-C_5	2.6888(9)	2.2074(9)	1.775(3)	TW
Phoban[3.3.1]-C_3NMe_2	2.6885(8)	2.2049(9)	1.778(4)	TW
PCp_3	2.674(9)	2.207(9)	1.782(4)	TW
$P(O\text{-}Ph)_3$	2.6722(4)	2.1224(4)	1.784(2)	10
PA-C_5	2.6691(13)	2.1875(13)	1.781(6)	TW
PMe_3	2.669(1)	2.175(1)	1.772(3)	11
Lim-C_{18}	2.6687(12)	2.197(2)	1.724(10)	12
$PPh_2CH_2C(O)Ph$	2.666(1)	2.171(2)	1.770(7)	13
P^nBu_3	2.665(14)	2.178(15)	1.75(3)	14
$PPh_2CH_2P(O)Ph_2$	2.660(1)	2.185(1)	1.783(23)	15
$P(O\text{-}^iPr)_3$	2.6544(12)	2.1350(12)	1.769(6)	16
Phoban[3.3.1]-Cy	2.6526(10)	2.1963(8)	1.783(2)	TW
$AsPh_3$	2.649(2)	2.293(2)	1.780(2)	17
PCy_3	2.6478(3)	2.1949(3)	1.782(14)	TW

* IMes = 1,3-bis(2,4,6-trimethylphenyl)imidazol-2-ylidene.

---

8 R. Meijboom, M. Haumann, A. Roodt and L. Damoense, *Helv. Chim. Acta*, 2005, **88**, 676.

9 H. van Rensburg, R. P. Tooze, D. F. Foster and A. M. Z. Slawin, *Inorg. Chem.*, 2004, **43**, 2468.

10 M. Haumann, R. Meijboom, J. R. Moss and A. Roodt, *Dalton Trans.*, 2004, 1679.

11 R. A. Jones, M. H. Seeberger, A. J. Stuart, B. R. Whiylesey and T. C. Wright, *Acta Cryst.*, 1986, **C42**, 399.

12 A. Polas, J. D. E. T. Wilton-Ely, A. M. Z. Slawin, D. F. Foster, P. J. Steynberg, M. J. Green and D. J. Cole-Hamilton, *Dalton Trans.*, 2003, 4669.

13 P. Braunstein, D. G. Kelly, Y. Dusausoy, D. Bayeul, M. Lanfranchi and A. Tiripicchio, *Inorg. Chem.*, 1994, **33** 233.

14 J. A. Ibers, *J. Organomet. Chem.*, 1968, **14** 423.

15 R. Weber, U. Englert, B. Ganter, W. Keim and M. Möthrath, *J. Chem. Soc., Chem. Commun.*, 2000, 1419.

16 D. H. Farrar, A. J. Lough and A. J. Poë, *Acta Cryst.*, 1995, **C51** 2008.

17 P. Macchi, L. G. Gariaschelli, S. Martinengo and S. Sironi, *Inorg. Chem.*, 1998, **37**, 6263.

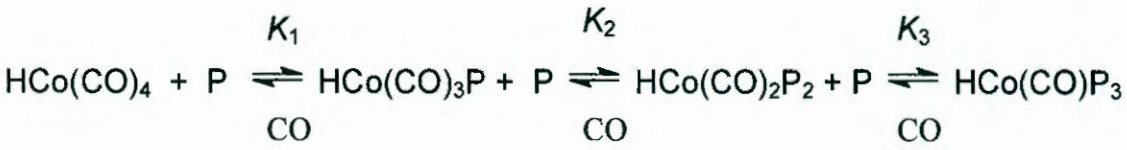

Figure 4.11: P/CO dependent equilibria for $HCo(CO)_{4-n}P_n$ (n = 0 - 3) species, where K_1 = equilibrium constant between modified and unmodified cobalt species, K_2 and K_3 are the equilibrium constants for the formation of the di- and tri- substituted phosphine hydrides.

However, not only ligand concentration influences the ratio of modified to unmodified catalytic species but also the nature of the ligand and the CO partial pressure employed. In the presence of an excess ligand some di- and tri- substituted phosphine hydrides, as shown in Figure 4.11, had been confirmed.[24] Since the coordinating ability of the ligands may differ and the differences in behaviour associated with modified and unmodified catalysis is so significant, it is imperative to compare the effect induced by different ligands at conditions resulting in an identical distribution between the modified and unmodified species. One way to achieve this is to conduct the reactions with different ligands under highly modified conditions to quantify the maximum effect that could be derived from each ligand while keeping all other variables constant (solvent, temperature and pressure).

In this study the hydroformylation catalysis of linear internal decene was compared for different Phoban derivatives under highly modified conditions. In order to do so hydroformylation reactions were performed at different ligand concentrations to verify that fully modified catalysis have been achieved for each ligand. Catalysis using P^nBu_3 under identical conditions were conducted as representative of conventional trialkyl phosphine behaviour. The kinetic and selectivity results for all the ligands utilized are shown in Table 4.7.

The observed first-order rate constants for all the ligand systems, given in Table 4.7, were obtained by fitting the kinetic data to the first-order rate expression given in Eqn. 4.1.

---

24 G. F. Pregaglia, A. Andreta, G. F. Ferrari and R. Ugo, *J. Organomet. Chem.*, 1671, **30**, 387.

with the cone angles differing from 132° to ~165° for P^nBu_3 and the Phoban[3.3.1] derivatives respectively.

The equilibrium constants K_1 as defined in Figure 4.11 can be calculated by Scientist fitting[25] of Eqns. (4.2) – (4.4) to the experimental concentration/catalytic parameter data, (where the catalytic parameter may be linearity or k_{obs}) with [Co] fixed and K_1, U_P (catalytic parameter associated with fully unmodified catalysis) and M_P (catalytic parameter associated with fully modified catalysis) as adjustable parameters, C denotes the observed catalytic behaviour at a specific set of conditions. Since all reactions were performed at constant syngas pressure, it was assumed that the CO and H_2 partial pressures remained constant and were thus included in the equilibrium constant for the given fixed set of conditions (temperature, pressure, reaction makeup and syngas ratio).

$$K_1 = [M]/([U][L_f]) \quad 4.2$$

$$C = (U_P[U] + M_P[M])/[Co] \quad 4.3$$

$$[M]^2K_1 + [M](-[Co]K_1 - K_1[L_a] - 1) + K_1[Co][L_a] = 0 \quad 4.4$$

In Eqns. 4.2 – 4.4, [Co] and $[L_a]$ refer to the total starting concentrations of cobalt and ligand respectively while [M], [U] and $[L_f]$ refer to the concentrations of the modified and unmodified species and the free ligand at equilibrium. The equilibrium concentrations of [U] = [Co] – [M] and $[L_f]$ in Eqns. 4.2 and 4.4 were calculated for each solution by using Eqn. 4.4. The concentration of ligand added is $[L_a] = [L_f] + [M]$. Since the value for U_P (fully unmodified catalysis) should be the same in the absence of all ligands at the given conditions it was fixed in the final calculations for K_1 (see Appendix B4.1). This mathematical manipulation was required due to the limited amount of data points for each ligand and significantly improved the statistics associated with the accuracy of the K_1 values. In addition, due to the limited data available, some values for K_1 were estimated by visually comparing simulated and experimental data and are given without s.u.'s in Table 4.11. It was found at lower ligand concentrations that the data points started deviating from the

---

25 *MicroMath Scientist for Windows, Version 2.01*, Copyright © 1986-1995, MicroMath, Inc.

	328	2.20	87.9	11.0	85.6			
Phoban-Cy	74	6.10	63.6	10.2	79.3	94 ± 16	165, 173	682, 703
	147	2.50	85.9	13.5	76.9			
	221	1.80	88.2	14.6	76.4			
	332	1.80	89.1	14.6	76.1			
Phoban-Ph	124	8.30	64.5	7.7	78.1	57 ± 15	167, 165	689, 717
	162	3.70	83.5	9.2	79.3			
	203	3.60	83.5	9.5	78.0			
	327	3.20	84.2	8.9	80.8			
	390	2.60	84.8	8.6	82.2			
	483	1.90	84.7	8.8	77.0			
*P^nBu_3	162	0.80	80.2	17.3	75.5		132	683
	239	0.70	80.4	17.0	75.9			
	325	0.60	80.7	16.6	76.8	> 150		

[$] Alcohol linearity.

[$$] Product yields calculated from the percentage molar ratio of the total products (aldehyde and alcohol) to the total olefins used during the reaction.

[$$$] Values for K_1 not containing s.u.'s are estimated, see Appendix B4.1.

* Cone angle not determined in this study and was taken from literature.[5]

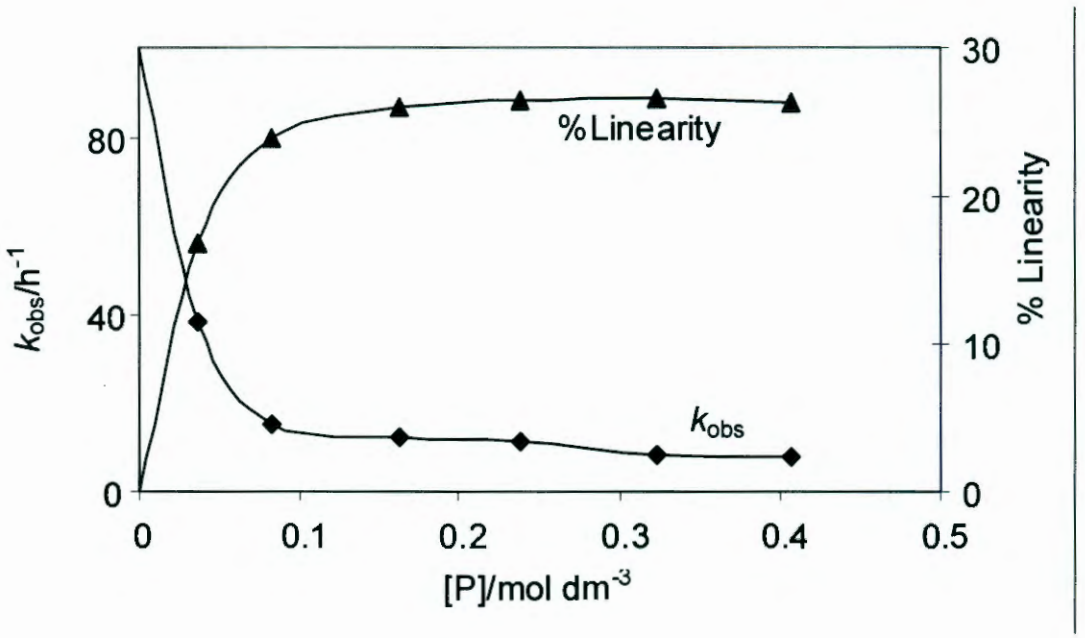

Figure 4.13: Linearity (%) of the alcohol fraction and k_{obs} (•) as a function of Phoban[4.2.1]-C_2 concentration, the solid lines represent Scientist fitting of the data points to eqns. 4.2 – 4.4, K_1 = 142 ± 15 mol^{-1} dm^3.

As shown from the study of the corresponding Phoban selenides in Chapter 3, the electronic differences induced by variation of the Q-substituent on the Phoban backbone at most could be described as moderate. In fact, the electronic differences between the [3.3.1] and [4.2.1] isomers were found to be much larger than any variation induced by changing the Q substituent. In addition, it was found that the cone angles are also very similar. From the data presented in Table 4.7, it is clear that fully modified catalysis for the less electron donating ligands ([4.2.1] isomers and Phoban-Ph) is reached at higher ligand concentrations as compared to the more electron rich [3.3.1] isomers. Feed losses through hydrogenation to the corresponding alkanes are lower for the less electron donating ligands but this advantage is offset by the formation of more aldol condensation products since hydrogenation of the aldehydes to alcohols are also less effective. The superiority of the Phoban family of ligands, in comparison to P^nBu_3, is clearly illustrated by the increased k_{obs}, higher selectivity towards linear alcohols and the higher yields.

Table 4.8: Rate and product distribution as a function of other phosphine ligands, [Co] = 13 mmol dm^{-3}, T = 180 °C, P = 60 bar (H_2:CO = 2:1).

Ligands	L:M	k_{obs}(± 0.01)/ h^{-1}	Conv./ %	Lin./ %	OH Yield/ %	Hydrog./ %	$^1J_{Se-P}$/ Hz	Tolman/ θ°
VCH-^{i}Bu	10:1	0.25	92.5	88.6	80.2	12.8	672, 687	~161[28]
PCy_3	10:1	0.15	91.4	84.7	69.5	22.5	676	174[28]
VCH-C_5	10:1	0.15	84.9	87.4	77.1	13.3	678	-
P^nBu_3	10:1	0.16	87.5	84.8	79.0	14.9	683	132[39]
Lim-C_5	11:1	0.41	97.8	83.2	86.8	9.0	684, 686	-
Phoban-C_5	8:1	0.38	95.5	90.8	83.4	10.0	686, 709	163[28]
PCp_3	13:1	0.10	81.2	84.8	56.1	40.2	687	169[28]
P^tBu_3	10:1	0.46	96.4	66.4	72.5	8.0	687	182[29, 30]
Lim-C_P	10:1	0.42	93.4	75.7	84.9	9.3	687, 690	-
P^iBu_3	10:1	0.26	97.8	73.2	82.8	11.9	688	143[30]
P(*p*-MeOPh)$_3$	8:1	0.13	13.8	77.8	41.4	12.4	708	145[5]
PPh_3	10:1	0.08	90.3	69.8	79.0	12.4	732	145[5]
PA-C_5	10:1	0.20	96.9	73.2	68.4	24.2	752	168[28]
P(2-furyl)$_3$	8:1	0.70	38.4	67.5	39.5	13.4	793	133[29]
Bislim	10:1	0.01	58.9	32.7	22.6	21.1	690, 690 689, 689	-

28 This work.

29 N. G. Andersen and B. A. Keay, *Chem. Rev.*, 2001, **101**, 997.

30 W. Cornely and B. Fell, *J. Mol. Catal.*, 1982, **16**, 89.

4.3.3.1. Effect of ligand electronic properties on modified cobalt hydroformylation

The results given in Table 4.8 are presented in a series of plots to relate the electronic nature of the ligands, as expressed in their first-order Se-P coupling constants ($^1J_{Se-P}$) to the catalytic results, Figures 4.14 – 4.16.

In general it was observed that the highly basic ligands would favour the modified complex according to the equilibrium in Figure 4.11.[31, 23] Increasing the concentration of the less basic ligands will affect the k_{obs} value more than the more basic ligands as more ligand will be required to reach fully modified conditions. The ligands used in the study could roughly be classified into three classes according to their relative reaction rates as shown in Figure 4.14: 0.1 - 0.2 h^{-1} (PCp_3, P(*p*-MeOPh)$_3$, PPh_3, PCy_3, VCH-C_5, P^nBu_3 and PA-C_5); 0.25 h^{-1} (VCH-^{i}Bu and P^iBu_3); 0.4 h^{-1} (Phoban-C_5, Lim-C_5 and Lim-C_P). The $^1J_{Se-P}$ coupling constant of the first class of ligands ranges from 676 to 752 Hz. The $^1J_{Se-P}$ coupling constant of the second and third class of ligands ranges from 672 to 687 Hz and 684 to 709 Hz. The overlapping in the ranges of the coupling constant indicates that the steric sizes of the ligands must also be playing a significant role.

These ligands cover a wide range of σ-donating abilities and exhibits reaction rates ranging from 0.1 – 0.4 h^{-1}, indicating that the electronic properties alone cannot explain the reactivity trend. Lim-C_5, Lim-Cp and Phoban-C_5 ligands that gave the highest observed rate constant also gave the highest product linearities (83 - 91%) and the lowest hydrogenation (9 - 10%).

---

31 R. J. Angelici and C. M. Ingemanson, *Inorg. Chem.*, 1969, **8**, 83.

The $^1J_{Se-P}$ coupling constants of four ligands (Phoban-C_5, PCp_3, Lim-Cp, P^iBu_3) were found to fall within the narrow range of 686 to 688 Hz but the product linearities associated with these differ significantly. The cone angle of Phoban-C_5 (163°) is smaller than that of PCp_3 (169°) and resulted in a higher product linearity. This was unexpected, as one would argue that the more bulky phosphine ligands should favour the formation of a less sterically crowded straight chain α-alkyl metal intermediate.[32] P^iBu_3 has the smallest cone angle (143°) and gave the least amount of linear product; unfortunately the cone angle for Lim-Cp is not known at this stage. Since the electronic properties of these ligands were similar while their steric sizes differ, the product linearities are therefore assumed to be influenced primarily by the steric effects of the ligands. A similar result was reported where phosphines with similar basicity but with different cone angles showed similar results in terms of product distribution in rhodium-catalysed hydroformylation of olefins.[32] The product linearities of the following ligands (VCH-^{i}Bu, PCy_3, VCH-C_5, P^nBu_3 and Lim-C_5) with $^1J_{Se-P}$ coupling constant ranging from 672 to 686 Hz decreased from 91 to 83%. Ligands with $^1J_{Se-P}$ coupling constant ranging from 688 to 752 Hz (P^iBu_3, P(*p*-MeOPh)$_3$, PPh_3 and PA-C_5) were more electron withdrawing and gave product linearities within the range 73 ± 5%. The results obtained in this study generally indicate that the $^1J_{Se-P}$ coupling constants of the ligands shows an inverse relationship with respect to the product linearities during modified cobalt hydroformylation with a few exceptions.

The effect of the electronic donating ability of the ligands (illustrated by their $^1J_{Se-P}$ coupling constant) on product yield as shown in Figure 4.16 indicate that PA-C_5, PCp_3 and PCy_3 ligands exhibited high hydrogenation and resulted in low yields of the total product. Lim-C_5, Lim-Cp and Phoban-C_5 catalysis were characterised by high product yields and low hydrogenation (6 - 10%). The higher yields obtained for the Lim ligand family, while maintaining

---

32 A. C. da Silva, K. C. B. De Oliveira, E. V. Gusevskaya and E. N. Dos Santos, *J. Mol. Catal. A: Chem.* 2002, **179**, 133.

4.3.3.2. Effect of ligand steric size on k_{obs} and product linearity

The effect of the steric sizes of the ligands, as expressed in term of their effective cone angle, on k_{obs} and product linearity is illustrated in Figures 4.17 and 4.18.

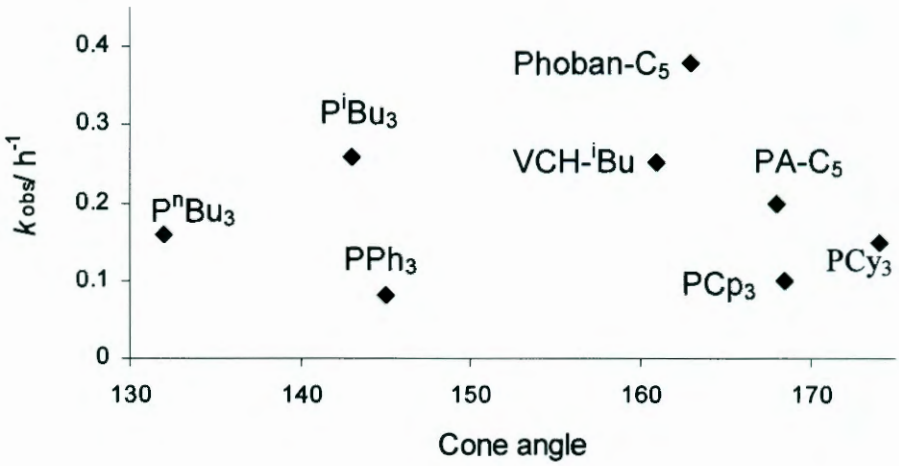

Figure 4.17: Effect of steric size of the ligands on the observe rate constant (k_{obs}) during modified cobalt hydroformylation of 1-octene.

All the ligands gave slower catalysis compared to the Phoban family over a wide range of cone angles indicating that the steric size of the ligands is probably not a determining factor in determining the rate of reaction.

The scattering of the points in Figure 4.18 indicate that the product linearities were independent of the cone angles of the ligands.

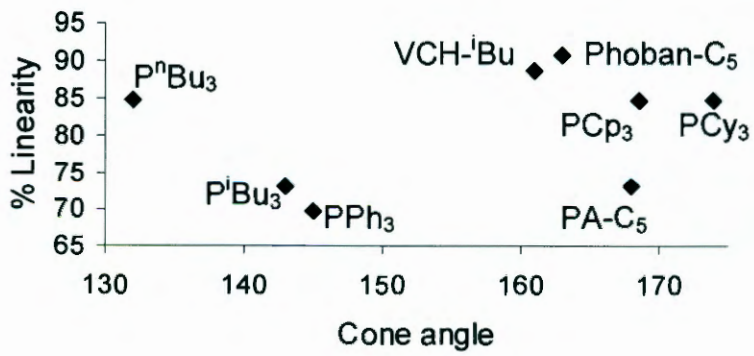

Figure 4.18: Effect of steric size of the ligands on % product linearity during modified cobalt hydroformylation of 1-octene.

hydrogenation of olefins during hydroformylation has been reported.[34] An electron withdrawing bulky phosphite, $P(OPh)_3$ (L:Co = 4) when used in the hydroformylation of 1-pentene showed no significant hydrogenation of the olefin and product hexanal to the corresponding pentane and hexanol respectively.[35] In general, the results obtained from this study seem to indicate that the electronic property of the ligands is not a driving force in olefin hydrogenation.

Even though some ligands with low reaction rates also gave low hydrogenation all the ligands giving hydrogenation > 20% had low reaction rates. None of the ligands displaying high reaction rates (> 0.4 h^{-1}) gave hydrogenation greater than 10%, see Figure 4.20.

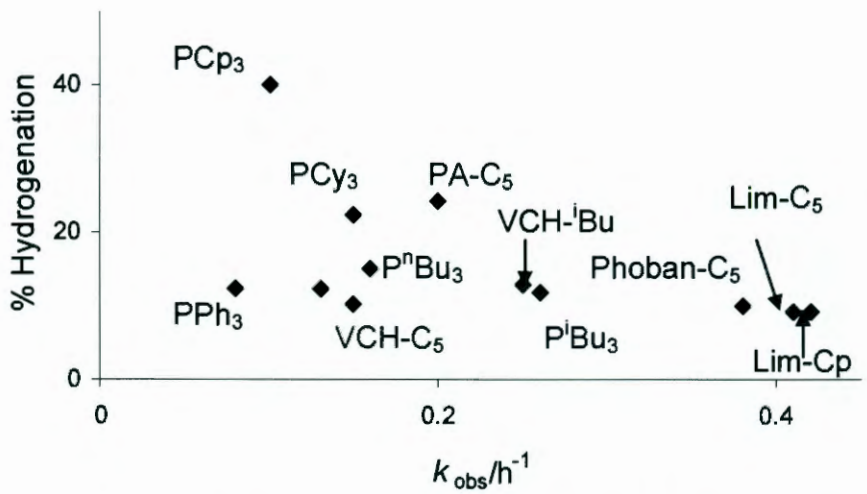

Figure 4.20: Effect of the reaction rate (k_{obs}) on the % hydrogenation during modified cobalt hydroformylation of 1-octene.

It is accepted that the k_{obs} of modified cobalt-catalysed hydroformylation is governed by dissociative CO substitution by the substrate olefin to give the π-complex.[36, 37, 38] It is thus expected that electron donating ligands will

34 E. R. Tucci, *Ind. Eng. Chem. Prod. Res. Develop.*, 1970, **9(4)**, 516.

35 M. Haumann, R. Meijboom, J. R. Moss and A. Roodt, *Dalton Trans.*, 2004, 1679.

36 a) R. F. Heck and D. S. Breslow, *J. Am. Chem. Soc.*, 1961, **83**, 4023; b) R. F. Heck and D. S. Breslow, *J. Am. Chem. Soc.*, 1962, **84**, 2499.

37 R. Whyman, *J. Organomet. Chem.*, 1974, **81**, 97.

Electron donating ligands on the cobalt metal will facilitate the alkyl migration process whereas electron-withdrawing ligands will strengthen the Co-alkyl bond making the process less feasible.[48] Generally slow alkyl migration will increase the residence time of the alkyl intermediate thereby creating the possibility of the alkyl complexes to react with either H_2 or $[HCo(CO)_3P]$ to form alkanes.[49, 50, 51]

Another possible explanation for the formation of paraffinic by-products during modified cobalt hydroformylation is the presence of a bisphosphine hydride species, $[HCo(CO)_2P_2]$, as suggested by Pregaglia and co-workers.[24] The formation of such disubstituted cobalt hydride species have been reported for P^nBu_3[41] and PCy_3.[52, 53] It was also shown that the formation of this disubstituted phosphine hydride was influence by the steric size of the ligands.[24, 22] The results obtained in this study as indicated in Figure 4.21 showed that hydroformylation with PCp_3, PA-C_5 and PCy_3 gave the highest paraffinic by-product among all the ligands studied even though they were the most bulky ligands in the series.

P^nBu_3 was one of the smallest ligands in terms of steric size (132°), but gave hydrogenation of only 15%. Lim and Phoban-C_5 (163°) which are more bulky than P^nBu_3, gave hydrogenation of 9 and 10% respectively. It is thus clear that the formation of bisphosphine complexes cannot be the only justification for the formation of the paraffinic by-product during modified cobalt hydroformylation as they could not explain why the three most bulky ligands

---

48 N. M. Makunya, R. Meijboom, A. Muller and A. Roodt, *J. Organomet. Chem.*, 2005, **690**, 4159.

49 N. Koga, C. Daniel, J. Han, X. Y. Fu and K. Morokuma, *J. Am. Chem. Soc.*, 1987, **109**, 3455.

50 C. N. Rowley, H. M. Foucault, T. K. Woo and D. E. Fogg, *Organometallics*, 2008, **27(8)**, 1661.

51 R. Tannenbaum and G. Bor, *J. Mol. Catal. A: Chem.*, 2004, **215**, 33.

52 C. Godard, S. B. Duckett, S. Polas, R. Tooze and A. C. Whitwood, *J. Am. Chem. Soc.*, 2005, **127(14)**, 4994.

53 C. Godard, S. B. Duckett, S. Polas, R. Tooze and A. C. Whitwood, *Dalton Trans.*, 2009, 2496.

aldehydes formed during the hydroformylation process correspond to the original position of the double bond in the olefins used.[30] The sum of the alcohol products and paraffins only accounted for ~44% of the converted substrate. If the conversion of the intermediate aldehydes to alcohols is slow (in accordance with the overall reaction) it can be expected that significant amounts are converted, via aldol condensation reactions, to undesired heavies. It is well known that the linear isomers would undergo heavies formation preferentially to branched isomers and would account for the low linearity of only 33% of the alcohol total products.

4.3.3.5. The mechanism of modified cobalt hydroformylation

From the results obtained in this study, and in agreement with literature[22, 36] a generalized mechanism for modified cobalt hydroformylation is given in Figure 4.22. According to Kirch and Orchin, all reaction steps are reversible except the hydrogenolysis step converting the acyl complex (**e**) to the corresponding aldehyde.[54] The aldehydes formed underwent hydrogenation to the corresponding alcohols through a series of reaction stages in the same reaction mixture.[34] The amount of olefin hydrogenated during the process is governed by the reaction between (**d**) and (**e**) and could be influence by the H_2/CO partial pressures, rate of alkyl-migration as well as the size and the electronic properties of the ligands. Even though there are different views as to whether step (**d**) to (**e**) occur through the H_2 or [$HCo(CO)_3P$] pathways[55], kinetic studies have supported the H_2 pathway.[51]

---

54 L. Kirch and M. Orchin, *J. Am. Chem. Soc.*, 1959, **81**, 3397.

55 http://chemistry.lsu.edu/stanley/webpub/4571-chapt16-hydroformylation.pdf, accessed on the 11/10/2009.

Whyman suggested that, irrespective of the olefin used during the hydroformylation process, the k_{obs} of the reaction is controlled by dissociative CO substitution.[37] This suggestion does not agree with the results of this study as the Lim-C_5, Lim-Cp and the Phoban ligands which are relatively good electron donors gave very high reaction rates and low paraffin formation. PA-C_5, PCy_3 and PCp_3, which are the most bulky ligands and PA-C_5 the most electron withdrawing, gave very slow catalysis and high hydrogenation. Based on Whyman's proposed rate-limiting step, one would expect these ligands to give relatively fast catalysis.

It is important to realise that even though the rate-limiting step is dissociative CO substitution, the alkyl-migration step (**d**) to (**e**) could also influence the overall rate of the reaction.

4.4. Conclusions

- Crystal structures of the cobalt dimers of the following ligands; Phoban[3.3.1]-C_2, Phoban[3.3.1]-C_5, Phoban[3.3.1]-C_3NMe2, Phoban[3.3.1]-Cy, PA-C_5, PCy_3, and PCp_3 were obtained.

  The P-Co-Co bond angles indicate that the molecules of all seven cobalt dimer structures deviate slightly from linearity and ranges from 170.49(3) to 174.39(13)° for the Phoban derivatives and 172.76(4) to 175.855(13) for PA, PCp_3 and PCy_3 respectively.

  Both the Co-Co (0.062(5) Å) and Co-C (0.060(10) Å) bonds vary within a narrow range while the Co-P bonds (0.085(10) Å) are slightly more sensitive to the nature of the P-ligand. The Co-P bond distances ranges from 2.1963(8) to 2.2074(9) Å for the Phoban derivatives and 2.1875(12) and 2.2071(10) for PA-C_5, PCy_3 and PCp_3 respectively. The shorter Co-P bond distance of the PA-C_5 ligand (2.1875(13) Å) compared to those of PCy_3 (2.1949(3) Å) and PCp_3 (2.207(9) Å) could be attributed to the higher electron withdrawing ability of the former.

even at high ligand concentrations. For that reason, these ligands were excluded from further discussion.

The Phoban-C_5 and the Lim ligand family generally gave the most active systems (0.38 and 0.41h^{-1}) and high product linearities (91 and 78 - 83%) and yields (83 and 85 – 87%) respectively compared to the rest of the ligands. A steric window was identified within which optimal hydroformylation occurs with the cone angle of 163° for the Phoban-C_5 ligand as the upper limit.

The ligands were also divided into two groups based on their hydrogenation capabilities. The first set of ligands, PCp_3 (169°), PA-C_5 (168°) and PCy_3 (174°), gave hydrogenation of 40, 25 and 22% respectively. All the other ligands fall within the second set ranging from P^nBu_3 (132°) to the Lim ligand family with hydrogenation of 9 - 15%. Bisphosphine cobalt hydrides thus could not be the only justification of paraffin formation during modified cobalt hydroformylation as the three bulkiest ligands gave the highest hydrogenation. All reactions displaying high reactivity gave low hydrogenation.

The bisphosphine ligand, Bislim, gave very slow catalysis (0.01 h^{-1}), low conversion and a high hydrogenation of 21% indicating that bisphosphine complexes to have a low impact on the overall catalysis as compared to more reactive systems (Lim-C_5, Lim-Cp and Phoban-C_5 > 0.4 h^{-1}).

5 Iodomethane oxidative addition and CO insertion in Rh-phosphine complexes

5.1. Introduction

The reaction of MeI with Rh(I) complexes of phosphine ligands have been shown to be an effective way to study the formation of metal alkyl and acyl complexes. Roodt and co-workers[1] manipulated the reactivities of the Rh(I) centre in the [Rh(BID)(CO)(PR_3)] type of complexes where PR_3 = monodentate phosphine ligands and BID = monoanionic bidentate ligands such as acetylacetonato[2] (acac), substituted acetylacetonato ligands[3], 8-hydroxyquinolinato[4] (ox) and cupferrato (cupf)[5]. The BID ligands contained donor atoms such as oxygen, nitrogen and sulphur. The intention was to study the reaction rates and equilibria involved in these reactions. The results illustrated that both *cis*- and *trans*-addition of the MeI may occur to the Rh(I) centre forming the corresponding *cis*- or *trans*- alkyl species, as in the case of *cis*-[Rh(I)(cupf)(CO)(CH_3)(PPh_3)][5] or *trans*-[Rh(I)(ox)(CO)(CH_3)(PPh_3)][4] respectively. The acyl complex such as [Rh(I)(Sacac)(COMe)(PPh_3)] was observed as the primary product when a bidentate ligand containing a sulphur atom was used.[6, 7] In this case the rate of disappearance of the Rh(I) acac complex was the same as the rate of formation of its acyl product with a small amount of the intermediate alkyl complex

---

1 A. Roodt and G. J. J. Steyn, in: S. G. Pandalai (Ed), *Res. Research Dev. Inorg. Chem., Transworld Research Network*, Trivandrum, 2000, **2**, 1.

2 S. S. Basson, J. G. Leipoldt, A. Roodt, J. A. Venter and T. J. van der Walt, *Inorg. Chim. Acta*, 1986, **119**, 35.

3 S. S. Basson, J. G. Leipoldt and J. T. Nel, *Inorg. Chim. Acta*, 1984, **84**, 167.

4 K. G. Van Aswegen, J. G. Leipoldt, I. M. Potgieter, G. J. Lamprecht, A. Roodt and G. J. Van Zyl, *Transition Met. Chem.*, 1991, **16**, 369.

5 S. S. Basson, J. G. Leipoldt, A. Roodt and J. A. Venter, *Inorg. Chim. Acta*, 1987, **128**, 31.

6 C. H. Cheng, B. D. Spivack and R. Eisenberg, *J. Am. Chem. Soc.*, 1977, **99**, 3003 and references there in.

7 J. G. Leipoldt, S. S. Basson and L. J. Botha, *Inorg. Chim. Acta*, 1990, **168**, 215.

The reactivity of the square planar rhodium monocarbonylphosphine complexes of the type [Rh(R'COCHCOR")(CO)(PPh_3)], where R' = Phenyl and R" = $(CH_2)_nCH_3$, in the oxidative addition reaction with MeI was reported. The focus was on varying the steric and electronic properties of the R' and R" groups to determine their effect on the oxidative addition of iodomethane to the Rh(I) complexes. The results suggested that an increase in the electron-donating ability of the R' and R" groups speeds up the oxidative addition reaction, but the sizes of the alkyl groups did not affect the rate of the reactions.[9]

The Eyring equation describes the temperature dependence of reaction rates and can be used to calculate the activation parameters for a reaction. Unlike the Arrhenius equation that can be applied to gaseous reaction only, the Eyring equation can be applied to the gaseous solutions as well as mixed phase reactions,[10] and is a theoretical derivation based on a transition state model. The principle behind the transition state theory involves a thermodynamic equilibrium between the transitory molecular species known as the activation complex and the reactants. The activated complex is the configuration of the atoms that corresponds energetically to the top of the energy barrier separating the reactants from the products.[11] The Eyring equation is given in Eqn. 5.4:

$$\ln(k/T) = -\Delta H^{\neq}/(R.T) + \ln(k_B/h) + \Delta S^{\neq}/R \qquad 5.4$$

The activation enthalpy and entropy are related to the Gibb's free energy of activation according to Eqn. 5.5:

$$\Delta G^{\neq} = \Delta H^{\neq} - T.\Delta S^{\neq} \qquad 5.5$$

---

9 N. F. Stuurman and J. Conradie, *J. Organomet. Chem.*, 2009, **694**, 259.

10 http://www.uni-r.de/Fakultaeten/nat_Fak_IV/Organische_Chemie/Didaktik/Keusch/eyr-e.htm, accessed on the 24/12/2009.

11 J. A. Ibemesi, *Physical Chemistry for Tertiary Institution*, University of Nigeria, Nsukka, 1994, 313.

5.2. Synthesis and spectroscopic characterisation of [Rh(acac)(CO)(P-Ph)] complexes

5.2.1. General experimental procedure

All manipulations involving air sensitive compounds were conducted in Schlenk glassware under an argon atmosphere using degassed solvents. ^{1}H, ^{13}C and ^{31}P NMR spectra were recorded as $CDCl_3$ solutions on a Varian Unity spectrometer operating at 400.428, 100.698 and 162.109 MHz, respectively. The spectra were calibrated relative to the solvent peaks for ^{1}H and ^{13}C and relative to an external standard of 85% H_3PO_4 at 0 ppm. For the IR spectroscopy the CO stretching frequencies, ν(CO), are reported as solutions in DCM.

5.2.1.1 Chemicals

Toluene (Riedel de Haen, 99%), DCM (Saarchem, 99%), $CDCl_3$ (Aldrich, 99%), $Pd(OAc)_2$ (Aldrich, 98%), acetonitrile (E-Lab. D. L, 99.9%), triethylamine (Fluka, 99.5%), hexane (Aldrich, 99%), acetone (Saarchem, 99.5%), [Rh(acac)$(CO)_2$] (Aldrich, 98%), PhI (Fluka, 99%), HCl (Aldrich, 37%), Na_2CO_3 (Saarchem, 99%), $MgSO_4$ (Promark Chemicals, 99.5%), Phoban-H (Rhodia, 60% m/m in toluene), Lim-H (Cytec, 40% m/m in toluene),VCH-H (Cytec, mixture of primary and secondary phosphines), PA-H (Cytec, 99%), neutral alumina (Aldrich, 99%) were used as received. All solvents were of the highest purity available and were dried according to standard procedures[15] where applicable.

---

15 W. L. F. Armarego and C. L. L. Chai, *Purification of Laboratory Chemicals*, Fifth Edition.

All the complexes were prepared according to the procedure as described in section 5.2.2.1.

5.2.2.1. Synthesis of [Rh(acac)(CO)(Phoban[3.3.1]-Ph)]

To a Schlenk tube containing a solution of $[Rh(acac)(CO)_2]$ (14.0 mg, 0.0542 mmol) in DCM (3 mL) was added a ligand solution containing Phoban[3.3.1]-Ph in DCM (2.9 mL, 18.97 mM, 0.0547 mmol) to give the product. The solvent was removed by passing a stream of nitrogen gas over the reaction mixture resulting in reddish brown oil. Treating the oil with few drops of diethyl ether and removal of the solvent under vacuum gave a yellowish powder, yield = 19.21 mg, 79%.

^{1}H NMR ($CDCl_3$): δ_H 1.40 - 2.21(m, 14H, 2CH, $6CH_2$), 1.86 (s, 3H, CH_3-acac, *cis* to phosphine), 2.01 (s, 3H, CH_3-acac, *trans* to phosphine), 5.41 (s, 1H, CH-acac), 7.30 - 7.39 (m, 3H, ArH), 7.39 - 7.46 (m, 2H, ArH).
^{31}P NMR ($CDCl_3$): δ_P 33.9 (d, $^1J_{Rh\text{-}P}$ = 164 Hz).

^{13}C NMR ($CDCl_3$): δ_C 189.87 (dd, $^1J_{Rh\text{-}C}$ = 77 Hz, $^2J_{P\text{-}C}$ = 25 Hz).
IR ν(CO) = 1962 cm^{-1} (s)

5.2.2.2. Synthesis of [Rh(acac)(CO)(Phoban[4.2.1]-Ph)]

After trituration, a yellowish brown powder was obtained, yield = 17.27 mg, 71%.
^{1}H NMR ($CDCl_3$): δ_H 1.49 - 2.18 (m, 14H, 2CH, $6CH_2$), 1.95 (s, 3H, CH_3-acac, *cis* to phosphine), 2.03 (s, 3H, CH_3-acac, *trans* to phosphine), 5.45 (s, 1H, CH-acac), 7.25 - 7.42 (m, 3H, ArH), 7.48 - 7.62 (m, 2H, ArH).
^{31}P NMR ($CDCl_3$): δ_P 65.1 (d, $^1J_{Rh\text{-}P}$ = 161 Hz).
^{13}C NMR ($CDCl_3$): δ_C 189.39 (dd, $^1J_{Rh\text{-}C}$ = 76 Hz, $^2J_{P\text{-}C}$ = 26 Hz).
IR ν(CO) = 1963 cm^{-1}(s)

4R, 8S-Lim

^{1}H NMR ($CDCl_3$): δ_H 0.60 - 2.10 (m, 12H, 4CH, $4CH_2$), 1.01-1.03 (d, 3H, CH_3 on 4R, 8S-carbon), 1.80 (d, 3H, CH_3 on 8S-carbon), 1.85 (s, 3H, CH_3-acac, *cis* to phosphine), 2.01 (s, 3H, CH_3-acac, *trans* to phosphine), 5.38 (s, 1H, CH-acac), 7.29 - 7.41 (m, 3H, ArH), 7.58 - 7.74 (m, 2H, ArH).

^{31}P NMR ($CDCl_3$): δ_P 20.7 (d, $^1J_{Rh\text{-}P}$ = 163 Hz).

^{13}C NMR ($CDCl_3$): δ_C 190.16 (dd, $^1J_{Rh\text{-}C}$ = 78 Hz, $^2J_{P\text{-}C}$ = 24 Hz).

4S, 8S-Lim

^{1}H NMR ($CDCl_3$): δ_H 0.60 - 2.10 (m, 12H, 4CH, $4CH_2$), 0.80 - 0.81 (d, 3H, CH_3- on 4S, 8S-carbon), 1.81 (d, 3H, on 8S-carbon), 1.83 (s, 3H, CH_3-acac, *cis* to phosphine), 2.01 (s, 3H, CH_3-acac, *trans* to phosphine), 5.39 (s, 1H, CH-acac), 18.51 (d, $^1J_{Rh\text{-}P}$ = 162 Hz), 7.29 - 7.41 (m, 3H, ArH), 7.58 - 7.74 (m, 2H, ArH).

^{31}P NMR ($CDCl_3$): δ_P 18.5 (d, $^1J_{Rh\text{-}P}$ = 162 Hz).

^{13}C NMR ($CDCl_3$): δ_C 189.96 (dd, $^1J_{Rh\text{-}C}$ = 79 Hz, $^2J_{P\text{-}C}$ = 24 Hz).

IR ν(CO) = 1967 cm^{-1}(s)

5.2.2.5. Synthesis of [Rh(acac)(CO)(PA-Ph)]

Yellow crystals of the complex suitable for X-ray data collection was obtained from slow evaporation of a 1:1 mixture of acetone and DCM. Details of the crystallographic characterisation are discussed in section 5.2.2.8, yield = 22.10 mg, 78%.

^{1}H NMR ($CDCl_3$): δ_H 1.42 - 1.43 (d, 6H, equivalent CH_3- bicyclic ring), 1.34 - 1.38 (d, 3H, CH_3-bicyclic ring away from CO), 1.69 - 1.72 (d, 3H, CH_3-bicyclic ring closer to CO), 1.20 - 2.20 (m, 14H, 2CH, $6CH_2$), 46.13 (d, $^1J_{Rh\text{-}P}$ = 183 Hz), 1.47 (s, 3H, CH_3-acac, *cis* to phosphine), 2.07 (s, 3H, CH_3-acac, *trans* to phosphine), 5.39 (s, 1H, CH-acac), 7.30 - 7.45 (m, 3H, ArH), 8.18 - 8.30 (m, 2H, ArH).

^{31}P NMR ($CDCl_3$): δ_P 46.1 (d, $^1J_{Rh\text{-}P}$ = 183.0 Hz).

^{13}C NMR ($CDCl_3$): δ_C 188.58 (dd, $^1J_{Rh\text{-}C}$ = 75 Hz, $^2J_{P\text{-}C}$ = 23 Hz).

IR ν(CO) = 1984 cm^{-1}(s)

The CO stretching frequencies of the complexes were very similar for all the ligands, ranging from 1962 – 1967 cm^{-1}, except that of PA-Ph (1984 cm^{-1}) which was significantly higher. This implies that the PA-Ph ligand is more electron withdrawing than the rest of the ligands. The $^{1}J_{Rh-P}$ coupling constants for the complexes of Phoban[3.3.1]-Ph, Phoban[3.3.1]-Ph, the two isomers of VCH-Ph and the two isomer of Lim-Ph were similar ranging from 161 - 164 Hz while that for PA-Ph (183 Hz) confirming that the latter ligand was the most electron withdrawing in the series. Electron withdrawing ligands such as PA-Ph will weaken the Rh-CO bond, account for the smaller $^{1}J_{Rh-C}$ coupling constant of 75 Hz compared to the rest of the complexes whose $^{1}J_{Rh-C}$ coupling constant ranges from 76 – 79 Hz. The similarities of the $^{1}J_{Rh-C}$ and $^{1}J_{Rh-P}$ for the Phoban, VCH and Lim ligands indicate that these ligands did not differ significantly in basicity.

5.2.2.7. ^{31}P NMR characterisation of the Rh(III) alkyl and acyl complexes

The $^{1}J_{Rh-P}$ coupling constants for the Rh(III) alkyl and acyl complexes ranges from 119 to 130 Hz and 142 to 150 Hz respectively as shown in Table 5.2. These values agree with those reported in similar systems elsewhere.[8] The $^{1}J_{Rh-P}$ coupling constant for the *cis*- and *trans*- Rh(III) alkyl species of the two Lim-Ph isomers could not be obtained from the ^{31}P NMR spectrum as the oxidative addition was very fast. The first-order Rh-P coupling constants for the Rh(III) acyl complexes of PA-Ph, Phoban[3.3.1]-Ph and VCH-Ph could also not be obtained because of the slow migratory CO-insertion. The complexes tend to decompose forming some unknown peaks when allowed to stand for over 3 – 4 days to enable the Rh(III) alkyl to convert to the corresponding acyl complexes.

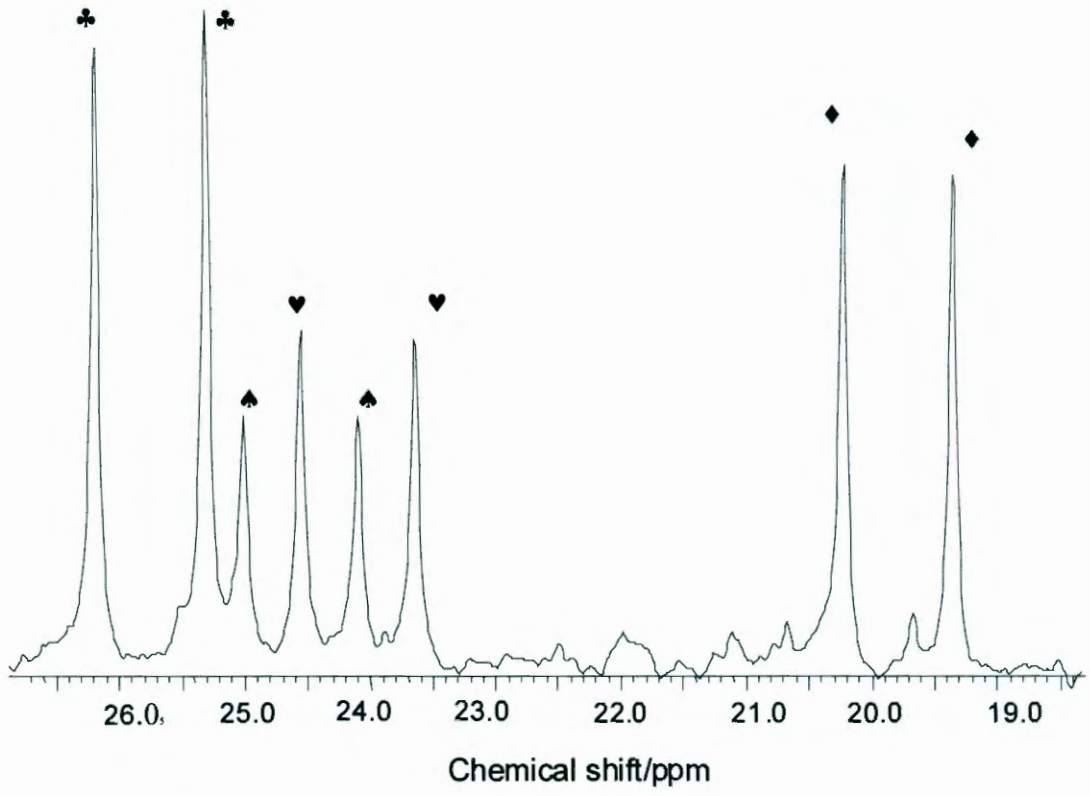

Figure 5.3: ^{31}P NMR spectrum showing the coupling of the Rh(III) acyl complex of the Lim-Ph system, solvent = DCM, [Rh] = 0.1 M, [MeI] = 0.2 M, number of NMR scans = 10000.

The couplings (♣) and (♦) correspond to the Rh(III) acyl species of 4S, 8S-Lim-Ph while (♠) and (♥) correspond to those of the 4R, 8S-Lim-Ph system derived from the *cis* and *trans* Rh(III) alkyl complexes. The presence of a larger amount of the Rh(III) acyl corresponding to the 4S, 8S-Lim-Ph compared to that of the other isomer could be attributed to the higher rate of formation of the former complex.

5.3. Crystallographic characterisation of complexes

The data collection of the crystals obtained in §5.2.5 and §5.2.6 was carried out on a Bruker X8 ApexII 4K Kappa CCD diffractometer using ϕ-scans and Mo K_α (0.71073 Å) radiation from a sealed tube. All reflections were merged and

Table 5.3: Crystallographic data and refinement parameters for [Rh(acac)(CO)(4R, 8S-Lim-Ph)] and [Rh(acac)(CO)(PA-Ph)]$_2$.

		4R, 8S-Lim-Ph	**PA-Ph**
Emp. formula		$C_{22}H_{30}O_3PRh$	$C_{22}H_{28}O_6PRh$
Form. weight		476.34	522.34
Crystal system		Monoclinic	Monoclinic
Space group		$P2_1$	$P2_1/c$
a / Å		7.6845(8)	18.5191(4)
b / Å		10.4236(9)	13.7525(4)
c / Å		13.1851(14)	19.0069(4)
α / °		90.00	90.00
β / °		100.041(3)	108.264(10)
γ / °		90.00	90.00
V / Å^3		1039.95(18)	4596.89(10)
Z		2	8
D_c / g.cm^{-3}		1.521	1.488
T / K		100(2)	100(2)
μ / mm^{-1}		0.917	0.844
F(000)		492	2092
Crystal size / mm		0.31x0.25x0.25	0.27x0.32x0.37
θ limit / °		1.57 to 28.42	1.16 to 28.29
Index ranges		$-6 \le h \le 10$	$-24 \le h \le 24$
		$-8 \le h \le 13$	$-18 \le h \le 18$
		$-17 \le h \le 15$	$-22 \le h \le 25$
Collected reflections		5327	32984
Unique reflections		3734	11420
R_{int}		0.030	0.045
Observed reflections (I>2σI)		3387	8091
Data / restraints / parameters		3734/1/248	11420/0/553
GooF		1.055	1.025
Absolute structure parameter		0.05(4)	-
R (I>4(σ)I)	R^a	0.0347	0.0362
	wR^b	0.0700	0.0742
R (all data)	R	0.0398	0.0599
	wR	0.0747	0.0865
$\Delta\rho_{max}$; $\Delta\rho_{min}$/ e.Å^{-3}		0.937; -0.523	0.684; -0.694

a) $R = [(\Sigma\Delta F)/(\Sigma F_o)]$ b) $wR = \Sigma[w(F_o^2 - F_c^2)^2]/\Sigma[w(F_o^2)^2]^{1/2}$

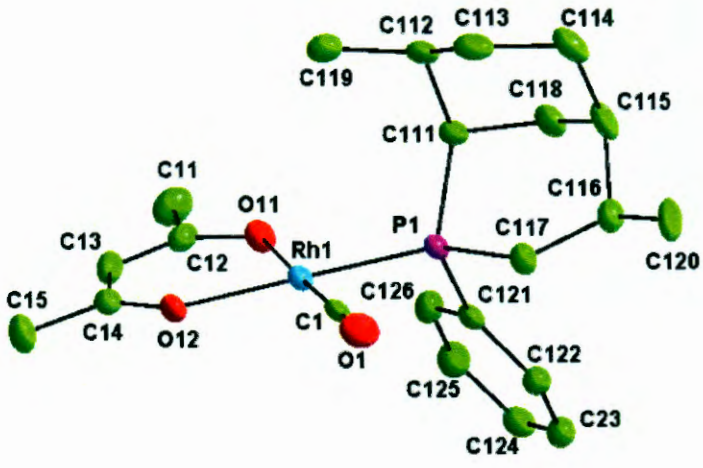

Figure 5.4: Molecular diagram showing the numbering scheme and displacement ellipsoids (30% probability) for [Rh(acac)(CO)(4R, 8S-Lim-Ph)]. In the numbering scheme, the first digit indicates the molecule number (n); second and third digits indicate numbers of the atom in the molecule. H-atoms are omitted for clarity.

The larger *trans* influence of the phosphine ligand with respect to the carbonyl ligand was indicated by the longer average Rh-O bonds of 2.0751(18) and 2.068(3) Å *trans* to PA-Ph and Lim-Ph respectively as compared to bond distances of Rh-O bond 2.037(19) and 2.049(3) Å respectively *trans* to the carbonyl ligand, see Table 5.4. The Rh(I) complexes of the two ligands showed deviation from the square planar geometry as indicated in Figures 5.4 and 5.6. The slightly longer Rh-C bond in the PA (1.817(3)) Å structure as compared to the Lim structure (1.800(5)) Å could be attributed to the weaker back bonding because of the higher electron withdrawing ability of the PA ligand. The bite angles of the acac moieties were very similar for both structures at 88.75(7) and 89.49(13)° for PA and Lim respectively. PA exhibits a slightly higher compression on the bond angle than the Lim ligand as the average C_1-Rh_1-P_1 angle of 92.63(9) for PA was larger than that of Lim (91.00(15)°). This compression did not affect the C_1-Rh_1-O_{12} angles, as they were similar in both cases. This analysis suggests that the steric demand for PA was larger than that of Lim, which is in agreement with their cone angles that were calculated as 165 and 158° respectively.

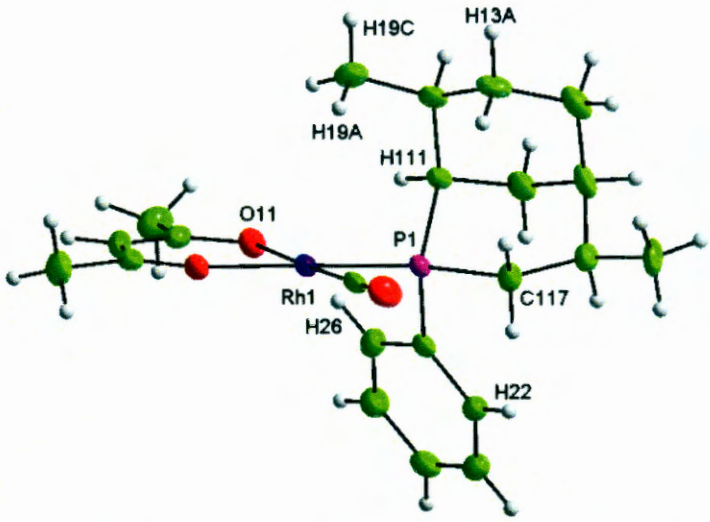

Figure 5.5: Numbering scheme for selected phosphine hydrogens in [Rh(acac)(CO)(4R, 8S-Lim-Ph)] showing the bicyclic backbone and the phenyl portions of the ligand occupying both sides of the equatorial plane.

Since H19A has a greater influence on the cone angle and is in close proximity to H13A, the influence of the later proton on the cone angle is therefore minimal. Thus, 158° was considered the more realistic cone angle for the ligand as the three substituents used in the calculation were more evenly distributed over the molecule.

The Rh complex, [Rh(acac)(CO)(PA-Ph)], crystallises in the monoclinic space group $P2_1/c$ as two independent molecules in the asymmetric unit. The complex possesses a distorted square planar configuration and a C1 symmetry in the solid state, see Figure 5.6.

Figure 5.7: Superimposed structure for molecule 1 and 2 of [Rh(acac)(CO)(PA-Ph)]$_2$.

The bicyclic portions of the two structures do coincide with each other indicating that the two molecules are not enantiomers.

The data in Table 5.5 was arranged in terms of increasing ν(CO) down the table indicating the metal centres being less electron rich. This is supported by the increasing values of $^1J_{Rh\text{-}P}$. As the metal centres become less electron rich, one would expect the Rh-C bond length to increase as the ability of the metal centre to donate electrons to CO decreases while the C-O and Rh-P bond lengths decrease. There are some indications based on the data reported here that this may generally be the case. The Rh-O bond length *trans* to the phosphine ligand was somehow irregular showing that the ligands (phosphine) exhibit minimal trans-influence to the Rh-P bond. However, the ligands on the two extremes, PCy_3 and $P(OPh)_3$, deviate only by 0.025(2) Å indicating that the Rh-O bond length for PCy_3 was slightly longer than that for $P(OPh)_3$. This was unexpected as one would expect the Rh-O bond length for PCy_3 to be shorter since the corresponding Rh-P bond *trans* to it was slightly longer 2.2537(4) Å than that of $P(OPh)_3$ 2.170(1) Å.

Some of these systems have been discussed in Chapter 2. In this section, the oxidative addition reaction of MeI to Rh(I) complexes of bicyclic phosphine ligands to form Rh(III) alkyl intermediate are discussed. In the section following after that, the conversion of these Rh(III) alkyl complexes to the corresponding acyl complexes are presented. All supporting information is given in Appendix C5.3 and includes observed rates as a function of [MeI] and temperature for all the complexes.

5.4.1 Experimental

IR Measurements

The rhodium species that resulted from the reaction of [Rh(acac)(CO)(P-Ph)] and MeI in DCM were identified via the analysis of well defined ν(CO) stretching frequencies. The infrared spectra of the rhodium phosphine complexes were collected in a CaF_2 liquid cell on an Equinox 55 Bruker IR spectrophotometer at room temperature. The temperature for each reaction was recorded using a thermometer and the time between successive spectra was monitored using a stopwatch. The ν(CO) stretching frequencies for the Rhodium species of all the ligands occur at the following wave numbers: Rh(III) alkyl 1 (2053 – 2062 cm^{-1}), Rh(III) alkyl 2 (2068 – 2083 cm^{-1}), Rh(I) acac (1963 - 1983 cm^{-1}), and Rh(III) acyl species (1711 - 1736 cm^{-1}). The two Rh(III) alkyl isomers resulting from the *cis*- and *trans*- coordination of MeI to the Rh(I) complexes were obtained for all the ligand systems.[4] Two sets of Rh(III) acyl complexes derived from the corresponding Rh(III) alkyl species of the Lim system, were observed by ^{31}P NMR analysis as shown in Figure 5.3. The first spectrum was divided by itself and taken as the zero line. All the other spectra were then divided by the first spectrum taken as the zero line as shown in section 5.4.2. The peaks above and below the zero lines indicate that the catalytic species are increasing and decreasing respectively.

---

37 P. M. Maitlis, A. Haynes, G. J. Sunley and M. J. Howard, *J. Chem. Soc., Dalton Trans.*, 1996, 2187.

Stopped Flow Measurements of fast reactions

The absorbance vs time data of the faster reactions ($t_{1/2}$ < 5s) were recorded by means of an Applied Photophysics Stopped Flow spectrophotometer using UV/vis detection. Pre-thermostated solutions of the metal complexes and MeI in DCM were injected simultaneously into the mixing chamber, where they begin to react and then moved quickly to the spectrophotometer cell. The progress of the reaction is followed by monitoring a change in absorbance of the reaction mixture at a specific wavelength as a function of time ranging from 50 to a maximum of 500 seconds.

The UV/vis and the Stopped Flow studies were monitored under pseudo-first-order conditions with MeI in at least 10-fold excess relative to the [Rh]. The observed first-order rate constants for all the ligand systems were calculated by least square fitting the kinetic data to the first-order rate expression given in Eqn. 5.6:

$$A_{obs} = A1-(A1-A0)*\exp(-k_{obs}*t) \qquad 5.6$$

Where; A_{obs} = Observed absorbance at time t

A0 = Initial absorbance

A1 = Final absorbance

k_{obs} = Pseudo first-order rate constant

t = time

All the kinetic data were processed by means of Microsoft Office Excel 2003[39] and Scientist for Windows.[38]

---

39 *Microsoft Office Professional Edition 2003 copyright*© 1985-2003 Microsoft Corporation.

The changes in the peak area of the Rh(I) acac and Rh(III) alkyl signals are illustrated in Figure 5.9 as a function of time. This Figure confirms that the rate of the formation of the Rh(III) alkyl complex and the disappearance of the Rh(I) acac complex is similar. The rate of change of peak area with time for the different rhodium species in Figure 5.9 was compared with UV/vis results to enable proper identification of the rhodium species.

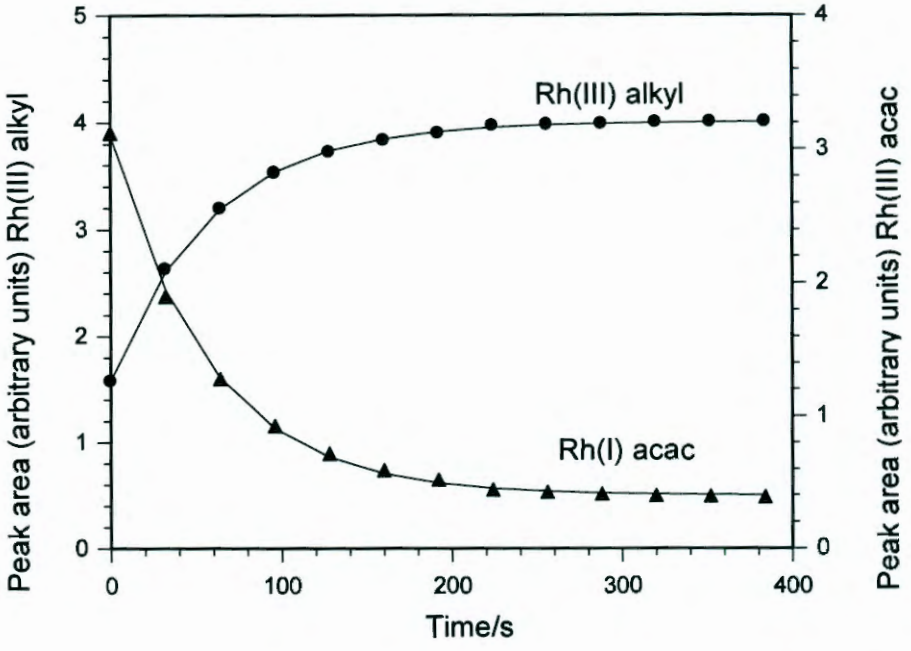

Figure 5.9: Changes in Rh species for the IR data in Figure 5.8 at 19 °C, [Rh] = 0.0025 mol dm^{-3}; [MeI] = 0.100 mol dm^{-3}; solvent = DCM; the solid lines represent least-squares fitting of the data points to Eqn. 5.6; $10^2 k_{obs}$ = 1.7 ± 0.3; $10^2 k_{obs}$ = 1.7 ± 0.2 s^{-1} for the disappearance of Rh(I) acac and appearance of Rh(III) alkyl species respectively.

The observed first-order rate constant for the oxidative addition reaction, obtained by UV/vis measurements at 380 nm, as shown in Figure 5.10 was about 1.2 times faster than that obtained by the IR for the same [MeI]. This could be attributed to variation in atmospheric temperature in the laboratory where the IR measurements were carried out.

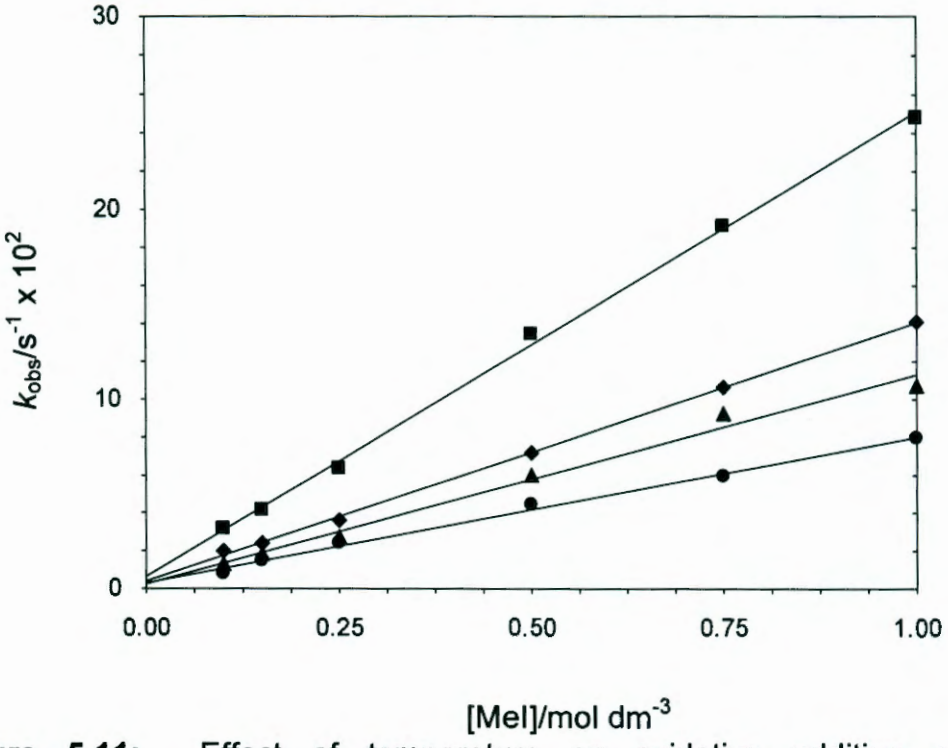

Figure 5.11: Effect of temperature on oxidative addition of MeI to [Rh(acac)(CO)(Phoban[3.3.1]-Ph)] in DCM with Stopped Flow spectrometer; λ = 380 nm; [Rh] = 0.00025 mol dm^{-3}, the solid lines represent linear fitting of the data points to Eqn. 5.2.[42]

Table 5.6: Effect of temperature on oxidative addition of MeI to [Rh(acac)(CO)(Phoban[3.3.1]-Ph)] in DCM with Stopped Flow spectrometer; λ = 380 nm; [Rh] = 0.00025 mol dm^{-3}.[42]

Temperature/ °C	$10^2 k_1$/mol^{-1} dm^3 s^{-1}	$10^2 k_{-1}$/s^{-1}	K/mol^{-1} dm^3
25	24.5 ± 0.5	0.6 ± 0.3	40 ± 18
15	13.7 ± 0.2	0.4 ± 0.1	36 ± 10
10	11.1 ± 0.6	0.3 ± 0.4	46 ± 67
5	7.7 ± 0.3	0.3 ± 0.2	27 ± 15

The large equilibrium constant was as a result of the pre-equilibrium favouring the Rh(III)alkyl formation with a slower reductive elimination reaction.

42 $K_1 = k_1/k_{-1}$

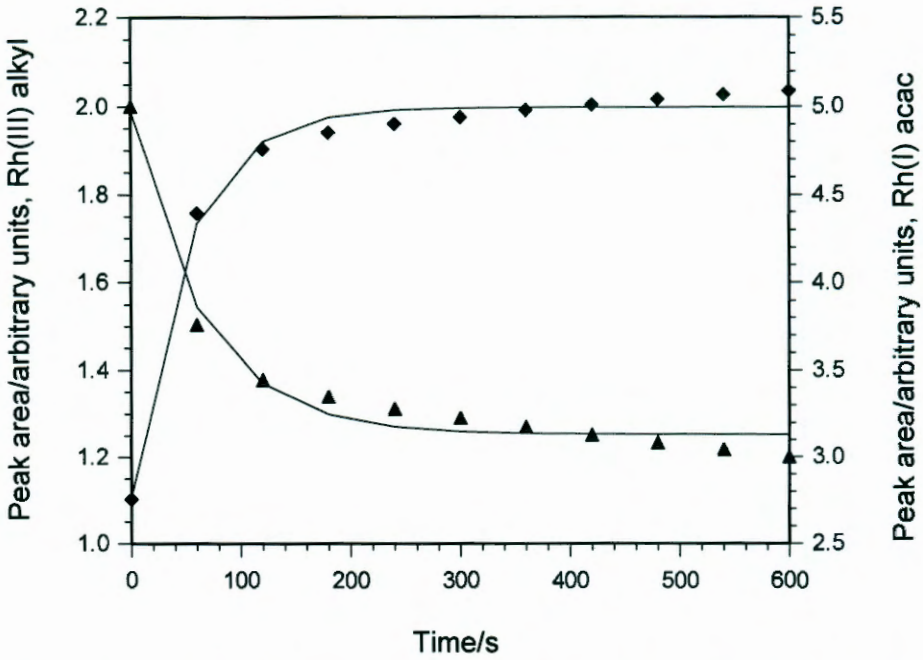

Figure 5.13: Changes in Rh species for the IR data in Figure 5.12 at 23 °C, [Rh] = 0.0025 mol dm^{-3}; [MeI] = 0.015 mol dm^{-3}; solvent = DCM; the solid lines represent least-squares fitting of the data points to Eqn. 5.6; $10^2 k_{obs}$ = 0.64 ± 0.01; $10^2 k_{obs}$ = 0.63 ± 0.01 s^{-1} for the disappearance of Rh(I) acac and appearance of Rh(III) alkyl species respectively.

Comparing Figures 5.13 and 5.14 it is observed that the rate of Rh(III) alkyl complex formation observed in the UV/vis at 313 nm was higher than that obtain in the IR experiment. This might be due to temperature differences during the measurements.

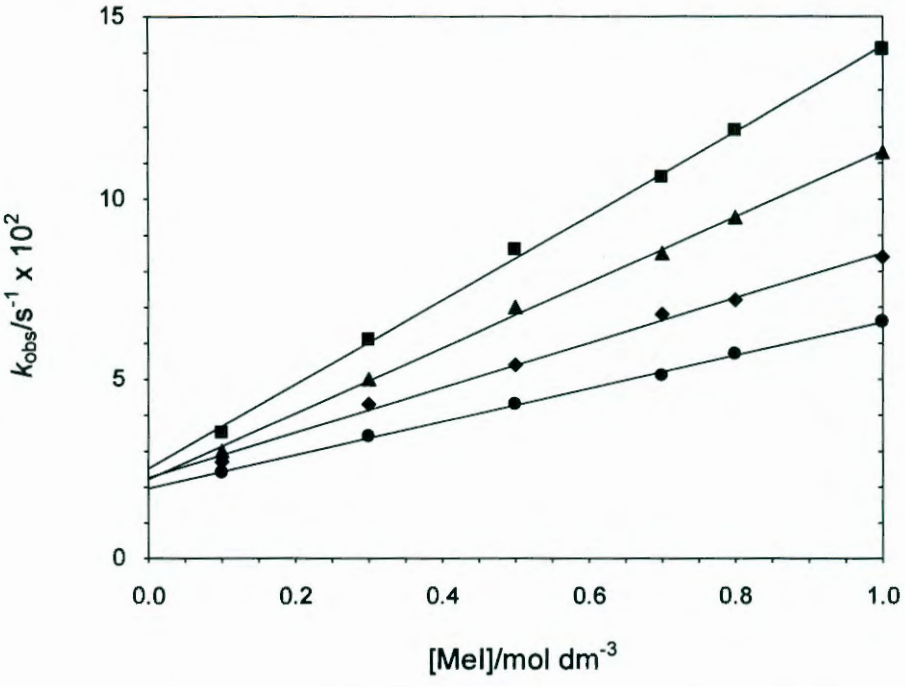

Figure 5.15: Effect of temperature on oxidative addition of MeI to [Rh(acac)(CO)(Phoban[4.2.1]-Ph)] in DCM with Stopped Flow spectrometer; λ = 313 nm; [Rh] = 0.00025 mol dm^{-3}, the solid lines represent linear fitting of the data points to Eqn. 5.2.[42]

Figure 5.15 illustrates the plots of k_{obs} with respect to [MeI] at four different temperatures. As expected the reaction rate increases as the reaction temperatures increases and the *K*-values at all temperatures were calculated (K_1 = k_1/k_{-1}). These *K*-values for this system were smaller than those of the Phoban[3.3.1]-Ph system indicating that the formation of the Rh(III) alkyl complexes of Phoban[4.2.1]-Ph was relatively less favoured.

Table 5.7: Effect of temperature on oxidative addition of MeI to [Rh(acac)(CO)(Phoban[4.2.1]-Ph)] in DCM with Stopped Flow spectrometer; λ = 313 nm; [Rh] = 0.00025 mol dm^{-3}.[42]

Temperature/ °C	10^2k_1/mol^{-1} dm^3 s^{-1}	10^2k_{-1}/s^{-1}	K/mol^{-1} dm^3
25	11.7 ± 0.2	2.5 ± 0.2	4.7 ± 0.3
20	9.1 ± 0.2	2.22 ± 0.12	4.1 ± 0.2
15	6.3 ± 0.2	2.26 ± 0.14	2.8 ± 0.2
10	4.6 ± 0.8	2.0 ± 0.5	2.4 ± 0.1

that the formation of the Rh(III) alkyl and disappearance of the Rh(I) acac complexes were similar.

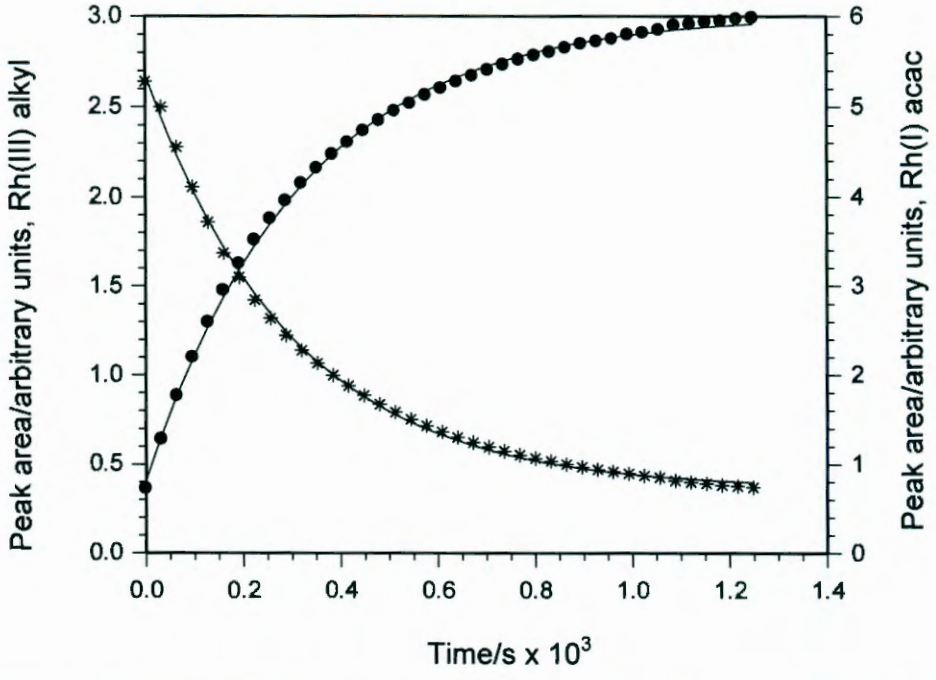

Figure 5.17: Changes in Rh species for the IR data in Figure 5.16 at 23 °C, [Rh] = 0.0025 mol dm^{-3}; [MeI] = 0.015 mol dm^{-3}; solvent = DCM; the solid lines represent least-squares fitting of the data points to Eqn. 5.6; $10^2 k_{obs}$ = 0.335 ± 0.004; $10^2 k_{obs}$ = 0.316 ± 0.004 s^{-1} for the disappearance of Rh(I) acac and appearance of Rh(III) alkyl species respectively.

In order to identify the oxidative addition with UV/vis, the same reaction was also studied at 23 °C, [Rh] = 0.00025 mol dm^{-3}; [MeI] = 0.015 mol dm^{-3} using the UV/vis spectrophotometer. The results indicate smooth first-order curves at 369 nm, which is given in Figure 5.18, corresponding to the oxidative addition reaction. The observed rate constants did not differ significantly from the IR result given in Figure 5.17.

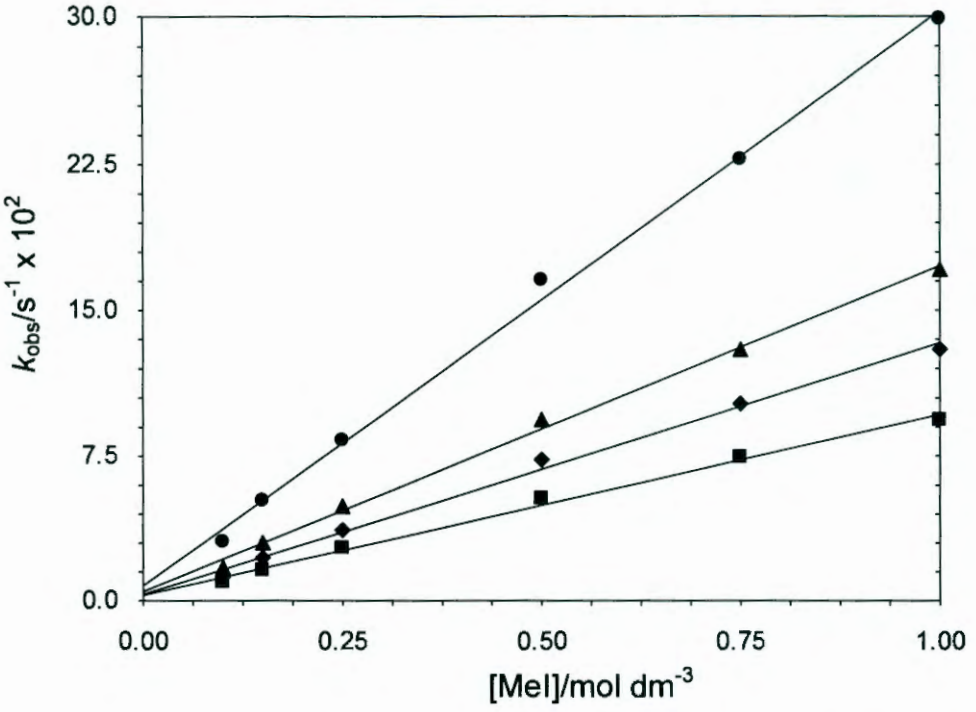

Figure 5.19: Effect of temperature on oxidative addition of MeI to [Rh(acac)(CO)(VCH[3.3.1 and 3.2.2]-Ph)] complexes in DCM with Stopped Flow spectrometer; λ = 369 nm; [Rh] = 0.00025 mol dm^{-3}, the solid lines represent linear fitting of the data points to Eqn. 5.2.[42]

The fairly large equilibrium constant, as shown in Table 5.8, indicates that the octahedral alkyl complex was favoured which may indicate that the ligand was less sterically hindered.

Table 5.8: Effect of temperature on oxidative addition of MeI to [Rh(acac)(CO)(VCH[3.3.1 and 3.2.2]-Ph)] in DCM with Stopped Flow spectrometer ; λ = 369 nm; [Rh] = 0.00025 mol dm^{-3}.[42]

Temperature/ °C	10^2k_1/mol^{-1} dm^3 s^{-1}	10^2k_{-1}/s^{-1}	K/mol^{-1} dm^3
25	29.5 ± 0.8	0.8 ± 0.5	37 ± 21
15	16.8 ± 0.5	0.5 ± 0.3	34 ± 17
10	13.0 ± 0.4	0.3 ± 0.3	39 ± 30
5	9.4 ± 0.3	0.39 ± 0.2	32 ± 21

The high stability of Rh(III) alkyl complexes formed during the oxidative addition reaction account for the large equilibrium constant observed.

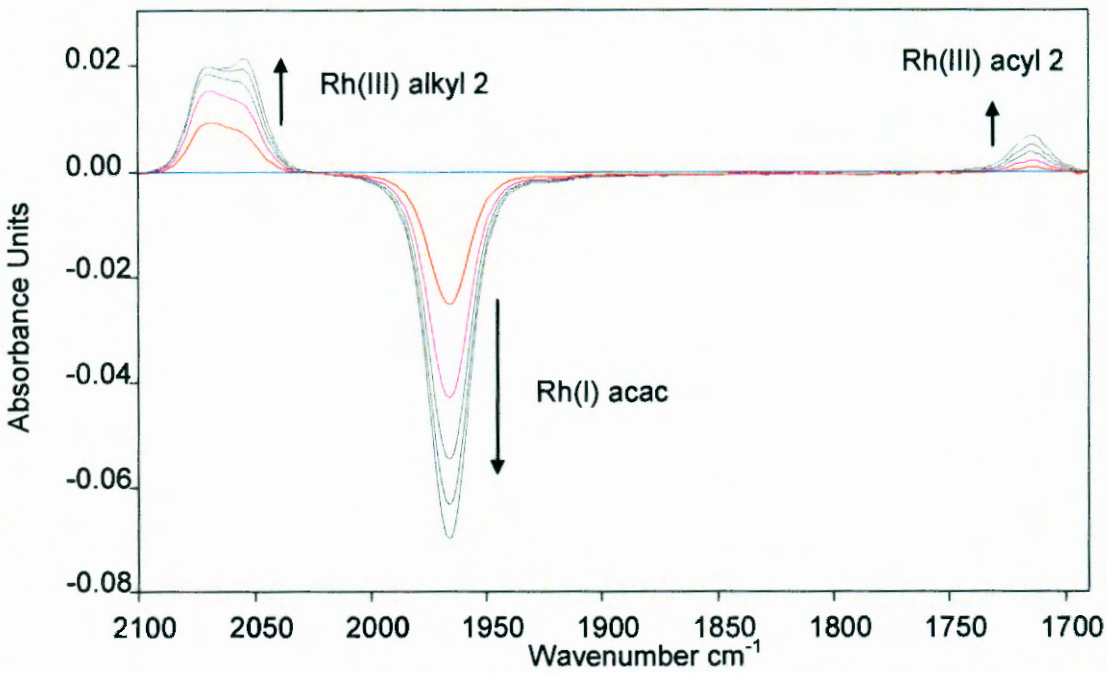

Figure 5.20: First five IR scans for the oxidative addition reaction of MeI to [Rh(acac)(CO)(4R, 8S- and 4S, 8S-Lim-Ph)] in DCM at 22 °C, [Rh] = 0.0025 mol dm^{-3}, [MeI] = 0.070 mol dm^{-3} and time gap between successive spectra = 10 s.

After the first five measurements the band at 2070 cm^{-3}(s) started to decrease while that at 2049 cm^{-3}(s), corresponding to the Rh(III) alkyl complex 1, start to increase resulting in an isobestic point as shown in Figure 5.21.

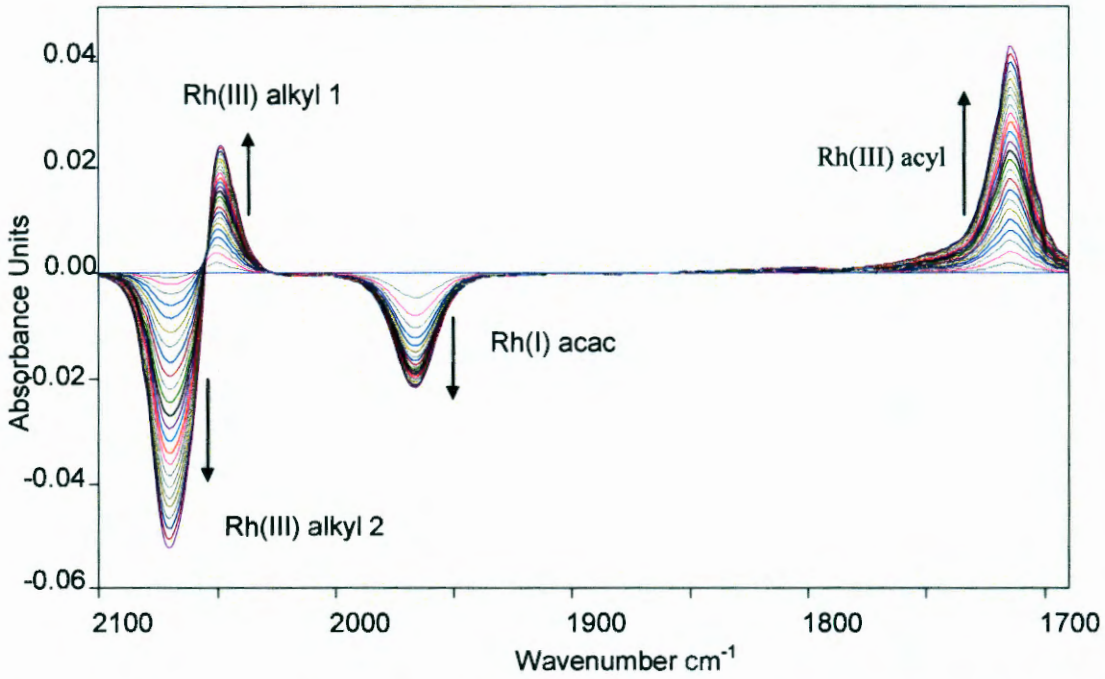

Figure 5.22: IR spectra for the oxidative addition reaction of MeI to [Rh(acac)(CO)(4R, 8S- and 4S, 8S-Lim-Ph)] in DCM at 22 °C after 80 seconds including the mixing time, [Rh] = 0.0025 mol dm^{-3}, [MeI] = 0.07 mol dm^{-3}, time gap between successive spectra = 10 s.

The formation of Rh(III) alkyl 2 was not observed at higher [MeI] = 0.250 mol dm^{-3} since the complex was rapidly converted to the Rh(III) acyl long before the first measurement was taken. This is illustrated by the rapid disappearance of Rh(III) alkyl 2 relative to Rh(III) alkyl 1.

The initial rate of increase of the Rh(III) acyl, shown in Figure 5.22, was not significantly different from the rate of disappearance of the Rh(III) alkyl 2. This is also illustrated in Figure 5.23 indicating that the rate of conversion of Rh(III) alkyl 1 to the corresponding acyl complex was very slow.

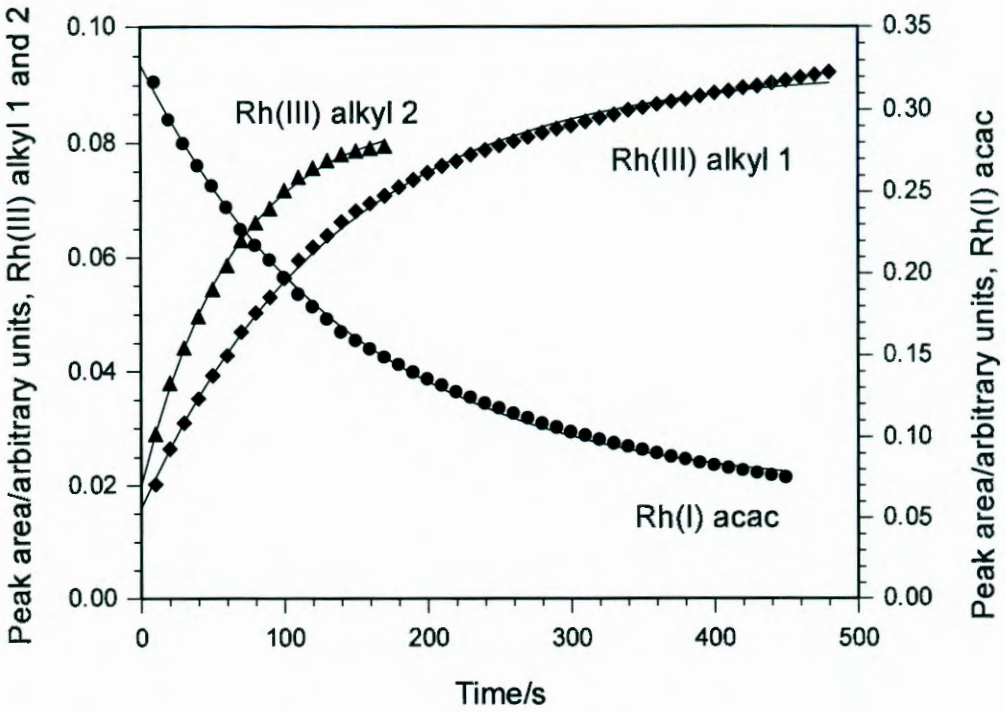

Figure 5.24: Changes in Rh species for the IR data in Figure 5.22 at 22 °C, [Rh] = 0.0025 mol dm^{-3}; [MeI] = 0.010 mol dm^{-3}; solvent = DCM; the solid lines represent least-squares fitting of the data points to Eqn. 5.6 with the Scientist programme; 10^2k_{obs} = 0.76 ± 0.01 s^{-1}; 10^2k_{obs} = 0.73 ± 0.01 s^{-1} and 10^2k_{obs} = 1.55 ± 0.05 s^{-1} for the disappearance of Rh(I) acac, appearance of Rh(III) alkyl 1 and Rh(III) alkyl 2 species respectively.

The oxidative addition of MeI to [Rh(acac)(CO)(4R, 8S-Lim-Ph)] complex was investigated with IR as a function of [MeI] at 22 °C. The rate of reaction was monitored at a specific wave number and the measurements were taken after every 10 seconds for about an hour. The results indicate a linear relationship with an equilibrium constant of 205 ± 60 mol^{-1} dm^3, see Table 5.9 and Figure 5.25.

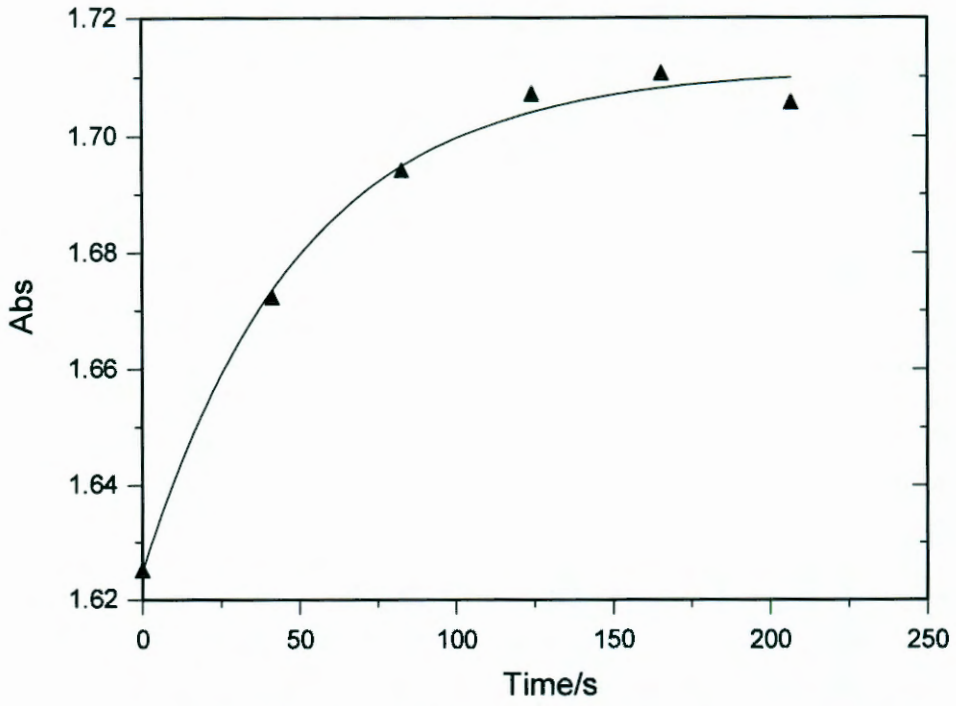

Figure 5.26: Rate of oxidative addition of MeI to [Rh(acac)(CO)(4S, 8S-Lim-Ph)] in DCM with UV/vis spectrometer at 26 °C, λ = 310 nm, [Rh] = 0.00025 mol dm^{-3} [MeI] = 0.015 mol dm^{-3}, $10^2 k_{obs}$ = 2.01 ± 0.26 s^{-1} for the appearance of Rh(III) alkyl 2 species; the solid lines represent least-squares fitting of the data points to Eqn. 5.6.

Comparing the results illustrated in Figure 5.24 to that in Figure 5.26 it can be seen that the formation of the Rh(III) alkyl 2 was identified. The oxidative addition of MeI to the [Rh(acac)(CO)(4S, 8S-Lim-Ph)] complex was subsequently investigated with Stopped Flow at 310 nm as a function of [MeI] and temperature, see Figure 5.27.

Table 5.10: Effect of temperature on oxidative addition of MeI to [Rh(acac)(CO)(4S, 8S-Lim-Ph)] in DCM with Stopped Flow spectrometer; λ = 310 nm; [Rh] = 0.0004 mol dm^{-3}.[42]

Temperature/ °C	$10^2 k_1$/mol^{-1} dm^3 s^{-1}	$10^2 k_{-1}$/s^{-1}	K/mol^{-1} dm^3
25	65.8 ± 0.8	3.5 ± 0.5	19 ± 2
20	50.8 ± 0.9	3.4 ± 0.5	15 ± 2
15	35.7 ± 1.8	5.5 ± 1.2	7 ± 1
10	28.3 ± 3	2.9 ± 0.2	10 ± 1

The large intercepts, as shown in Figure 5.27, verify that the rate of reductive elimination was significant resulting in the smaller equilibrium constants obtained relative to those of the Phoban[3.3.1]-Ph and VCH systems. The equilibrium constant at 22 – 25 °C for the formation of the Rh(III) alkyl 1 and 2 were about 5 and 49 times larger than that of Phoban[4.2.1]-Ph.

5.4.2.5. Iodomethane oxidative addition to [Rh(acac)(CO)(PA-Ph)]

In the PA-Ph system, the oxidative addition reaction of the Rh(I) complex and MeI was monitored using IR and UV/vis spectrophotometers. The IR results, as illustrated in Figure 5.28, show the reaction progress in the 1700 - 2100 cm^{-1} range. The bands at 2063 cm^{-1}(s), 1982 cm^{-1}(s), and 1712 cm^{-1}(m) were assigned to the Rh(III) alkyl, Rh(I) acac, and Rh(III) acyl complexes respectively while, according to an earlier report[1], the band at 1750 cm^{-1}(vw) was assigned to MeI.

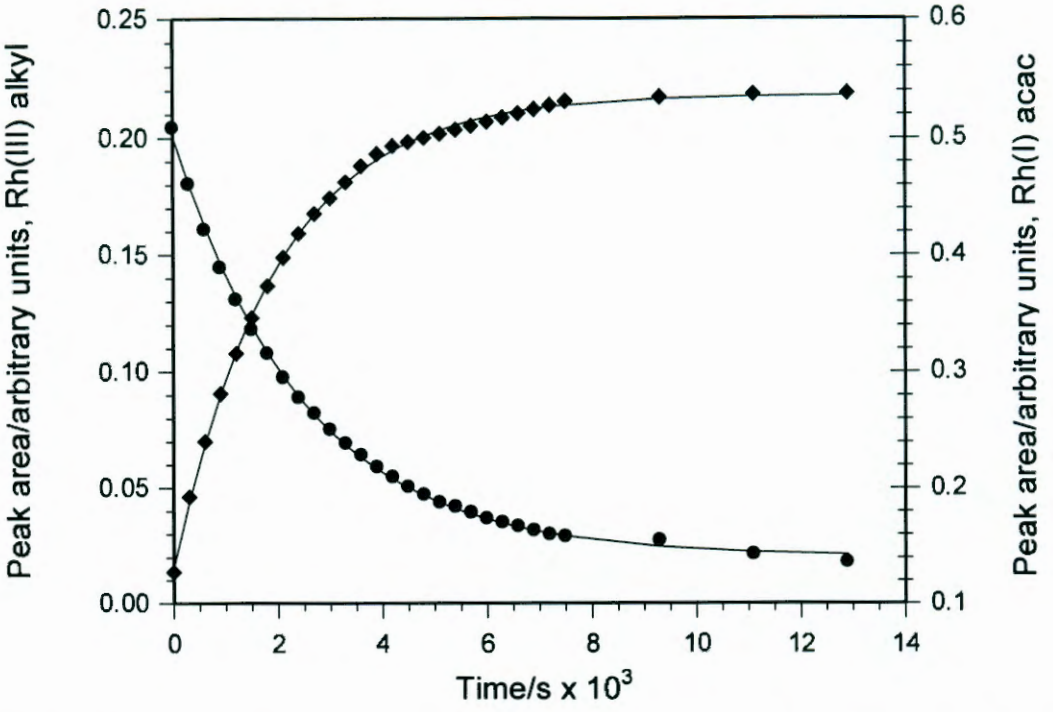

Figure 5.29: Changes in Rh species for the IR data in Figure 5.28 at 18 °C, [Rh] = 0.0025 mol dm^{-3}; [MeI] = 0.250 mol dm^{-3}; solvent = DCM; the solid lines represent least-squares fitting of the data points to Eqn. 5.6 ; $10^2 k_{obs}$ = 0.040 ± 0.001 s^{-1}; $10^2 k_{obs}$ = 0.051 ± 0.001 s^{-1} for the disappearance of Rh(I) acac species and appearance of Rh(III) alkyl species respectively.

The reaction was monitored at 0.250 mol dm^{-3} using the UV/vis and graphs of absorbance versus time obtained at 322 nm for the oxidative addition reaction is illustrated in the Figure 5.30.

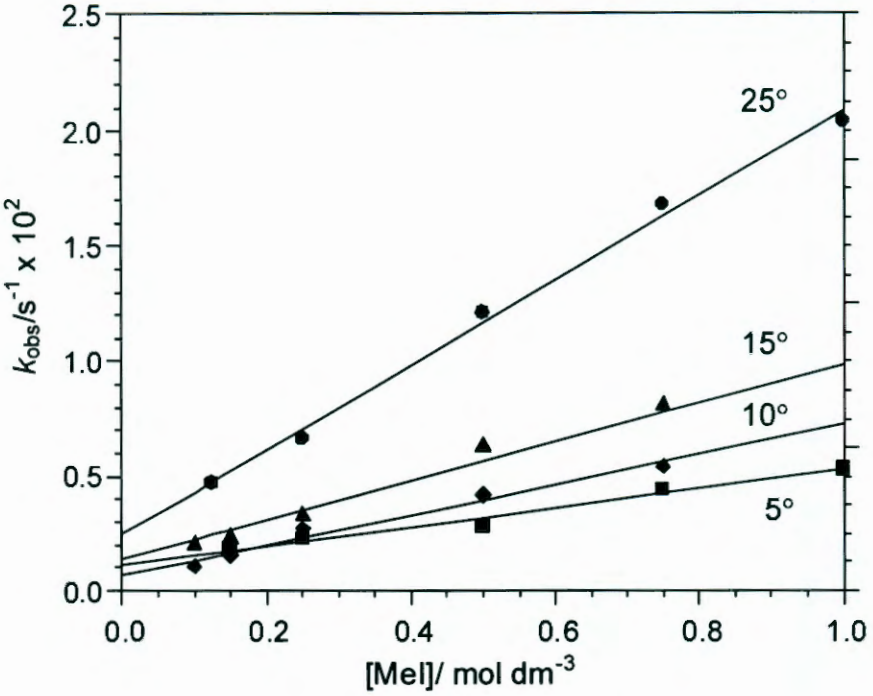

Figure 5.31: Effect of temperature on oxidative addition of MeI to [Rh(acac)(CO)(PA-Ph)] in DCM with UV/vis spectrometer; λ = 322 nm; [Rh] = 0.00025 mol dm^{-3}, the solid lines represent linear fitting of the data points to Eqn. 5.2.[42]

It is not expected that the equilibrium constant should be sensitive to temperature in the 20 °C range investigated here. The slight deviation at 5 °C could be attributed to a degree of inaccuracy associated with it.

Table 5.11: Effect of temperature on oxidative addition of MeI to [Rh(acac)(CO)(PA-Ph)] in DCM with UV/vis spectrometer; λ = 322 nm; [Rh] = 0.00025 mol dm^{-3}.[42]

Temperature/ °C	10^2k_1/mol^{-1} dm^3 s^{-1}	10^2k_{-1}/s^{-1}	K/mol^{-1} dm^3
25	0.18 ± 0.01	0.03 ± 0.01	7 ± 1
15	0.10 ± 0.01	0.011 ± 0.002	9 ± 2
10	0.07 ± 0.01	0.006 ± 0.003	10 ± 5
5	0.042 ± 0.004	0.011 ± 0.002	4 ± 1

Table 5.12: Effect of the steric and electronic properties of selected ligands on the oxidative addition of MeI to the solutions of [Rh(acac)(CO)(L)] in DCM at 23 – 25 °C, [Rh] = 0.00025 mol dm^{-3}; [MeI] = 0.01 - 1 mol dm^{-3}.[42]

	Ligand (L)	$10^2 k_1$/ mol^{-1} $dm^3 s^{-1}$	ν (CO)/* cm^{-1}	K/ mol^{-1} dm^3	$^1J_{Se-P}$/ Hz	θ/ °
1	*PCy_3[8]	2.71 ± 0.02	1945	92 ± 29	676 (TW)	174[27]
2	Phoban[3.3.1]- Ph	24.5 ± 0.5	1962	36 ± 16	691	165
3	**4S, 8S-Lim-Ph	65.8 ± 0.8	1965	19 ± 2	692	~ 149
4	VCH-Ph	29.5 ± 0.8	1964	37 ± 21	695	~ 149
5	4R, 8S-Lim-Ph	49.1 ± 1.0	1965	205 ± 60	699	158
6	Phoban[4.2.1]-Ph	11.7 ± 0.2	1963	4.7 ± 0.3	717	165
7	*PPh_3[8]	3.1 ± 0.1	1977	27 ± 4	732	149
8	PA-Ph	0.18 ± 0.01	1984	7 ± 1	752	165

*[Rh] = 0.003 mol dm^{-3}; **[Rh] = 0.0004 mol dm^{-3}

The results of PCy_3 and PPh_3 from previous studies were included for comparison with the results reported here.[8] As we go down Table 5.12, an approximately one order of magnitude variation in the rate constants is observed.

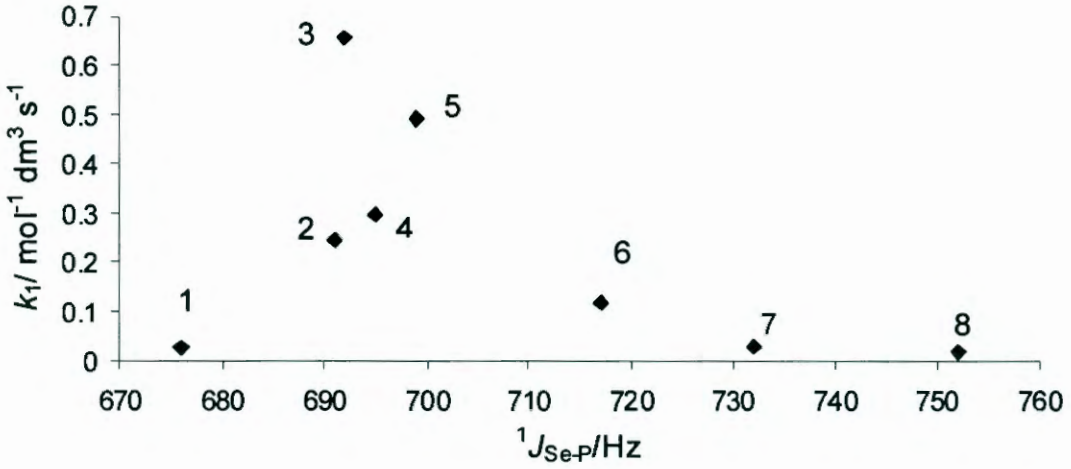

Figure 5.32: Effect of the electronic properties of selected ligands on the oxidative addition of MeI to [Rh(acac)(CO)(L)] in DCM at 23 – 25 °C, [Rh] = 0.00025 – 0.0004 mol dm^{-3}; [MeI] = 0.01 - 1 mol dm^{-3}, L = Phosphine ligands given in Table 5.12.

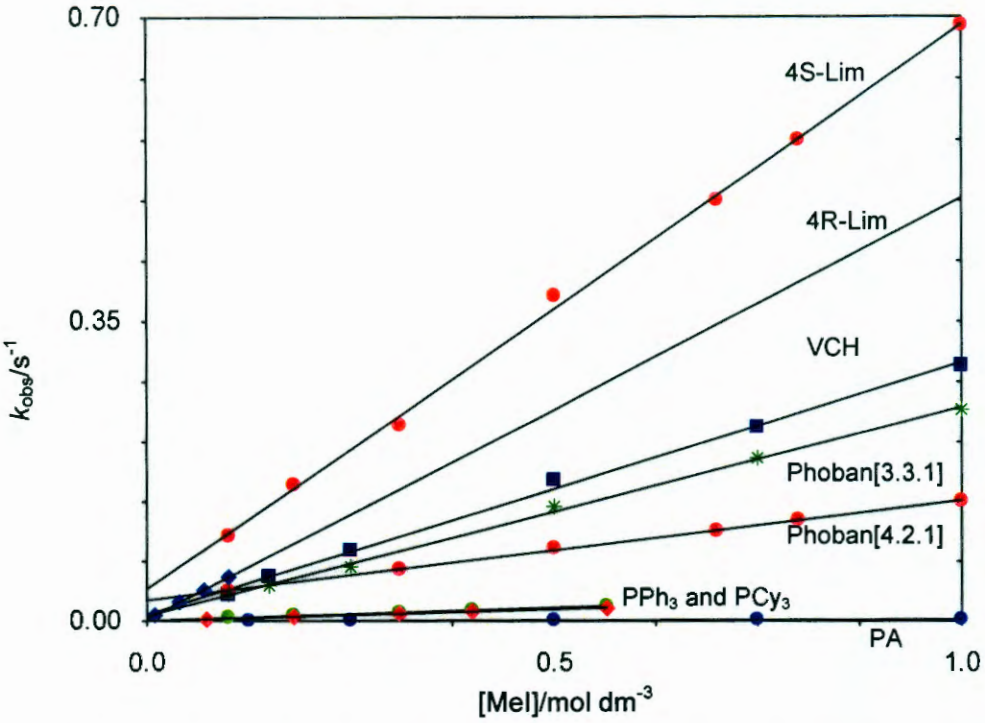

Figure 5.33: Effect of [MeI] on the rate of oxidative addition of MeI to [Rh(acac)(CO)(L)] in DCM at 25 °C, [Rh] = 0.00025 – 0.0004 mol dm^{-3}; [MeI] = 0.01 - 1 mol dm^{-3}, L = Phosphine ligands given in Table 5.12. The results of PCy_3 and PPh_3 from previous studies were included for comparison.[8]

PCy_3 which is the most electron-donating ligand in the series, gave a slower reaction rate compared to Phoban[3.3.1]-Ph , the two Lim-Ph isomers, VCH-Ph, Phoban[4.2.1]-Ph but similar to that of PPh_3. The slow rate could be attributed to the large steric size of the ligand which would hinder its coordination to the metal centre during the reaction process. The similarities in the rate of oxidative addition reaction for PCy_3 and PPh_3, despite their differences in electron donating ability, confirms that the steric differences between the two ligands is contributing to their activity toward oxidative addition.

The reaction rates of oxidative addition of PCy_3 and PPh_3 were faster than that of the PA-Ph even though the former ligands have larger and smaller steric sizes than the PA-Ph ligand, respectively. The slower reactivity of PA-Ph could be attributed to the more electron withdrawing nature of the ligand.

The reaction rate constant for the Rh(I) acac species of 4S, 8S-Lim-Ph towards oxidative addition was about 1.3 times faster than that of the 4R, 8S-Lim-Ph even

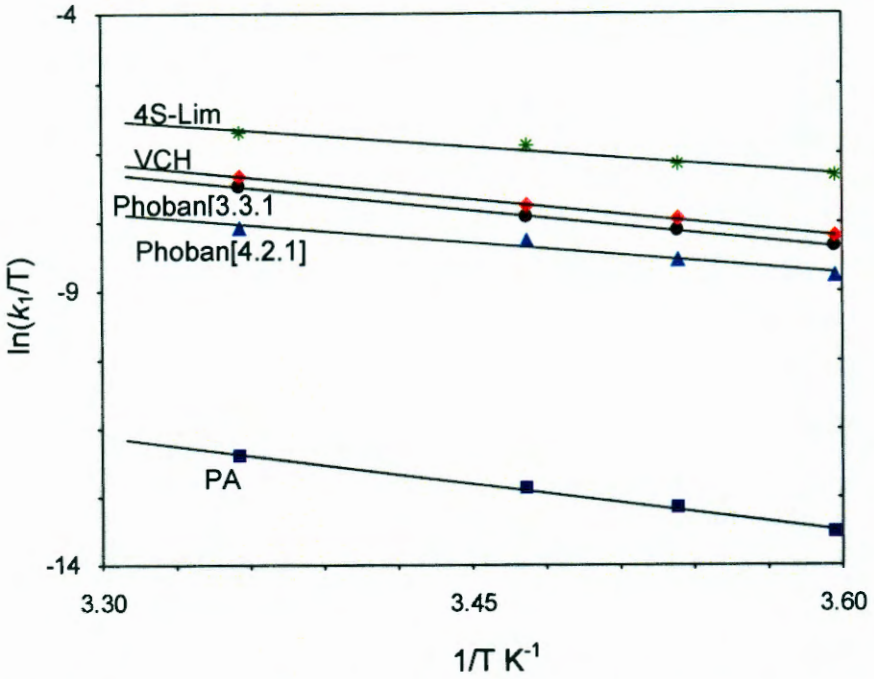

Figure 5.34: Plots from the Eyring equation (Eqn. 5.4) for the oxidative addition reaction of MeI to the solutions of [Rh(acac)(CO)(L)] in DCM at 23 – 25 °C, [Rh] = 0.00025 – 0.0004 mol dm^{-3}; [MeI] = 0.01 - 1 mol dm^{-3}, L = Phosphine ligands.

The results presented in Figure 5.34 are in agreement with that in Table 5.12 and Figure 5.33 indicating that the reactivity of the ligands occur according to the following trend: 4S, 8S-Lim-Ph > VCH-Ph > Phoban[3.3.1]-Ph > Phoban[4.2.1]-Ph > PA-Ph.

Table 5.13: Activation parameters from (Eqn. 5.4 and 5.5) for the oxidative addition reaction of [MeI] to the solutions of [Rh(acac)(CO)(L)] in DCM at 23 – 25 °C, [Rh] = 0.00025 – 0.0004 mol dm^{-3}; [MeI] = 0.01 - 1 mol dm^{-3}.

Ligand (L)	$\Delta G^{\neq}$ / kJ mol^{-1}	$\Delta H^{\neq}$ / kJ mol^{-1}	$\Delta S^{\neq}$ / J K mol^{-1}
4S, 8S-Lim-Ph	74 ± 7	36 ± 2	-127 ± 7
VCH[3.3.1 and 3.2.2]-Ph	76 ± 3	37.0 ± 1.0	-131 ± 3
Phoban[3.3.1]-Ph	77 ± 2	37.0 ± 1.0	-131 ± 3
Phoban[4.2.1]-Ph	78 ± 6	40 ± 2	-129 ± 6
PPh_3[8]	82 ± 4	38.0 ± 1.0	-146 ± 3
PCy_3[8]	82 ± 9	36 ± 3	-154 ± 9
PA-Ph	89 ± 8	48 ± 3	-136 ± 8

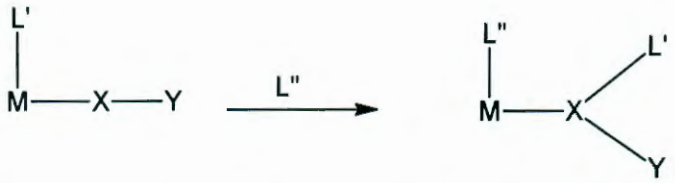

Figure 5.35: A general reaction showing the 1, 1 shift of ligand L' to an unsaturated fragment XY.

The migratory CO-insertion reaction is an intramolecular nucleophilic attack of the coordinated alkyl group (L') to a coordinated *cis*-CO (XY) to give an acyl complex. The reaction is expressed as the second step in Eqn. 5.1 with the rate constant given as k_2. Several factors are known to govern alkyl migration or migratory CO-insertion reactions, these include solvent effects[47] as well as the effect of participating[48] and non-participating ligands.[49]

5.5.1. Experimental

The absorbance of the reaction mixture as a function of time was recorded using a Varian Cary 300 Conc UV/vis spectrophotometer with a Julabo F12-mV temperature cell regulator at 25 °C in a 1.00 cm quartz curvette in DCM. The reactions were monitored at different [MeI] at a fixed wavelength depending on the ligand used and [Rh] = 0.00025 mol dm^{-3}. The k_{obs}-value for all the ligand systems were calculated by fitting the kinetic data to the first-order rate equation, Eqn. 5.6, using the Scientist software of which a typical example is shown in Figure 5.37. Estimated values of equilibrium constants that fall within 95% confident level were use to fit the data. Values that gave the best fit resulting to k_2-values that are more accurate were used.

---

47 R. George, J. M. Anderson and J. R. Moss, *J. Organomet. Chem.*, 1995, **505**, 131.

48 J. D. Cotton, M. M. Kroes, R. D. Markwell and E. A. Miles, *J. Organomet. Chem.*, 1990, **388**, 133.

49 C. Masters, *Homogeneous Transition-metal Catalysis*, 1980 and references there in.

Scientist software resulted in a straight line horizontal to the x-axis as shown in Figure 5.38.

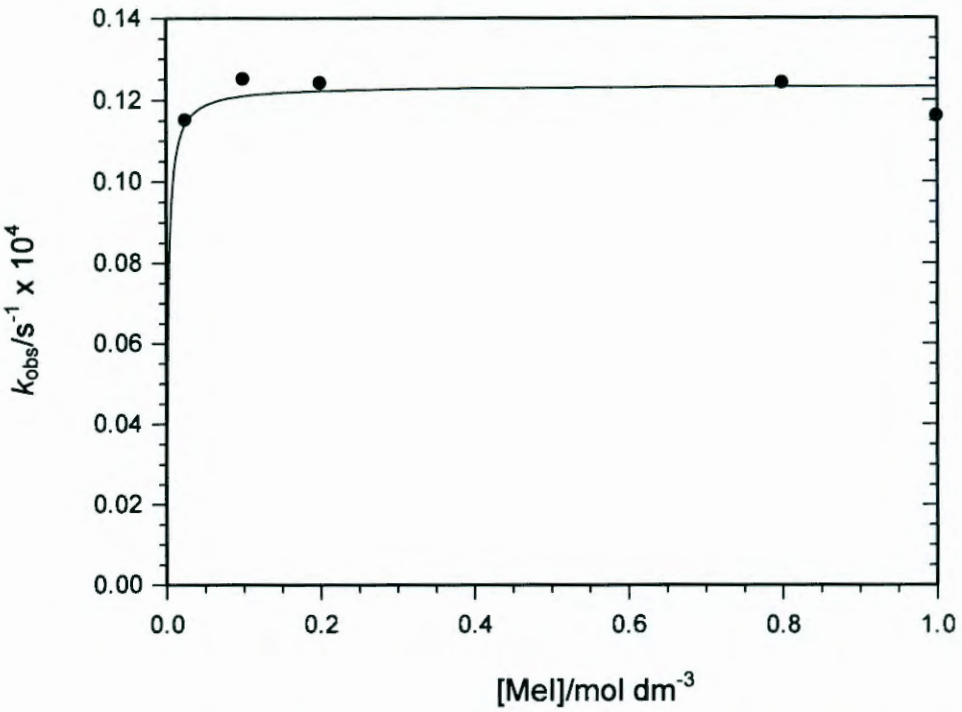

Figure 5.38: Effect of [MeI] on the rate of migratory CO-insertion at [Rh(acac)(Me)(I)(CO)(Phoban[3.3.1]-Ph)] in DCM at 25 °C, λ = 370 nm, [Rh] = 0.00025 mol dm^{-3}, $10^4 k_2$ = 0.123 ± 0.002 s^{-1}, K was fixed at 500 mol^{-1} dm^3, the solid lines represent least-squares fitting of the data points to Eqn. 5.3.

The results indicate that the observed rate constant, k_{obs}, for the migratory CO-insertion reaction was independent to the [MeI] used during the experiment, resulting in $k_{obs} = k_2$, implying that in Eqn. 5.3, K[MeI] >> 1. However, from Figure 5.11 it cannot be confidently stated that the intercept is very small. This might be interpreted as a small solvent pathway to be operative but was not investigated further in this study.

The value obtained for k_2 is in good agreement with the k_{obs} calculated from the oxidative addition absorption-time graph in Figure 5.37 at a fixed [MeI]. Since the curve at lower [MeI] is not well defined, an apparently large value for the equilibrium constant, of about 500 mol^{-1} dm^3 gave the best fit of the kinetic data.

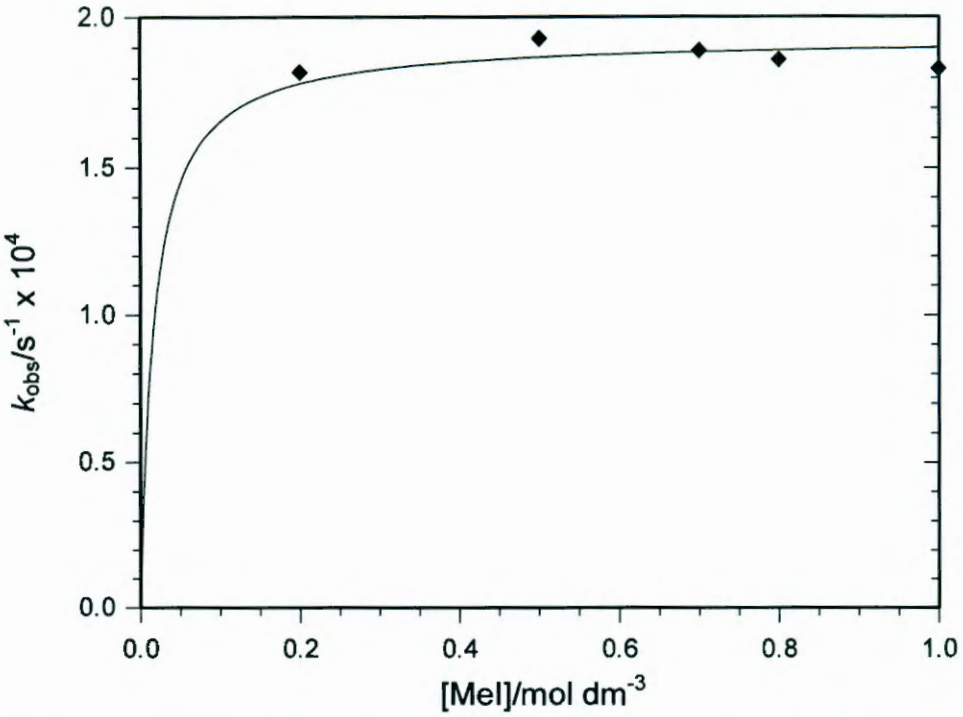

Figure 5.40: Effect of [MeI] on the rate of migratory CO-insertion at [Rh(acac)(Me)(I)(CO)(Phoban[4.2.1]-Ph)] in DCM at 25 °C, λ = 380 nm, [Rh] = 0.00025 mol dm^{-3}, $10^4 k_2$ = 1.93 ± 0.02 s^{-1}, K was fixed at 60 mol^{-1} dm^3, the solid lines represent least-squares fitting of the data points to Eqn. 5.3.

The rate constant at 0.100 mol dm^{-3} was higher than the rate at 0.200 mol dm^{-3}. At lower [MeI], the oxidative addition reaction interfere with the migratory CO-insertion reaction hence the point was excluded in the plot, see Figure 5.40. Both reactions were observed at the same wavelength in a consecutive manner such that as the oxidation addition is finished, the migratory CO-insertion reaction starts. Hence lowering the [MeI] in order to observe the linear relationship between k_{obs} and [MeI] in Figure 5.40 was indeed impossible and the point 0.100 mol dm^{-3} [MeI] was excluded from the plot.

The value obtained for k_2 is in good agreement with the k_{obs} calculated from the oxidative addition absorption-time graph at 0.2 mol dm^{-3} [MeI] as shown in Figure 5.39.

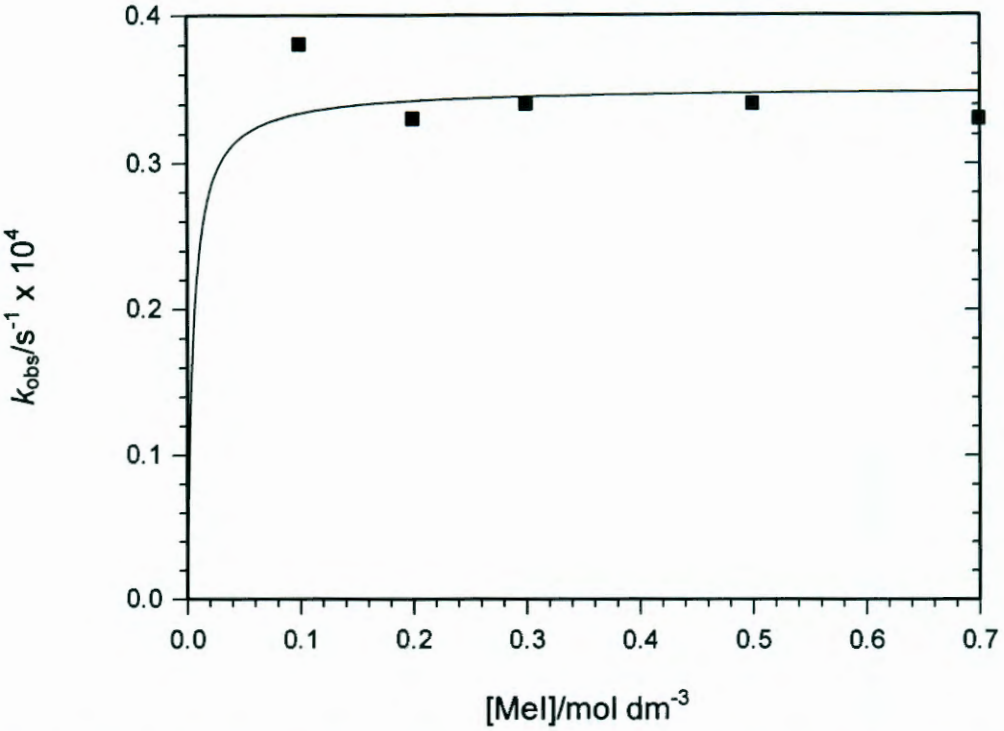

Figure 5.42: Effect of [MeI] on the rate of migratory CO-insertion at [Rh(acac)(Me)(I)(CO)(VCH[3.3.1 and 3.2.2]-Ph)] in DCM at 25 °C, λ = 370 nm, [Rh] = 0.00025 mol dm^{-3}, $10^4 k_2 = 0.343 \pm 0.004$ s^{-1}, K was fixed at 200 mol^{-1} dm^3, the solid lines represent least-squares fitting of the data points to Eqn. 5.3.

The results here indicate slightly higher reaction rates at 0.1 mol dm^{-3} as compared to 0.2 mol dm^{-3} [MeI]. As discussed above, this shows the interference of the oxidative addition reaction on migratory CO-insertion at lower [MeI]s. The k_2 rate constant ($k_2 = (0.343 \pm 0.004) \times 10^{-4}$ s^{-1}) agrees well with the observed rate constant (k_{obs}) for the Rh(III) acyl formation at 0.2 mol dm^{-3} [MeI] given in Figure 5.41.

5.5.2.4a. Kinetics of migratory CO-insertion at [Rh(acac)(Me)(I)(CO)(4R, 8S-Lim-Ph)]

The migratory CO-insertion reaction was monitored using the UV/vis spectrophotometer at 25 °C. The absorption-time graph for the reaction at 0.200 mol dm^{-3} is given in Figure 5.43.

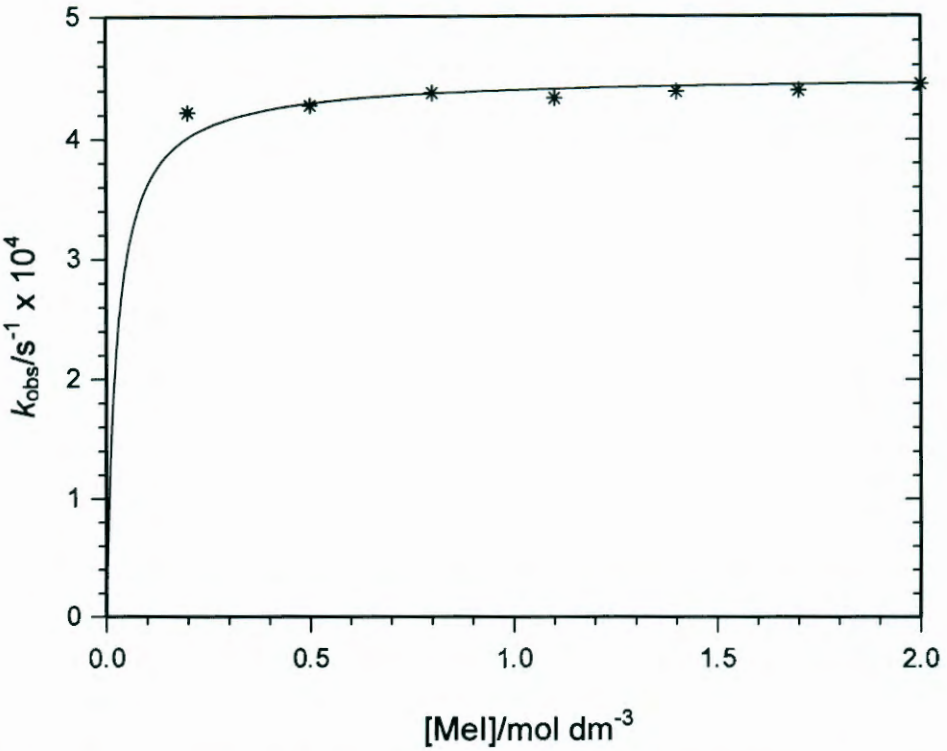

Figure 5.44: Effect of [MeI] on rate of migratory CO-insertion at [Rh(acac)(Me)(I)(CO)(4R, 8S-Lim-Ph)] in DCM at 25 °C, λ = 370 nm, [Rh] = 0.00025 mol dm^{-3}, $10^4 k_2 = 4.51 \pm 0.04$ s^{-1}, K was fixed at 90 mol^{-1} dm^3, the solid lines represent least-squares fitting of the data points to Eqn. 5.3.

Fitting the data obtained into Eqn. 5.3 at a fixed K-value of 90 mol^{-1} dm^3 using the Scientist software resulted in a straight line horizontal to the x-axis as shown in Figure 5.44. Under this reaction condition, $k_{obs} = k_2$, implying that K[MeI] >> 1.

The k_2-value, as shown in Figure 5.44, was in good agreement with the k_{obs} calculated from the absorption-time graph at 0.2 mol dm^{-3} [MeI] in Figure 5.43.

5.5.2.4b. Kinetics of migratory CO-insertion at [Rh(acac)(Me)(I)(CO)(4S, 8S-Lim-Ph)]

The migratory CO-insertion reaction was monitored using the UV/vis spectrophotometer at 25 °C. The absorption-time graph for the reaction at 0.200 mol dm^{-3} is given in Figure 5.45. The results indicate that the migratory CO-insertion reaction for the complex of the 4S, 8S-Lim-Ph isomer was about 15

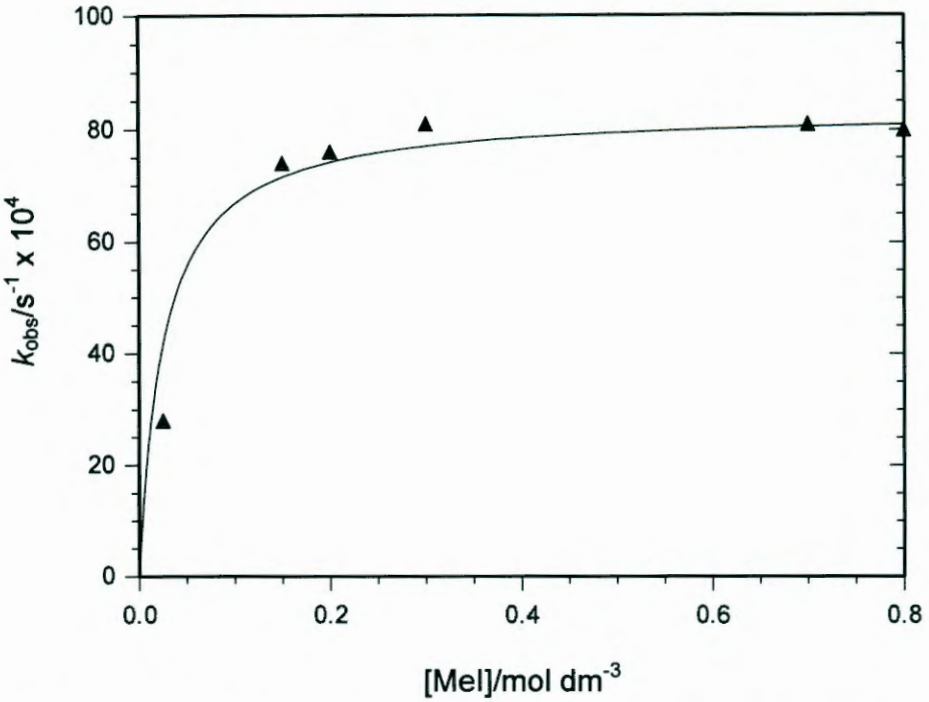

Figure 5.46: Effect of [MeI] on rate of migratory CO-insertion at [Rh(acac)(Me)(I)(CO)(4S, 8S-Lim-Ph)] in DCM at 25 °C, λ = 370 nm, [Rh] = 0.00025 mol dm^{-3}, $10^4 k_2$ (4S, 8S-Lim) = 83 ± 3 s^{-1}, K was fixed at 40 mol^{-1} dm^3, the solid lines represent least-squares fitting of the data points to Eqn. 5.3.

The k_2-value as shown in Figure 5.46 is in good agreement with the k_{obs} calculated from the absorption-time graph at 0.2 mol dm^{-3} [MeI] in Figure 5.45. These results indicate that the migratory CO-insertion for the two Lim-Ph systems were very different. The migratory CO-insertion of both isomers was observed at the same wavelength but at different rates. The initial rate of the migratory CO-insertion reaction was attributed predominantly to the 4S, 8S-Lim-Ph isomer while that for the 4R, 8S-Lim-Ph was relatively slow, compared to the 4S, 8S-Lim-Ph complex. The result is consistence with the IR results presented in Figures 5.22 which indicates that the formation of the Rh(III) acyl within the first 250 seconds was the same as the disappearance of Rh(III) alkyl species 2 of the 4S, 8S-Lim-Ph isomer.

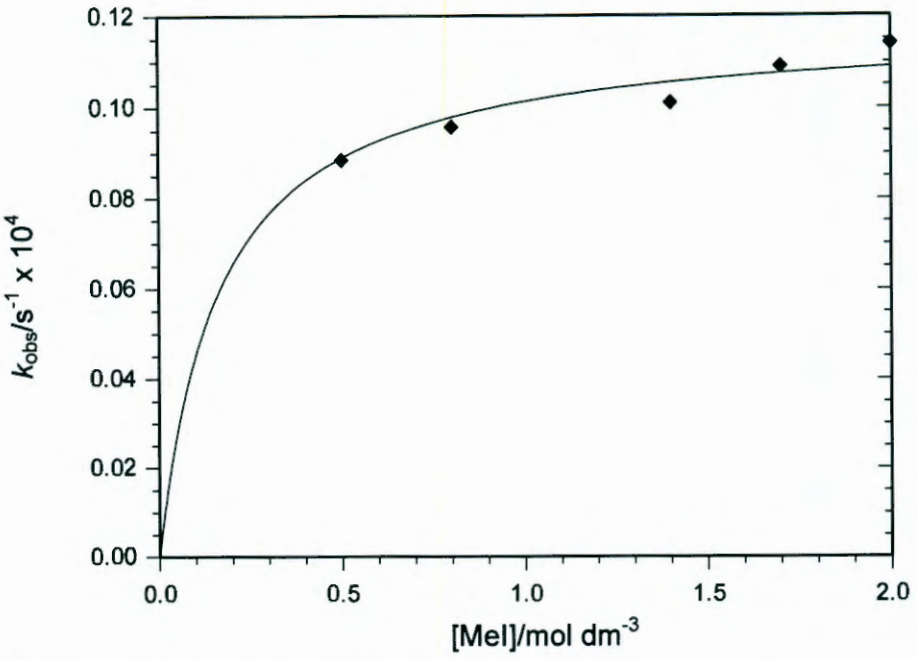

Figure 5.48: Effect of [MeI] on rate of migratory CO-insertion at [Rh(acac)(Me)(I)(CO)(PA-Ph)] in DCM at 25 °C, 380 nm, [Rh] = 0.00025 mol dm^{-3}, $10^4 k_2 = 0.12 \pm 0.01$ s^{-1}, $K = 6.2 \pm 1.3$ mol^{-1} dm^3, the solid lines represent least-squares fitting of the data points to Eqn. 5.3.

The curve obtained in Figure 5.48 is consistence with fast pre-equilibrium followed by a second slow reaction.[1] The migratory CO-insertion reaction for this system is dependence on [MeI] over the range investigated during the study.

The rate constant, $k_2 = (0.12 \pm 0.01) \times 10^{-4}$ s^{-1} was in good agreement with the k_{obs} calculated from the absorption-time graph at 0.2 mol dm^{-3} [MeI] in Figure 5.47. The equilibrium constant, $K = 6.2 \pm 1.3$ mol^{-1} dm^3, with the associated small standard deviation did not differ significantly from the value obtained from the oxidative addition reaction, $K = 7.4 \pm 0.7$ mol^{-1} dm^3.

5.5.3. Discussion on migratory CO-insertion of [Rh(acac)(Me)(I)(CO)(P-Ph)] complex

The rate of Rh(III) acyl formation was slower compared to the rate of formation of the Rh(III) alkyl species. The reaction in most of the systems except of the 4S, 8S-Lim-Ph proceeded with a fast pre-equilibrium step with rate constant k_1

Table 5.14: Effect of the steric and electronic properties of selected ligands on the migratory CO-insertion at [Rh(acac)(Me)(I)(CO)(P-Ph)] in DCM at 25 °C [Rh] = 0.00025 mol dm^{-3}; [MeI] = 0.01 - 2 mol dm^{-3}.

Ligands	ν (CO)/* cm^{-1}	$10^4 k_2/s^{-1}$	$10^4 k_{obs}/s^{-1}$*	$^1J_{Se-P}$/ Hz	θ/°
PA-Ph	1984	0.12 ± 0.04	0.12 ± 0.01	752	165
Phoban[3.3.1]-Ph	1962	0.123 ± 0.002	0.127 ± 0.002	691	167
VCH[3.3.1 & 3.2.2]-Ph	1964	0.34 ± 0.10	0.38 ± 0.01	695	~149
Phoban[4.2.1]-Ph	1963	1.89 ± 0.04	2.02 ± 0.02	717	165
4R, 8S-Lim-Ph	1965	4.42 ± 0.08	4.45 ± 0.02	699	158
4S, 8S-Lim-Ph	1965	83 ± 3	65.70 ± 0.20	692	~149

* The reaction was monitored at a [MeI] of 0.2 mol dm^{-3}.

The reaction rate constants k_2 obtained in this study could be divided into two groups as shown in Figure 5.49. The values for the first set of ligands, PA-Ph, Phoban[3.3.1] -Ph and VCH-Ph are (0.12, 0.12 and 0.34) x 10^{-4} s^{-1} while those for the second set, 4S, 8S-Lim-Ph, 4R, 8S-Lim-Ph and Phoban[4.2.1] -Ph are (83, 4.42 and 1.89) x 10^{-4} s^{-1} respectively. The reaction trend for the migratory CO-insertion reaction was determined as 4S, 8S-Lim-Ph > 4R, 8S-Lim-Ph > Phoban[4.2.1]-Ph > VCH-Ph > Phoban[3.3.1]-Ph > PA-Ph.

The low rate of migratory CO-insertion obtained for the Phoban[3.3.1]-Ph and VCH-Ph ligands is in agreement with the high stability of the [Rh(acac)(Me)(I)(CO)(P-Ph)] complexes. This was unusual as one would expect a higher reaction rate due to the high electron-donating nature of the ligands which was believed to increase the nucleophilicity of the Rh(I) centre.[1, 9] The slowest rate was observed for the PA-Ph ligand compared to the rest of the ligands and could be attributed by the electron withdrawing nature of the ligand. The electron withdrawing nature of the PA-Ph ligand would strengthen the Rh-Me bond making the alkyl migration process slow. Makunya and co-workers showed that electron withdrawing phosphine ligands in [CpFe(CO)(P)(PR_3)] type

The crystal structures of [Rh(acac)(CO)(4R, 8S-Lim-Ph)] and [Rh(acac)(CO)(PA-Ph)] were determined and the cone angles of 4R, 8S-Lim-Ph and PA-Ph were calculated as 158° and 165° respectively.

The larger *trans*-influence of the phosphine ligands was evident from the longer Rh-O bonds of 2.0751(18) and 2.068(3) Å *trans* to PA-Ph and Lim-Ph respectively compared the Rh-O bonds of 2.0371(19) and 2.049(3) Å, *trans* to the carbonyl ligands, respectively.

The effect of these bicyclic ligands on the rate of oxidative addition as well as migratory CO-insertions reactions were determined in DCM at temperatures ranging from 5 – 25 °C.

The two Rh(III) alkyl complexes as well as their acyl derivatives corresponding to the *cis* and *trans* isomers of all the ligands were identified using IR and ^{31}P NMR spectroscopy, while the oxidative additions and migratory CO-insertion of the two isomers, 4R, 8S-Lim-Ph and 4S, 8S-Lim-Ph, were studied independently even though they were synthesized as mixtures of isomers.

The formation of the [Rh(acac)(Me)(I)(CO)(4S, 8S-Lim-Ph)] was only about 1.3 times faster than [Rh(acac)(Me)(I)(CO)(4R, 8S-Lim-Ph)] whereas the equilibrium constant for the 4R, 8S-Lim-Ph system was about an order of magnitude larger than that of the 4S, 8S-Lim-Ph system indicating that the former is thermodynamically the more stable complex.

The oxidative addition of the two Lim-Ph ligands were about 2 – 3 times faster than those of the Phoban[3.3.1]-Ph and VCH-Ph ligands. Overall, these four ligands gave the highest rate of oxidative addition suggested to be due to the high electron density introduced by the ligands.

The general reactivity trend for the oxidative addition was found to be: 4S, 8S-Lim-Ph > 4R, 8S-Lim-Ph > VCH-Ph > Phoban[3.3.1]-Ph > Phoban[4.2.1]-Ph > PPh_3 ~ PCy_3 > PA-Ph.

6 Evaluation and future work

6.1. Introduction

The aim of this research was to improve the fundamental understanding of the role different phosphine ligands play in modified cobalt-catalyzed hydroformylation.

The electronic and steric properties of Phoban derived ligands, Phoban-Q (Q = CH_2CH_3 (C_2), $(CH_2)_4CH_3$ (C_5), $(CH_2)_9CH_3$ (C_{10}), $(CH_2)_{19}CH_3$ (C_{20}), $(CH_2)_3N(CH_3)_2$ (C_3NMe_2), C_6H_{11} (Cy) and C_6H_5 (Ph), were systematically manipulated by altering the side chain on the phosphorus atoms. The effects of electronic and steric properties of the Phoban derived ligands were determined in cobalt-catalyzed hydroformylation of linear internal decene.

Other bicyclic ligands added for comparison are: a mixture of 4S, 8S- and 4R, 8S isomers of Lim-C_5 and Lim-Cp, [3.3.1] and [3.2.2] isomers of VCH-^{i}Bu, VCH-C_5, PA-C_5 and Phoban-C_5 and were selected based on differences in their electronic and steric properties. The bicyclic ligands were compared to the following conventional ligands: P^nBu_3, P^tBu_3, P^iBu_3, PCy_3, PCp_3, P(*p*-$C_6H_4OCH_3)_3$, PPh_3 and P(2-furyl)$_3$ and their effects on cobalt-catalyzed hydroformylation of 1-octene were evaluated.

To gain further information on some of the ligands used in the hydroformylation studies, their effect on the MeI oxidative addition was investigated in a model [Rh(acac)(CO)(L) (L = selected bicyclic phosphine ligands) system. This system involves an investigation of the rate of formation of rhodium alkyl and acyl species in oxidative and CO-insertion reactions at ambient temperature and pressure. The information obtained from this study

The [3.3.1] and [4.2.1] isomers of Phoban ligands differ significantly in their electronic properties with $\Delta^1 J_{Se\text{-}P}$ = 20 - 30 Hz. The maximum difference in $^1J_{Se\text{-}P}$ coupling constant of 14 and 7 Hz could be induce between the Phoban[4.2.1] and [3.3.1] isomers respectively for Q = Cy and Ph, the most electron donating and withdrawing substituents.

The bicyclic back bone have a significant effect on the electronic properties of the ligands with the VCH[3.3.1]-^{i}Bu and VCH-C_5 being the most electronic donating in the series with $^1J_{Se\text{-}P}$ ranging from 673 – 678 Hz while PA-C_5 and PA-Ph ligands were the most electron withdrawing ligands with $^1J_{Se\text{-}P}$ ranging from 751 – 752 Hz.

The first VCH-^{i}Bu crystal structure, Se-VCH[3.3.1]-^{i}Bu, as well as the structures of other bicyclic ligands Se-Phoban[3.3.1]-C_2, Se-Phoban[3.3.1]-Cy, Se-Phoban[4.2.1]-Cy, Se-Phoban[3.3.1]-Ph and Se-Phoban[4.2.1]-Ph were obtained. The selenide complexes of the [3.3.1] and [4.2.1] isomers of Phoban-Cy and Phoban-Ph ligands co-crystallizes within the same unit cell indicating that both isomers were similar in steric size. In the crystal structures of these Se-P complexes the bicyclic ligands, the alkyl or aryl side chains and the selenium atoms coordinates to the phosphorus atoms in a tetrahedral fashion.

6.2.2. Ligand evaluation in modified cobalt hydroformylation

The role different phosphine ligands play in modified cobalt-catalyzed hydroformylation were evaluated. The first part of chapter 4 focused on the effect of Phoban derived ligands in modified cobalt hydroformylation of linear internal decene at fully modified conditions. The electronic and steric properties of the ligands were systematically manipulated by altering the side chain on the phosphorus atoms. The results of all the Phoban derived ligands were very similar with linearities ranging from 85 - 90%, alcohol yields from 77 - 85%, hydrogenation from 9 – 15% and rates of 1.8 – 2.4 h^{-1}confirming that

be observed by common spectroscopic technique such as IR at standard hydroformylation conditions.[1] As such, a model study was designed to investigate the effect of selected bicyclic ligands on the rate of oxidative addition as well as CO insertion reactions as discussed in the next section.

Crystal structures of the cobalt dimers of the following ligands; Phoban[3.3.1]-C_2, Phoban[3.3.1]-C_5, Phoban[3.3.1]-C_3NMe_2, Phoban[3.3.1]-Cy, PA-C_5, PCy_3, and PCp_3 were obtained and characterised by X-ray crystallography.

The P-Co-Co bond angles indicate that the molecules of all seven cobalt dimer structures slightly deviate from linearity and ranges from 170.49(3) to 174.39(13)° for the Phoban derivatives and 172.76(4) to 175.855(13) Å for PA, PCp_3 and PCy_3 respectively. Both the Co-Co 0.062(5) Å and Co-C 0.060(10) Å bonds vary within a narrow range while the Co-P bonds 0.085(10) Å are slightly more sensitive to the nature of the P-ligand.

The Co-P bond distances ranges from 2.1963(8) to 2.2074(9) Å for the Phoban derivatives and 2.1875(12) Å and 2.2071(10) Å for PA-C_5, PCy_3 and PCp_3 respectively. The shorter Co-P bond distance of the PA-C_5 ligand 2.1875(13) Å compared to those of PCy_3 2.1949(3) Å and PCp_3 2.207(9) Å could be attributed to the more electron withdrawing ability of the former.

6.2.3. MeI oxidative addition and insertion reactions in Rh-phosphine complexes

The effects of electronic and steric properties of selected bicyclic ligands were investigated to determine their effect on the rate of oxidative addition as well as CO insertion reactions at ambient temperature and pressure.

A series of [Rh(acac)(CO)(P-Ph)] complexes where P-Ph = Phoban[3.3.1]-Ph, Phoban[4.2.1]-Ph, a mixture of 4R, 8S- and 4S, 8S-Lim-Ph, a mixture of VCH[3.3.1]-Ph and VCH[3.2.2]-Ph and PA-Ph were successfully synthesized and characterised by multinuclear NMR and IR spectroscopic techniques.

Crystal structures of the Rh(III) alkyl and acyl complexes of these bicyclic ligands should be pursued in the future as they could give useful informations on the discreet catalytic steps.

Modelling should be use to investigate these systems to derive further understanding on the mechanism of the oxidative addition as well as CO insertion reactions of these systems. The study may also give information on the most stable structural form of the Rh(III) alkyl and acyl complexes of the ligands.

Abstract

The aim of this research work was to improve the fundamental understanding of the role selected tertiary bicyclic and conventional phosphine ligands play in modified cobalt-catalyzed hydroformylation.

Selected bicyclic ligands were synthesized by radical addition of 1-alkenes to the 2° phosphines shown in Figure 1.

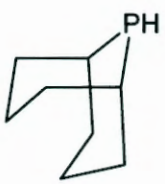

Phoban[3.3.1]

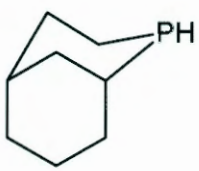

VCH[3.3.1]

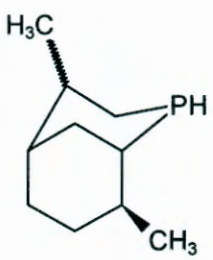

Lim

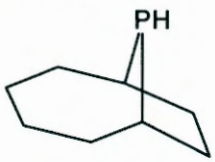

Phoban[4.2.1]

VCH[3.2.2]

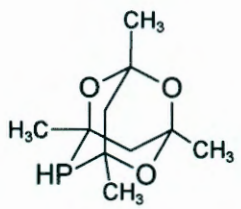

PA

Figure 1: Secondary phosphines used as precursors for making phosphine ligands.

The following ligands were synthesized in this way: Phoban-Q (Q = CH_2CH_3 (C_2), $(CH_2)_4CH_3$ (C_5), $(CH_2)_3N(CH_3)_2$ (C_3NMe_2), Lim-C_5, VCH-C_5 and PA-C_5. Phoban-Cy was made from the reaction between a diene and a 1° phosphine, H_2PCy, with a radical initiator at 100°C.

the second set ranging from P^nBu_3 to the Lim family with hydrogenation ranging from 9 - 15% respectively.

Crystal structures of the cobalt dimers of the following ligands; Phoban[3.3.1]-C_2, Phoban[3.3.1]-C_5, Phoban[3.3.1]-C_3NMe_2, Phoban[3.3.1]-Cy, PA-C_5, PCy_3, and PCp_3 were obtained and characterised by X-ray crystallography.

A series of [Rh(acac)(CO)(P-Ph)] complexes where P-Ph = Phoban[3.3.1]-Ph, Phoban[4.2.1]-Ph, a mixture of 4R, 8S- and 4S, 8S-Lim-Ph, a mixture of VCH[3.3.1]-Ph and VCH[3.2.2]-Ph and PA-Ph were successfully synthesized and characterised by NMR and IR spectrophotometers.

The crystal structures of [Rh(acac)(CO)(4R, 8S-Lim-Ph)] and [Rh(acac)(CO)(PA-Ph)] were obtained and characterised by X-ray crystallography.

The oxidative addition and CO-insertion reactions of the rhodium complexes of these ligands were carried out and the results indicate that the Lim-Ph systems were the most active among the bicyclic ligands included in the study.

The general reactivity trend for the oxidative addition was found to be: 4S, 8S-Lim-Ph > 4R, 8S-Lim-Ph > VCH-Ph > Phoban[3.3.1]-Ph > Phoban[4.2.1]-Ph > PPh_3 ~ PCy_3 > PA-Ph.

The overall reactivity trend for the CO-insertion reaction was determined as 4S, 8S-Lim-Ph > 4R, 8S-Lim-Ph > Phoban[4.2.1]-Ph > VCH-Ph > Phoban[3.3.1]-Ph > PA-Ph.

Keywords: Catalysis, Cobalt, Hydroformylation, Autoclave, Crystallography, Phosphine ligands, Selenide complexes, Coupling constant, Rhodium, Oxidative addition, CO-insertion, UV/vis, Infra Red, Stopped flow, Kinetics.

Opsomming

Die doel van die navorsing was om die fundamentele begrip vir die rol wat geselekteerde tersiêre bisikliese en konvensionele fosfien ligande in gemodifiseerde kobalt gekataliseerde hidroformilering speel te verbeter.

Geselekteerde bisikliese ligande is gesintetiseer deur die radikaal addisie van 1-alkene aan die 2° fosfiene in Figuur 1.

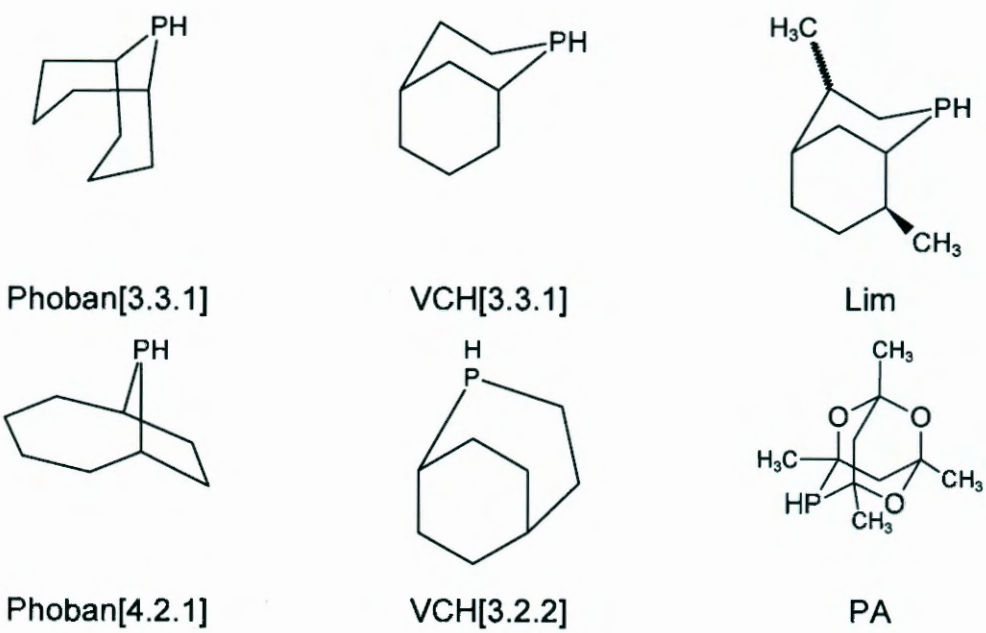

Figuur 1: Sekondêre fosfiene wat gebruik is as uitgangstowwe om fosfien ligande te maak.

Die volgende ligande is op die manier gesintetiseer: Phoban-Q (Q = CH_2CH_3 (C_2), $(CH_2)_4CH_3$ (C_5), $(CH_2)_3N(CH_3)_2$ (C_3NMe_2), Lim-C_5, VCH-C_5 en PA-C_5. Phoban-Cy is gemaak deur die reaksie tussen 'n dieen en 'n 1° fosfien, H_2PCy, met 'n radikaal inisieerder by 100°C.

groep en wissel van P^nBu_3 tot die Lim familie met hidroginering wat wissel van 9 - 15% onderskeidelik.

Kristalstrukture van kobalt dimere van die volgende ligande Phoban[3.3.1]-C_2, Phoban[3.3.1]-C_5, Phoban[3.3.1]-C_3NMe_2, Phoban[3.3.1]-Cy, PA-C_5, PCy_3 en PCp_3 is verkry en gekarakteriseer met X-straal kristallografie.

'n Reeks [Rh(acac)(CO)(P-Ph)] komplekse waar P-Ph = Phoban[3.3.1]-Ph, Phoban[4.2.1]-Ph, 'n mengsel van 4R, 8S- en 4S, 8S-Lim-Ph, 'n mengsel van VCH[3.3.1]-Ph en VCH[3.2.2]-Ph en PA-Ph is suksesvol gesintetiseer en gekarakteriseer met KMR en IR spektroskopie.

Die kristalstrukture van [Rh(acac)(CO)(4R, 8S-Lim-Ph)] en [Rh(acac)(CO)(PA-Ph)] is verkry en gekarakteriseer met X-straal kristallografie.

Die oksidatiewe addisie en CO-inlassings reaksies van die rhodium komplekse van die ligande is uitgevoer en die resultate dui aan dat die Lim-Ph sisteem die meeste aktief was van al die bisikliese ligande wat ingesluit is in die studie.

Die algemene reaktiwiteits reeks vir die oksidatiewe addisie is bepaal as: 4S, 8S-Lim-Ph > 4R, 8S-Lim-Ph > VCH-Ph > Phoban[3.3.1]-Ph > Phoban[4.2.1]-Ph > PPh_3 ~ PCy_3 > PA-Ph.

Die totale reaktiwiteits orde vir die CO-inlassings reaksie is bepaal as 4S, 8S-Lim-Ph > 4R, 8S-Lim-Ph > Phoban[4.2.1]-Ph > VCH-Ph > Phoban[3.3.1]-Ph > PA-Ph.

Sleutelwoorde: Katalise, Kobalt, Hidroformilering, Autoklaaf, Kristallografie, Fosfien ligande, Selenied komplekse, Koppelings konstante, Rhodium, Oksidatiewe addisie, CO inlassing, UV-Sig, Infrarooi, Staak vloei, kinetika.

Appendix

Table of content

Appendix

Appendix A of Chapter 3

A3.1. Electronic data

Table A3.1: ^{31}P NMR data and cone angles for conventional ligands.

Ligands	Se-Phoban / ppm	$^{1}J_{Se-P}$ / Hz	θ °
$P^{i}Bu_3$	33.5	688	
$P^{n}Bu_3$	36.5	683	
$P^{t}Bu_3$	92.8	687	
PCp_3	62.8	687	169
PCy_3	59.4	676	174
PPh_3	36.5	731	
$P(p\text{-MeOPh})_3$	31.6	708	
$P(2\text{-furyl})_3$	21.8	793	

Table A3.3: ^{31}P NMR data and cone angles for bicyclic phosphine derivatives (P-Q) with aliphatic or alicyclic side chains.

Q	Abbreviation	Source	$\theta°$	Yield		P-Q/ δ		Bp	Se-Phoban		$^{1}J_{Se-P}$	
				g	%	ppm		°C	ppm		Hz	
Lim									**4R**	**4S**	**4R**	**4S**
H	Lim-H	Cytec				-73.6	-97.6					
C_2H_5	Lim-C_5			34.30	78	-45.6	-52.2	312	26.8	22.1	686	684
C_5H_4	Lim-Cp	Cytec				-29.6	-37.5	321	40.7	36.6	687	690
C_6H_5	Lim-Ph		158	14.59	74	-32.7	-43.9	343	20.7	18.5	699	693
	BisLim	Cytec				-39.8,-40.4	-46.9, -47.0	438	29.1, 28.9	26.0, 25.7	690, 690	689, 689
VCH												
									[3.3.1]	**[3.2.2]**	**[3.3.1]**	**[3.2.2]**
H	VCH-H	Cytec				-59.9		-				
C_2H_5	VCH-C_5			1.84	56.5	-31.9		303	31.4		678	
C_4H_9	VCH-^{i}Bu	Cytec	168			-35.3	-36.3		29.8	29.7	673	688
C_6H_5	VCH-Ph			2.71	55.2	-20.5	-23.8	330	27.1	25.6	696	695
PA												
H	PA-H	Cytec				-49.6	-	-				
C_2H_5	PA-C_5	20.85	168	20.85	77	-28.5	-	297	36.3		751	
C_6H_5	PA-Ph			19.32	70	-24.1	-	315	31		752	

Table A3.5: Hydrogen coordinates (x 10^4) and isotropic displacement parameters ($Å^2$ X 10^4) for Se-Phoban[3.3.1]-C_2.

	x	y	z	U(eq)
H11	6443	-628	9678	450
H12A	4225	-3532	9881	520
H12B	3169	-2353	9109	520
H13A	2169	-5057	8115	550
H13B	4358	-5195	8189	550
H14A	2764	-3200	6485	560
H14B	3691	-4708	6160	560
H15	5802	-1854	5635	480
H16A	7585	-3884	6102	640
H16B	8919	-1920	6455	640
H17A	9530	-3590	8028	670
H17B	7239	-4640	8107	670
H18A	8078	-2834	9833	600
H18B	9296	-1182	9096	600
H21A	8779	2250	8030	560
H21B	9627	776	7516	560
H22A	8783	1345	5494	1060
H22B	9989	3194	6142	1060
H22C	7630	2635	5943	1060

Table A3.6: Anisotropic displacement parameters ($Å^2$ X 10^4) for Se-Phoban[3.3.1]-C_2. The anisotropic displacement factor exponent takes the form: $-2\pi^2[h^2a^{*2}U11 + ... + 2hka^*b^*U12]$.

	U11	U22	U33	U23	U13	U12
Se	434(2)	514(2)	618(2)	496(16)	189(15)	251.8(16)
P	302(4)	333(4)	376(4)	10(3)	9(3)	97(3)
C11	408(16)	383(16)	336(14)	-55(12)	5(12)	144(13)
C12	476(18)	460(18)	388(16)	89(14)	92(14)	171(15)
C13	410(17)	365(16)	571(19)	48(14)	25(14)	78(13)
C14	472(19)	418(17)	479(18)	-101(14)	-49(15)	101(14)
C15	413(17)	431(17)	366(15)	-4(14)	29(13)	139(14)
C16	500(2)	570(2)	590(2)	-87(17)	126(16)	222(17)
C17	437(19)	580(2)	740(2)	-38(18)	10(17)	291(17)
C18	410(18)	560(2)	560(2)	64(16)	-57(15)	186(15)
C21	338(16)	486(18)	541(19)	-2(15)	15(14)	69(14)
C22	640(2)	690(2)	610(2)	120(2)	108(19)	-79(19)

Table A3.8: Bond angles [°] for Se-Phoban[3.3.1]-C_2.

Bond angle	Å/°	Bond angle	Å/°
C15-P-C21	109.85(14)	C16-C15-H15	108.0
C15-P-C11	97.00(13)	C14-C15-H15	108.0
C21-P-C11	108.30(14)	P-C15-H15	108.0
C15-P-Se	114.98(10)	C17-C16-C15	116.0(2)
C21-P-Se	110.64(11)	C17-C16-H16A	108.3
C11-P-Se	115.22(9)	C15-C16-H16A	108.3
C18-C11-C12	115.0(2)	C17-C16-H16B	108.3
C18-C11-P	110.2(2)	C15-C16-H16B	108.3
C12-C11-P	107.69(19)	H16A-C16-H16B	107.4
C18-C11-H11	107.9	C16-C17-C18	115.9(3)
C12-C11-H11	107.9	C16-C17-H17A	108.3(
P-C11-H11	107.9	C18-C17-H17A	108.3
C13-C12-C11	115.6(2)	C16-C17-H17B	108.3
C13-C12-H12A	108.4	C18-C17-H17B	108.3
C11-C12-H12A	108.4	H17A-C17-H17B	107.4
C13-C12-H12B	108.4	C11-C18-C17	116.4(2)
C11-C12-H12B	108.4	C11-C18-H18A	108.2
H12A-C12-H12B	107.4	C17-C18-H18A	108.2
C12-C13-C14	115.9(2)	C11-C18-H18B	108.2
C12-C13-H13A	108.3	C17-C18-H18B	108.2
C14-C13-H13A	108.3	H18A-C18-H18B	107.3
C12-C13-H13B	108.3	C22-C21-P	113.3(2)
C14-C13-H13A	108.3	C22-C21-H21A	108.9
H13A-C13-H13B	107.4	P-C21-H21A	108.9
C13-C14-C15	116.3(3)	C22-C21-H21B	108.9
C13-C14-H14A	108.2	P-C21-H21B	108.9
C15-C14-H14A	108.2	H21A-C21-H21B	107.7
C13-C14-H14B	108.2	C21-C22-H22A	109.5
C15-C14-H14B	108.2	C21-C22-H22B	109.5
H14A-C14-H14B	107.4	H22A-C22-H22B	109.5
C16-C15-C14	114.9(2)	C21-C22-H22C	109.5
C16-C15-P	109.9(2)	H22A-C22-H22C	109.5
C14-C15-P	107.73(19)	H22B-C22-H22C	109.5

Table A3.10: Hydrogen coordinates (x 10^4) and isotropic displacement parameters ($Å^2$ X 10^4) for Se-Phoban[3.3.1]-Cy.

	x	y	z	U(eq)
H11A	8497	206	2772	260
H12A	9164	505	169	260
H12B	8402	497	-388	260
H13A	8846	1415	-1757	260
H13B	9212	1630	108	260
H14A	8367	2372	-260	260
H14B	7847	1809	-750	260
H15A	7570	2222	2181	260
H16A	8622	2633	3277	260
H16B	8276	2192	4829	260
H17A	9365	1900	4967	260
H17B	9436	1871	2759	260
H18A	9484	791	3648	260
H18B	8908	874	5136	260
H11B	8524	228	1720	240
H12C	9134	1106	-337	240
H12D	8452	798	-1028	240
H13C	8042	1802	-1178	240
H13D	8704	2103	-306	240
H14C	7544	2166	1445	240
H15B	8025	2488	4168	240
H15C	8453	2782	2511	240
H16C	9251	2491	4283	240
H16D	8830	1948	5327	240
H17C	9809	1592	4037	240
H17D	9506	1712	2025	240
H18C	9517	568	2943	240
H18D	8997	735	4539	240
H21	7308	844	-204	160
H22A	6264	992	2518	180
H22B	6491	1563	1114	180
H23A	5521	1002	-68	210
H23B	6122	932	-1496	210
H24A	5704	-84	1073	220
H24B	5622	-122	-1139	220
H25A	6785	-201	1528	190
H25B	6549	-773	-142	190
H26A	6901	-133	2498	190
H26B	7513	-225	1111	190

Table A3.12: Bond length [Å] for Se-Phoban[3.3.1]-Cy.

Bond length	Å/°	Bond length	Å/°
Se-P	2.1160(9)	C13B-C14B	1.576(15)
P-C14B	1.89(2)	C13B-H13C	9700
P-C11A	1.817(7)	C13B-H13D	9700
P-C15A	1.810(10)	C14B-C15B	1.497(19)
P-C21	1.832(3)	C14B-H14C	9800()
P-C11B	1.922(13)	C15B-C16B	1.503(13)
C11A-C12A	1.530(7)	C15B-H15B	9700()
C11A-C18A	1.540(8)	C15B-H15C	9700
C11A-H11A	9800	C16B-C17B	1.440(13)
C12A-C13A	1.502(7)	C16B-H16C	9700
C12A-H12A	9700	C16B-H16D	9700
C12A-H12B	9700	C17B-C18B	1.532(13)
C13A-C14A	1.529(7)	C17B-H17C	9700
C13A-H13A	9700()	C17B-H17D	9700
C13A-H13B	9700	C18B-H18C	9700
C14A-C15A	1.525(8)	C18B-H18D	9700
C14A-H14A	9700	C21-C26	1.528(4)
C14A-H14B	9700	C21-C22	1.534(4)
C15A-C16A	1.560(9)	C21-H21	9800
C15A-H15A	9800	C22-C23	1.533(4)
C16A-C17A	1.532(7)	C22-H22A	9700
C16A-H16A	9700	C22-H22B	9700
C16A-H16B	9700	C23-C24	1.526(4)
C17A-C18A	1.533(7)	C23-H23A	9700
C17A-H17A	9700	C23-H23B	9700
C17A-H17B	9700	C24-C25	1.519(4)
C18A-H18A	9700()	C24-H24A	9700()
C18A-H18B	9700	C24-H24B	9700
C11B-C18B	1.515(16)	C25-C26	1.536(4)
C11B-C12B	1.562(14)	C25-H25A	9700
C11B-H11B	9800	C25-H25B	9700
C12B-C13B	1.521(13)	C26-H26A	9700
C12B-H12C	9700	C26-H26B	9700
C12B-H12D	9700		

Table A3.14: Bond angles [°] for Se-Phoban[3.3.1]-Cy, continue.

Bond angle	Å/°	Bond angle	Å/°
P-C15A-H15A	109.0	C23-C22-H22A	109.6
C17A-C16A-C15A	117.4(5)	C21-C22-H22A	109.6
C17A-C16A-H16A	108	C23-C22-H22B	109.6
C15A-C16A-H16A	108	C21-C22-H22B	109.6
C17A-C16A-H16B	108	H22A-C22-H22B	108.2
C15A-C16A-H16B	108	C24-C23-C22	111.1(3)
H16A-C16A-H16B	107.2	C24-C23-H23A	109.4
C16A-C17A-C18A	115.9(4)	C22-C23-H23A	109.4
C16A-C17A-H17A	108.3	C24-C23-H23B	109.4
C18A-C17A-H17A	108.3	C22-C23-H23B	109.4
C16A-C17A-H17B	108.3	H23A-C23-H23B	108.0
C18A-C17A-H17B	108.3	C25-C24-C23	111.4(3)
H17A-C17A-H17B	107.4	C25-C24-H24A	109.4
C11A-C18A-C17A	117.6(5)	C23-C24-H24A	109.4
C11A-C18A-H18A	107.9	C25-C24-H24B	109.4
C17A-C18A-H18A	107.9	C23-C24-H24B	109.4
C11A-C18A-H18B	107.9	H24A-C24-H24B	108.0
C17A-C18A-H18B	107.9	C24-C25-C26	110.6(3)
H18A-C18A-H18B	107.2	C24-C25-H25A	109.5
C18B-C11B-C12B	113.0(9)	C26-C25-H25A	109.5
C18B-C11B-P	111.7(8)	C24-C25-H25B	109.5
C12B-C11B-P	102.0(8)	C26-C25-H25B	109.5
C18B-C11B-H11B	110.0	H25A-C25-H25B	108.1
C12B-C11B-H11B	110.0	C21-C26-C25	109.8(3)
P-C11B-H11B	110.0	C21-C26-H26A	109.7
C13B-C12B-C11B	113.5(10)	C25-C26-H26A	109.7
C13B-C12B-H12C	108.9	C21-C26-H26B	109.7
C11B-C12B-H12C	108.9	C25-C26-H26B	109.7
C13B-C12B-H12D	108.9	H26A-C26-H26B	108.2

Table A3.16: Hydrogen coordinates (x 10^4) and isotropic displacement parameters ($Å^2$ X 10^4) for Se-Phoban[3.3.1]-Ph.

	x	y	z	U(eq)
H11A	1969	3309	5654	350
H12A	1218	2434	3576	350
H12B	1165	3498	3043	350
H13A	-940	3536	3110	350
H13B	-617	2573	2256	350
H14A	-1163	1730	4416	350
H14B	-2243	2468	4146	350
H15A	-1793	2299	6874	350
H16A	-1631	3824	7711	350
H16B	-2465	3825	6149	350
H17A	-1024	4556	4655	350
H17B	-981	5088	6325	350
H18A	873	4476	6984	350
H18B	1005	4769	5156	350
H11B	2128	2968	5399	310
H12C	610	3486	3026	310
H12D	1205	2470	3152	310
H13C	-577	1827	3665	310
H13D	-1185	2799	3172	310
H14C	-1653	2102	5918	310
H15B	-2544	3512	5394	310
H15C	-1854	3634	7054	310
H16C	-1732	4948	5336	310
H16D	-907	4345	4149	310
H17C	-133	4596	7365	310
H17D	131	5398	6096	310
H18C	1567	4569	4816	310
H18D	1820	4341	6643	310
H22	2408	1575	5319	370
H23	2885	22	4837	430
H24	1565	-1154	5662	400
H25	-256	-781	6986	410
H26	-729	776	7503	350

Table A3.18: Bond length [Å] for Se-Phoban[3.3.1]-Ph.

Bond length	Å/°	Bond length	Å/°
Se-P	2.1090()	C118-C12B	1.585(13)
P-C21.1.	1.8109(8)	C11B-H11B	1.0000()
P-C15A-	1.816(6)	C12B-C13B	1.537(12)
P-C11A	1809(8)	C12B-H12C	0.9900
P-C21	1.816(3)	C12B-H12D	0.9900
P-C115A	1.837(6)	C13B-C14B	1.540(10)
P-C14B	1.853(8)	C13B-H13C	0.9900
P-C11B	1.863(12)	C13B-H13D	0.9900
P-C118	1.863(12)	C14B-C15B	1.527(11)
C11A-C12A	1.523(10)	C14B-H14C	1.0000
C11A-C18A	1.552(8)	C15B-C16B	1.508(10)
C11A-H11A	1.0000	C15B-H15B	0.9900
C12A-C13A	1.570(9)	C15B-H15C	0.9900
C12A-H12A	0.9900	C16B-C17B	1.537(10)
C12A-H12B	0.9900	C16B-H16C	0.9900
C13-C14A	1.506 (7)	C16B-H16D	0.9900
C13A-H13A	0.9900	C17B-C188	1.549(11)
C13A-H13B	0.9900	C17B-H17C	0.9900
C14A-C15A	1.526(8)	C17B-H17D	0.9900
C14-H14A	0.9900	C18B-H18C	0.9900
C14A-H14B	0.9900	C18B-H18D	0.9900
C15A-C16A	1.543(7)	C21-C26	1.390(4)
C15A-H15A	1.0000	C21-C22	1.399(4)
C16A-C17A	1.548(7)	C22-C23.	1.382(4)
C16A-H16A	0.9900	C22-H22	0.9500
C16A-H16B	0.9900	C23-C24	1.381(5)
C17A-C18A	1.547(7)	C23-H23	0.9500
C17A-H17A	0.9900	C24-C25	1.387(5)
C17A-H17B	0.9900	C24-H24	0.9500
C18A-H18A	0.9900	C25-C26	1.389(4)
C18-H18B	0.9900	C25-H25	0.9500
C11B-C18B	1.532(13)	C26-H26	0.9500

Table A3.20: Bond angles [°] for Se-Phoban[3.3.1]-Ph, continue.

Bond angle	Å/°	Bond angle	Å/°
C13B-C12B-H12C	109.4	C16B-C17B-C188	117.1(6)
C11B-C12B-H12C	109.4	C16B-C17B-H17C	108.0
C13-C12B-H12D	109.4	C18B-C17B-H17C	108.0
C11B-C12B-H12D	109.4	C16B-C17B-H17D	108.0
H12C-C12B-H12D	108.0	C18B-C17B-H17D	108.0
C12B-C13B-C14B	111.9(8)	H17C-C17B-H17D	107.3
C12B-C13B-H13C	109.2	C11B-C18B-C17B	120.4(7)
C14B-C13B-H13C	109.2	C11B-C18D-H18C	107.2
C12B-C13B-H13D	109.2	C17-C18B-H18C	107.2
C14B-C13B-H13D	109.2	C11-C18B-H18B	107.2
H13C-C13B-H13D	107.9	C17B-C18B-H18D	107.2
C15B-C14B-C13B	112.7 (7)	H18C-C18B-H18D	106.9
C15B-C14B-P	111.9(6)	C26-C21-C2	118.9(3)
C13B-C14B-P	102.5(5)	C26-C21-P	118.4(2)
C15B-C14B-H14C	109.9	C22-C21-P	122.7(2)
C13B-C14B-H14C	109.9()	C23-C22-C21	120.1(3)
P-C14B-H14C	109.9	C23-C22-H22	119.9
C16B-C15B-C14B	110.4(7)	C21-C22-H22	119.9
C16B-C15B-H15B	107.5	C24-C23-C22	120.5(3)
C14B-C15B-H15B	107.5	C24-C23-H23	119.8
C16B-C15B-H15C	107.5	C22-C23-H23	119.8
C14B-C15B-H15C	107.5	C23-C24-C25	120.1(3)
H15B-C15B-H15C	107.0	C23-C24-H24	119.9
C15B-C16B-C17B	113.7(6)	C24-C25-C26	119.5(3)
C15B-C16B-H16C	108.8	C24-C25-H25	120.2
C17B-C16B-H16C	108.8	C26-C25-H25	120.2
C15B-C16BH16D	108.8	C25-C26-C21	120.8(3
C17B-C16B-H16D	108.8	C25-C26-H26	119.6
H16C-C16B-H16D	107.7	C21-C26-H26	119.6

A3.2.4. Se-VCH[3.3.1]-^{i}Bu

Table A3.22: Atomic coordinates (x 10^4) and equivalent isotropic displacement parameters ($Å^2$ x10^4) for Se-VCH[3.3.1]-^{i}Bu. U(eq) is defined as one third of the trace of the orthogonalized Uij tensor.

	x	y	z	U(eq)
Se	2330.8(6)	-934(2)	240.5(4)	633(3)
P	2184.7(13)	-934(2)	-335.5(8)	418(4)
C11	1179(6)	-851(9)	-1269(3)	588(16)
C12	1797(6)	105(11)	-1899(4)	712(19)
C13	3099(7)	-640(12)	-1997(4)	780(2)
C14	3999(6)	-340(10)	-1255(4)	699(19)
C15	3697(5)	-1675(8)	-582(4)	528(15)
C16	3785(6)	-3676(8)	-870(4)	610(17)
C17	2984(7)	-4081(11)	-1622(4)	820(2)
C18	3119(8)	-2667(14)	-2240(5)	910(2)
C21	1449(5)	-2707(7)	190(3)	452(13)
C22	1795(5)	-2755(8)	1068(3)	490(14)
C23	893(6)	-4026(10)	1427(4)	680(18)
C24	3154(6)	-3372(10)	1303(4)	708(19)

Table A3.25: Bond length [Å] for Se-VCH[3.3.1]-^{i}Bu.

Bond length	Å/°	Bond length	Å/°
P-C15	1.822(6)	C16-H16A	0.9700
P-C21	1.825(6)	C16-H16B	0.9700
P-C11	1.835(6)	C17-C18	1.514(12)
P-Se	2.1360(16)	C17-H17A	0.9700
C11-C12	1.531(9)	C17-H17B	0.9700
C11-H11A	9700	C18-H18A	0.9700
C11-H11B	9700	C18-H18B	0.9700
C12-C13	1.534(10)	C21-C22	1.533(8)
C12-H12A	0.9700	C21-H21A	0.9700
C12-H12B	0.9700	C21-H21B	0.9700
C13-C14	1.527(9)	C22-C24	1.530(9)
C13-C18	1.532(12)	C22-C23	1.536(8)
C13-H13	9800	C22-H22	0.9800
C14-C15	1.594(9)	C23-H23A	0.9600
C14-H14A	0.9700	C23-H23B	0.9600
C14-H14B	0.9700	C23-H23C	0.9600
C15-C16	1.544(8)	C24-H24A	0.9600
C15-H15	0.9800	C24-H24B	0.9600
C16-C17	1.501(9)	C24-H24C	0.9600

Table A3.26: Bond angles [°] for Se-VCH[3.3.1]-^{i}Bu.

Bond angle	Å/°	Bond angle	Å/°
C15-P-C21	112.0(3)	C18-C13-C12	114.7(6)
C15-P-C11	103.6(3)	C14-C13-H13	107.4
C21-P-C11	103.3(3)	C18-C13-H13	107.4
C15-P-Se	111.27(19)	C12-C13-H13	107.4
C21-P-Se	113.12(19)	C13-C14-C15	112.0(5)
C11-P-Se	112.9(3)	C13-C14-H14A	109.2
C12-C11-P	113.3(4)	C15-C14-H14A	109.2
C12-C11-H11A	108.9	C13-C14-H14B	109.2
P-C11-H11A	108.9	C15-C14-H14B	109.2
C12-C11-H11B	108.9	H14A-C14-H14B	107.9
P-C11-H11B	108.9	C16-C15-C14	107.5(5)
H11A-C11-H11B	107.7	C16-C15-P	116.8(4)
C11-C12-C13	114.6(6)	C14-C15-P	106.0(4)
C12-C11-H12A	108.6	C16-C15-H15	108.7
C13-C12-H12A	108.6	C14-C15-H15	108.7
C11-C12-H12B	108.6	P-C15-H15	108.7
C13-C12-H12B	108.6	C17-C16-C15	114.7(6)
H12A-C12-H12B	108.6	C17-C16-H16A	108.6
C14-C13-C18	110.0(7)	C15-C16-H16A	108.6
C14-C13-C12	109.6(6)	C17-C16-H16B	108.6

Appendix B of Chapter 4

B4.1. Calculation of equilibrium constants of modified-unmodified cobalt hydroformylation systems

The equilibrium between unmodified- and modified catalysis, as depicted below, was determined for selected ligands based on the results of the batch autoclave studies. The unmodified catalysis component is associated with high reaction rates, low hydrogenation and low linearities of the aldehyde products. In contrast, modified catalysis is characterised by lower reaction rates, increased hydrogenation (also resulting in paraffins as side products) and high linearity of the alcohol products.

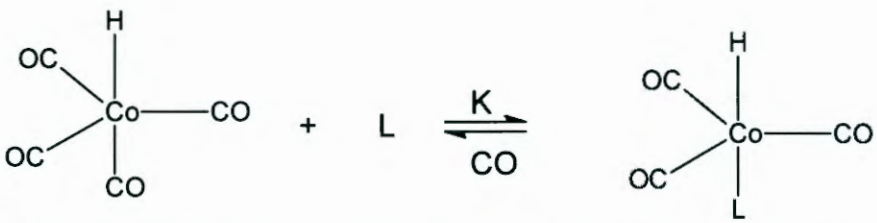

Figure B4.1: The ligand dependant equilibrium between the unmodified- and modified cobalt hydride species.

Values obtained for the reaction rate or alcohol linearity, as a function of ligand concentration, were fitted to the model given below:

Table B4.1: Models and catalytic parameters for calculating equilibrium constant.

Independant Variable: L_a	L_a = Ligand added initially
Dependant Variable: C	C = Catalytic parameter fitted, i.e. reaction rate or linearity
Parameters: C_M, C_U, K	C_M = Catalysis at fully modified conditions
	C_U = Catalysis at fully unmodified conditions
	K = Equilibrium constant
$K = M/(U*L_f)$	M = Concentration of modified catalyst
	U = Concentration of unmodified catalyst
	L_f = Concentration of free ligand at equilibrium
$C = (Up*U + Mp*M)/(Co)$	
$M = Co - U$	
$L_a = L_f + M$	
$Co = 0.040$	Co = Initial Co concentration
$M*M*K + M*(-K*Co - K*L_a - 1) + Co*K*L_a = 0$	

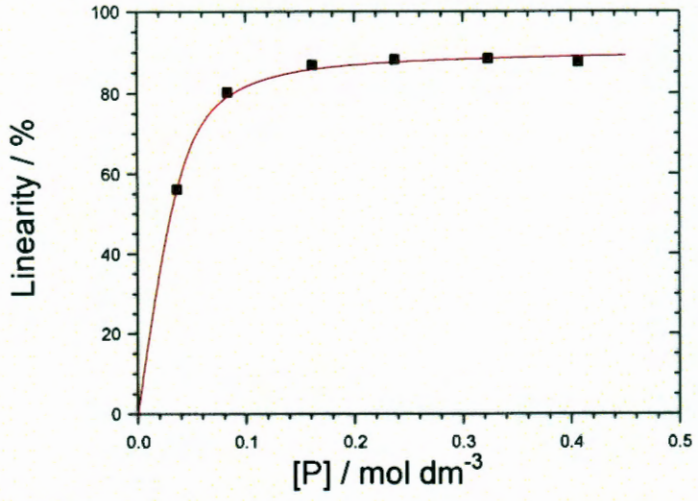

Figure B4.2: Linearity of the alcohol fraction as a function of Phoban[4.2.1]-C_2 concentration.

Parameter Name : M_P
Estimate Value = 90.73 ± 0.76

Parameter Name : K
Estimate Value =142 ± 15

Fix: K = 142

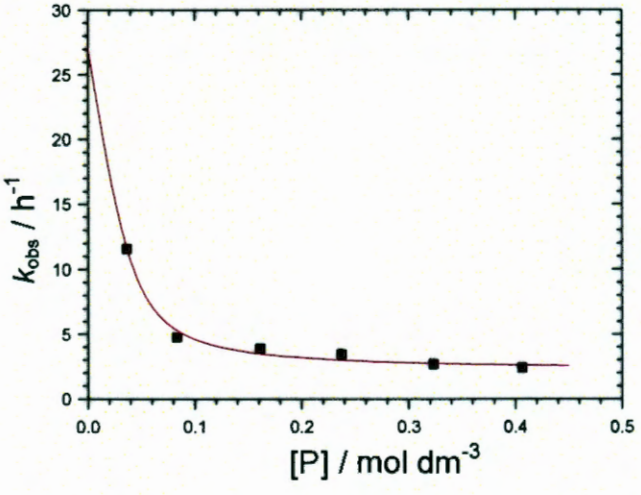

Figure B4.3: Rate of the alcohol formation as a function of Phoban[4.2.1]-C_2 concentration.

Parameter Name : M_P
Estimate Value =2.14 ± 0.22

Parameter Name : U_P
Estimate Value = 27 ± 1

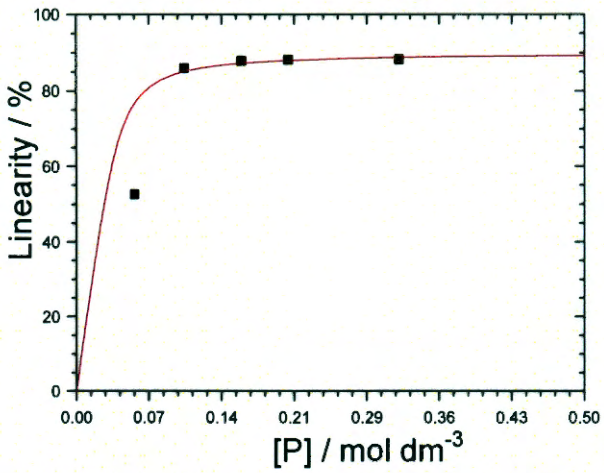

Figure B4.5: Linearity of the alcohol fraction as a function of Phoban-C_2 (mixture of isomers) concentration.

Parameters were adjusted and the simulation was visually evaluated to give the best fit.

M_P = 90; U_P = 0 K = 250

Table B4.5: Effect of concentration of Phoban-C_5 (mixture of isomers) on rate and product distribution.

[L]	L:M	k_{obs} (± 0.1)	Linearity	Hydrogenation	Yield
mmol dm^{-3}		h^{-1}	%	%	%
54	1.34	4.5	76.3	8.9	84.4
107	2.65	3.0	85.5	9.7	83.3
120	3.01	3.1	84.6	10.5	80.4
162	4.05	2.7	87.3	11.3	80.2
277	6.92	2.6	88.1	11.2	80.5
314	7.82	2.4	87.9	10.4	80.4

Fix: U_P = 0

Table B4.8: Effect of concentration of Phoban-C_3NMe_2 (mixture of isomers) on rate and product distribution.

[L]	L:M	k_{obs} (± 0.1)	Linearity	Hydrogenation	Yield
mmol dm^{-3}		h^{-1}	%	%	%
240	6.00	2.3	87.9	11.3	86.0
328	8.20	2.2	87.9	11.0	85.6

Table B4.9: Effect of concentration of Phoban-Cy (mixture of isomers) on rate and product distribution.

[L]	L:M	k_{obs} (± 0.1)	Linearity	Hydrogenation	Yield
mmol dm^{-3}		h^{-1}	%	%	%
74	1.84	6.1	63.6	10.2	79.3
147	3.68	2.5	85.9	13.5	76.9
221	5.53	1.8	88.2	14.6	76.4
332	8.30	1.8	89.1	14.6	76.1

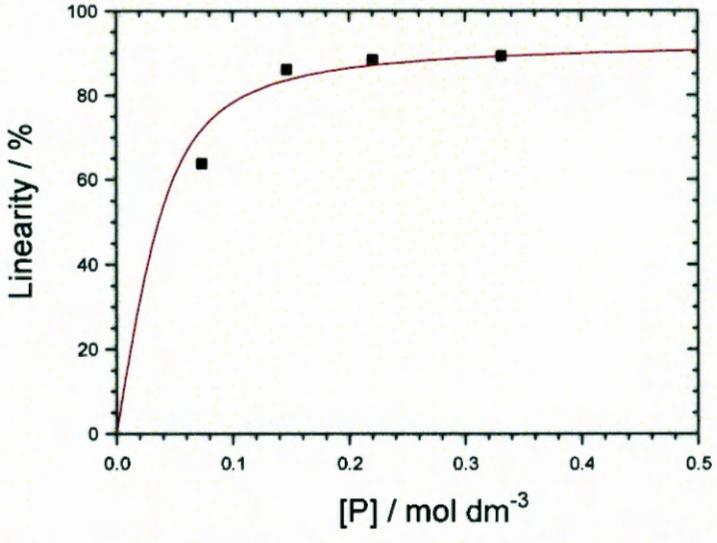

Figure B4.7: Linearity of the alcohol fraction as a function of Phoban-Cy (mixture of isomers) concentration.

Parameters were adjusted and the simulation was visually evaluated to give the best fit.

$M_P = 93$; $U_P = 0$ $K = 80$

Fix: $U_P = 27$

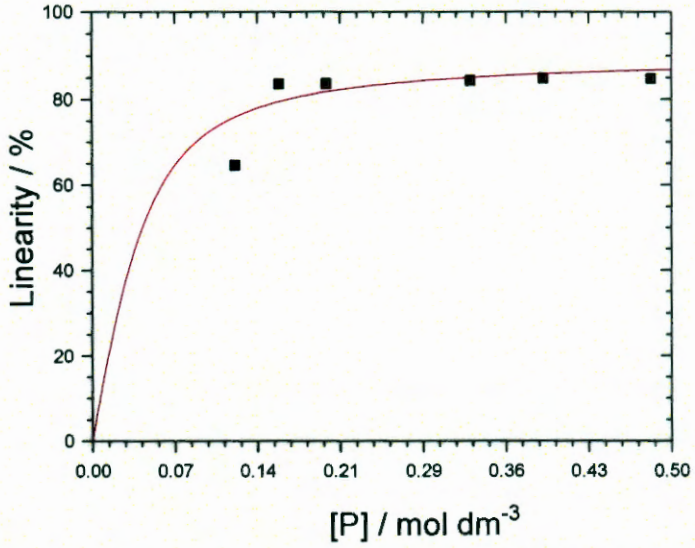

Figure B4.9: Linearity of the alcohol fraction as a function of Phoban-Ph (mixture of isomers) concentration.

Parameters were adjusted and the simulation was visually evaluated to give the best fit.

$M_P = 90$; $U_P = 0$; $K = 60$

Fix: $U_P = 27$ and $M_P = 2$

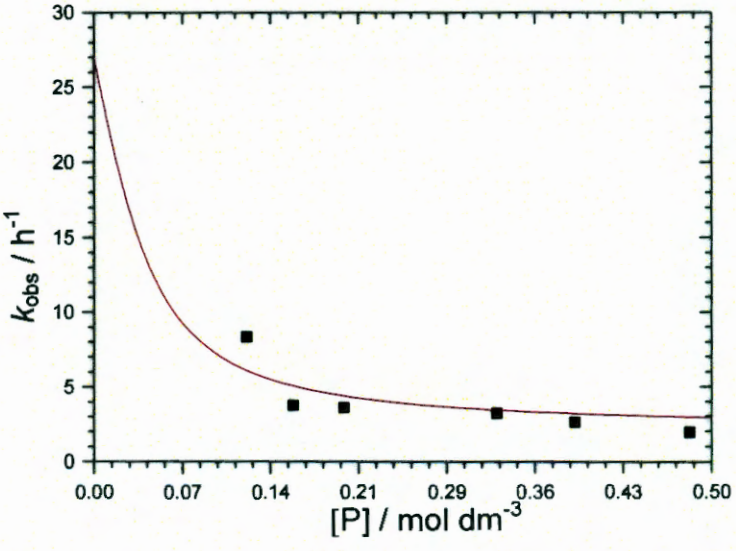

Figure B4.10: Rate of the alcohol formation as a function of Phoban-Ph (mixture of isomers) concentration.

Parameter Name : *K*

Table B4.13: Hydrogen coordinates (x 10^4) and isotropic displacement parameters ($Å^2$ X 10^4) for $[Co(Phoban[3.3.1]\text{-}C_2)(CO)_3]_2$.

	x	y	z	U(eq)
H21A	4349	3854	7388	780
H21B	4828	2920	7643	780
H22A	6121	4384	7356	1140
H22B	6622	3443	7587	1140
H22C	5825	3964	8195	1140
H11	3070	2583	6222	1020
H12A	3269	1440	5261	1330
H12B	3784	2336	4938	1330
H18A	3813	1882	7371	1830
H18B	3243	1165	6811	1830
H13A	5000	1313	4501	1770
H13B	5000	796	5320	1770
H17A	5000	609	6455	2690
H17B	5000	686	7394	2690

Table B4.14: Anisotropic displacement parameters ($Å^2$ X 10^4) for $[Co(Phoban[3.3.1]\text{-}C_2)(CO)_3]_2$. The anisotropic displacement factor exponent takes the form: $-2\pi^2[h^2a^{*2}U11 + \ldots + 2hka^*b^*U12]$.

	U11	U22	U33	U23	U13	U12
Co	552(9)	329(7)	395(8)	38(6)	000	000
C2	770(7)	530(5)	590(5)	140(4)	-90(5)	-100(5)
O2	950(6)	1140(7)	1160(6)	330(5)	-470(6)	-550(6)
C1	990(11)	360(6)	460(7)	70(5)	000	000
O1	2300(17)	630(7)	440(6)	-30(5)	000	000
P	650(2)	318(14)	367(14)	12(11)	000	000
C21	1120(12)	420(7)	420(7)	-30(5)	000	000
C22	930(15)	870(14)	480(11)	-160(10)	-140(11)	-250(13)
C11	1270(10)	660(6)	610(6)	-20(5)	190(7)	-510(7)
C12	1980(17)	790(8)	560(6)	-70(6)	-140(8)	-870(10)
C18	310(3)	830(9)	640(7)	-40(7)	320(12)	-1170(4)
C13	3300(4)	560(10)	530(10)	-250(8)	000	000
C17	570(8)	400(10)	660(12)	130(10)	000	000

Table B4.17: Torsion angles [°] for $[Co(Phoban[3.3.1]\text{-}C_2)(CO)_3]_2$.

Torsion angles	Å/°	Torsion angles	Å/°	Torsion angles	Å/°
C2-Co-C2-O2	130(11)	C2-Co-P-C11	-60.7(6)	C21-P-C11-C18	-48.0(11)
C1-Co-C2-O2	-67(12)	C2-Co-P-C11	175.1(6)	Co-P-C11-C18	-173.7(9)
P-Co-C2-O2	35(12)	C1-Co-P-C11	57.2(4)	C11-P-C11-C12	-64.6(10)
Co-Co-C2-O2	-150(12)	Co-Co-P-C11	-122.8(4)	C21-P-C11-C12	172.2(9)
C2-Co-C1-O1	-81.9(4)	C2-Co-P-C11	62.1(3)	Co-P-C11-C12	62.0(10)
C2-Co-C1-O1	81.9 (4)	C2-Co-P-C21	-62.1(3)	C18-C11-C12-C13	-62.4(17)
P-Co-C1-O1	180.00(8)	C1-Co-P-C21	180.000(2)	P-C11-C12-C13	59.9(14)
Co-Co-C1-O1	0.00(8)	Co-Co-P-C21	0.000(5)	C12-C11-C18-C17	59.7(19)
C2-Co-P-C11	-175.1(6)	C11-P-C21-C22	160.4(14)	P-C11-C18-C17	-60.3(14)
C2-Co-P-C11	60.7(6)	C11-P-C21-C22	60.6(15)	C11-C12-C13-C12	-44(2)
C1-Co-P-c11	-57.2(4)	Co-P-C21-C22	-69.5(14)	C11-C18-C17-C18	50(3)
Co-Co-P-C11	122.8 (4)	C11-P-C11-C18	59.6(11)		

B4.2.2. $[Co(Phoban[3.3.1]\text{-}C_5)(CO)_3]_2$

Table B4.18: Atomic coordinates (x 10^4) and equivalent isotropic displacement parameters (Å^2 x10^4) for $[Co(Phoban[3.3.1]\text{-}C_5)(CO)_3]_2$. U(eq) is defined as one third of the trace of the orthogonalized Uij tensor.

	x	y	z	U(eq)
Co	4552.7(4)	5882.3(4)	5653.8 (3)	442.9 (13)
P	4042.2(8)	7195.2(7)	6995.6(6)	427.9(16)
C1	3176(4)	6022(3)	4196(3)	601(7)
C2	3892(4)	4216(3)	6282(3)	613(7)
C3	6616(4)	7219(3)	6172(3)	537(6)
O1	2317(3)	6087(3)	3246(2)	988(8)
O2	3414(4)	3180(3)	6721(2)	950(8)
O3	7926(3)	8135(3)	6445(2)	749(6)
C11	1885(3)	6750(3)	6845(2)	516(6)
C12	1787(4)	7612(4)	7952(3)	678(8)
C13	2601(4)	9355(4)	8196(3)	751(9)
C14	4305(4)	10023(3)	8112(3)	6950(8)
C15	4515(3)	9261(3)	7004(2)	533(6)
C16	3455(4)	9451(3)	5741(3)	605(7)
C17	1572(4)	8714(4)	5306(3)	674(8)
C18	932(3)	7078(3)	5595(3)	592(7)
C21	5050(4)	6921(4)	8574(3)	624(7)
C22	6871(4)	7211(4)	9029(3)	744(9)
C231	7564(18)	7050(3)	10344(14)	860(7)
C241	9375(16)	7810(2)	11050(13)	1200()
C251	10460(3)	7460(3)	10520(2)	1360(10)
C232	7494(9)	6631(15)	10234(7)	820(3)
C242	9230(8)	6679(10)	10668(7)	1080(3)
C252	10481(12)	8232(12)	11053(13)	1560(5)

Table B4.20: Anisotropic displacement parameters ($Å^2$ X 10^4) for $[Co(Phoban[3.3.1]\text{-}C_5)(CO)_3]_2$. The anisotropic displacement factor exponent takes the form: $-2\pi^2[h^2a^{*2}U11 + ... + 2hka^*b^*U12]$.

	U11	U22	U33	U23	U13	U12
Co	470(2)	443(2)	522(2)	58.5(15)	230.8(16)	255.4(16)
P	424(3)	429(3)	488(4)	37(3)	190(3)	214(3)
C1	671(19)	685(18)	623(18)	69(14)	285(15)	430(16)
C2	770(2)	513(16)	699(19)	48(14)	366(16)	325(15)
C3	540(17)	582(17)	625(17)	86(13)	285(14)	308(14)
O1	1080(2)	1490(2)	602(14)	156(14)	170(13)	882(19)
O2	1560(2)	580(14)	1132(19)	335(13)	885(18)	493(15)
O3	526(13)	768(15)	914(16)	26(12)	316(12)	156(11)
C11	476(15)	501(15)	638(16)	39(12)	290(13)	188(12)
C12	627(19)	900(2)	671(19)	49(16)	345(16)	386(17)
C13	800(2)	860(2)	700(2)	-177(16)	273(17)	474(19)
C14	780(2)	568(18)	680(19)	-121(14)	157(16)	321(16)
C15	472(15)	424(14)	703(18)	-4(12)	225(13)	174(12)
C16	760(2)	467(15)	717(19)	163(13)	340(16)	308(15)
C17	720(2)	780(2)	636(19)	89(15)	182(15)	485(18)
C18	371(14)	724(19)	651(17)	-40(14)	159(13)	220(13)
C21	658(18)	726(19)	568(17)	109(14)	217(14)	365(16)
C22	652(19)	1030(3)	650(2)	258(18)	226(16)	428(19)
C231	760(8)	880(13)	980(13)	10(9)	200()	(520)8
C241	780(8)	990(15)	184(16)	80(12)	480(10)	360(10)
C251	900(14)	210(3)	1260(18)	480(18)	600(13)	530(19)
C232	720(4)	1000(7)	700(5)	440(4)	160(3)	330(3)
C242	860(4)	1220(6)	1000(5)	360(4)	50(4)	470(4)
C252	910(7)	1340(8)	1890(14)	170(7)	160(8)	160(6)

Table B4.22: Bond angles [°] for $[Co(Phoban[3.3.1]\text{-}C_5)(CO)_3]_2$.

Bond angles	Å/°	Bond angles	Å/°	Bond angles	Å/°
C2-Co-C3	125.90(14)	C13-C14-C15	116.1(2)	C231-C22-C232	14.5(15)
C2-Co-C1	117.62(15)	C13-C14-H14A	108.3	C21-C22-C232	113.3(4)
C3-Co-C1	114.72(14)	C15-C14-H14A	108.3	C231-C22-H22A	109.0
C2-Co-P	89.41(9)	C13-C14-H14B	108.3	C21-C22-H22A	109.0
C3-Co-P	91.65(9)	C15-C14-H14B	108.3	C232-C22-H22A	95.9
C1-Co-P	103.00(9)	H14A-C14-H14B	107.4	C231-C22-H22B	109.0
C2-CoCo	84.39(9)	C16-C15-C14	114.6(2)	C21-C22-H22B	109.0
C3-Co-Co	86.20(9)	C16-C15-P	107.67(18)	C232-C22-H22B	120.5
C1-Co-Co	86.29(8)	C14-C15-P	111.02(19)	H22A-C22-H22B	107.8
P-Co-Co	170.49(3)	C16-C15-H15	107.8	C241-C231-C22	118.7(13)
C15-P-C21	108.44(14)	C14-C15-H15	107.8	C241-C231-H23A	107.6
C15-P-C11	95.19(13)	P-C15-H15	107.8	C22-C231-H23A	107.6
C21-P-C11	103.37(13)	C15-C16-C17	116.8(2)	C241-C231-H23B	107.6
C15-P-Co	118.47(9)	C15-C16-H16A	108.1	C22-C231-H23B	107.6
C21-P-Co	110.73(10)	C17-C16-H16A	108.1	H23A-C231-H23B	107.1
C11-P-Co	118.76(9)	C15-C16-H16B	108.1	C251-C241-C231	117.2
O1-C1-Co	177.9(2)	C17-C16-H16B	108.1	C251-C241-H24A	108.0
O2-C2-Co	175.7(2)	H166-C16-H16B	107.3	C231-C241-H24A	108.0
O3-C3-Co	176.9(2)	C18-C17-C16	115.4(2)	C251-C241-H24B	108.0
C18-C11-C12	113.6(2)	C18-C17-H17A	108.4	C231-C241-H24B	108.0
C18-C11-P	108.65(17)	C16-C17-H17A	108.4	H24A-C241-H24B	107.3
C12-C11-P	111.34(19)	C18-C17-H17B	108.4	C242-C232-C22	117.1(6)
C18-C11-H11	107.7	C16-C17-H17B	108.4	C242-C232-H23C	108.0
C12-C11-H11	107.7	H17A-C17-H17B	107.5	C22-C232-H23C	108.0
P-C11-H11	107.7	C17-C18-C11	116.7(2)	H23C-C232-H23D	107.3
C13-C12-C11	116.3(3)	C17-C18-H18A	108.1	C252-C242-C232	114.0 (9)
C13-C12-H12A	108.2	C11-C18-H18A	108.1	C252-C242-H24C	108.8
C11-C12-H12A	108.2	C17-C18-H18B	108.1	C232-C242-H24C	108.8
C13-C12-H12B	108.2	C11-C18-H18B	108.1	C252-C242-H24D	108.8
C11-C12-H12B	108.2	H18A-C18-H18B	107.3	C232-C242-H24D	108.8
H12A-C12-H12B	107.4	C22-C21-P	118.1(2)	H24C-C242-H24D	107.7
C12-C13-C14	116.9(2)	C22-C21-H21A	107.8	C242-C252-H25D	109.5
C12-C13-H13A	108.1	P-C21-H21A	107.8	C242-C252-H25E	109.5
C14-C13-H13A	108.1	C22-C21-H21B	107.8	H25D-C252-H25E	109.5
C12-C13-H13B	108.1	P-C21-H21B	107.8	C242-C252-H25F	109.5
C14-C13-H13B	108.1	H21A-C21-H21B	107.1	H25D-C252-H25F	109.5
H13A-C13-H13B	107.3	C231-C22-C21	112.9(7)	H25E-C252-H25F	109.5

B4.2.3. [Co(Phoban[3.3.1]-Cy)$(CO)_3]_2$

Table B4.24: Atomic coordinates (x 10^4) and equivalent isotropic displacement parameters ($Å^2$ x10^4) for [Co(Phoban[3.3.1]-Cy)$(CO)_3]_2$. U(eq) is defined as one third of the trace of the orthogonalized Uij tensor.

	x	y	z	U(eq)
Co	4056(88)16	8313.96(17)	4888(54)11	131.4(6)
P	2582.9(3)	2308.4(2)	4842.2(2)	130.6(8)
O1	4610.8(10)	8494(10)	3110.2(6)	211(2)
O2	2477.6(11)	-1403.8(11)	5211(8)	316(3)
O3	5684.1(9)	2631.8(11)	5992.1 (7)	253 (2)
C1	4369.5(12)	8494(13)	3799.2(9)	164(3)
C2	3104.9(13)	-524.4(14)	5113.9(9)	203(3)
C3	5046.5(13)	1884.3(14)	5590.1(9)	179(3)
C11	2977(13)	3998.4(13)	4514.1(9)	182(3)
C12	1931.2(15)	4991.3(15)	4568.7(10)	249(3)
C13	6993(15)	4630.0(17)	4027.4(10)	292(4)13
C14	269.6 (13)	3185.5 (17)	4084.0 (10)	256(3)
C15	1235.4(13)	2102.5(15)	4006.4(9)	195(3)
C16	1677.4(14)	2064.9(16)	3117.3(9)	234(3)
C17	2408.9(14)	3208.6(16)	2882.3(9)	255(3)
C18	3352.9(14)	3892.5(14)	3601.8(10)	221(3)
C21	1954.0(12)	2503.8(13)	5871.9(8)	156(3)
C22	2922.9(13)	2921.2(15)	6633.3(9)	192(3)
C23	2332.2(14)	3153.8(15)	7446.5(9)	224.3()
C24	1662.3(15)	1913.2(15)	7683.5(9)	248(3)
C25	698.7(15)	1488.2(16)	6913.9(10)	269(3)
C26	1273.5(14)	1259.3(15)	6110.0(10)	225(3)

Table B4.26: Anisotropic displacement parameters ($Å^2$ X 10^4) for $[Co(Phoban[3.3.1]\text{-}Cy)(CO)_3]_2$. The anisotropic displacement factor exponent takes the form: $-2\pi^2[h^2a^{*2}U11 + ... + 2hka^*b^*U12]$.

	U11	U22	U33	U23	U13	U12
Co	155.1(10)	122.0(10)	121.5(9)	-4(9)	35.0(7)	35.9(7)
P	151.3(17)	121.5(16)	122.9(16)	1.7(12)	32.8(12)	29.0(12)
O1	268(5)	213(5)	163(5)	-17(4)	73(4)	-2(4)
O2	366(7)	190(6)	444(7)	-46(5)	231(6)	-32(5)
O3	232(5)	276(6)	245(5)	-91(4)	18(4)	10(4)
C1	171(6)	134(6)	186(7)	-14(5)	18(5)	11(5)
C2	244(7)	176(7)	208(7)	-12(5)	93(6)	67(6)
C3	192(7)	189(7)	165(6)	-7(5)	53(5)	71(5)
C11	229(7)	132(6)	198(7)	21(5)	75(5)	30(5)
C12	344(8)	166(7)	269(8)	51(6)	151(7)	94(6)
C13	323(9)	328(9)	242(8)	86(7)	102(6)	203(7)
C14	182(7)	386(9)	192(7)	1(6)	0000(5)	102(6)
C15	169(6)	250(7)	160(6)	-4(5)	9(5)	16(5)
C16	223(7)	320(8)	150(7)	-24(6)	1(5)	65(6)
C17	315(8)	309(8)	157(7)	55(6)	88(6)	118(7)
C18	294(8)	161(7)	236(7)	55(6)	129(6)	46(6)
C21	172(6)	152(6)	156(6)	-3(5)	66(5)	43(5)
C22	214(7)	207(7)	165(7)	-30(5)	58(5)	20(6)
C23	283(8)	230(7)	168(7)	-43(6)	60(6)	31(6)
C24	370(9)	212(7)	189(7)	5(6)	130(6)	60(6)
C25	341(9)	233(8)	273(8)	-23(6)	172(7)	-40(6)
C26	300(8)	193(7)	203(7)	-19(6)	108(6)	-31(6)

Table B4.27: Bond length [Å] for $[Co(Phoban[3.3.1]\text{-}Cy)(CO)_3]_2$.

Bond length	Å/°	Bond length	Å/°	Bond length	Å/°
Co-C3	1.7755(15)	C13-C14	1.532(3)	C21-C22	1.534(2)
Co-C1	1.7871(15)	C13-H13A	0.9700	C21-H21	0.9800
Co-C2	1.7875(16)	C13-H13B	0.9700	C22-C23	1.5314(19)
Co-P	2.1963(8)	C14-C15	1.541(2)	C22-H22A	0.9700
Co-Co	2.6526(10)	C14-H14A	0.9700	C22-H22B	0.9700
P-C15	1.8393(15)	C14-H14B	0.9700	C23-C24	1.523(2)
P-C11	1.8393(16)	C15-C16	1.541(2)	C23-H23A	0.9700
P-C21	1.8556(14)	C15-H15	0.9800	C23-H23B	0.9700
O1-C1	1.1474(17)	C16-C17	1.539(2)	C24-C25	1.522(2)
O2-C2	1.1467(19)	C16-H16A	0.9700	C24-H24A	0.9700
O3-C3	1.1490(18)	C16-H16B	0.9700	C24-H24B	0.9700
C11-C12	1.539(2)	C17-C18	1.541(2)	C25-C26	1.534(2)
C11-C18	1.5472(19)	C17-H17A	0.9700	C25-H25A	0.9700
C11-H11	0.9800	C17-H17B	0.9700	C25-H25B	0.9700
C12-C13	1.534(2)	C18-H18A	0.9700	C26-H26A	0.9700()
C12-H12A	0.9700	C18-H18B	0.9700	C26-H26B	0.9700
C12-H12B	0.9700	C211.-C26	1.533(2)		

B4.2.4. [Co(Phoban[3.3.1]-C_3NMe_2)$(CO)_3]_2$

Table B4.29: Atomic coordinates (x 10^4) and equivalent isotropic displacement parameters ($Å^2$ x10^4) for [Co(Phoban[3.3.1]-C_3NMe_2)$(CO)_3]_2$. U(eq) is defined as one third of the trace of the orthogonalized Uij tensor.

	x	y	z	U(eq)
Co	9682.2(4)	86.4(4)	4004.6(3)	306.6(16)
P	9440.5(7)	268.1(10)	2416.3(6)	349(2)
N	13369(4)	156(4)	2791(3)	670(11)
O1	7334(2)	-257(3)	3971(2)	523(7)
O2	11145(3)	-2134(3)	4173(2)	713(10)
O3	10481(3)	2722(3)	4356(2)	539(7)
C1	8240(3)	-137(3)	3960(2)	374 (8)
C2	10572(3)	-1261(4)	4124(3)	441(9)
C3	10192(3)	1682(4)	4242(2)	380(8)
C11	8666(4)	-1070(5)	1551(3)	586(12)
C12	8707(4)	-810(6)	518(3)	690(15)
C13	8233(5)	415(6)	25(4)	728(15)
C14	8554(4)	1580(5)	633(3)	531(11)
C15	8485(3)	1522(4)	1676(3)	401(8)
C16	7266(3)	1288(4)	1677(3)	425(8)
C17	6683(3)	44(4)	1212(3)	493(10)
C18	7396(3)	-1160(4)	1570(3)	445(9)
C21	10819(4)	353(5)	2256(3)	605(12)
C22	11657(4)	1307(6)	2846(4)	681(14)
C23	12766(4)	1381(5)	2632(4)	594(12)
C24	13790(7)	-182(7)	3826(6)	1180(3)
C25	14336(5)	245(5)	2464(5)	799(17)

Table B4.31: Anisotropic displacement parameters ($Å^2$ X 10^4) for $[Co(Phoban[3.3.1]\text{-}C_3NMe_2)(CO)_3]_2$. The anisotropic displacement factor exponent takes the form: $-2\pi^2[h^2a^{*2}U11 + ... + 2hka^*b^*U12]$.

	U11	U22	U33	U23	U13	U12
Co	313(2)	372(3)	199(2)	-28.3(18)	51.3(17)	29.0(19)
P	289(4)	520(6)	214(4)	-56(4)	62(3)	16(4)
N	570(2)	780(3)	640(3)	20(2)	190(2)	-50(2)
O1	408(15)	760(2)	408(15)	2(14)	162(13)	-29(14)
O2	950(3)	720(2)	462(18)	80(16)	256(18)	430(2)
O3	700(2)	447(17)	421(16)	-86(13)	151(15)	-85(14)
C1	409(19)	450(2)	226(15)	-9(14)	70(14)	39(15)
C2	520(2)	520(2)	266(17)	4(16)	120(16)	124(18)
C3	392(19)	480(2)	227(16)	-36(14)	70(14)	25(16)
C11	610(3)	730(3)	320(2)	-70(2)	51(19)	250(2)
C12	510(3)	1190(5)	380(2)	-210(3)	160(2)	50(3)
C13	810(4)	990(3)	490(3)	-70(3)	360(3)	-100(3)
C14	510(2)	760(3)	330(2)	148(19)	165(18)	100(2)
C15	470(2)	420(2)	316(18)	9(15)	151(16)	-20(16)
C16	440(2)	470(2)	390(2)	90(16)	173(17)	118(16)
C17	319(17)	640(3)	500(2)	90(2)	131(17)	-1(18)
C18	470(2)	480(2)	332(19)	-86(16)	91(17)	-10(17)
C21	390(2)	1050(4)	370(2)	-10(2)	141(18)	-30(2)
C22	530(3)	990(4)	520(3)	-40(3)	190(2)	-160(3)
C23	410(2)	770(3)	610(3)	-20(2)	200(2)	-160(3)
C24	1110(6)	1420(7)	800(5)	210(4)	90(4)	420(5)
C25	530(3)	770(4)	1120(5)	-150(3)	320(3)	-10(2)

Table B4.33: Bond angles [°] for [Co(Phoban[3.3.1]-C_3NMe_3)$(CO)_3]_2$.

Bond angles	Å/°	Bond angles	Å/°	Bond angles	Å/°
C2-Co-C3	124.47(19)	H12A-C12-H12B	107.1	P-C21-H21A	107.9
C2-Co-C1	119.08(18)	C14-C13-C12	117.4(4)	C22-C21-H21B	107.9
C2-Co-C1	114.45(17)	C14-C13-H13A	108.0	C11-C18-H18B	108.8
C2-Co-P	90.70(12)	C12-C13-H13A	108.0	C17-C18-H18B	108.8
C3-Co-P	91.25(11)	C14-C13-H13B	108.0	C11-C18-H18B	108.8
C1-Co-P	102.76(11)	C12-C13-H13B	108.0	H18A-C18-H18B	107.7
C2-Co-Co	85.01(12)	H13A-C13-H13B	107.2	C22-C21-P	117.7(4)
C3-Co-Co	85.02(11)	C13-C14-C15	116.7(4)	P-C21-H21B	107.9
C1-Co-Co	85.91(11)	C13-C14-H14A	108.1	H21A-C21-H21B	107.2
P-Co-Co	171.33(4)	C15-C14-H14A	108.1	C21-C22-C23	115.1(4)
C21-P-C15	108.6(2)	C13-C14-H14B	108.1	C21-C22-H22A	108.5
C21-P-C11	103.4(2)	C15-C14-H14B	108.1	C23-C22-H22A	108.5
C15-P-C11	94.68(19)	H14A-C14-H14B	107.3	C21-C22-H22B	108.5
C21-P-Co	111.08(15)	C14-C15-C16	114.6(3)	C23-C22-H22B	108.5
C15-P-Co	18.61 (12)	C14-C15-P	109.9(3)	H22A-C22-H22B	107.5
C11-P-Co	117.60(15)	C16-C15-P	108.5(2)	N-C23-C22	112.1(4)
C24-N C25	108.9(5)	C14-C16-H15	107.9	N-C23-H23A	109.2
C24-N-C23	110.6(5)	C16-C15-H15	107.9	C22-C23-H23A	109.2
C25-N-C23	109.5(4)	P-C15-H15	107.9	N-C23-H23B	109.2
O1-C1-Co	177.1(3)	C17-c16-c15	116.6(3)	C22-C23-H23B	109.2
O2-C2-C0	178.0(3)	C17-C16-H16A	108.1	H23A-C23-H23B	107.9
O3-C3-Co	177.0(3)	C15-C16-H16B	108.1	N-C24-H24A	109.5
C12-C11-C18	114.4(3)	C17-C16-H16B	108.1	N-C24-H24B	109.5
C12-C11-P	108.5(4)	C15-C16- H16B	108.1	H24A-C24-H24B	109.5
C18-C11-P	107.6(3)	H16A-C16-H16B	107.3	N-C24-H24C	109.5
C12-C11-H11	108.7	C18-C17-C16	115.8(3)	H24A-C24-H24C	109.5
C18-C11-H11	108.7	C18-C17H17A	108.3	H24B-C24-H24C	109.5
P-C11-H11	108.7	C16-C17-H17A	108.3	N-C25-H25A	109.5
C13-C12-C11	118.1(4)	C18-C17-H17B	108.3	N-C25-H25B	109.5
C13-C12-H12A	107.8	C16-C17-H17B	108.3	H25A-C25-H25B	109.5
C11-C12-H12A	107.8	H17A-C17-H17B	107.4	N-C25-H25C	109.5
C13-C12-H12B	107.8	C17-C18-C11	113.9(3)	H25A-C25-H25C	109.5
C11-C12-H12B	107.8	C17A-C18-H18A	108.8	H25B-C25-H25C	109.5

Table B4.35 mol. 2: Atomic coordinates (x 10^4)and equivalent isotropic displacement parameters (Å^2 x10^4) for molecule 2, [Co(PA-C_5)$(CO)_3]_2$. U(eq) is defined as one third of the trace of the orthogonalized Uij tensor; continue.

Co2	5957.8(3)	280.2(3)	4736.4(3)	196.8(11)
P2	7513.9(6)	845.9(6)	4379.8(5)	164.7(18)
O21	6591(2)	-1427(2)	5890.0(17)	383(7)
O22	5366(2)	1962(2)	5192(2)	630(11)
O23	5323(2)	99(3)	3224.8(18)466	8()
O24	7352.3(18)	1419.9(18)	2830.8(14)	270(6)
O25	9076.2(19)	1125.6(19)	2518.2(15)	287(6)
O26	9461.1(17)	6131(18)	3842(15)	258(6)
C21	6351(2)	-755(3)	5438(2)	256(8)
C22	5589(3)	1290(3)	5021(3)	377(10)
C23	5586(3)	173(3)	3808(2)	293(9)
C211	7635(3)	1812(2)	3450(2)	238(8)
C212	8751(3)	2159(3)	3305(2)	258(8)
C213	9441(3)	1394(3)	3160(2)	246(8)
C214	8057(3)	740(3)	2664(2)	260(8)
C215	8093(3)	-132(2)	3340(2)	221(7)
C216	8494(2)	94(2)	4054(2)	212(7)
C217	6878(3)	2604(3)	3422(3)	383(10)
C218	1055(3)	1699(3)	2967(3)	408(11)
C219	7709(3)	551(3)	1929(2)	341(9)
C220	8763(3)	-773(3)	4700(2)	312(9)
C221	8176(3)	1332(3)	5075(2)	253(8)
C222	7951(3)	879 (3)	5926(2)	306(9)
C223	8608(3)	1257(3)	6449(2)	256(8)
C224	8354(4)	924(4)	7298(3)	547(14)
C225	9126(3)	1174(3)	7817(2)	397(10)

Table B4.37: Hydrogen coordinates (x 10^4) and isotropic displacement parameters ($Å^2$ X 10^4) for molecule 1, $[Co(PA\text{-}C_5)(CO)_3]_2$.

	x	y	z	U(eq)
H11A	6431	3091	6701	230
H11B	7569	3448	6465	230
H11C	6175	6064	7247	210
H11D	6004	6374	6351	210
H11E	5682	3578	5387	370
H11F	6828	3751	5065	370
H11G	6007	4550	4815	370
H11H	7946	3064	7932	420
H11I	6798	2715	8114	420
H11J	7218	3506	8456	420
H11K	4032	4622	7140	390
H11L	4149	5680	6663	390
H11M	4400	5373	7545	390
H12A	7994	6451	7223	380
H12B	7973	6942	6330	380
H12C	8789	6158	6651	380
H12A	6086	6287	5101	250
H12B	7029	6939	5115	250
H12C	7775	6494	4023	300
H12D	6734	5971	3983	300
H12E	6897	7927	3792	390
H12F	5849	7411	3770	390
H12G	6418	7047	2631	460
H12H	6417	8138	2509	460
H12I	8227	8083	2675	690
H12J	7926	7756	1950	690
H12K	8199	7008	2722	690

Table B4.39: Hydrogen coordinates (x 10^4) and isotropic displacement parameters ($Å^2$ X 10^4) for molecule 3, $[Co(PA\text{-}C_5)(CO)_3]_2$, continue.

	x	y	z	U(eq)
H31A	4815	7594	7941	360
H31B	4541	8206	8511	360
H31C	5953	5537	10299	280
H31D	6936	6185	10057	280
H31E	7297	8569	7977	530
H31F	6247	9104	7796	530
H31G	6535	8296	7414	530
H31H	3282	6566	8438	630
H31I	2966	7110	9048	630
H31J	3163	6023	9320	630
H31K	6428	4681	9339	570
H31L	7412	5306	9033	570
H31M	6564	5215	8456	570
H32A	5068	7396	11010	400
H32B	6155	6919	11150	400
H32C	5159	6297	11216	400
H32D	7639	7742	10232	290
H32E	7839	7520	9434	290
H1A	7810	9413	9485	440
H1B	8326	9022	8829	440
H1C	7962	9215	8872	440
H1D	8026	9288	9721	440
H32F	9619	9367	9660	390
H32G	9100	8627	10369	390
H32H	10171	8192	9125	460
H32I	9588	7432	9790	460
H32J	11245	8504	10074	930
H32K	11379	7481	9991	930
H32L	10715	7653	10688	930
H32M	9631	9412	9065	510
H32N	9515	8357	9048	510
H32O	9388	7870	10412	610
H32P	9454	8920	10442	610
H32Q	11098	7929	9934	850
H32R	11090	8272	10688	850
H32S	11170	9007	9871	850
H1A	8237	4963	2410	1610
H1B	8049	4819	1591	1610
H1C	7652	5732	1792	1610
H2A	10942	3846	8932	800
H2B	10650	3889	8083	800
H3A	9369	4552	8713	1710
H3B	9785	5260	7949	1710
H4A	10633	6164	8678	1680
H4B	9450	6065	8929	1680
H5A	10882	4776	9680	1420
H5B	10689	5695	9927	1420

Table B4.41: Anisotropic displacement parameters ($Å^2$ X 10^4) for molecule 2, $[Co(PA\text{-}C_5)(CO)_3]_2$. The anisotropic displacement factor exponent takes the form: $-2\pi^2[h^2a^{*2}U11 + ... + 2hka^*b^*U12]$, continue.

	U11	U22	U33	U23	U13	U12
Co2	109(2)	230(3)	283(3)	-126(2)	12.3(18)	-14.5(17)
P2	121(4)	164(4)	213(5)	-57(3)	-10(3)	-3(3)
O21	343(15)	379(18)	350(17)	22(14)	52(12)	-20(13)
O22	322(16)	500(2)	1270(3)	-630(2)	351(18)	-173(14)
O23	250(14)	840(3)	408(19)	-341(18)	-31(13)	-73(15)
O24	290(13)	277(14)	253(14)	-83(11)	-69(11)	28(11)
O25	300(13)	322(15)	254(14)	-115(11)	75(11)	-110(11)
O26	144(11)	280(14)	324(15)	-41(11)	26(10)	-53(10)
C21	140(15)	330(2)	310(2)	-125(17)	77(14)	-57(14)
C22	159(17)	430(3)	630(3)	-310(2)	104(18)	-72(16)
C23	132(16)	380(2)	420(2)	-198(19)	9(15)	-30(15)
C211	271(18)	137(17)	300(2)	-47(15)	-34(15)	7(14)
C212	295(18)	206(19)	260(2)	-40(15)	15(15)	-91(15)
C213	238(17)	260(2)	236(19)	-70(15)	39(14)	-106(14)
C214	255(18)	260(2)	290(2)	-126(16)	18(15)	-62(15)
C215	197(16)	181(18)	310(2)	-128(15)	75(14)	-25(13)
C216	148(15)	181(17)	290(2)	-45(14)	28(13)	9(13)
C217	480(2)	210(2)	450(3)	-70(18)	-80(2)	126(18)
C218	320(2)	510(3)	400(3)	-160(2)	141(18)	-235(19)
C219	390(2)	400(2)	290(2)	-178(19)	-20(17)	-35(18)
C220	243(18)	240(2)	440(3)	-80(17)	-2(17)	72(15)
C221	201(16)	270(2)	300(2)	-100(16)	2(14)	-60(14)
C222	315(19)	350(2)	270(2)	-122(17)	28(16)	-130(16)
C223	236(17)	260(2)	290(2)	-118(16)	-1(15)	-41(14)
C224	710(3)	660(4)	280(2)	-140(2)	90(2)	-380(3)
C225	480(2)	410(3)	340(2)	-150(2)	-44(19)	-20(2)

Table B4.43: Bond length [Å] for molecule 1, $[Co(PA\text{-}C_5)(CO)_3]_2$.

Bond length	Å/°	Bond length	Å/°	Bond length	Å/°
Co1-C11	1.776(4)	C112-C113	1.508(5)	C120-H12A	0.9600
Co1-C12	1.780(4)	C112-H11A	0.9700	C120-H12B	0.9600
Co1-C13	1.795(4)	C112-H11B	0.9700	C120-H12C	0.9600
Co1-P1	2.1887(12)	C113-C118	1.502(5)	C121-C122	1.522(5)
Co1-Co1	2.6632(12)	C114-C119	1.501(4)	C121-H12A	0.9700
P1-C121	1.841(3)	C114-C115	1.509(5)	C121-H12B	0.9700
P1-C116	1.872(4)	C115-C116	1.521(4)	C122-C123	1.513(5)
P1-C111	1.877(3)	C115- H11C	0.9700	C122-H12C	0.9700
O11-C11	1.145(4)	C115-H11D	0.9700	C122-H12D	0.9700
O12-C12	1.154(5)	C116-C120	1,509(5)	C123-C124	1.524(6)
O13-C13	1.143(4)	C117-H11E	0.9600	C123-H12E	0.9700
O14-C114	1.430(4)	C117-H11F	0.9600	C123-H12F	0.9700
O14-C111	1.451 (4)	C117-H11G	0.9600	C124-C125	1.517(6)
O15-C114	1.424(4)	C118-H11H	0.9600	C124-H12G	0.9700
O15-C13	1.427(4)	C118-H11I	0.9600	C124-H12H	0.9700
O16-C113	1.430(4)	C118-H11J	0.9600	C125-H12I	0.9600
O16-C116	1.452(4)	C119-H11K	0.9600	C125-H12J	0.9600
C111-C117	1.506(5)	C119-H11L	0.9600	C125-H12K	0.9600
C111-C112	1.523(4)	C119-H11M	0.9600		

Table B4.44: Bond length [Å] for molecule 2, $[Co(PA\text{-}C_5)(CO)_3]_2$.

Bond length	Å/°	Bond length	Å/°	Bond length	Å/°
Co2-C22	1.761(4)	C212-C213	1.508(5)	C220-H22A	9600
Co2-C21	1.781(4)	C212-H21A	0.9700	C220-H22B	9600
Co2-C23	1.799(4)	C212-H21B	0.9700	C220-H22C	9600
Co2-P2	2.1882(11)	C213-C218	1.505(5)	C221-C222	1.508(5)
Co2-Co2	2.6717(12)	C214-C219	1.505(5)	C221-H22A	9700
P2-C221	1.839(4)	C214-C215	1.510(5)	C221-H22B	9700
P2-C216	1.861(3)	C215-C216	1.519(5)	C222-C223	1.504(5)
P2-C211	1.877(4)	C215- H21C	9700	C222-H22C	9700
O21-C21	1.146(4)	C215-H21D	9700	C222-H22D	9700
O22-C22	1.149(5)	C216-C220	1.523(5)	C223-C224	1.491(5)
O23-C23	1.144(5)	C217-H21E	9600	C223-H22E	9700
O24-C214	1.436(4)	C217-H21F	9600	C223-H22F	9700
O24-C211	1.444(4)	C217-H21G	9600	C224-C225	1.503(6)
O25-C213	1.413(4)	C218-H21H	9600	C224-H22G	9700
O25-C214	1.426(4)	C218-H21I	9600	C224-H32H	9700
O26-C213	1.434(4)	C218-H21J	9600	C225-H22I	9600
O26-C216	1.454(4)	C219-H21K	9600	C225-H22J	9600
C211-C217	1.514(5)	C219-H21L	9600	C225-H22K	9600
C211-C212	1.524(5)	C219-H21M	9600		

Table B4.46: Bond angles [°] for molecule 1, $[Co(PA\text{-}C_5)(CO)_3]_2$.

Bond angles	Å/°	Bond angles	Å/°	Bond angles	Å/°
C11-Co1-C12	119.91(18)	O15-C113-C112	107.2(3)	H11K-C119-H11M	109.5
C11-Co1-C13	117.94(18)	O16-C113-C112	111.8(3)	H11L-C119-H11M	109.5
C12-Co1-C13	119.79(18)	C118-C113-C112	113.6(3)	C116-C120-H12A	109.5
C11-Co1-P1	92.15(11)	O15-C114-O14	110.9(3)	C116-C120-H12B	109.5
C12-Co1-P1	95.94(11)	O15-C114-C119	107.0(3)	H12A-C120-H12B	109.5
C13-Co1-P1	97.25(11)	O14-C114-C119	106.6(3)	C116-C120-H12C	109.5
C11-Co1-Co1	82.98(11)	O15-C114-C115	108.6(3)	H12A-C120-H12C	109.5
C12-Co1-Co1	84.39(11)	O14-C114-C115	110.5(3)	H12B-C120-H12C	109.5
C13-Co1-Co1	87.29(11)	C119-C114-C115	113.3(3)	C122-C121-P1	116.4(2)
P1- Co1-Co1	174.52(4)	C114-C115-C116	110.8(3)	C122-C121-H12A	108.2
C121-P1-C116	104.11(15)	C114-C115-H11C	109.5	P1-C121-H12A	108.2
C121-P1-C111	104.69(15)	C116-C115-H11C	109.5	C122-C121-H12B	108.2
C116-P1-C111	93.82(15)	C114-C115-H11D	109.5	P1-C121-H12B	108.2
C121-P1-Co1	115.11 (11)	C116-C115-H11D	109.5	H12A-C121-H12B	107.4
C116-P1-Co1	116.33(10)	H11C-C115-H11D	108.1	C123-C122-C121	111.7(3)
C111-P1-Co1	119.77(11)	O16-C116-C120	105.5(3)	C123-C122-H12C	109.3
C114-O14-C111	115.7(2)	O16-C116-C115	108.9(2)	C121-C122-H12C	109.3
C114-O15-C113	112.1(2)	C120-C116-C115	112.4(3)	C123-C122-H12D	109.3
C113-O16-C116	116.1(2)	O16-C116-P1	106.8(2)	C121-C122-H12D	109.3
O11-C11-Co1	178.7(3)	C120-C116-P1	113.4(2)	H12C-C122-H12D	107.9
O12-C12-Co1	179.6(3)	C115-C116-P1	109.6(2)	C122-C123-C124	113.7(3)
O13-C13-Co1	176.9(3)	C111-C117-H11E	109.5	C122-C123-H12E	108.8
O14-C111-C117	105.1(3)	C111-C117-H11F	109.5	C124-C123-H12E	108.8
O14-C111-C112	108.7(3)	H11E-C117-H11F	109.5	C122-C123-H12F	108.8
C117-C111-C112	113.2(3)	C111-C117-H11G	109.5	C124-C123-H12F	108.8
O14-C111-P1	109.3(2)	H11E-C117-H11G	109.5	H12E-C122-H12F	107.7
C117-C111-P1	113.1(2)	H11F-C117-H11G	109.5	C125-C124-C123	114.0(3)
C112-C111-P1	107.4(2)	C113-C118-H11H	109.5	C125-C124-H12G	108.8
C113-C112-C111	110.9(3)	C113-C118-H11I	109.5	C123-C124-H12G	108.8
C113-C112-H11A	109.5	H11H-C118-H11I	109.5	C125-C124-H12H	108.8
C111-C112-H11A	109.5	C113-C118-H11J	109.5	C123-C124-H12H	108.8
C113-C112-H11B	109.5	H11H-C118-H11J	109.5	H12G-C124-H12H	107.7
C111-C112-H11B	109.5	H11I-C118-H11J	109.5	C124-C125-H12I	109.5
H11A-C112-H11B	109.5	C114-C119-H11K	109.5	C124-C125-H12J	109.5
O15-C113-O16	110.4(3)	C114-C119-H11L	109.5	H12I-C125-H12J	109.5
O15-C113-O18	107.3(3)	H11K-C119-H11L	109.5	C124-C125-H12K	109.5
O16-C113-O18	106.5(3)	C114-C119-H11M	109.5	H12I-C125-H12K	109.5
				H12J-C125-H12K	109.5

Table B4.48: Bond angles [°] for molecule 3, $[Co(PA\text{-}C_5)(CO)_3]_2$.

Bond angles	Å/°	Bond angles	Å/°	Bond angles	Å/°
C33-Co3-C32	118.72(18)	C320-C316-P3	112.8(2)	H32F-C323-H32G	107.4
C33-Co3-C31	120.54(17)	C315-C316-P3	110.9(2)	C323-C324-C325	112.6(8)
C32-Co3-C31	118.09(18)	C311-C317-H31E	109.5	C323-C324-H32H	109.1
C33-Co3-P3	89.77(12)	C311-C317-H31F	109.5	C325-C324-H32H	109.1
C32-Co3-P3	99.40(13)	H31E-C317-H31F	109.5	C323-C324-H32I	109.1
C31-Co3-P3	97.17(12)	C311-C317-H31G	109.5	C325-C324-H32I	109.1
C33-Co3-Co3	80.74(12)	H31E-C317-H31G	109.5	H32H-C324-H32I	107.8
C32-Co3-Co3	88.27(13)	H31F-C317-H31G	109.5	C322-C326-C327	107.1(10)
C31-Co3-Co3	84.84(12)	C313-C318-H31H	109.5	C322-C326-H32M	110.3
P3- Co3-Co3	169.90(4)	C313-C318-H31I	109.5	C327-C326-H32M	110.3
C321-P3-C316	104.40(40)	H31H-C318-H31I	109.5	C322-C326-H32N	110.3
C321-P3-C311	103.79(17)	C313-C318-H31J	109.5	C327-C326-H32N	110.3
C316-P3-C311	93.89(16)	H31H-C318-H31J	109.5	H32M-C326-H32N	108.6
C321-P3-Co3	116.05(13)	H31I-C318-H31J	109.5	C326-C327-C328	110.9(11)
C316-P3-Co3	113.34(12)	C314-C319-H31K	109.5	C326-C327-H320	109.5
C311-P3-Co3	122.05(12)	C314-C319-H31L	109.5	C328-C327-H320	109.5
C314-O34-C311	115.5(3)	H31K-C319-H31L	109.5	C326-C327-H32P	109.5
C313-O35-C314	112.0(3)	H31K-C319-H31M	109.5	C328-C327-H32P	109.5
C313-O36-C316	116.3(3)	H31L-C319-H31M	109.5	H320-C327-H32P	108.0
O31-C31-Co3	178.1(4)	C316-C320-H32A	109.5	C327-C328-H32Q	109.5
O32-C32-Co3	177.3(4)	C316-C320-H32B	109.5	C327-C328-H32R	109.5
O33-C33-Co3	176.4(3)	H32A-C320-H32B	109.5	H32Q-C328-H32R	109.5
O34-C311-C317	176.4(3)	C316-C320-H32C	109.5	C327-C328-H32S	109.5
O34-C311-C312	108.9(3)	H32A-C320-H32C	109.5	H32Q-C328-H32S	109.5
C317-C311-C312	113.4(3)	H32B-C320-H32C	109.5	H32R-C328-H32S	109.5
O34-C311-P3	109.8(2)	C322-C321-P3	116.0(2)	C2-C1-H1A	109.5
C317-C311-P3	113.4(3)	C322-C321-H32D	108.3	C2-C1-H1B	109.5
C312-C311-P3	106.9(3)	P3-C321-H32D	108.3	H1A-C1-H1C	109.5
C313-C312-C311	110.7(3)	C322-C321-H32E	108.3	H1B-C1-H1C	109.5
C313-C312-H31A	109.5	P3-C321-H32E	108.3	C1-C2-C3	114.3(7)
C311-C312-H31A	109.5	H32D-C321-H32E	107.4	C1-C2-H2A	108.7
C313-C312-H31B	109.5	C326-C322-C321	118.0(6)	C3-C2-H2A	108.7
C311-C312-H31B	109.5	C326-C222-C323	32.1(5)	C1-C2-H2B	108.7
H31A-C312-H31B	108.1	C321-C322-C323	109.3(4)	C3-C2-H2B	108.7
O35-C313-O36	110.4(3)	C326-C322-H1A	126.2	H2A-C2-H1B	107.6
O35-C313-O318	108.2(3)	C321-C322-H1A	109.8	C2-C3-C4	120.7(7)
O35-C313-C312	108.1(3)	C323-C322- H1A	109.8	C2-C3-H3A	107.1
O36-C313-C312	106.4(3)	C326-C322- H1B	78.0	C4-C3-H3A	107.1
C318-C313-C312	112.6(3)	C321-C322-H1B	109.8	C2-C3-H3B	107.1
O35-C314-O34	1102.7(3)	C323-C322-H1B	109.8	C4-C3-H3B	107.1
O35-C314-C319	108.0(3)	C321-C322-H1C	107.8	H3A-C3-H3B	106.8
O34-C314-C319	107.3(3)	C323-C322-H1C	136.2	C5-C4-C3	107.1(7)
O35-C314-C3	108.4(3)	H1A-C322-H1C	78.0	C5-C4-H4A	110.3
O34-C314-C315	110.3(3)	H1B-C322-H1C	33.8	C3-C4-H4A	110.3
C319-C314-C315	112.1(3)	C326-C322-H1D	107.8	C5-C4-H4B	110.3
C314-C315-C316	111.2(3)	C321-C322-H1D	107.8	C3-C4-H4B	110.3
C314-C315-H31C	109.4	C323-C322-H1D	82.8	H4A-C4-H4B	108.6
C316-C315-H31C	109.4	H1A-C322-H1D	30.4	C5-C5-C4	123.3(11)
C314-C315-H31D	109.4	H1B-C322-H1D	132.8	C5-C5-H5A	106.5
C316-C315-H31D	109.4	H1C-C322-H1D	107.1	C4-C5-H5A	106.5

Table B4.50: Hydrogen coordinates (x 10^4) and isotropic displacement parameters ($Å^2$ X 10^4) for $[Co(PCy_3)(CO)_3]_2$.

	x	y	z	U(eq)
H11	7745	2274	1251	120
H12A	6004	1746	295	140
H12B	6181	1181	-580	140
H13A	7030	188	1442	180
H13B	6163	-462	445	180
H14A	7785	-1406	946	180
H14B	7349	-802	-152	180
H15A	9099	-244	864	170
H15B	8869	326	1704	170
H16A	8119	1324	-306	170
H16B	8958	1967	712	170
H21	7833	3579	-1205	130
H22A	6744	1785	-1657	160
H22B	5766	2655	-2224	160
H23A	7321	2369	-2809	180
H23B	6186	1851	-3442	180
H24A	5516	3844	-3913	180
H24B	6425	3720	-4169	180
H25A	6508	5639	-3315	180
H25B	7533	4855	-2721	180
H26A	5946	4955	-2166	150
H26B	7037	5597	-1538	150
H31	8979	3941	920	140
H32A	8034	5570	1716	180
H32B	8431	4218	2141	180
H33A	9674	5740	3175	220
H33B	10148	4811	2699	220
H34A	9446	7267	1968	220
H34B	13610	6830	2502	220
H35A	10282	5570	1101	220
H35B	9894	6928	690	220
H36A	8636	5434	-362	170
H36B	8171	6341	139	170

Table B4.52: Bond length [Å] for $[Co(PCy_3)(CO)_3]_2$.

Bond length	Å/°	Bond length	Å/°	Bond length	Å/°
Co-C3	1.7787(12)	C14-H14A	0.9700	C25-H25B	0.9700
Co-C1	1.7829(12)	C14-H14B	0.9700	C26-H26A	0.9700
Co-C2	1.7841(13)	C15-C16	1.5300(16)	C26-H26B	0.9700
Co-P	2.1949(3)	C15-H15A	0.9700	C31-C36	1.5361(16)
Co-Co	2.6478(3)	C15-H15B	0.9700	C31-C32	1.5383(16)
P-C11	1.8619(11)	C16-H16A	0.9700	C31-H31	0.9800
P-C21	1.8619(11)	C16-H16B	0.9700	C32-C33	1.5322(17)
P-C31	1.8707(12)	C21-C22	1.5384(16)	C32-H32A	0.9700
O1-C1	1.1466(15)	C21-C26	1.5429(16)	C32B-H32B	0.9700
O2-C2	1.1463(15)	C21-H21	0.9800	C33-C34	1.5240(18)
O3-C3	1.1466(15)	C22-C23	1.5324(16)	C33-H33A	0.9700
O11-C16	1.5398(16)	C22-H22A	0.9700	C33-H33B	0.9700
O11-C12	1.5403(16)	C22-H22B	0.9700	C34-C35	1.5220(18)
O11-H11	0.9800	C23-C24	1.5215(17)	C34-H34A	0.9700
C12-C13	1.5282(16)	C23-H23A	0.9700	C34-H34B	0.9700
C12-H12A	0.9700	C23-H23B	0.9700	C35-C36	1.5325(17)
C12-H12B	0.9700	C24-C25	1.5222(17)	C35-H35A	0.9700
C13-C14	1.5242(17)	C24-H24A	0.9700	C35-H35B	0.9700
C13-H13A	0.9700	C24-H24B	0.9700	C36-H36A	0.9700
C13-H13B	0.9700	C25-C26	1.5327(16)	C36-H36B	0.9700
C14-C15	1.5215(17)	C25-H25A	0.9700		

B4.2.7. $[Co(PCp_3)(CO)_3]_2$

Table B4.54: Atomic coordinates (x 10^4) and equivalent isotropic displacement parameters ($Å^2$ x10^4) for $[Co(PCp_3)(CO)_3]_2$. U(eq) is defined as one third of the trace of the orthogonalized Uij tensor.

	x	y	z	U(eq)
Co1	5654.3(4)	9157.2(4)	4577.0(3)	122.2(13)
Co2	10584.5(4)	4085.2(4)	458.7(3)	130.6(14)
P1	6507.0(8)	7696.6(7)	3841.3(6)	111.8(19)
P2	11498.9(8)	2510.4(7)	1142.2(6)	118.7(19)
O11	3564(3)	7873(2)	5351.4(19)	250(6)
O12	5172(3)	10562(2)	2939.3(18)	267(6)
O13	7910(3)	9533(3)	5674(2)	331(7)
O21	13035(3)	4830(3)	-343(2)	307(7)
O22	8905(3)	2830(2)	-596(2)	307(7)
O23	9565 (4)	5268(3)	2026(2)	403(8)
C11	4365(4)	8397(3)	5054(2)	167(7)
C12	5367(4)	10032(3)	3590(2)	169(7)
C13	7048(4)	9363(3)	5243(2)	196(7)
C21	12082(4)	4523(3)	-32(2)	196(7)
C22	9548(4)	3333(3)	-178(2)	200(7)
C23	9969(4)	4791(3)	1418(3)	231(8)
C111	6407(3)	6337(3)	4472(2)	140(7)
C112	7160 (4)	5235(3)	4105(2)	177(7)
C113	7895(4)	4615(3)	4907(3)	215(8)
C114	7198(4)	5110 (3)	5721 (3)	215 (8)
C115	6871(4)	6355(3)	5438(2)	172(7)
C121	5587(3)	7621(3)	2812(2)	135(6)
C122	4047(3)	7652(3)	2946(2)	168(7)
C123	3552(4)	7071(4)	2150(3)	248(8)
C124	4778(4)	6770(3)	1564(2)	201(8)
C125	5934(4)	6620(3)	2222(2)	184(7)
C131	8242(3)	7697(3)	3434(2)	142(7)
C132	8575(3)	8836(3)	3006(2)	166(7)
C133	10103(4)	8661(3)	2882(3)	228(8)
C134	10601(4)	7818(4)	3635(3)	269(9)

Table B4.56: Hydrogen coordinates (x 10^4) and isotropic displacement parameters ($Å^2$ X 10^4) for $[Co(PCp_3)(CO)_3]_2$.

	x	y	z	U(eq)
H111	5460	6216	4505	170
H11A	6534	4767	3869	210
H11B	7790	5422	3640	210
H11C	7831	3806	4908	260
H11D	8829	4744	4890	260
H11E	7782	5019	6227	206
H11F	6393	4755	5869	260
H11G	7652	6762	5469	210
H11H	6168	6707	5811	210
H121	5740	8303	7446	160
H12A	3833	7248	3497	200
H12B	3640	8427	2959	200
H12C	3149	6394	2348	300
H12D	2895	7579	1825	300
H12E	4899	7373	1121	240
H12F	4704	6075	1270	240
H12G	5955	5902	2562	220
H12H	6787	6667	1920	220

Table B4.58: Anisotropic displacement parameters ($Å^2$ X 10^4) for $[Co(PCp_3)(CO)_3]_2$. The anisotropic displacement factor exponent takes the form: $-2\pi^2[h^2a^{*2}U11 + ... + 2hka^*b^*U12]$.

	U11	U22	U33	U23	U13	U12
Co1	111(2)	98(2)	154(2)	-14.9(17)	0.9(17)	8.9(17)
Co2	120(2)	107(2)	157(3)	5.5(17)	-197(17)	19.5(17)
P1	96(4)	103(4)	134(4)	-5(3)	-7(3)	3(3)
P2	101(4)	119(4)	134(4)	-6(3)	-17(3)	4(3)
O11	241(15)	236(14)	285(15)	-51(11)	94(12)	-78(12)
O12	332(17)	214(14)	240(15)	45(11)	-50(12)	17(12)
O13	231(16)	310(17)	448(19)	-123(14)	-173(14)	78(13)
O21	163(14)	291(16)	443(18)	102(13)	59(12)	9(12)
O22	348(17)	189(14)	389(17)	13(12)	-196(14)	-33(12)
O23	610(2)	300(17)	250(16)	-21(13)	65(15)	198(16)
C11	142(17)	142(16)	212(18)	-65(13)	-5(13)	39(13)
C12	174(18)	106(16)	221(18)	-35(13)	-12(14)	24(13)
C13	194(18)	144(17)	237(19)	-24(14)	-22(15)	55(14)
C21	223(19)	124(17)	222(18)	49(13)	-41(14)	46(14)
C22	217(19)	147(17)	220(18)	63(14)	-62(15)	30(14)
C23	260(2)	180(18)	225(19)	34(15)	-17(15)	74(15)
C111	145(16)	100(15)	175(17)	-19(12)	2(13)	-7(13)
C112	185(18)	123(16)	224(18)	-20(13)	-15(14)	-13(13)
C113	240(2)	142(17)	260(2)	-8(14)	-50(15)	4(15)
C114	260(2)	140(17)	242(19)	45(14)	-54(15)	-15(15)
C115	222(19)	133(17)	157(17)	15(13)	-13 (14)	-2(14)
C121	151(16)	106(15)	145(16)	-1(12)	-16(12)	-1(13)
C122	111(16)	216(18)	181(17)	-24(14)	-28(13)	-15(14)
C123	161(18)	390(2)	211(19)	-77(16)	-31(14)	-77(17)
C124	210(19)	244(19)	166(17)	-35(14)	-34(14)	-38(15)
C125	192(18)	203(18)	159(17)	-37(14)	-24(13)	-14(14)
C131	130(16)	115(16)	180(17)	-4(12)	11(13)	-16(13)
C132	126(16)	162(17)	204(17)	39(13)	9(13)	-16(13)
C133	171(18)	209(19)	300(2)	69(15)	39(15)	-35(15)
C134	123(18)	290(2)	380(2)	77(17)	22(16)	-24(16)
C135	127(17)	182(18)	250(19)	48(14)	-26(14)	3(14)
C211	113(16)	176(17)	137(16)	-12(13)	-19(12)	-22(13)
C212	115(16)	187(18)	212(18)	-12(14)	11(13)	30(13)
C213	220(2)	360(2)	290(2)	-38(18)	7(16)	-159(18)
C214	195(19)	195(19)	290(2)	-33(15)	-73(15)	-18(15)
C215	188(18)	175(18)	209(18)	-22(14)	-63(14)	-35(14)
C221	133(16)	155(16)	146(16)	6(13)	-25(12)	-24(13)
C222	165(17)	203(18)	174(17)	-19(14)	-7(13)	-10(14)
C223	188(19)	370(2)	162(18)	-26(16)	32(14)	8(16)
C224	157(19)	400(2)	250(2)	-10(17)	24(15)	12(17)
C225	144(17)	300(2)	190(18)	-15(15)	-22(14)	-64(15)
C231	147(16)	128(16)	147(16)	-7(12)	-7(12)	-7(13)
C232	212(18)	159(17)	161(17)	-12(13)	-24(14)	37(14)
C233	194(18)	172(17)	170(17)	-12(13)	-2(13)	20(14)
C234	208(18)	131(17)	232(19)	-35(14)	7(14)	5(14)
C235	204(18)	118(16)	191(17)	-15(13)	4(14)	22(14)

Table B4.60: Bond angles [°] for $[Co(PCp_3)(CO)_3]_2$.

Bond angles	Å/°	Bond angles	Å/°	Bond angles	Å/°
C11-Co1-C12	120.34(17)	C112-C113-H11C	110.7	P1-C131-H131	107.6
C11-Co-C13	118.88(17)	C114-C113-H11D	110.7	C131-C132-C133	103.2(3)
C12-Co1-C13	118.43(17)	C112-C113-H11D	110.7	C131-C132-H13A	111.1
C11-Co1-P1	92.38(11)	H11C-C113-H11D	108.8	C133-C132-H13A	111.1
C12-Co1-P	92.81(11)	C113-C114-C115	103.4(3)	C131-C132-H13B	111.1
C13-Co1-P	100.17(12)	C113-C114-H11E	111.1	C133-C132-H13B	111.1
C11-Co1-Co1	82.26(11)	C115-C114-H11E	111.1	H13A-C132-H13B	109.1
C12-Co1-Co1	86.39(11)	C113-C114-H11F	111.1	C134-C133-C132	105.5(3)
C13-Co1-Co1	86.09(12)	C115-C114-H11F	111.1	C134-C133-H13C	110.6
P1-Co1-Co1	173.23(4)	H11E-C114-H11F	109.0	C132-C133-H13C	110.6
C22-Co2-C21	118.96(17)	C114-C115-C111	104.0(3)	C134-C133-H13D	110.6
C22-Co2-C23	121.80(19)	C114-C115-H11G	111.0	C132-C133-H13D	110.6
C21-Co2-C23	116.42(18)	C111-C115-H11G	111.0	H13C-C133-H13D	108.8
C22-Co2-P2	92.26(12)	C114-C115-H11H	111.0	C133-C134-C135	106.6(3)
C21-Co2-P2	96.85(12)	C111-C115-H11H	111.0	C133-C134-H13E	110.4
C23-Co2-P2	97.78(13)	H11G-C115-H11H	109.0	C135-C134-H13E	110.4
C22-Co2-Co2	84.03(12)	C125-C122-C122	103.5(3)	C133-C134-H13F	110.4
C21-Co2-Co2	83.93(12)	C125-C121-P1	119.6(2)	C134-C134-H13F	110.4
C23-Co2-C02	85.26(12)	C122-C121-P1	114.2(2)	H13E-C134-H13F	108.6
P2-Co2-Co2	176.09(7)	C125-C121-H121	106.2	C131-C135-C134	103.9(3)
C121-P1-C111	106.55(15)	C122-C121-H121	106.2	C131-C135-H13G	111.0
C121-P1-C131	102.32(15)	P1-C12`-H121	106.2	C134-C135-H13G	111.0
C111-P1-C131	106.60(16)	C123-C122-C121	105.6(3)	C131-C135-H13H	111.0
C121-P1-Co1	110.20(11)	C123-C122-H12A	110.6	C134-C135-H13H	111.0
C111-P2-Co1	112.67(11)	C123-C122-H12B	110.6	H13G-C135-H13H	109.0
C131-P1-Co1	117.53(11)	C121-C122-H12B	110.6	C212-C211-C215	101.5(3)
C211-P2-C221	101.63(15)	H12A-C122-H12B	108.8	C212-C21P2	117.2(2)
C211-P2-C231	105.52(16)	C124-C123-C122	106.3(3)	C215-C211-P2-	114.9 (2)
C221-P2-C231	99.19(15)	C124-C123-H12C	110.5	C212-C211-H211	107.6
C231-P2-Co2	112.98(12)	C122-C123-H12C	110.5	C215-C211-H211	107.6
O11-C11-Co1	177.5(3)	C124-C123-H12D	110.5	P2-C211-H211	107.6
O12-C12-Co11	177.6(3)	C122-C123-H12D	110.5	C213-C212-C211	105.7(3)
O13-C13-Co1	177.4(3)	H12C-C123-H12D	108.7	C213-C212-H21A	110.6
O21-C21-C02	178.3(3)	C123-C124-C125	103.6(3)	C211-C212-H21A	110.6
O22-C22-Co2	178.3(4)	C123-C124-H12E	111.0	C213-C212-H21B	110.6
O23-C23-Co2	178.5(4)	C125-C124-H12E	111.0	C211-C212-H21B	110.6
C115-C111-C112	105.2(3)	C123-C124-H12F	111.0	H21A-C212-H21B	108.7
C115-C111-P1	112.9(2)	C125-C124-H12F	111.0	C212-C213-C214	106.4(3)
C112-C111-P1	119.0(2)	H12E-C124-H12F	109.0	C212-C213-H21C	110.5
C115-C111-H111	106.3	C121-C125-C124	102.0(3)	C214-C213-H21C	110.5
C112-C111-H111	106.3	C121-C125-H12G	111.4	C212-C213-H21D	110.5
P1-C111-H111	106.3	C124-C125-H12G	111.4	C214-C213-H21D	110.5
C113-C112-C111	105.4(3)	C121-C125-H12H	111.4	H21C-C213-H21D	108.6
C113-C112-H11A	110.7	C124-C125-H12H	111.4	C215-C214-C213	105.7(3)
C111-C112-H11A	110.7	H12G-C125-H12H	109.2	C215-C214-H21E	110. 6
C113-C112-H11B	110.7	C132-C135-C135	102.0 (3)	C213-C214-H21E	110.6
C111-C112-H11B	110.7	C132-C131-P1	114.2(2)	C215-C214-H21F	110.6
H11A-C112-H11B	108.8	C135-C131-P1	117.2(2)	C213-C214-H21F	110.6
C114-C113-C112	105.4(3)	C132-C131-H131	107.6	H21E-C214-H21F	108.7
C114-C113-H11C	110.7	C135-C131-H131	107.6	C214-C215-C211	103.2(3)

Appendix C of Chapter 5

C5.1. Results of oxidative addition reaction

C5.1.1. [Rh(acac)(CO)(Phoban[3.3.1]-Ph)]

Table C5.1: IR kinetic data in Fig 5.8 for the oxidative addition of MeI to [Rh(acac)(CO)(Phoban[3.3.1]-Ph)] in DCM at 19°C, [Rh] = 0.0025 mol dm^{-3}; [MeI] = 0.100 mol dm^{-3}.

Rh Specie	$10^2 k_{obs}$ (s^{-1})
Rh(I) acac	1.74 ± 0.03
Rh(III) alkyl	1.71 ± 0.02
Rh(III) acyl*	0.00125 ± 0.00002

* Reaction done at 25°C with UV-VIS spectrophotometer.

Table C5.2: Kinetic data for the oxidative addition of MeI to [Rh(acac)(CO)(Phoban[3.3.1]-Ph)] in DCM using stopped Flow spectroscopy, [Rh] = 0.00025 mol dm^{-3}, λ = 380 nm.

[MeI]/ (mol dm^{-3})	5°C/ $10^2 k_{obs}$ (s^{-1})	10°C/ $10^2 k_{obs}$ (s^{-1})	15.2°C/ $10^2 k_{obs}$(s^{-1})	24.7°C/ $10^2 k_{obs}$ (s^{-1})
0.100	0.8 ± 0.1	1.3 ± 0.1	2.0 ± 0.1	3.15 ± 0.01
0.150	1.5 ± 0.1	1.8 ± 0.1	2.4 ± 0.1	4.15 ± 0.01
0.250	2.4 ± 0.3	2.7 ± 0.1	3.60 ± 0.10	6.4 ± 0.1
0.500	4.4 ± 0.1	6.0 ± 0.1	7.19 ± 0.02	13.45 ± 0.01
0.750	6.0 ± 0.1	9.3± 0.1	10.64 ± 0.02	19.15 ± 0.01
1.000	8.0 ± 0.1	10.7 ± 0.1	14.1 ± 0.2	24.8 ± 0.1
$10^2 k_1$ (mol^{-1} dm^3 s^{-1})	7.7 ± 0.3	11.1 ± 0.6	13. 7 ± 0.2	24.5 ± 0.5
$10^2 k_{-1}$ (s^{-1})	0.3 ± 0.2	0.2 ± 0.4	0.4 ± 0.1	0.6 ± 0.3
K (mol^{-1} dm^3)	27 ± 15	46 ± 67	36 ± 10	36 ± 16

Table C5.6: Kinetic data for the oxidative addition of MeI to [Rh(acac)(CO)(Phoban[4.2.1]-Ph)] in DCM using stopped Flow spectroscopy, [Rh] = 0.0005 mol dm^{-3}, λ = 313 nm.

[MeI]/ (mol dm^{-3})	10°C/ 10^2k_{obs} (s^{-1})	15°C/ 10^2k_{obs} (s^{-1})	20°C/ 10^2k_{obs} (s^{-1})	25°C/ 10^2k_{obs} (s^{-1})
0.100	2.4 ± 0.4	2.7 ± 0.4	3.0 ± 0.2	3.5 ± 0.2
0.300	3.4 ± 0.6	4.3 ± 0.6	5.0 ± 0.8	6.1 ± 0.2
0.500	4.3 ± 0.6	5.4 ± 0.5	7.0 ± 0.7	8.6 ± 0.3
0.700	5.1 ± 0.9	6.8 ± 0.8	8.5 ± 1.0	10.6 ± 0.3
0.800	5.7 ± 0.7	7.2 ± 1.0	9.5 ± 1.0	11.9 ± 0.4
1.000	6.6 ± 1.4	8.4 ± 0.1	11.3 ± 0.2	14.1 ± 0.6
10^2k_1 (mol^{-1} dm^3 s^{-1})	4.6 ± 0.1	6.3 ± 0.2	9.1 ± 0.2	11.7 ± 0.2
10^2k_{-1} (s^{-1})	2.0 ± 0.1	2.3 ± 0.1	2.2 ± 0.1	2.5 ± 0.2
K (mol^{-1} dm^3)	2.4 ± 0.1	2.8 ± 0.2	4.1 ± 0.2	4.7 ± 0.3

Table C5.7: Data used for constructing the Eyring plot for the oxidative addition of MeI to [Rh(acac)(CO)(Phoban[4.2.1]-Ph)] in DCM using stopped Flow spectroscopy, [Rh] = 0.0005 mol dm^{-3}, λ = 313 nm.

T (°C)	T (K)	k_1 (mol^{-1} dm^3 s^{-1})	1/T (K^{-1})	k_1/T	ln(k_1/T)
25	298.35	1.17E-01	0.003354	3.92E-04	-7.844033
20	293.25	9.12E-02	0.00341	3.11E-04	-8.075726
14.8	287.95	6.25E-02	0.003473	2.17E-04	-8.435376
9.5	282.65	4.62E-02	0.003538	1.63E-04	-8.718985

Table C5.8: Activation parameters for the oxidative addition (k_1) of MeI to [Rh(acac)(CO)(Phoban[3.3.1]-Ph)] in DCM, [Rh] = 0.0005 mol dm^{-3}, λ = 313

	All data points
Slope (m)	-4803 ± 226
Intercept(C)	8 ± 1
$\Delta H^{\neq}$	40 ± 2 kJ mol^{-1}
$\Delta S^{\neq}$	-129 ± 6 J $K^{-1}mol^{-1}$
$\Delta G^{\neq}$	78 ± 6 kJ mol^{-1}

Table C5.12: Activation parameters for the oxidative addition (k_1) of MeI to [Rh(acac)(CO)(VCH[3.3.1 and 3.2.2]-Ph)] in DCM, [Rh] = 0.0005 mol dm^{-3}, λ = 368.5.

	All data points
Slope (m)	-4432 ± 109
Intercept(C)	8.0 ± 0.4
$\Delta H^{\neq}$	37 ± 1 kJ mol^{-1}
$\Delta S^{\neq}$	-131 ± 3 J K mol^{-1}
$\Delta G^{\neq}$	76 ± 3 kJ mol^{-1}

C5.1.4. [Rh(acac)(CO)(Lim-Ph)]

Table C5.13: IR kinetic data in Fig 5.22 for the oxidative addition of MeI to [Rh(acac)(CO)(4R, 8S and 4S, 8S-Lim-Ph)] in DCM at 26°C, [Rh] = 0.0025 mol dm^{-3}; [MeI] = 0.150 mol dm^{-3}.

Rh Specie	**$10^2 k_{obs}$ (s^{-1})**
Rh(I) acac	0.76 ± 0.01
Rh(III) alkyl 1	0.73 ± 0.01
Rh(III) alkyl 2	1.6 ± 0.1
Rh(III) acyl (1)*	0.0445 ± 0.0002
Rh(III) acyl (2)*	0.83 ± 0.03

* Reaction done at 25°C with UV-VIS spectrophotometer at 370 nm, [Rh] = 0.00025 mol dm^{-3}, [MeI] = 0.200 mol dm^{-3}.

Table C5.14: IR kinetic data for the oxidative addition of MeI to [Rh(acac)(CO)(4R, 8S-Lim-Ph)] in DCM, [Rh] = 0.00025 mol dm^{-3}.

[MeI]/ (mol dm^{-3})	**22°C/ $10^2 k_{obs}$ (s^{-1})**
0.010	0.73 ± 0.01
0.040	2.3 ± 0.1
0.070	3.6 ± 0.1
0.100	5.19 ± 0.02
$10^2 k_1$ (mol^{-1} dm^3 s^{-1})	49.1 ± 1.0
$10^2 k_{-1}$ (s^{-1})	0.3 ± 0.1
K (mol^{-1} dm^3)	205 ± 60

C5.1.4.2. MeI variation of [Rh(acac)(CO)(4R, 8S-Lim-Ph)] at 22°C

C5.1.5 . [Rh(acac)(CO)(PA-Ph)]

Table C5.18: IR kinetic data in Fig 5.22 for the oxidative addition of MeI to [Rh(acac)(CO)(PA-Ph)] in DCM at 18°C, [Rh] = 0.0025 mol dm^{-3}; [MeI] = 0.250 mol dm^{-3}.

Rh Specie	$10^2 k_{obs}$ (s^{-1})
Rh(I) acac	0.040 ± 0.001
Rh(III) alkyl	0.051 ± 0.001
Rh(III) acyl	0.0016 ± 0.0003

Table C5.19: Kinetic data for the oxidative addition of MeI to [Rh(acac)(CO)(PA-Ph)] in DCM using UV/vis, [Rh] = 0.00025 mol dm^{-3}, λ = 322 nm.

[MeI]/ (mol dm^{-3})	5°C/ $10^2 k_{obs}$ (s^{-1})	10°C/ $10^4 k_{obs}$ (s^{-1})	15°C/ $10^2 k_{obs}$ (s^{-1})	25°C/ $10^2 k_{obs}$ (s^{-1})
0.100	0.0168 ± 0.0004	0.0103 ± 0.0002	0.0209 ± 0.0004	
0.125				0.0471 ± 0.0002
0.150	0.0180 ± 0.0003	0.0151 ± 0.0002	0.024± 0.001	
0.250	0.023 ± 0.001	0.0271 ± 0.0001	0.0339 ± 0.0010	0.067 ± 0.001
0.500	0.028 ± 0.001	0.0419 ± 0.0004	0.064 ± 0.001	0.121 ± 0.001
0.750	0.0442 ± 0.0002	0.054 ± 0.001	0.082± 0.001	0.168 ± 0.002
1.000	0.0530 ± 0.0002	0.0500± 0.0004	0.077 ± 0.001	0.204 ± 0.004
$10^2 k_1$ (mol^{-1} $dm^{-3} s^{-1}$)	0.042 ± 0.004	0.067 ± 0.006	0.098 ± 0.006	0.184 ± 0.007
$10^2 k_{-1}$ (s^{-1})	0.011 ± 0.002	0.006 ± 0.003	0.0106± 0.0024	0.025 ± 0.005
K (mol^{-1} dm^{-3})	4 ± 1	10 ± 5	9 ± 2	7 ± 1

Table C5.20: Data for the construction of the Eyring plot for the oxidative addition of MeI to [Rh(acac)(CO)(PA-Ph)] in DCM at 322 nm, [Rh] = 0.00025 mol dm^{-3}.

T (°C)	T (K)	k_1 (mol^{-1} dm^{-3} s^{-1})	1/T, (K^{-1})	k_1/T	$\ln(k_1/T)$
25	298.15	1.84E-03	0.003354	6.17E-06	-11.9956
15	288.15	9.80E-04	0.00347	3.40E-06	-12.5914
10	283.15	6.70E-04	0.003532	2.37E-06	-12.9542
5	278.15	4.20E-04	0.003595	1.51E-06	-13.4034

C5.2.2. [Rh(acac)(CO)(Phoban[4.2.1]-Ph)]

Table C5.23: Effect of [MeI] on the rate of migratory CO-insertion at [Rh(acac)(Me)(I)(CO)(Phoban[4.2.1]-Ph)] in DCM at 25°C, λ = 380 nm, [Rh] = 0.00025 mol dm^{-3}.

[MeI]/mol dm^{-3}	$10^4 k_{obs}$/s^{-1}
0.200	1.82 ± 0.02
0.500	1.93 ± 0.02
0.700	1.89 ± 0.02
0.800	1.86 ± 0.02
1.000	1.83 ± 0.02
$10^4 k_2$ (s^{-1})	1.93 ± 0.02
K (mol^{-1} dm^3)	Fix at 60

C5.2.3. [Rh(acac)(CO)(VCH[3.3.1 and 3.2.2]-Ph)]

Table C5.24: Effect of [MeI] on the rate of migratory CO-insertion at [Rh(acac)(CO)(VCH[3.3.1 and 3.2.2]-Ph)] in DCM at 25°C, λ = 370 nm, [Rh] = 0.00025 mol dm^{-3}.

[MeI]/mol dm^{-3}	$10^4 k_{obs}$/s^{-1}
0.100	0.38 ± 0.01
0.200	0.33 ± 0.01
0.300	0.34 ± 0.01
0.500	0.34 ± 0.01
0.700	0.33 ± 0.01
$10^4 k_2$ (s^{-1})	0.35 ± 0.01
K (mol^{-1} dm^3)	Fix at 200

C5.2.6. [Rh(acac)(CO)(PA-Ph)]

Table C5.27: Effect of [MeI] on the rate of migratory CO-insertion at [Rh(acac)(Me)(I)(CO)(PA-Ph)] in DCM at 25°C, λ = 380 nm, [Rh] = 0.00025 mol dm^{-3}.

[MeI]/mol dm^{-3}	**$10^4 k_{obs}/s^{-1}$**
0.500	0.0885 ± 0.0002
0.800	0.0958 ± 0.0003
1.400	0.101 ± 0.001
1.700	0.109 ± 0.001
2.000	0.114 ± 0.001
$10^4 k_2$ (s^{-1})	0.118 ± 0.002
K (mol^{-1} dm^3)	Fix at 6.2

C5.3. Crystallographic data

C5.3.1. [Rh(acac)(CO)(4R, 8S-Lim-Ph)]

Table C5.29: Atomic coordinates (x 10^4)and equivalent isotropic displacement parameters ($Å^2$ x10^4) for [Rh(acac)(CO)(4R, 8S-Lim-Ph)]. U(eq) is defined as one third of the trace of the orthogonalized Uij tensor.

	x	y	z	U(eq)
Rh1	7635.6(4)	5023.7(2)	70814(9)	176.4(9)
P1	6587.7(16)	6592.5(11)	7955.9(9)	169(2)
O11	6580(4)	5977(3)	5757(2)	236(8)
O12	8623(4)	3645(3)	6207(3)	217(7)
C1	8494(6)	4193(5)	8260(4)	210(10)
O1	9021(4)	3524(3)	8997(3)	298(8)
C11	5859(7)	6572(5)	4015(4)	349(13)
C12	6706(6)	5958(5)	4837(4)	223(10)
C13	7590(7)	4577(5)	4566(4)	260(11)
C14	8500(6)	3666(5)	5231(4)	239(11)
C15	9435(8)	2595(6)	4780(5)	373(14)
C111	4207 (6)	6965(4)	7556(4)	192(10)
C112	2923(6)	5837(5)	7525(4)	235 (10)
C113	2934(6)	5278(4)	8588(4)	270(13)
C114	2677(7)	6294 (5)	9359(4)	299(12)
C115	3802(7)	7495(5)	9370(4)	283(12)
C116	5741(6)	7344(5)	9897(4)	247(11)
C117	6845(6)	6447(5)	9352(3)	223(10)
C118	3695(7)	7999(5)	8274(4)	259(11)
C119	3125(6)	4776(5)	6755(4)	328(15)
C120	5904(8)	6945(6)	11018(4)	319(13)
C121	7612(6)	8139(5)	7757(4)	206(10)
C122	8709(6)	8790(5)	8532(4)	228()
C23	9451(5)	9960(7)	8342(3)	291(10)
C124	9120(7)	10487(5)	7370(4)	302(12)
C125	8046(6)	9856(7)	6592(4)	328(13)
C126	7283(7)	8685(5)	6771(4)	275(11)

Table C5.31: Anisotropic displacement parameters ($Å^2$ X 10^4) for [Rh(acac)(CO)(4R, 8S-Lim-Ph)]. The anisotropic displacement factor exponent takes the form: $-2\pi^2[h^2a^{*2}U11 + ... + 2hka^*b^*U12]$.

	U11	U22	U33	U23	U13	U12
Rh1	15.58(14)	19.24(15)	18.80(16)	-0.3(2)	4.94 (10)	1.5(2)
P1	15.2(6)	19.8(6)	16.5(6)	0.4(5)	5.0(4)	1.5(5)
O11	24.0(19)	24.5(18)	23(2)	3.3(15)	5.8(14)	4.9(15)
O12	18.6(17)	21.1(17)	26(2)	-4.0(2)	6.2(14)	3.5(14)
C1	13(2)	25(2)	27(3)	-6(2)	8.4(19)	0(2)
O1	29(2)	33(2)	28(2)	12.2(17)	4.8(15)	2.5(16)
C11	39(3)	35(3)	28(3)	7(2)	-2(2)	-4(3)
C12	23(3)	23(2)	20(3)	0(2)	2.9(19)	-7(2)
C13	30(3)	30(3)	20(3)	-6(2)	9(2)	-8(2)
C14	19(2)	24(3)	29(3)	-7(2)	7(2)	-5(2)
C15	36(3)	41(3)	36(3)	-15(3)	10(2)	6(3)
C111	15(2)	22(2)	20(2)	2.8(19)	3.4(17)	0(19)
C112	12(2)	29(2)	30(3)	-1(2)	2.9(17)	0.6(19)
C113	18(2)	23(3)	40(3)	8(2)	4.7(18)	-4 (2)
C114	25(3)	31(3)	37(3)	6(2)	15(2)	8(2)
C115	31(3)	30(3)	28(3)	-1(2)	17(2)	6(2)
C116	29(3)	25(3)	22(3)	-3(2)	8(2)	-2(2)
C117	24(3)	24(2)	19(3)	0(2)	3.6(19)	5(2)
C118	23(3)	22(2)	35(3)	0(2)	10(2)	6(2)
C119	20(2)	36(4)	42(3)	-8(3)	1.0(19)	-3(2)
C120	46(4)	36(3)	17(3)	-5(2)	13(2)	2(3)
C121	16(2)	24(2)	24(3)	-3(2)	7.8(18)	1.5(19)
C122	21(2)	25(3)	23(3)	-3(2)	4.0(19)	-1(2)
C23	25(2)	30(2)	32(2)	-10(4)	5.8(17)	-2(3)
C124	26(3)	25(2)	44(3)	-6(2)	15(2)	-5(2)
C125	34(3)	33(4)	33(3)	-4(3)	11(2)	-5(3)
C126	28(3)	30(3)	24(3)	-5(2)	4(2)	-1(2)

Table C5.33: Bond angles [°] for [Rh(acac)(CO)(4R, 8S-Lim-Ph)].

Bond length	Å/°	Bond length	Å/°
C1-Rh1-O11	178.08(18)	C13-C14-C15	118.5(5)
C1-Rh1-O12	91.83(18)	C14-C15-H15A	109.5
O11-Rh1-O12	89.49(13)	C14-C15-H15B	109.5
C1-Rh1-P1	91(15)	H15A-C15-H15B	109.5
O11-Rh1-P1	87.71(10)	C14-C15-H15C	109.5
O12-Rh1-P1	176.75(10)	H15A-C15-H15C	109.5
C117-P1-C121	104.1(2)	H15B-C15-H15C	109.5
C117-P1-C111	103.5(2)	C118-C111-C112	108.9(4)
C121-P1-C111	101.7(2)	C118-C111-P1	108.6(3)
C117-P1-Rh1	118.40(16)	C112-C111-P1	116.5(3)
C121-P1-Rh1	111.59(15)	C118-C111-H111	107.5
C111-P1-Rh1	115.70(16)	C112-C111-H111	107.5
C12-O11-Rh1	126.8(3)	P1-C111-H111	7.5()
C14-O12-Rh1	125.5(3)	C113-C112-C119	110.6(4)
O1-C1-Rh1	177.7(4)	C113-C112-C111	111.8(4)
C12-C11-H11A	109.5	C119-C112-C111	115.7(4)
C12-C11-H11B	109.5	C113-C112-H112	106.0
H11A-C11-H11B	109.5	C119-C112-H112	106.0
C12-C11-H11C	109.5	C111-C112-H112	106.0
H11A-C11-H11C	109.5	C114-C113-C112	112.0(4)
H11B-C11-H11C	109.5	C114-C113-H13A	109.2
O11-C12-C13	125.0(5)	C112-C113-H13A	109.2
O11-C12-C11	115.2(5)	C114-C113-H13B	109.2
C13-C12-C11	119.7(5)	C112-C113-H13B	109.2
C14-C13-C12	127.0(5)	H13A-C113-H13A	107.9
C14-C13-H13	116.5	C113-C114-C115	114.5(4)
C12-C13-H13	116.5	C113-C114-H14A	108.6
O12-C14-C13	126.0(5)	C115-C114-H14A	108.6

C5.3.2. [Rh(acac)(CO)(PA-Ph)]

Table C5.35: Atomic coordinates (x 10^4) and equivalent isotropic displacement parameters ($Å^2$ x10^4) for molecule 1, [Rh(acac)(CO)(PA-Ph)]. U(eq) is defined as one third of the trace of the orthogonalized Uij tensor for molecule 1.

	x	y	z	U(eq)
Rh1	1006.26(12)	8273.52(16)	1108.08(12)	114.0(6)
P1	1893.4(4)	9192.8(5)	962.8(4)	111.7(15)
O11	1378.7(11)	8796.5(14)	2166.3(10)	161(4)
O12	164.7(11)	7514.6(14)	1382.3(11)	177(4)
C1	668.3(16)	7808(2)	165.8(16)	154(6)
O1	420.8(12)	7497.3(15)	-421.8(11)	225(5)
C11	1556.7(18)	9025(2)	3430.5(17)	273(8)
C12	1124.6(16)	8575 (2)	2694.7(16)	172(6)
C13	505.2(16)	7974(2)	2648.8(16)	184(6)
C14	55.8(16)	7512(2)	2014.3(16)	188(7)
C15	-636.4(18)	6951(3)	2037.6(19)	339(9)
O13	2147.6(10)	11028.9(13)	412.8(10)	128(4)
O14	1800.4(10)	10622.7(13)	-852.1(10)	138(4)
O15	1567.0(10)	8994.2(13)	-608.6(10)	134(4)
C111	1547.9(15)	10446.3(19)	540.1(16)	121(6)
C112	920.5(15)	10316(2)	-192.7(15)	139(6)
C113	1239.2(15)	9948(2)	-789.2(15)	134(6)
C114	2417.2(16)	10701(2)	-178.0(15)	138(6)
C115	2798.6(15)	9704(2)	-5.0(16)	140(6)
C116	2223.8(15)	8933(2)	46.3(15)	130(6)
C117	1283.5(16)	10982(2)	1113.7(16)	156(6)
C118	653.1(16)	9856(2)	-1535.7(16)	188(6)
C119	2942.3(17)	11483(2)	-285.7(16)	183(6)
C120	2526.8(16)	7913(2)	62.3(16)	176(6)
C121	2763.3(15)	9295(2)	1644.9(2)	130(6)
C122	3018.2(16)	8445(2)	2040.6(16)	159(6)
C123	3673.3 (16)	8446(2)	2648.9(17)	188(6)
H123	3845	7870	2904	230
C124	4070.2	9301	2876.3	192
C125	3822.4(16)	10157(2)	2481.5(16)	177(6)
H125	4093	10731	2631	210
C126	3174.5(16)	10156(2)	1866.7(16)	154(6)

Table C5.37: Hydrogen coordinates (x 10^4) and isotropic displacement parameters ($Å^2$ X 10^4) for molecule 1, [Rh(acac)(CO)(PA-Ph)].

	x	y	z	U(eq)
H11A	2082	8842	3562	410
H11B	1348	8800	3804	410
H11C	1514	9720	3394	410
H13	383	7874	3082	220
H15A	-1085	7246	1707	510
H15B	-666	6959	2533	510
H15C	-599	6291	1888	510
H11D	666	10933	-346	170
H11E	548	9857	-130	170
H11F	3014	9527	-391	170
H11G	3209	9734	461	170
H11H	1698	11034	1567	230
H11I	873	10629	1203	230
H11J	1112	11621	934	230
H11K	396	10466	-1673	280
H11L	292	9363	-1518	280
H11M	896	9678	-1895	280
H11N	3139	11298	-678	280
H11O	3356	11567	165	280
H11P	2667	12083	-412	280
H12A	2148	7457	101	260
H12B	2976	7841	481	260
H12C	2649	7791	-385	260
H22	2748	7870	1897	190
H123	3845	7870	2904	230
H124	4501	9305	3292	230
H125	4093	10731	2631	210
H126	3014	10727	1602	180

Table C5.39: Anisotropic displacement parameters ($Å^2$ X 10^4) for molecule 1, [Rh(acac)(CO)(PA-Ph)]. The anisotropic displacement factor exponent takes the form: $-2\pi^2[h^2a^{*2}U11 + ... + 2hka^*b^*U12]$.

	U11	U22	U33	U23	U13	U12
Rh1	112.5(11)	116.5(11)	114.2(12)	4.3(9)	37.2(9)	-12.7(9)
P1	119(3)	99(3)	122(4)	10(3)	45(3)	9(3)
O11	162(10)	184(11)	136(10)	-28(9)	46(8)	-16(8)
O12	161(10)	219(11)	145(11)	-16(9)	40(9)	-56(9)
C1	150(14)	136(15)	181(16)	27(13)	59(12)	-38(12)
O1	247(12)	247(13)	162(11)	-32(10)	39(10)	-78(10)
C11	298(18)	340(2)	169(17)	-70(15)	59(14)	-59(15)
C12	182(15)	195(15)	135(15)	14(13)	42(12)	41(12)
C13	191(15)	256(17)	127(15)	28(13)	81(13)	31(13)
C14	170(15)	197(17)	190(16)	56(13)	46(13)	-3(12)
C15	265(18)	480(2)	290(2)	43(18)	114(16)	-163(17)
O13	157(10)	111(10)	152(10)	2(8)	101(8)	-10(8)
O14	157(10)	134(10)	131(10)	14(9)	55(8)	-21(8)
O15	133(10)	132(10)	131(10)	-3(8)	33(8)	15(8)
C111	128(13)	72(13)	184(15)	13(12)	81(12)	8(11)
C112	129(13)	126(14)	167(15)	5(12)	52(12)	19(11)
C113	109(13)	124(14)	172(15)	13(12)	46(12)	12(11)
C114	175(14)	156(15)	112(14)	14(12)	85(12)	8(12)
C115	106(13)	169(15)	157(15)	0(12)	58(12)	20(11)
C116	129(13)	121(14)	146(15)	-8(12)	53(12)	15(11)
C117	163(14)	128(14)	199(16)	-6(13)	91(12)	22(12)
C118	185(15)	206(16)	167(15)	31(13)	48(13)	22(13)
C119	238(16)	150(15)	186(16)	-3(13)	101(13)	-37(12)
C120	187(15)	156(15)	213(16)	15(13)	105(13)	46(12)
C121	111(13)	156(14)	134(14)	7(12)	56(11)	-1(11)
C122	159(14)	154(15)	171(15)	2(13)	60(12)	-14(12)
C123	172(15)	182(16)	207(16)	48(13)	54(13)	35(12)
C124	104(14)	250(17)	203(16)	-32(14)	19(12)	1(12)
C125	140(14)	171(15)	231(16)	-27(13)	75(12)	-27(12)
C126	171(14)	126(14)	178(15)	2(13)	75(12)	17(12)

Table C5.41: Bond length [Å] for molecule 1, [Rh(acac)(CO)(PA-Ph)].

Bond length	Å/°	Bond length	Å/°
Rh1-C1	1.818(3)	C112-H11E	9700
Rh1-O11	2.0418(19)	C113-C118	1.497(4)
Rh1-O12	2.0733(18)	C114-C119	1.507(4)
Rh1-P1	2.2350(7)	C114-C115	1.530(4)
P1-C121	1.823(3)	C115-C116	1.827(4)
P1-C116	1.872(3)	C115-H11F	0.9700
P1-C111	1.874(3)	C115-H11G	0.9700
O11-C12	1.273(3)	C116-C120	1.508(4)
O12-C14	1.279(3)	C117-H11H	0.9600
C1-O1	1.149(3)	C117-H11I	0.9600
C11-C12	1.509(4)	C117-H11J	0.9600
C11-H11A	0.9600	C118-H11K	0.9600
C11-H11B	0.9600	C118-H11L	0.9600
C11-H11C	0.9600	C118-H11M	0.9600
C12-C13	1.394(4)	C119-H11N	0.9600
C13-C14	1.386(4)	C119-H11O	0.9600
C13-H13	0.9300	C119-H11P	0.9600
C14- C15	1.508(4)	C120-H12A	0.9600
C15-H15A	0.9600	C120-H12B	0.9600
C15-H15B	0.9600	C120-H12C	0.9600
C15-H15C	0.9600	C121-C122	1.391(4)
O13-C114	1.437(3)	C121-C126	1.399(4)
O13-C111	1.450(3)	C122-C123	1.389(4)
O14-C113	1.425(3)	C122-H122	0.9300
O14-C114	1.429(3)	C123-C124	1.383(4)
4O15-C113	1.442(3)	C123-H123	0.9300
O15-C116	1.445(3)	C124-C125	1.394(4)
C111-C112	1.519(4)	C124-H124	0.9300
C111-C117	1.518(4)	C125-C126	1.388(4)
C112-C113	1.520(4)	C125-H125	0.9300
C112-H11D	0.9700	C126-H126	0.9300

Table C5.43: Bond angles [°] for molecule 1, [Rh(acac)(CO)(PA-Ph)].

Bond angles	[°]	Bond angles	[°]
C1-Rh1-O11	179.63(10)	C13-C14-C15	119.5(3)
C1-Rh1-O12	90.95(10)	C14-C15-H15A	109.5
O11-Rh1-O12	88.75(7)	C14-C15-H15B	109.5
C1-Rh1-P1	92.42(8)	H15A-C15-H15B	109.5
O11-Rh1-P1	87.87(6)	C14-C15-H15C	109.5
O12-Rh1-P1	175.41(6)	H15A-C15-H15C	109.5
C121-P1-C116	104.83(12)	H15B-C15-H15C	109.5
C121-P1-C111	108.64(13)	C114-O13-C111	115.4(2)
C116-P1-C111	94.08(12)	C113-O14-C114	111.9(2)
C121-P1-Rh1	113.14(9)	C113-O15-C116	115.9(2)
C116-P1-Rh1	121.16(9)	O13-C111-C112	108.5(2)
C111-P1-Rh1	113.00(8)	O13-C111-C117	106.7(2)
C12-O11-Rh1	126.78(18)	C112-C111-C117	112.9(2)
C14-O12-Rh1	126.15(19)	O13-C111-P1	111.23(17)
O1-C1-Rh1	176.4(2)	C112-C111-P1	106.06(18)
C12-C11-H11A	109.5	C117-C111-P1	111.42(19)
C12-C11-H11B	109.5	C111-C112-C113	111.0(2)
H11A-C11-H11B	109.5	C111-C112-H11D	109.4
C12-C11-H11C	109.5	C113-C112-H11D	109.4
H11A-C11-H11C	109.5	C111-C112-H11E	109.4
H11B-C11-H11C	109.5	C113-C112-H11E	109.4
O11-C12-C13	126.4(3)	H11D-C112-H11E	108.0
O11-C12-C11	114.4(3)	O14-C113-O15	110.4(2)
C13-C12-C11	119.2(3)	O14-C113-C118	107.9(2)
C14-C13-C12	125.7(3)	O15-C113-C118	105.9(2)
C14-C13-H13	117.1	O14-C113-C112	108.0(2)
C12-C13-H13	117.1()	O15-C113-C112	111.0(2)
O12-C14-C13	126.0(3)	C118-C113-C112	113.6(2)
O12-C14-C15	114.5(3)	O14-C114-O13	110.4(2)

Table C5.45 : Bond angles [°] for molecule 2, [Rh(acac)(CO)(PA-Ph)].

Bond angles	[°]	Bond angles	[°]
C2-Rh2-O21	178.14(10)	C23-C24-C25	118.6(3)
C2-Rh2-O22	92.70(10)	C24-C25-H25A	109.5
O21-Rh2-O22	89.14(7)	C24-C25-H25B	109.5
C2-Rh2-P2	92.83(9)	H25A-C25-H25B	109.5
O21-Rh2-P2	85.31(5)	C24-C25-H25C	109.5
O22-Rh2-P2	171.86(6)	H25A-C25-H25C	109.5
C221-P2-C216	108.73(13)	H25B-C25-H25C	109.5
C221-P2-C211	104.91(12)	C214-O23-C213	111.5(2)
C211-P2-C216	94.27(12)	C213-O24-C216	115.6(2)
C221-P2-Rh2	112.93(9)	C214-O25-C211	115.3(2)
C216-P2-Rh2	111.78(8)	O25-C211-C212	109.4(2)
C211-P2-Rh2	122.28(9)	O25-C211-C217	106.7(2)
C22-O21-Rh2	127.00(19)	C212-C211-C217	111.7(2)
C24-O22-Rh2	124.95(18)	O25-C211-P2	107.18(16)
O2-C2-Rh2	177.5(2)	C212-C211-P2	109.79(19)
C22-C21-H21A	109.5	C217-C211-P2	111.92(19)
3C22-C21-H21B	109.5	C211-C212-C213	110.2(2)
H21A-C21-H21B	109.5	C211-C212-H21D	109.6
C22-C21-H21C	109.5	C213-C212-H21D	109.6
H21A-C21-H21C	109.5	C211-C212-H21E	109.6
H21B-C21-H21C	109.5	C213-C212-H21E	109.6
O21-C22-C23	126.2(3)	H21D-C212-H21E	108.1
O21-C22-C21	113.5(3)	O24-C213-O23	110.3(2)
C23-C22-C21	120.3(3)	O24-C213-C218	106.2(2)
C24-C23-C22	125.5(3)	O23-C213-C218	107.4(2)
C24-C23-H23	117.2	O24-C213-C212	111.8(2)
C22-C23-H23	117.2	O25-C213-C212	107.8(2)
O22-C24-C23	126.6(3)	C218-C213-C212	113.2(2)
O22-C24-C25	114.8(3)	O23-C214-O25	110.0(2)